EFFECTS OF CHANNEL MISMATCHES ON BEAMFORMING AND SIGNAL DETECTION

THESIS

Christopher I. Allen, Captain, USAF

AFIT/GE/ENG/10-01

DEPARTMENT OF THE AIR FORCE
AIR UNIVERSITY

AIR FORCE INSTITUTE OF TECHNOLOGY

Wright-Patterson Air Force Base, Ohio

The views expressed in this thesis are those of the author and do not reflect the official policy or position of the United States Air Force, Department of Defense, or the United States Government.

AFIT/GE/ENG/10-01

EFFECTS OF CHANNEL MISMATCHES ON BEAMFORMING AND SIGNAL DETECTION

THESIS

Presented to the Faculty

Department of Electrical and Computer Engineering

Graduate School of Engineering and Management

Air Force Institute of Technology

Air University

Air Education and Training Command

In Partial Fulfillment of the Requirements for the

Degree of Master of Science in Electrical Engineering

Christopher I. Allen, B.S.E.E.

Captain, USAF

March 2010

AFIT/GE/ENG/10-01

EFFECTS OF CHANNEL MISMATCHES ON BEAMFORMING AND SIGNAL DETECTION

Christopher I. Allen, B.S.E.E.

Captain, USAF

Approved:

Richard K. Martin — 11 Mar 2010

Dr. Richard K. Martin, Thesis Advisor — Date

Michael A. Saville — 11 Mar 2010

Maj. Michael A. Saville, Committee Member — Date

Matthew C. Fickus — 11 Mar 2010

Dr. Matthew C. Fickus, Committee Member — Date

Table of Contents

AFIT/GE/ENG/10-01

Abstract

Tuner gain measurements of a multichannel receiver are reported. A linear regression model is used to characterize the gain, as a function of channel number, tuner set-on frequency, and intermediate frequency. Residual errors of this model are characterized by a t distribution. Very strong autocorrelation of tuner gain at various frequencies is noted. Tuner performance from one channel to the next is diverse; several defects at specific frequencies are noted. The Wilcoxon signed rank test is used to test normality of tuner gain among devices; normality is rejected.

Antenna directivity and phase pattern measurements are also reported. An antenna element pattern is presented, along with residual errors. An array pattern model is constructed using steering vectors. Simulated gain and phase mismatches are used to predict their effects on antenna beamforming and signal detection.

List of Figures

List of Tables

List of Abbreviations

Abbreviation Page

EFFECTS OF CHANNEL MISMATCHES ON BEAMFORMING AND SIGNAL DETECTION

I. Introduction

In radar, Electronic Intelligence (ELINT), and various antenna applications, we are concerned with beamforming using antenna arrays, and with detection of signals within noise. In a multichannel analog Radio Frequency(RF) system, it is desirable to have equal performance from one channel to the next, and to compensate for mismatches via calibration. Using statistical methods, we can characterize the detrimental effects of channel mismatches. In this thesis, for a multichannel receiver, "mismatch" means any undesired variation in gain and/or phase among the channels. This thesis seeks to answer two questions: (1) how do channel mismatches affect beamforming, and (2) how do channel mismatches affect detector performance?

Each channel within the RF system is characterized by its gain and its phase delay. These parameters vary with frequency. The transmit path of a radar may contain mixers, amplifiers, filters, and cables for each individual array element. Each of these RF channels will have a slightly different gain and phase response. The antenna elements themselves will vary somewhat from one to the next. If there is coupling between antenna elements, the elements at the edges of the array will not perform the same as the ones toward the center. On the receive path, the antenna elements once again contribute to channel mismatches. Each channel may have its own Low Noise Amplifier (LNA), Intermediate Frequency (IF) downconverter, and Analog to Digital (A/D) converter; each of these components may contribute to mismatches in gain and phase. For a single channel, the overall gain is equal to the product of the gains of all the components; the overall phase equals the sum of the phase delays of all the components.

A single component will perform differently from the equivalent component in each of the other channels. Such variations can be characterized by statistical distributions of gain and phase from one component to the next. The same can be said of the entire

system—there is a statistical distribution of gain and phase from one channel to the next. These statistical distributions are frequency-dependent.

The basic signal detection problem for the system is to decide whether or not a signal is present within a noisy environment. We start with two hypotheses: a signal is present, or it is not. The system has to decide which hypothesis is true at any given time. Detection becomes easier as the signal strength increases relative to the noise level. The figures of merit for a detector are the detection probability P_d and the false alarm probability P_f. P_f is the likelihood the system will make a Type I error, and P_d is the likelihood the system will *not* make a Type II error. Both of these probabilities vary negatively with the detection threshold τ. The functional variation between P_f and P_d is known as the Receiver Operating Characteristic (ROC).

Each channel contributes to the detector performance. If we assume the gain or loss of each component is known precisely, and all the channels have the same overall gain, then we can analytically compute the ROC. If one channel is functioning poorly, we can expect this to affect the ROC. If, however, we assume a statistical variation of gain from one channel to the next, then we can transform this information into a statistical variation of the ROC curve.

The antenna pattern of a given antenna is a function of azimuth angle ϕ, elevation angle θ, and frequency ω. To analytically predict the antenna pattern of an array, we must first have a mathematical model of each element. We may choose to use a simple isotropic, omnidirectional, or forward-looking model for each element. To predict the array pattern, we use the azimuth steering vector $\mathbf{a}$ and the elevation steering vector $\mathbf{e}$, and our chosen element model. This gives us an antenna gain pattern and an antenna phase pattern. We may also need to apply a phase delay, or weight, $\mathbf{w}_k$ to each element, which changes the antenna pattern and gives the antenna beam a squint angle. Other figures of merit for the antenna pattern are the Half Power Beamwidth (HPBW), First Null Beamwidth (FNBW), and Sidelobe Level (SLL).

Mismatches in performance between channels are equivalent to weighting each antenna element in amplitude as well as phase. We would expect this to affect the squint

angle, beamwidth, and sidelobe level. If we can characterize the statistical distribution of gain and phase from one channel to the next, we can predict a statistical distribution of antenna patterns, including squint angles, beamwidths, and sidelobe levels.

We apply these concepts to measured data from the Multi-Channel Wideband Electronic Support System (MCWESS), a testbed at the Air Force Research Laboratory (AFRL) Sensors Directorate at Wright-Patterson Air Force Base, Ohio. In support of this research, we conducted extensive measurements of antenna patterns and tuner gain of the MCWESS, and have applied mathematical models to each. We use these data to investigate the effects of channel mismatches on beamforming and signal detection.

II. Literature Review

The beamforming problem consists of using a multichannel phased antena array to focus on desired sources at various conditions of azimuth, elevation, and frequency, while similarly tuning out sources of interference. The design concept is achieved via steering vectors. A beamforming network is subject to errors due to receiver noise, or channel-to-channel mismatches in gain, phase response, or antenna element patterns. Such errors can cause the array pattern to form improperly. Numerous articles address the problem of robust beamforming in the presence of steering vector errors. Wax and Anu [10] provide an analysis of the signal-to-interference-plus-noise ratio (SINR) of a minimum variance beamformer in the presence of steering vector errors. The article considers error sources such as noise, interference, angular distance between the desired signal and the interferences, array dimensions, correlation between the desired signal and the interferences, and sampling errors. This article models a single desired signal source, and any number of interference sources. The signal samples, noise samples, and steering vector errors are each assumed to be normally distributed.

The diagonal loading algorithm is commonly used to design adaptive beamformers which are robust against steering vector errors. Vincent and Besson [9] describe how to maximize SINR, in the presence of steering vector errors, via optimum diagonal loading; and the optimum loading is negative. The paper considers a single desired signal source, any number of interference sources, and noise. No assumption is made about the distribution of the steering vector errors, but their statistical expectation and covariance are assumed known.

The formula described in [6] is a generalized method to design constraints into a minimum variance adaptive beamformer. The authors define two types of constraints. The first constraint determines the quiescent response of the system, which is the response when there is only noise, and no signal. The other constraints ensure the desired signal is not tuned out when it is present. Clearly, in order to use this formula, we must have prior knowledge about the location and frequency of the desired signal, unless we want the antenna to scan free space and a wide bandwidth.

The algorithm proposed in [11] models steering vector errors as generalized phase errors. The algorithm iteratively corrects the steering vector in order to maximize beamformer output power. The paper considers a single desired signal source, multiple interference sources, and noise. The algorithm assumes the interference sources are separated from the desired signal in angle or frequency.

III. Experimental Procedure

3.1 Test Item Description

The MCWESS is a sixteen-channel, wideband RF receiver which is being developed as a demonstrator for ELINT applications. It was manufactured by Harris Corporation, Government Communication Systems Division, for the Air Force Research Laboratory, Sensors Directorate. The receiver is tunable between 1-8 GHz, and provides 500 MHz of instantaneous bandwidth, within each of the sixteen input channels simultaneously. A phased array antenna collects inputs to the system, which then pass through a passive analog Beamforming Network (BFN). The signals pass through power dividers to the sixteen tuner modules. A Local Oscillator (LO) provides a 1 GHz Intermediate Frequency (IF). The tuner modules down convert the input signals to 1 GHz $\pm$ 250 MHz. The signals then go to a sixteen-channel high-speed digitizer. A Windows-based Personal Computer (PC) reads the data from the digitizer; the PC also controls the input frequency band (0.5 to 18 GHz, $\pm$ 250 MHz) of the tuner modules.

The Current Sheet Antenna (CSA) is the front-end of the MCWESS system. The active region of the CSA consists of 512 Printed Wire Board (PWB) antenna elements: a 16×16 array of horizontally polarized elements, interlaced with a 16×16 array of vertically polarized elements. The CSA collects signals within the 1-8 GHz band.

The Beam Forming Network consists of sixteen passive beam former cards. Each beam former consists of a balun which combines the inputs from a column of sixteen horizontally-polarized antenna elements into a single RF output, and a balun which combines a column of sixteen vertically-polarized elements into another RF output. A Low Noise Amplifier (LNA) is connected to the output of each balun, and is built into the beam former card. The output of each LNA has a SubMiniature version A (SMA) connector at the rear of the assembly; there are 32 in all. There is no beam steering capability within the antenna or BFN. Thus, in its current configuration, the MCWESS antenna is effectively a fixed array with a single row of sixteen superelements, which can be polarized either horizontally or vertically according to which set of sixteen SMA connectors are being

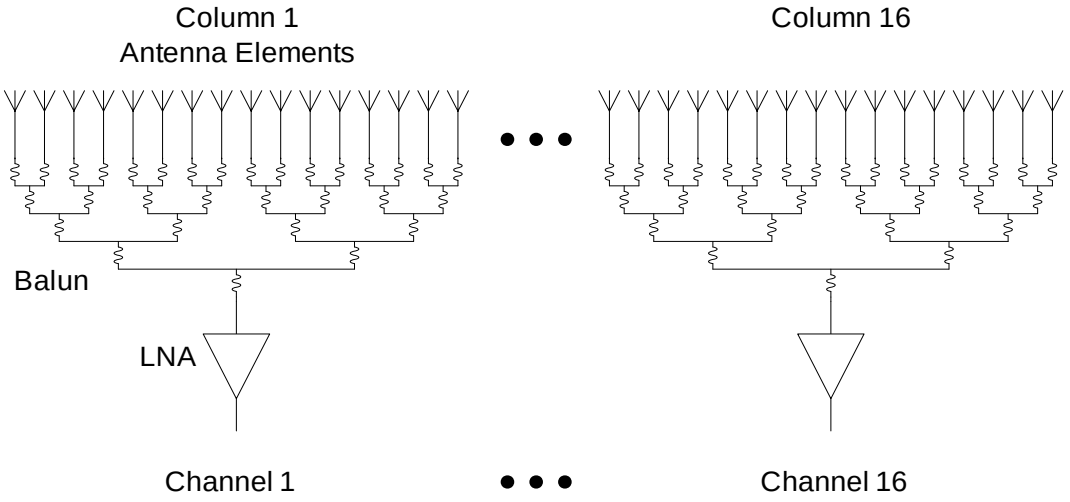

Figure 3.1 Schematic of the MCWESS antenna and beamforming network assembly. Only one polarization is shown, but both horizontally and vertically polarized elements are interlaced with each other. Throughout these tests, only one polarization was used at any given time.

used. The antenna superelement pattern is designed to have ±60 degrees of scan coverage in azimuth. A schematic of the CSA/BFN assembly is shown in Fig. 3.1.

After leaving the BFN, the signals pass through 50-ohm coaxial cables approximately 1.1 m long, into two-way power dividers, manufactured by ET Industries. There is one power divider per channel. The purpose of the power dividers is to provide signals to both the low and high band input ports of each tuner. Each of these power dividers is connected to each tuner via two coaxial cables, which are each approximately 1.2 m long.

A synthesizer provides the 1 GHz intermediate frequency for the system. The 1 GHz carrier goes through four eight-way power dividers before going through to the tuner modules. All these components are manufactured by Mid-Atlantic RF Systems; Mid-Atlantic calls them Low Cost Receiver (LCR) systems. The synthesizer, or LO module, is part number LCR1600, and the power dividers are part number LCR-PS8-01.

The sixteen tuner modules down-convert the input signals to the 1 GHz intermediate frequency. The tuner modules are also manufactured by Mid-Atlantic, and the part number is LCR400SNBG20, except for one tuner which is a part number LCR1600SNBG20; both part numbers are built according to the same design. The tuner center frequency is

selectable from 0.5-18 GHz at intervals of 1 MHz. Each tuner has a low band (0.5-5.999 GHz) input port, and a high band (6-18 GHz) input port. The specified nominal power gain of each tuner is 20 dB (equivalent to 10 dB voltage gain). The relationship of input vs. output frequency is different above 12 GHz than it is below 12 GHz:

$$f_{IF} = \begin{cases} f_{in} - f_c + 1\,\text{GHz} & f_c < 12\,\text{GHz} \\ f_c - f_{in} + 1\,\text{GHz} & f_c \geq 12\,\text{GHz} \end{cases} \tag{3.1}$$

where f_c is the frequency the tuner is centered on, f_{in} is the input frequency, and f_{IF} is the output frequency.

Two interface boxes, manufactured by Mid-Atlantic, are connected to the Windows-based PC via a 25-pin parallel port. These boxes allow the computer to tune the tuner modules within their 0.5-18 GHz frequency range. The interface boxes also control the frequency of the local oscillator, although MCWESS only uses a 1 GHz intermediate frequency. A 28-volt DC power supply provides power to the interface boxes, the LO module, and the tuner modules.

The down-converted RF signals which leave the tuner modules pass through bandpass filters, and then through 4.5-meter coaxial cables, to a high-speed digitizer. The filters were custom-made by K&L. The high-speed digitizer is made by Acqiris. The digitizer is connected to the PC via an Ethernet cable.

Fig. 3.2 is a block diagram of the MCWESS. The power dividers, tuners, and anti-aliasing filters, as well as the associated LOs, LCR1600 control module, and RF cables, are collectively referred to as the Microwave Block Downconverter (BDC).

3.2 Tuner Gain

A tuner is designed to operate linearly, meaning the magnitude of the output equals the magnitude of the input, plus a constant gain. When this is happening, the input in dBm can be plotted against the output in dBm, and the result is a straight line with a slope of one, and a y-intercept that coincides with the gain in dB. This is illustrated in

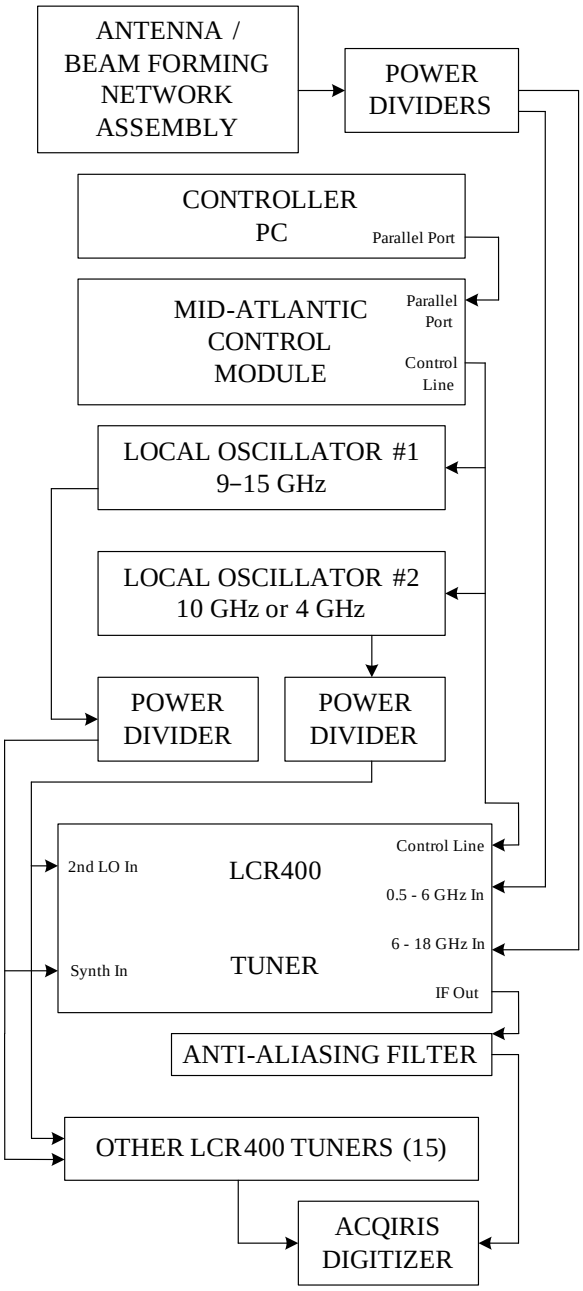

Figure 3.2 MCWESS configuration. The Microwave Block Downconverter (BDC) consists of everything in the figure except for the beamforming network, the controller PC, and the digitizer. One of the sixteen tuners is enlarged, but all of them are connected the same way.

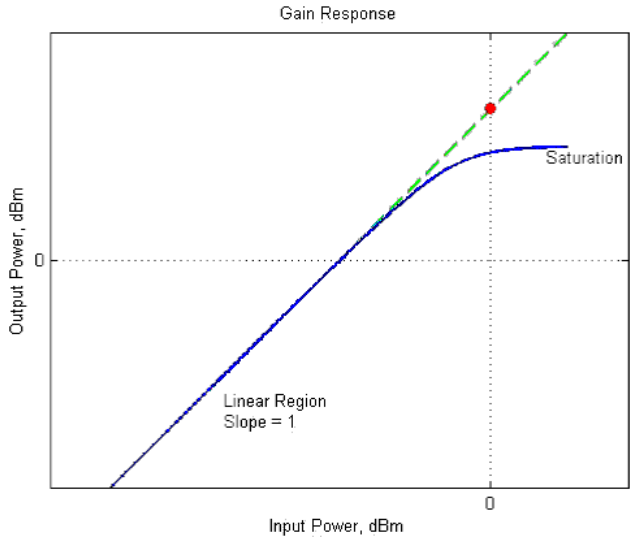

Figure 3.3 Gain response of a device, showing linear and saturation regions.

Fig. 3.3 and summarized in (3.2):

$$G_1 = P_{out} - P_{in} \tag{3.2}$$

where P_{out} is output power in dBm, P_{in} is input power in dBm, and G_1 is gain. However, when the output reaches a certain level, various components within the tuner begin to saturate, and the output magnitude begins to level off. This is also illustrated in Fig. 3.3. The level at which the output begins to saturate can be characterized as the 1 dB compression point [7]. This is the level of input (or output) at which the output deviates from the linear region defined in (3.2). Our experience with the LCR400 tuners leads us to assume that an input level of -40 dBm is within the linear region of the device.

The gain measurements were conducted as follows. The center frequency of the tuner was set to 0.500 GHz. The input frequency was set to the center frequency, and then varied at +10 MHz intervals until the gain dropped below 0 dBm. The input frequency was again set to the center frequency, and then varied at -10 MHz intervals until the gain dropped below 0 dBm. The center frequency was then incremented by 15 MHz (except tuner #3 was incremented at 10 MHz intervals). At all times, the input power level was -40 dBm. A low band sweep (0.5-5.999 GHz) had to be conducted separately from the high band

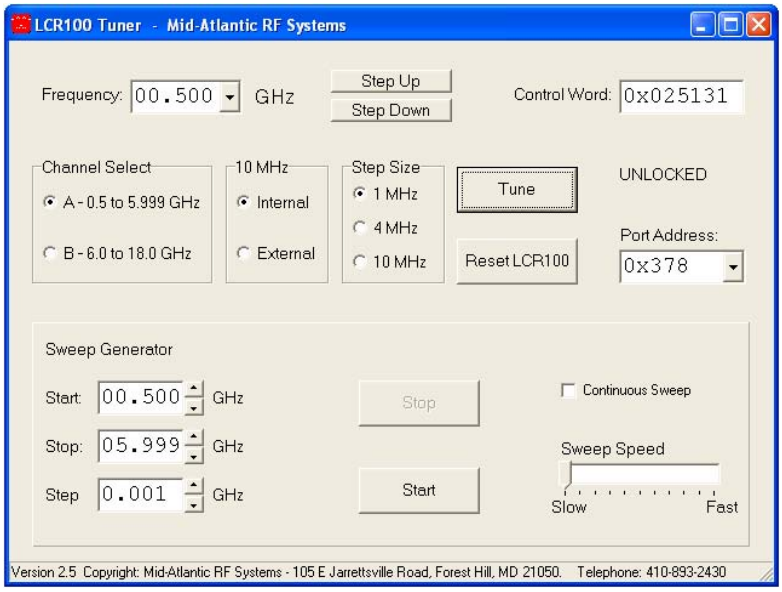

Figure 3.4 Screen shot of the Graphical User Interface which sets the center frequency of the Mid-Atlantic LCR400 tuners.

sweep (6-18 GHz), because the LCR400 tuner has separate input ports for the two bands, so the RF input cable had to be swapped in between sweeps.

The tuner control software provided by Mid-Atlantic does not support the test methodology just described. Mid-Atlantic's software provides a Graphical User Interface (GUI), shown in Fig. 3.4, to set the center frequency of the tuners. This GUI does not communicate with the command line, Matlab, GPIB, or any other application. It was therefore impossible to know or control what frequency the tuners were set on. To solve this problem, a separate executable application was created, which takes in the desired center frequency via the command line, and then emulates the mouse and the keyboard to communicate with Mid-Atlantic's GUI. This application was implemented in C using Microsoft Visual Studio and Microsoft Platform Software Development Kit (SDK); the code is given in Appendix B and is available in electronic form from [12]. Matlab is then able to call the program using Matlab's `dos` or `system` function.

3.2.1 Temperature Monitoring and Control. We expected that the gain of the tuners would vary with temperature. A thermocouple was attached to the tuner under test, to monitor the temperature. We found that by placing cooling fans next to the tuners, the

tuner temperature would remain stable near the ambient temperature of 23°C. Without the cooling fans, the tuner would stabilize at about 17°C above ambient temperature when using low band, and 10°C above ambient temperature when using high band. All results described in Sections 4.1-4.2 were obtained using cooling fans, except for one sweep of Tuner #3.

The gains of tuners 4 and 6 were measured at different temperatures (-3°C and +50°C), by placing the BDC inside the Tenney Thermal Product Solutions (TPS) model T10RC Environmental Test Chamber. This chamber can create temperatures from -75°C to +200°C. The chamber measures 10 cubic feet, and is just wide enough to contain the BDC metal chassis with the tuners, oscillators, control modules, and power dividers. A small opening on the side allows cables to pass into the chamber.

3.2.2 Test Setup. An Agilent swept spectrum analyzer with a 26 GHz bandwidth was used to collect all gain measurements. An Anritsu signal generator, with a bandwidth from 10 MHz – 40 GHz, was used to generate the input tones. These devices are controllable via the General Purpose Interface Bus (GPIB). A Windows-based computer, with a National Instruments GPIB interface card, and Matlab with the Instrument Control Toolbox, was used to control the signal generators and spectrum analyzer. This computer was the same computer used by MCWESS to control the center frequency of the tuners.

The controller computer communicates with the tuners via its 25-pin parallel interface. As mentioned earlier, a special application had to be developed to allow Matlab to command the tuner to set on each desired frequency. The C code for this application is given in Appendix B.

A thermocouple was attached to the casing of each tuner as it was tested. The thermocouple reader, the Omegaette model HH306, communicates with the controller computer via the computer's serial COM port. The Omegaette driver application records time/temperature data to the computer's hard drive in tab- or comma-delimited text format. As the tuner temperature remained stable throughout each test, little needed to be done but to make a note of it after each sweep.

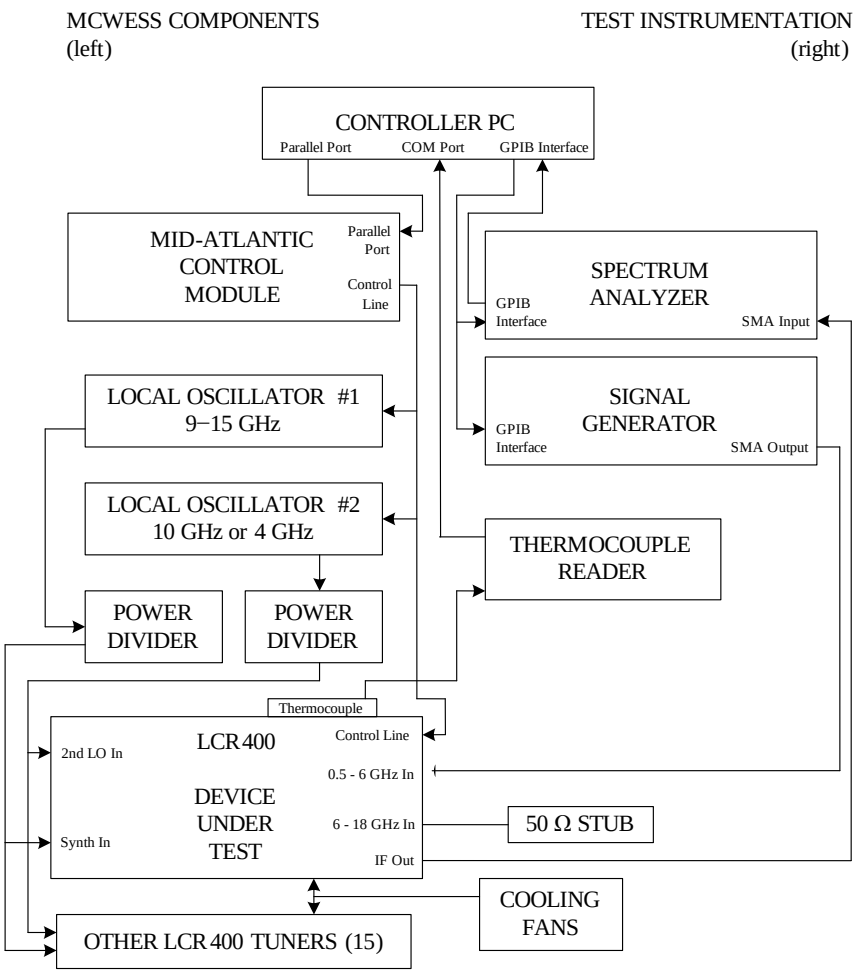

Figure 3.5 Single tone test (low band), used for gain tests.

The baseline MCWESS setup without instrumentation is shown in Fig. 3.2. The single tone test setups, used for gain tests, are illustrated in Fig. 3.5 and 3.6. Matlab was used to control the center frequency sweeps and input frequency sweeps, and to read the outputs from the spectrum analyzer.

Results are displayed with reference to the shorthand notation "Tuner #1" etc.; Table 3.1 matches the shorthand with the serial number of each tuner. This notation is consistent with the channel number nomenclature used on the Aqiris digitizer displays.

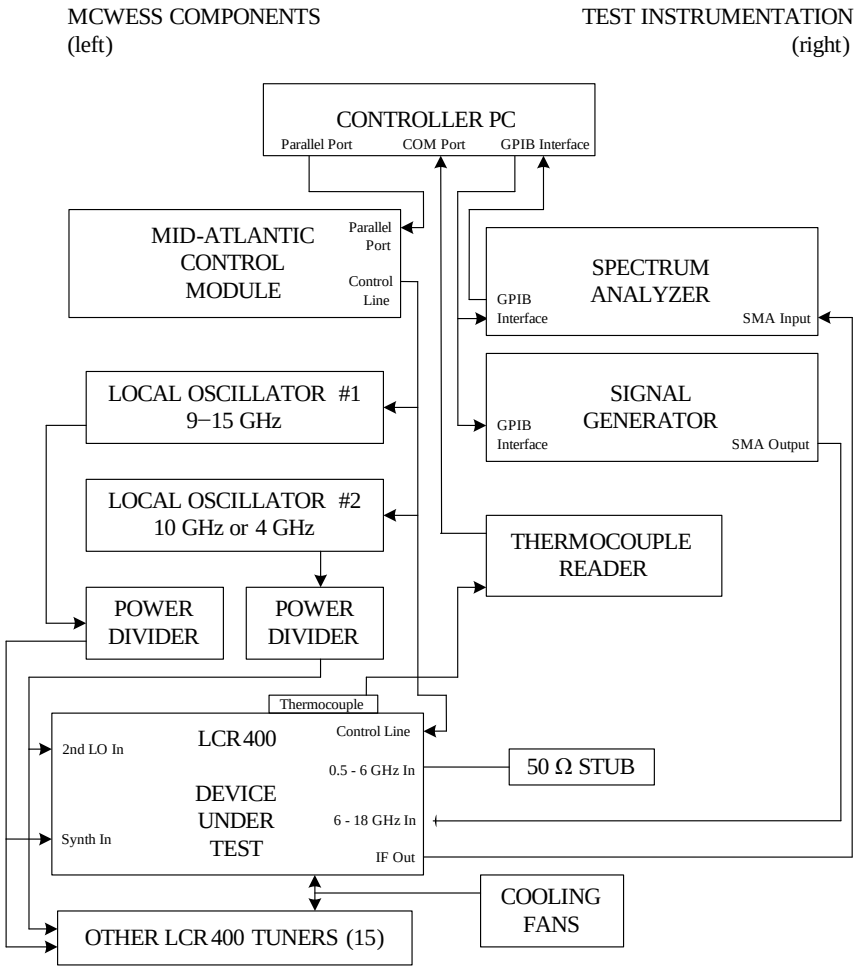

Figure 3.6 Single tone test (high band), used for gain tests.

Table 3.1 Mid-Atlantic LCR400 tuner serial numbers used in MCWESS. The serial number includes the year (first two digits) and week (second two digits) in which the tuner was built.

Tuner #	**Serial #**	**Tuner #**	**Serial #**
1	0649.2-4	9	0732.1
2	0831.1	10	0732.7
3	0649.1-3	11	0732.4
4	0649.1-2	12	0732.6
5	0649.1-4	13	0732.5
6	0649.2-1	14	0732.2
7	0649.2-3	15	0732.3
8	0649.2-2	16	0732.8

3.3 Microwave Block Downconverter Gain

The gain of the entire downcoverter section was measured in a similar fashion. These measurements take into account losses due to the power dividers, the cables, and the K&L bandpass filters, as well as the tuner gain. All measurements were conducted at room temperature, with cooling fans to maintain tuner temperatures at approximately 23°C. As a power divider distributes the input signal to both the low and the high-band inputs of the tuner under test, there is no changing of instrumentation cables between low and high-band test runs.

3.4 Antenna Pattern

3.4.1 Setup. Various antenna patterns were measured for the MCWESS antenna assembly. Note that the baluns and LNAs can not be separated from the antenna (Fig. 3.1). These measurements were performed in the near-field anechoic chamber at the Air Force Research Laboratory, Sensors Directorate, at Wright-Patterson Air Force Base, using the NSI2000 equipment from Near Field Systems, Inc. (NSI). Although the measurements were conducted in the near field region, all data were transformed into a far-field coordinate system using a Fast Fourier Transform (FFT) algorithm. This algorithm is resident within the NSI2000 software [4]. Inside the anechoic chamber, the Antenna Under Test (AUT) remained fixed, while a network analyzer transmitted test signals though a movable instrumentation probe. The probe moved across the (x, z) plane parallel to the array face, and sampled the antenna pattern from –69.3 cm to +69.3 cm in the x direction at intervals of 1.75 cm, and likewise in the z direction. The coordinate system is shown in Fig. 3.7. Only the front hemisphere was measured. A total of $80 \times 80 = 6400$ samples were taken for each antenna pattern. The NSI2000 software reported the far-field antenna patterns in terms of azimuth angle ϕ, elevation angle θ, and antenna voltage pattern measured in dBi. After performing the far-field transformation, the software reported valid antenna patterns over the domain from $(|\phi| \leq 90°, |\theta| \leq 67°)$ at increments of 0.9° in each direction, with the exception of a notched domain from approximately $(|\phi| > 60°, |\theta| < 30°)$. The domain limitations are due to the limitations of the chamber setup and of the FFT.

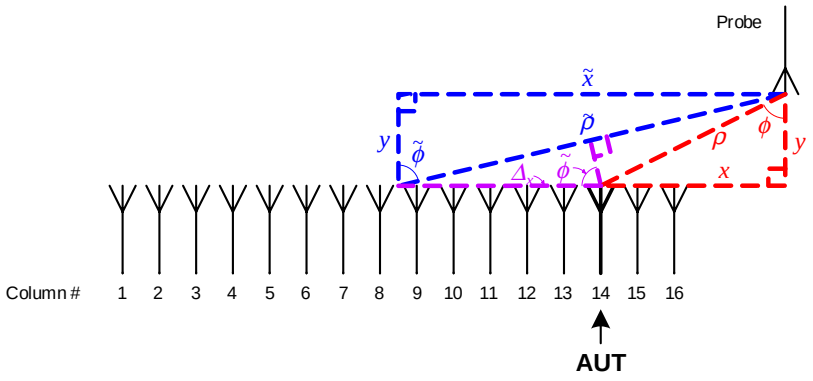

(a)

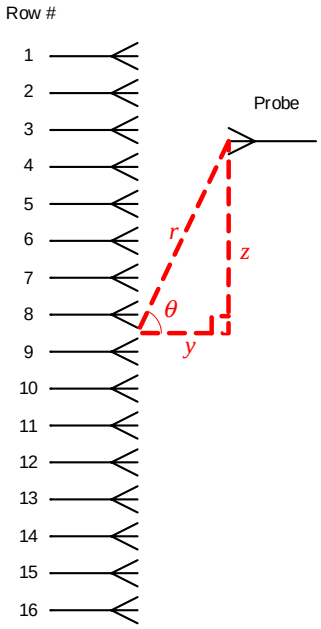

(b)

Figure 3.7 Coordinate system used for the antenna pattern measurements, showing (a) a top view and (b) a side view. The rows and columns are spaced 0.45 inches (1.14 cm) apart. In this example, superelement #14 is the antenna under test.

Antenna pattern measurements were performed for each superelement individually, as shown in Fig. 3.8. The voltage pattern of the kth superelement is denoted $A_k(\phi, \theta)$. Additional measurements were performed for the entire array combined; this is denoted $A(\phi, \theta)$. This configuration required external power combiners be added to the system, as shown in Fig. 3.9; the devices used were power "dividers" which can also be used as combiners. Measurements of both the horizontally and vertically polarized antenna elements were conducted. The frequency varied from 2.6 to 8.2 GHz at intervals of 100 MHz; measurements below 2.6 GHz will require a different test setup, and have not yet been conducted. Three different Open-Ended Waveguide (OEWG) probes were used to cover the various frequencies: size WR284 for 2.6-3.9 GHz, size WR187 for 4.0-5.8 GHz, and size WR137 for 5.9-8.2 GHz. Also, antenna patterns were sampled for the WR284, WR187, and WR137 standard gain horns at the various frequencies. By sampling these known references, it is possible to know the absolute amplitudes of the antenna patterns of the device under test. Excluding the standard gain horn measurements, a total of $57 \times 2 \times (16 + 1) = 1938$ antenna patterns were generated—57 frequencies, 2 polarizations, 16 superelements, and one entire array.

3.4.2 Phase Measurement. In addition to providing antenna voltage patterns, the NSI2000 reported an antenna phase pattern $\tilde{\Psi}_k(\tilde{\phi}, \tilde{\theta})$ measured in degrees, where $\tilde{\phi}$ and $\tilde{\theta}$ are the azimuth and elevation angles according to the chamber coordinate system, whose origin was at the center of the array, *not* the superelement under test, as shown in Fig. 3.7a. Apparently, the NSI2000 did not perform a far-field transformation on $\tilde{\Psi}_k$, because in a far-field coordinate system, signals radiate spherically, and therefore the phase should be independent of $\tilde{\phi}$ and $\tilde{\theta}$. We wish to use the (ϕ, θ) coordinate system shown in Fig. 3.7, whose origin is at the superelement under test. The NSI2000 performed a far-field coordinate transformation for each A_k to the effect that $(\tilde{\phi}, \tilde{\theta}) \rightarrow (\phi, \theta)$, but for $\tilde{\Psi}_k$ we had to externally compute the coordinate correction. In this thesis, we are only interested in determining the mismatches of the phase Ψ_k from channel to channel, and as such we only need to sample Ψ_k at one point in the pattern for each superelement; for simplicity, we choose Ψ_k at boresight, i.e. $\phi = \theta = 0$ and $x = z = 0$. Since the MCWESS array is effectively a single row, $\tilde{\theta} = 0$ always implies $\theta = 0$; therefore, we can ignore the

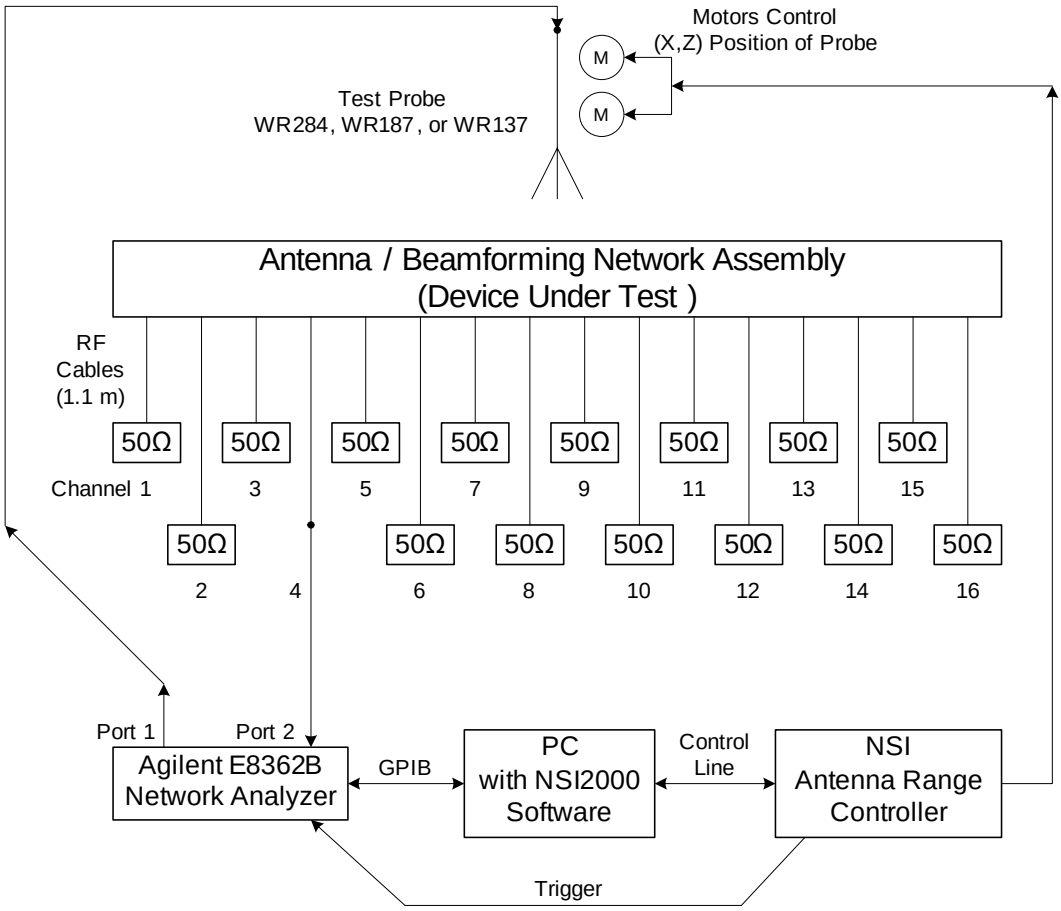

Figure 3.8 Test setup for measuring the antenna pattern of a single superelement (column) of the MCWESS antenna. The CSA/BFN assembly and test probe were inside a near-field anechoic chamber. Sixteen other outputs for the unused polarization are present but not shown; these had 50Ω stubs immediately at the output of the antenna assembly.

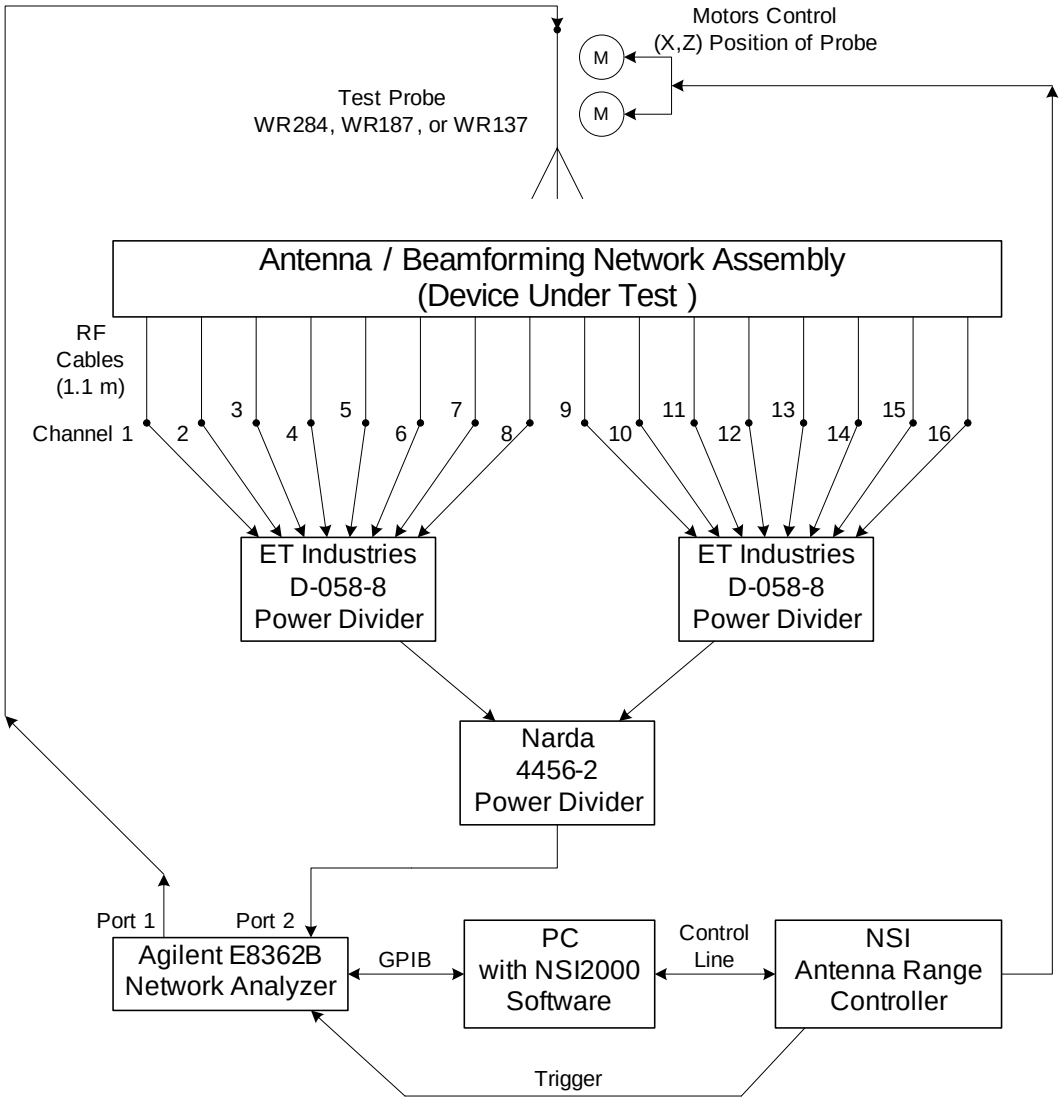

Figure 3.9 Test setup for measuring the antenna pattern of the entire MCWESS antenna. The CSA/BFN assembly and test probe were inside a near-field anechoic chamber. The power "dividers" are reversed, and used as summing devices.

elevation correction, and focus on correcting the azimuth angle. From Fig. 3.7a, we make the following assumptions for the far-field coordinate system:

$$\phi \approx \tilde{\phi} \tag{3.3}$$

and

$$\tilde{\rho} \approx \rho + \Delta_x \sin \tilde{\phi}. \tag{3.4}$$

The element displacement Δ_x for the kth superelement is

$$\Delta_x = (k - 8.5)\, d_x, \tag{3.5}$$

where d_x is the linear spacing between elements, which is $0.45\,\text{in} = 1.14\,\text{cm}$. The phase Ψ_k from the probe to the AUT is related to the distance ρ by

$$\rho = \frac{\lambda \Psi_k\,(\phi, 0)}{2\pi} - \tilde{\psi}_k, \tag{3.6}$$

where $\tilde{\psi}_k$ is a constant particular to the kth superelement, and likewise from the probe to the center of the array:

$$\tilde{\rho} = \frac{\lambda \tilde{\Psi}_k(\tilde{\phi}, 0)}{2\pi} - \tilde{\psi}_k. \tag{3.7}$$

Therefore, to convert from the measured $\Psi_k(\tilde{\phi}, 0)$ to the desired $\Psi_k\,(\phi, 0)$, we substitute (3.6-3.7) into (3.4) as follows:

$$\frac{\lambda \tilde{\Psi}_k(\tilde{\phi}, 0)}{2\pi} - \tilde{\psi}_k \approx \frac{\lambda \Psi_k\,(\phi, 0)}{2\pi} - \tilde{\psi}_k + (k - 8.5)\, d_x \sin \tilde{\phi}, \tag{3.8}$$

$$\Psi_k\,(\phi, 0) \approx \tilde{\Psi}_k(\tilde{\phi}, 0) - \frac{2\pi\,(k - 8.5)\, d_x \sin \tilde{\phi}}{\lambda}, \tag{3.9}$$

and given (3.3-3.4) we have

$$\Psi_k\,(\phi, 0) \approx \tilde{\Psi}_k\,(\phi, 0) - \frac{2\pi \Delta_x \sin \phi}{\lambda}. \tag{3.10}$$

Using (3.10) gives a data set centered about $\phi = 0$ such that

$$\min_{\phi,\theta} \Psi_k(\phi,\theta) = \Psi_k(0,0). \tag{3.11}$$

Theoretically, from Fig. 3.7a, $\Psi_k(\phi,0)$ should follow a secant function according to

$$\Psi_k(\phi,0) = \frac{2\pi y}{\lambda}\sec\phi + \tilde{\psi}_k, \tag{3.12}$$

where y is constant, as illustrated in Fig. 3.10. Next, we define ψ_k as

$$\psi_k \equiv \min_{\phi,\theta} \Psi_k(\phi,\theta) \tag{3.13}$$

where

$$\psi_k = \Psi_k(0,0) = \frac{2\pi y}{\lambda} + \tilde{\psi}_k \tag{3.14}$$

Now, the absolute values of $\tilde{\psi}_k$ for each k are unknown, and furthermore, the NSI2000 provides the data set $\tilde{\Psi}_k(\tilde{\phi},\tilde{\theta})$ modulo 360°, but we can still compare each $\tilde{\psi}_k$ relative to each other. Using (3.13-3.14) enables us to ignore the constant y and compare the relative ψ_k for each superelement, which is what we are really interested in. From (3.10) and Fig. 3.10 we see that $\tilde{\Psi}_k(\phi,0)$ intersects $\Psi_k(\phi,0)$ at $\phi = 0$. Experimentally, we find letting

$$\psi_k \approx \tilde{\Psi}_k(0,0) \tag{3.15}$$

gives the most satisfactory results.

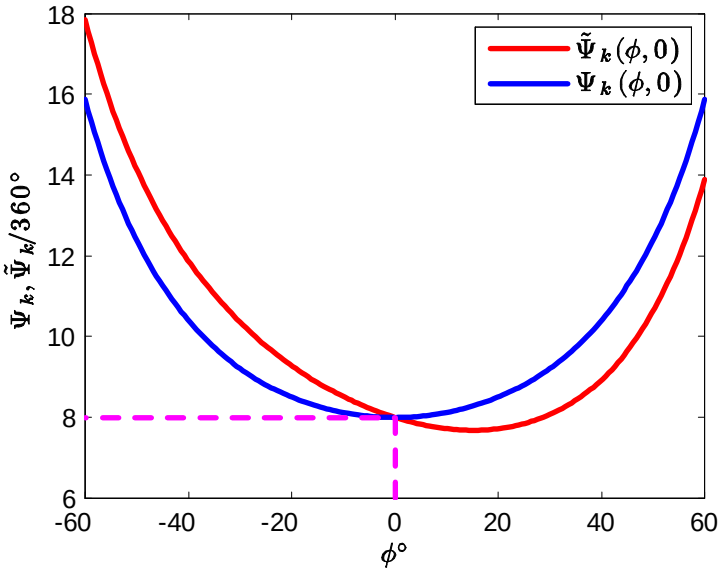

Figure 3.10 Theoretical $\Psi_k(\phi,0)$ and $\tilde{\Psi}_k(\phi,0)$ predicted by (3.12). In this example, $\lambda = 3.8\,\text{cm}$, $k = 16$, $y = 30\,\text{cm}$, and $\psi_k = 8.0 \times 360° = 2880°$.

IV. Experimental Results

4.1 Tuner Gain

The results of the gain measurements for the Mid-Atlantic LCR400 tuners are shown in Tables 4.1-4.18 and Figs. 4.1-4.35, and summarized in Table 4.19 and Figs. 4.37-4.40. Each color plot (Figs. 4.1, 4.4 etc.) shows the raw gain measurements for a single tuner at each point in the frequency spectrum; the color represents gain. In the line plots, (Figs. 4.2, 4.3 etc.) the solid black line shows the mean gain as the input frequency varies across the passband ($f_c - 0.25 \leq f_{in} \leq f_c + 0.25$ GHz), with f_c constant; the red line is the maximum, the blue line is the minimum, the green line is the standard deviation, and the dotted purple line is the passband ripple (the difference between the maximum and the minimum). Unless stated otherwise, all gain values are voltage gain (not power gain) in linear scale (not decibels).

For each tuner, there is significant variation in gain from one frequency to the next. There is also significant variation in performance from one tuner to the next. The motivation behind this thesis is to study channel-to-channel mismatches; the raw data are shown in Figs. 4.37-4.40 and Table 4.19. Basically, tuner gain can be expected to be within a certain envelope, i.e. between the maximum and minimum shown in Table 4.19.

Out-of-band performance was very poor, as shown in the color plots; hence the need for the K&L anti-aliasing filters. In each color plot, the edges of the passband are highlighted with purple lines. For each tuner, there was significant output up to 300 MHz outside of the passband. Section 4.2 shows the performance of the system with the anti-aliasing filters in place.

Tuner gain was very stable with respect to temperature. From Figs. 4.7-4.10 and 4.13-4.16 and Tables 4.4, 4.5, 4.7, and 4.8, we can see that the shape of the overall gain pattern for each tuner is virtually unchanged, but the gain shifts very slightly as temperature changes. As the temperature increases from -3°C to 22°C, the gain of tuner 4 decreases about 0.3 dB in the low band ($0.5 \leq f_c < 6$ GHz), and is virtually unchanged in the high band ($6 \leq f_c \leq 18$ GHz). As the temperature increases from 22°C to 50°C, the gain of tuner 6 decreases about 0.6 dB in the low band, and about 0.3 dB in the high band.

Table 4.1 Measured voltage gain, within the passband, for Tuner 1.

	Linear Scale					Decibels				
f_c [GHz]	Max	Mean	Min	Ripple	Std Dev	Max	Mean	Min	Ripple	Std Dev
0.5	7.28	5.86	4.16	3.11	0.76	8.62	7.64	6.19	2.43	0.58
1	7.55	6.07	4.34	3.21	0.90	8.78	7.78	6.38	2.41	0.66
2	6.88	5.59	4.02	2.86	0.57	8.38	7.45	6.04	2.34	0.46
3	5.67	4.57	3.34	2.34	0.53	7.54	6.57	5.24	2.30	0.51
4	7.24	5.19	3.44	3.80	1.08	8.60	7.06	5.37	3.23	0.92
5	6.53	4.99	3.17	3.36	0.85	8.15	6.91	5.02	3.14	0.78
5.99	4.51	3.73	3.02	1.49	0.40	6.54	5.70	4.80	1.74	0.46
6	8.23	6.57	4.96	3.27	0.77	9.15	8.15	6.95	2.20	0.52
7	9.66	8.16	6.61	3.05	0.79	9.85	9.10	8.20	1.65	0.43
8	10.75	9.08	7.30	3.45	0.99	10.32	9.56	8.63	1.68	0.48
9	9.66	8.44	7.04	2.62	0.69	9.85	9.25	8.48	1.37	0.36
10	8.67	7.43	6.18	2.49	0.65	9.38	8.70	7.91	1.47	0.38
11	8.90	7.69	5.97	2.93	0.84	9.50	8.83	7.76	1.73	0.49
12	9.00	7.80	6.54	2.46	0.65	9.54	8.91	8.15	1.39	0.36
13	8.60	7.62	6.48	2.12	0.63	9.35	8.80	8.12	1.23	0.36
14	7.18	6.39	5.55	1.63	0.43	8.56	8.05	7.44	1.12	0.29
15	6.37	5.64	4.85	1.52	0.43	8.04	7.50	6.86	1.19	0.33
16	6.89	6.01	4.87	2.02	0.57	8.38	7.77	6.88	1.51	0.42
17	6.34	5.44	4.08	2.26	0.63	8.02	7.32	6.11	1.92	0.54
18	6.05	5.28	4.26	1.79	0.49	7.81	7.21	6.29	1.52	0.41

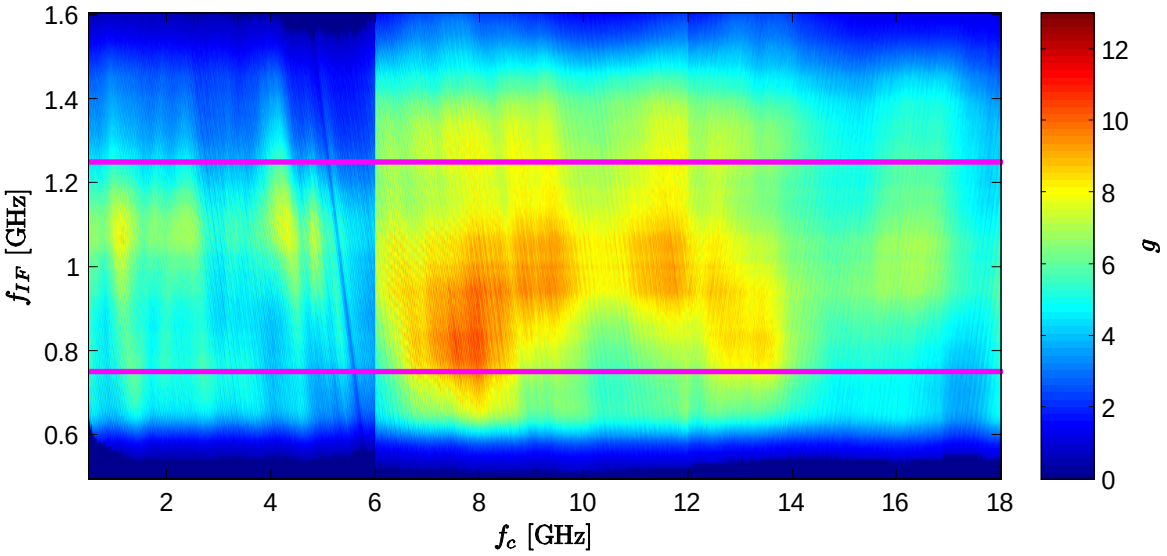

Figure 4.1 Tuner 1 voltage gain (linear scale). The purple lines highlight the edges of the passband ($0.75 \leq f_{IF} \leq 1.25$ GHz).

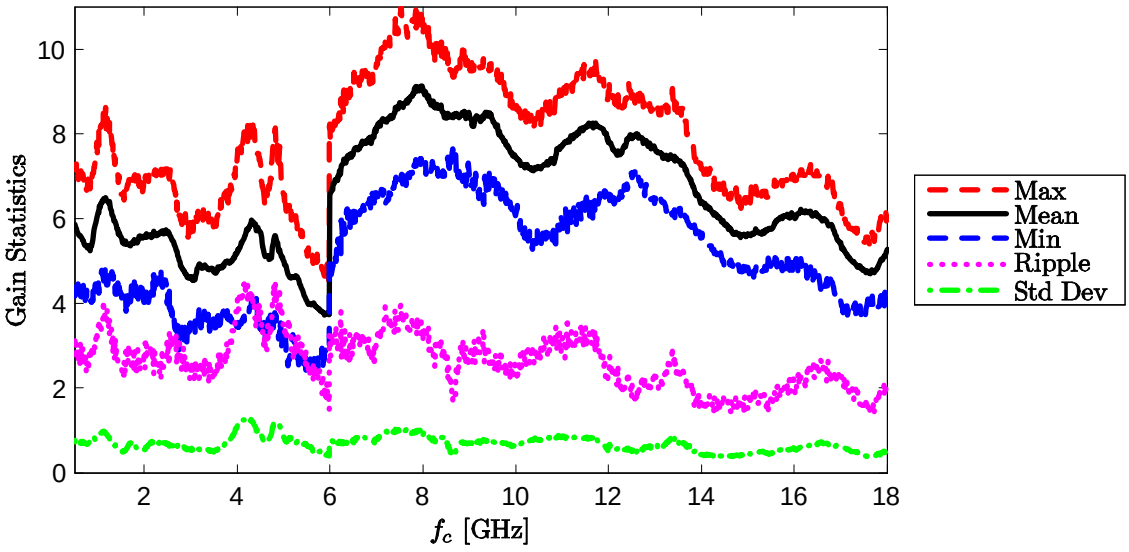

Figure 4.2 Tuner 1 voltage gain statistics, within the passband (linear scale). At each point, the statistics are computed with f_c held constant.

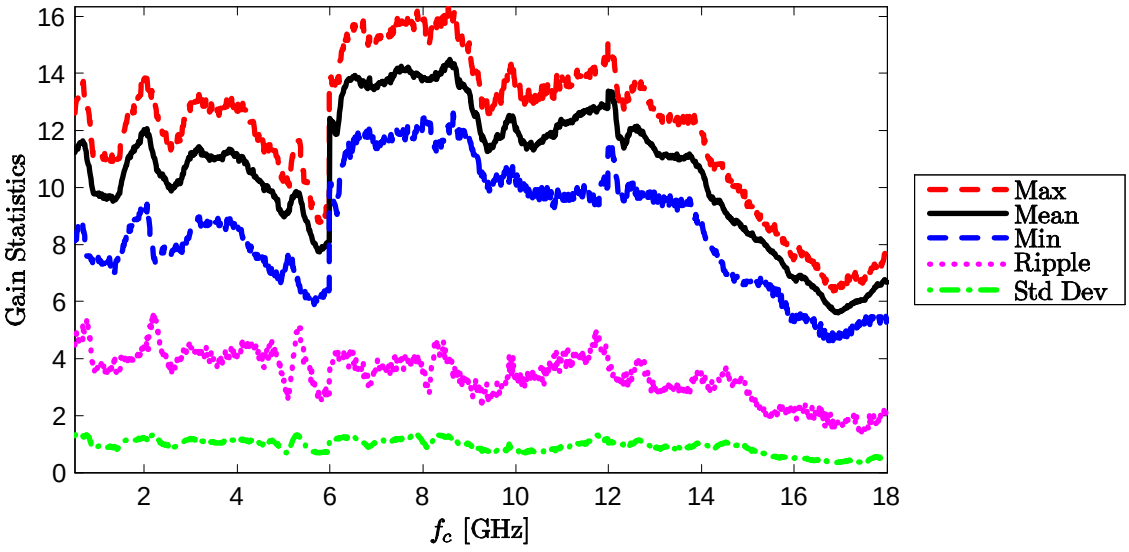

Figure 4.3 Tuner 2 gain statistics, within the passband (linear scale).

Table 4.2 Measured voltage gain, within the passband, for Tuner 2.

	Linear Scale					Decibels				
f_c [GHz]	Max	Mean	Min	Ripple	Std Dev	Max	Mean	Min	Ripple	Std Dev
0.5	12.62	11.23	8.13	4.48	1.29	11.01	10.47	9.10	1.91	0.53
1	11.12	9.78	7.39	3.73	0.93	10.46	9.88	8.69	1.77	0.43
2	13.80	12.03	9.36	4.44	1.23	11.40	10.78	9.71	1.69	0.46
3	12.98	11.22	8.58	4.40	1.20	11.13	10.47	9.33	1.80	0.48
4	12.68	11.18	8.68	4.00	1.14	11.03	10.46	9.39	1.64	0.46
5	10.12	8.97	6.92	3.20	0.82	10.05	9.51	8.40	1.65	0.41
5.99	9.16	8.11	6.40	2.76	0.73	9.62	9.07	8.06	1.56	0.41
6	13.70	12.43	10.12	3.58	1.09	11.37	10.93	10.05	1.31	0.40
7	15.22	13.58	11.57	3.65	1.12	11.82	11.31	10.63	1.19	0.37
8	15.89	13.81	12.21	3.67	1.06	12.01	11.39	10.87	1.14	0.33
9	15.08	13.32	11.81	3.27	0.99	11.78	11.23	10.72	1.06	0.32
10	13.59	12.09	10.07	3.52	0.81	11.33	10.82	10.03	1.30	0.29
11	14.00	12.32	9.92	4.08	0.91	11.46	10.89	9.97	1.50	0.33
12	15.06	13.37	11.38	3.68	1.03	11.78	11.25	10.56	1.22	0.34
13	12.55	11.28	9.49	3.06	0.87	10.99	10.51	9.77	1.21	0.34
14	12.10	10.61	8.58	3.51	1.03	10.83	10.23	9.34	1.49	0.44
15	9.49	8.38	6.69	2.79	0.86	9.77	9.21	8.26	1.52	0.47
16	7.60	6.83	5.41	2.19	0.51	8.81	8.33	7.33	1.48	0.34
17	6.49	5.65	4.78	1.72	0.38	8.13	7.51	6.79	1.33	0.29
18	7.40	6.67	5.36	2.04	0.56	8.69	8.23	7.29	1.40	0.38

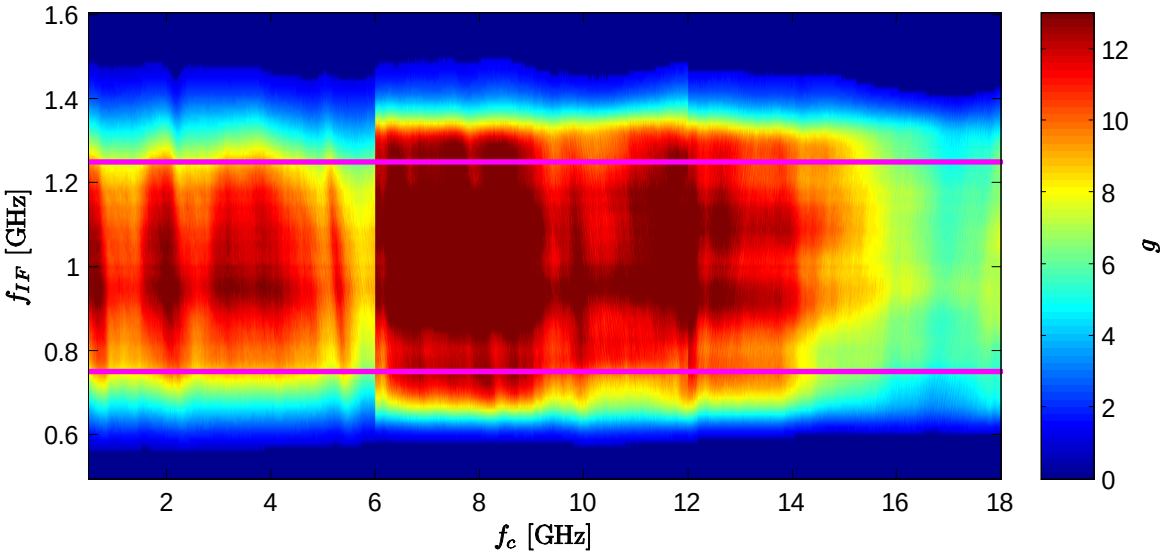

Figure 4.4 Tuner 2 gain (linear scale).

Table 4.3 Measured voltage gain, within the passband, for Tuner 3.

	Linear Scale					Decibels				
f_c [GHz]	Max	Mean	Min	Ripple	Std Dev	Max	Mean	Min	Ripple	Std Dev
0.5	9.06	6.62	3.77	5.28	1.18	9.57	8.14	5.77	3.80	0.82
1	10.71	7.53	4.22	6.49	1.33	10.30	8.70	6.25	4.05	0.79
2	7.86	6.00	3.86	4.00	0.92	8.95	7.73	5.86	3.09	0.70
3	7.44	5.60	3.69	3.76	0.89	8.72	7.43	5.67	3.05	0.70
4	9.92	6.92	4.04	5.89	1.38	9.97	8.32	6.06	3.91	0.86
5	9.41	7.37	3.92	5.50	1.31	9.74	8.60	5.93	3.81	0.87
5.99	5.76	4.15	2.69	3.08	0.67	7.61	6.12	4.29	3.31	0.71
6	11.39	8.98	6.86	4.53	1.01	10.56	9.50	8.36	2.20	0.49
7	10.51	9.04	7.73	2.77	0.80	10.21	9.55	8.88	1.33	0.39
8	10.40	9.23	7.80	2.60	0.76	10.17	9.64	8.92	1.25	0.37
9	11.45	10.09	8.50	2.94	0.96	10.59	10.02	9.30	1.29	0.42
10	9.88	8.84	7.78	2.10	0.60	9.95	9.45	8.91	1.04	0.30
11	8.17	7.59	6.87	1.30	0.34	9.12	8.80	8.37	0.76	0.19
12	10.10	8.53	7.09	3.02	0.85	10.04	9.29	8.50	1.54	0.43
13	10.66	9.04	7.55	3.11	0.87	10.28	9.54	8.78	1.50	0.42
14	9.91	8.51	6.33	3.58	1.02	9.96	9.27	8.02	1.95	0.55
15	8.02	7.15	6.21	1.81	0.47	9.04	8.53	7.93	1.11	0.29
16	7.03	6.31	5.45	1.57	0.40	8.47	7.99	7.37	1.10	0.28
17	6.66	6.14	5.46	1.20	0.29	8.23	7.88	7.37	0.86	0.21
18	6.92	6.27	5.45	1.47	0.31	8.40	7.97	7.36	1.04	0.22

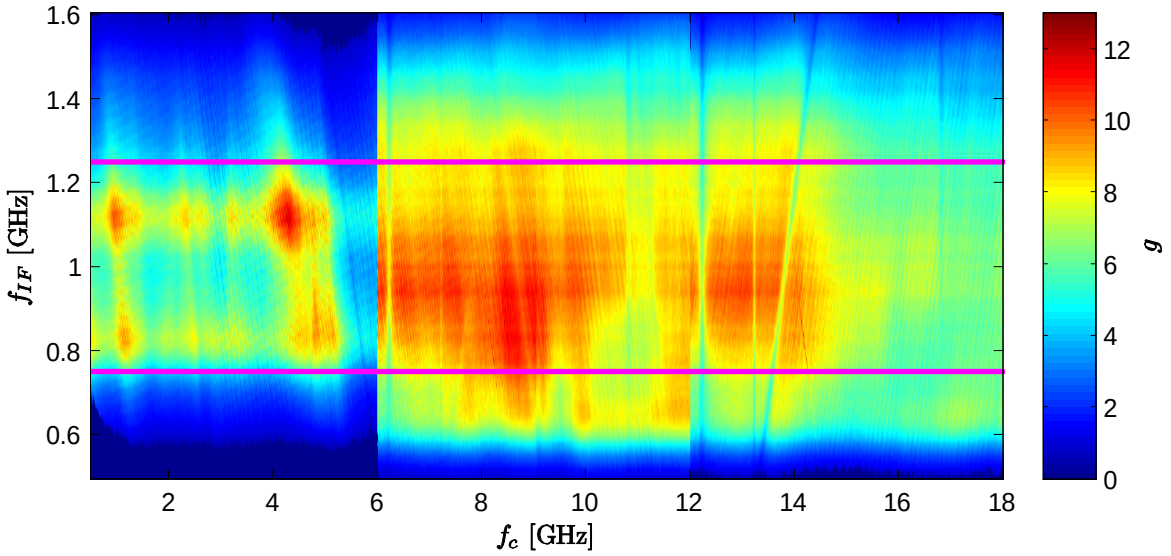

Figure 4.5 Tuner 3 gain (linear scale).

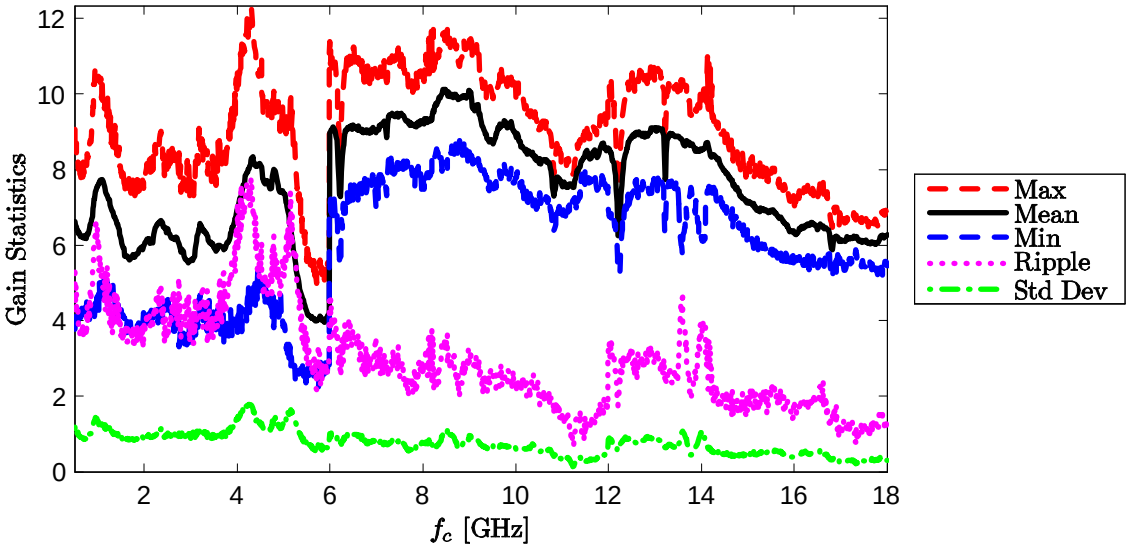

Figure 4.6 Tuner 3 gain statistics, within the passband (linear scale).

Table 4.4 Measured voltage gain, within the passband, for Tuner 4 at 22°C.

	Linear Scale					Decibels				
f_c [GHz]	Max	Mean	Min	Ripple	Std Dev	Max	Mean	Min	Ripple	Std Dev
0.5	11.57	8.09	5.44	6.12	1.19	10.63	9.04	7.36	3.27	0.62
1	12.45	8.95	6.25	6.20	1.57	10.95	9.46	7.96	2.99	0.73
2	9.35	7.06	4.59	4.75	1.01	9.71	8.44	6.62	3.08	0.63
3	8.87	6.34	4.46	4.41	1.01	9.48	7.97	6.50	2.98	0.70
4	12.17	7.48	4.97	7.21	1.90	10.85	8.61	6.96	3.89	1.05
5	9.23	6.58	4.40	4.83	1.10	9.65	8.13	6.44	3.22	0.72
5.99	7.41	4.88	3.55	3.86	0.87	8.70	6.82	5.50	3.20	0.75
6	7.24	5.67	3.31	3.93	1.12	8.60	7.44	5.20	3.40	0.95
7	7.99	6.86	5.29	2.70	0.70	9.03	8.34	7.23	1.79	0.46
8	8.59	7.59	6.62	1.97	0.51	9.34	8.79	8.21	1.13	0.30
9	8.29	7.17	5.81	2.48	0.65	9.18	8.53	7.64	1.54	0.40
10	7.17	6.12	4.73	2.44	0.64	8.56	7.85	6.75	1.81	0.47
11	7.09	5.84	3.99	3.10	1.01	8.51	7.59	6.01	2.50	0.82
12	7.99	6.74	4.64	3.35	0.95	9.03	8.24	6.67	2.36	0.65
13	8.37	7.26	5.75	2.63	0.66	9.23	8.59	7.59	1.63	0.41
14	7.44	6.72	6.05	1.39	0.37	8.72	8.27	7.82	0.90	0.24
15	5.67	5.04	4.03	1.64	0.44	7.54	7.01	6.05	1.48	0.39
16	5.37	4.40	3.19	2.17	0.55	7.30	6.40	5.04	2.26	0.57
17	5.66	4.71	3.18	2.48	0.75	7.53	6.67	5.02	2.51	0.75
18	5.19	4.33	3.24	1.95	0.50	7.15	6.33	5.10	2.05	0.52

Table 4.5 Measured voltage gain, within the passband, for Tuner 4 at -3°C.

	Linear Scale					Decibels				
f_c [GHz]	Max	Mean	Min	Ripple	Std Dev	Max	Mean	Min	Ripple	Std Dev
0.5	12.02	8.48	5.54	6.47	1.28	10.80	9.24	7.44	3.36	0.65
1	13.19	9.43	6.83	6.36	1.74	11.20	9.68	8.34	2.86	0.77
2	9.89	7.40	4.59	5.30	1.11	9.95	8.64	6.62	3.34	0.67
3	9.58	6.72	4.47	5.12	1.10	9.81	8.21	6.50	3.31	0.72
4	12.63	7.64	4.88	7.76	2.01	11.01	8.69	6.88	4.13	1.08
5	9.78	6.78	4.41	5.38	1.22	9.90	8.25	6.44	3.46	0.77
5.99	7.83	5.26	3.91	3.92	0.94	8.94	7.15	5.92	3.02	0.75
6	7.51	5.85	3.44	4.07	1.11	8.76	7.58	5.37	3.39	0.91
7	8.12	6.85	5.29	2.82	0.70	9.09	8.33	7.24	1.86	0.46
8	8.75	7.61	6.36	2.40	0.58	9.42	8.80	8.03	1.39	0.34
9	8.43	7.11	5.93	2.50	0.69	9.26	8.50	7.73	1.53	0.42
10	7.59	6.33	4.73	2.86	0.72	8.80	7.98	6.75	2.05	0.51
11	6.95	5.79	3.92	3.04	0.92	8.42	7.56	5.93	2.49	0.75
12	8.17	6.88	4.75	3.43	0.96	9.12	8.33	6.77	2.36	0.64
13	8.38	7.25	5.64	2.75	0.72	9.23	8.58	7.51	1.72	0.44
14	7.74	6.76	5.98	1.75	0.43	8.89	8.29	7.77	1.12	0.27
15	6.13	5.14	4.25	1.87	0.49	7.87	7.09	6.29	1.58	0.42
16	5.48	4.45	3.19	2.28	0.53	7.39	6.46	5.04	2.34	0.55
17	5.99	4.90	3.24	2.75	0.79	7.77	6.84	5.10	2.67	0.76
18	5.29	4.46	3.36	1.93	0.53	7.23	6.46	5.26	1.97	0.53

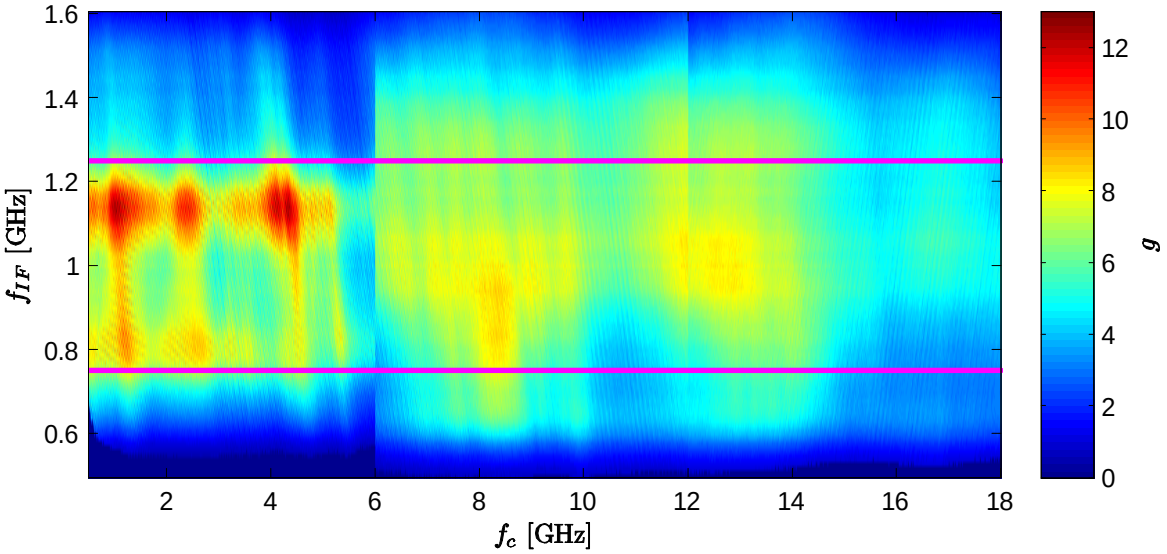

Figure 4.7 Tuner 4 gain at 22°C (linear scale).

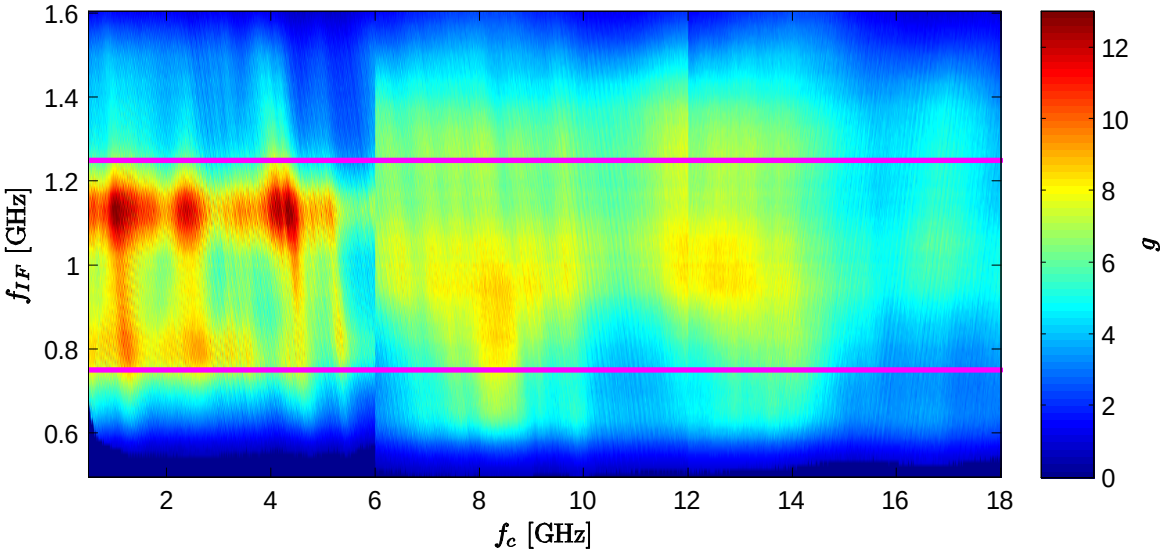

Figure 4.8 Tuner 4 gain at -3°C (linear scale).

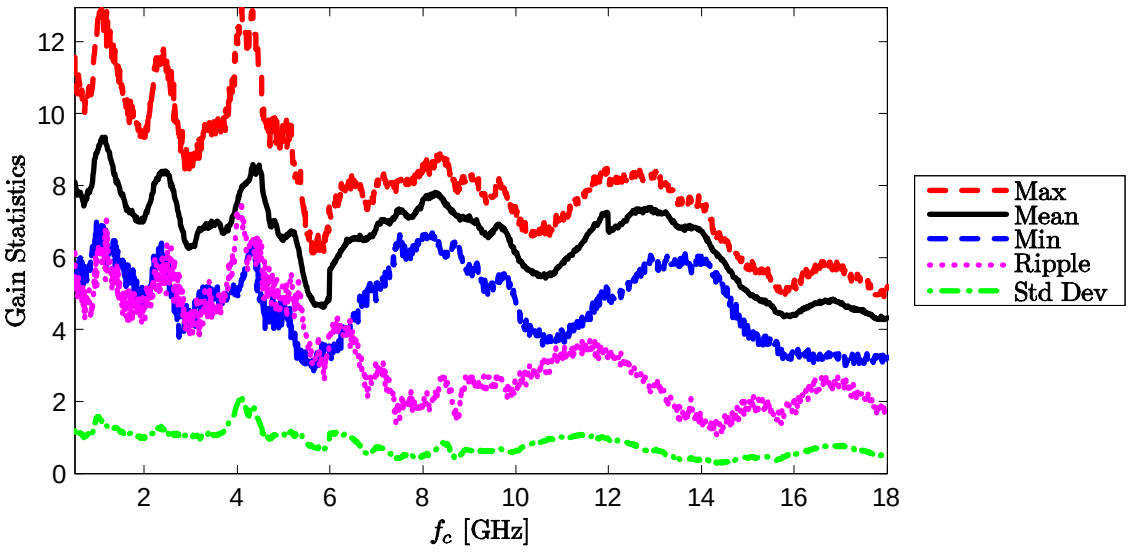

Figure 4.9 Tuner 4 gain statistics at 22°C, within the passband (linear scale).

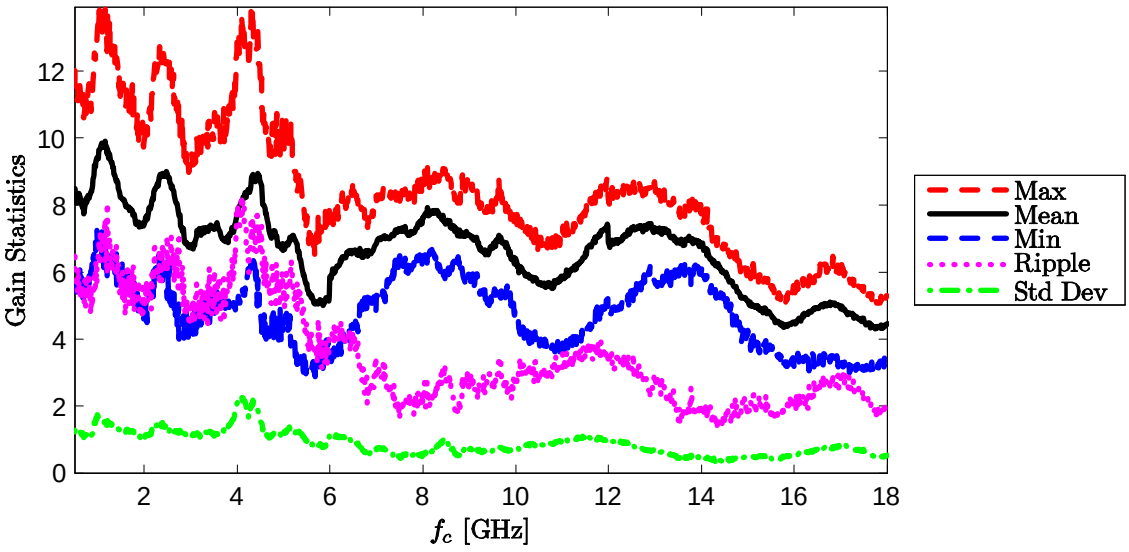

Figure 4.10 Tuner 4 gain statistics at -3°C, within the passband (linear scale).

Table 4.6 Measured voltage gain, within the passband, for Tuner 5.

	Linear Scale					Decibels				
f_c [GHz]	Max	Mean	Min	Ripple	Std Dev	Max	Mean	Min	Ripple	Std Dev
0.5	9.01	6.82	5.04	3.97	0.80	9.55	8.31	7.03	2.52	0.50
1	11.60	8.32	5.57	6.03	1.54	10.64	9.13	7.46	3.19	0.80
2	9.15	7.29	5.15	4.01	0.76	9.62	8.60	7.12	2.50	0.46
3	8.20	6.24	4.46	3.74	0.80	9.14	7.91	6.50	2.64	0.57
4	11.71	7.31	4.49	7.23	2.10	10.69	8.46	6.52	4.17	1.23
5	7.71	5.34	2.77	4.94	1.28	8.87	7.15	4.43	4.44	1.09
5.99	7.27	5.11	4.05	3.23	0.79	8.62	7.03	6.07	2.55	0.65
6	11.63	9.20	7.00	4.62	1.20	10.65	9.60	8.45	2.20	0.57
7	11.03	9.16	7.73	3.30	0.91	10.42	9.60	8.88	1.54	0.43
8	11.26	9.55	8.19	3.06	0.87	10.51	9.78	9.13	1.38	0.40
9	11.70	10.05	8.70	3.01	0.89	10.68	10.00	9.39	1.29	0.38
10	11.08	9.96	8.74	2.34	0.67	10.45	9.97	9.42	1.03	0.30
11	6.60	5.45	4.77	1.84	0.42	8.20	7.35	6.78	1.42	0.33
12	10.91	9.02	7.19	3.72	1.12	10.38	9.52	8.57	1.81	0.54
13	11.41	9.77	8.13	3.29	0.96	10.57	9.88	9.10	1.47	0.43
14	10.51	8.97	7.33	3.18	0.78	10.22	9.51	8.65	1.56	0.38
15	9.52	8.17	6.85	2.67	0.76	9.79	9.10	8.36	1.43	0.41
16	8.84	7.93	7.28	1.56	0.43	9.46	8.98	8.62	0.84	0.23
17	4.94	4.25	3.78	1.16	0.27	6.94	6.27	5.78	1.16	0.27
18	8.40	7.58	6.75	1.65	0.41	9.24	8.79	8.29	0.95	0.24

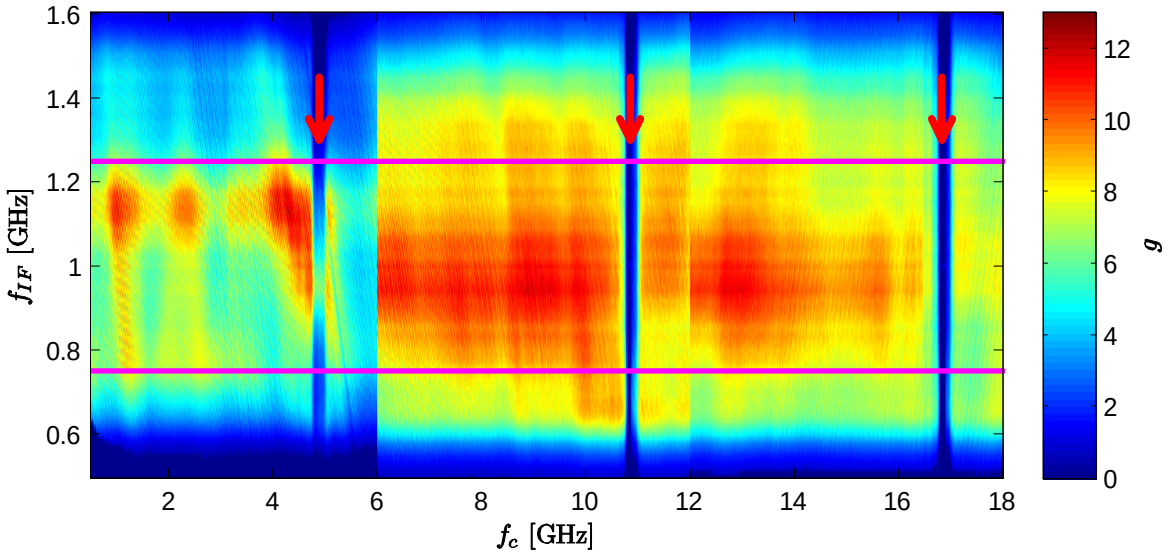

Figure 4.11 Tuner 5 gain (linear scale). The following defective areas are highlighted: $4.75 \leq f_c \leq 5.02$ GHz, $10.62 \leq f_c \leq 11.09$ GHz, and $16.59 \leq f_c \leq 17.09$ GHz.

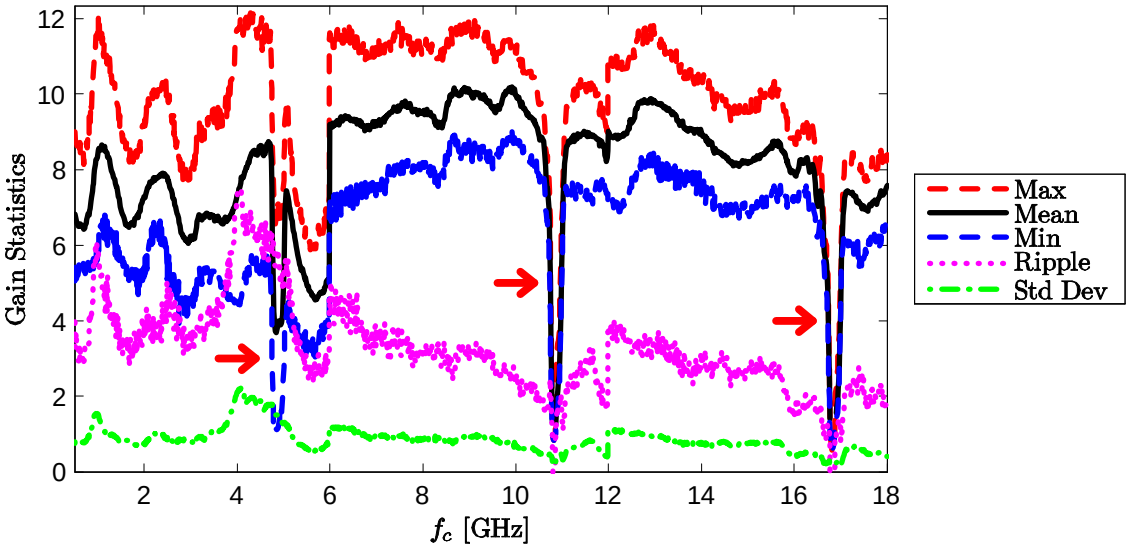

Figure 4.12 Tuner 5 gain statistics, within the passband (linear scale).

Table 4.7 Measured voltage gain, within the passband, for Tuner 6 at 22°C.

	Linear Scale					Decibels				
f_c [GHz]	Max	Mean	Min	Ripple	Std Dev	Max	Mean	Min	Ripple	Std Dev
0.5	7.89	5.30	2.81	5.09	1.08	8.97	7.15	4.48	4.49	0.93
1	10.05	7.63	4.27	5.78	1.42	10.02	8.74	6.30	3.72	0.85
2	8.37	6.38	4.52	3.85	0.88	9.23	8.01	6.55	2.68	0.60
3	8.28	6.26	4.41	3.87	0.86	9.18	7.92	6.45	2.73	0.60
4	9.46	6.72	4.74	4.73	1.15	9.76	8.21	6.75	3.01	0.74
5	8.07	6.57	4.74	3.33	0.76	9.07	8.15	6.76	2.31	0.52
5.99	5.78	4.47	3.42	2.36	0.58	7.62	6.47	5.33	2.28	0.56
6	8.91	6.84	4.69	4.22	0.96	9.50	8.31	6.71	2.79	0.62
7	10.41	8.56	6.78	3.63	1.02	10.17	9.30	8.31	1.86	0.52
8	9.84	8.43	7.03	2.81	0.79	9.93	9.24	8.47	1.46	0.41
9	10.02	8.47	6.62	3.39	1.08	10.01	9.24	8.21	1.80	0.57
10	8.48	6.93	5.73	2.75	0.72	9.28	8.38	7.58	1.70	0.45
11	7.92	6.70	5.15	2.77	0.80	8.99	8.23	7.12	1.87	0.53
12	9.36	7.58	6.20	3.17	0.89	9.71	8.77	7.92	1.79	0.51
13	8.88	7.33	5.97	2.91	0.83	9.48	8.63	7.76	1.73	0.49
14	8.83	7.35	6.34	2.49	0.64	9.46	8.65	8.02	1.44	0.37
15	7.01	6.12	5.05	1.96	0.50	8.46	7.86	7.03	1.43	0.36
16	6.25	5.08	4.09	2.16	0.50	7.96	7.03	6.12	1.84	0.43
17	6.11	5.19	4.01	2.10	0.58	7.86	7.13	6.03	1.83	0.49
18	6.18	5.14	4.18	2.00	0.51	7.91	7.09	6.21	1.70	0.43

Table 4.8 Measured voltage gain, within the passband, for Tuner 6 at 50°C.

	Linear Scale					Decibels				
f_c [GHz]	Max	Mean	Min	Ripple	Std Dev	Max	Mean	Min	Ripple	Std Dev
0.5	6.84	4.59	2.36	4.48	0.96	8.35	6.51	3.73	4.62	0.96
1	8.97	6.71	3.65	5.31	1.23	9.53	8.19	5.63	3.90	0.85
2	7.18	5.47	4.11	3.07	0.74	8.56	7.34	6.14	2.43	0.58
3	7.38	5.56	4.01	3.37	0.74	8.68	7.41	6.03	2.65	0.58
4	7.96	5.61	3.91	4.05	0.98	9.01	7.43	5.92	3.09	0.74
5	6.81	5.51	4.14	2.67	0.64	8.33	7.38	6.18	2.16	0.52
5.99	5.14	3.98	2.95	2.19	0.52	7.11	5.96	4.70	2.41	0.57
6	8.41	6.37	4.34	4.07	0.89	9.25	8.00	6.38	2.87	0.62
7	9.14	7.86	6.28	2.86	0.84	9.61	8.93	7.98	1.63	0.47
8	9.11	7.84	6.63	2.48	0.67	9.60	8.93	8.22	1.38	0.37
9	9.43	7.79	6.03	3.40	0.99	9.75	8.88	7.81	1.94	0.57
10	7.71	6.44	5.52	2.19	0.62	8.87	8.07	7.42	1.45	0.41
11	7.19	6.09	4.68	2.52	0.72	8.57	7.82	6.70	1.87	0.53
12	8.37	6.89	5.53	2.84	0.77	9.22	8.36	7.43	1.80	0.48
13	8.22	6.72	5.52	2.69	0.77	9.15	8.25	7.42	1.72	0.49
14	8.03	6.72	5.76	2.27	0.57	9.05	8.26	7.60	1.44	0.36
15	6.38	5.52	4.59	1.78	0.45	8.05	7.41	6.62	1.43	0.35
16	5.80	4.56	3.59	2.21	0.47	7.64	6.56	5.56	2.08	0.44
17	5.99	4.87	3.65	2.34	0.57	7.77	6.84	5.62	2.15	0.52
18	5.20	4.48	3.86	1.33	0.38	7.16	6.50	5.87	1.29	0.37

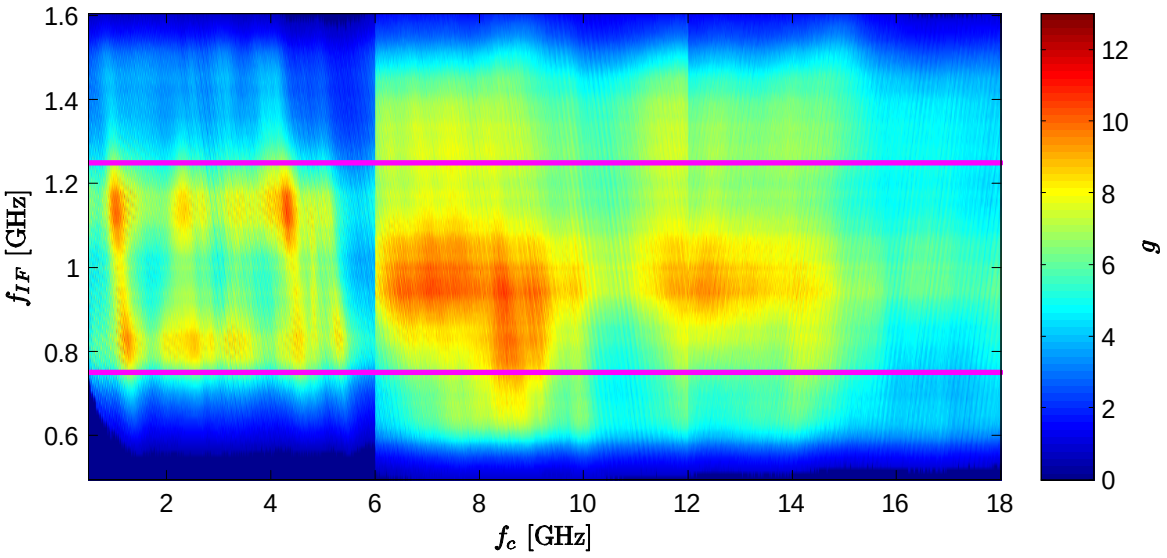

Figure 4.13 Tuner 6 gain at 22°C (linear scale).

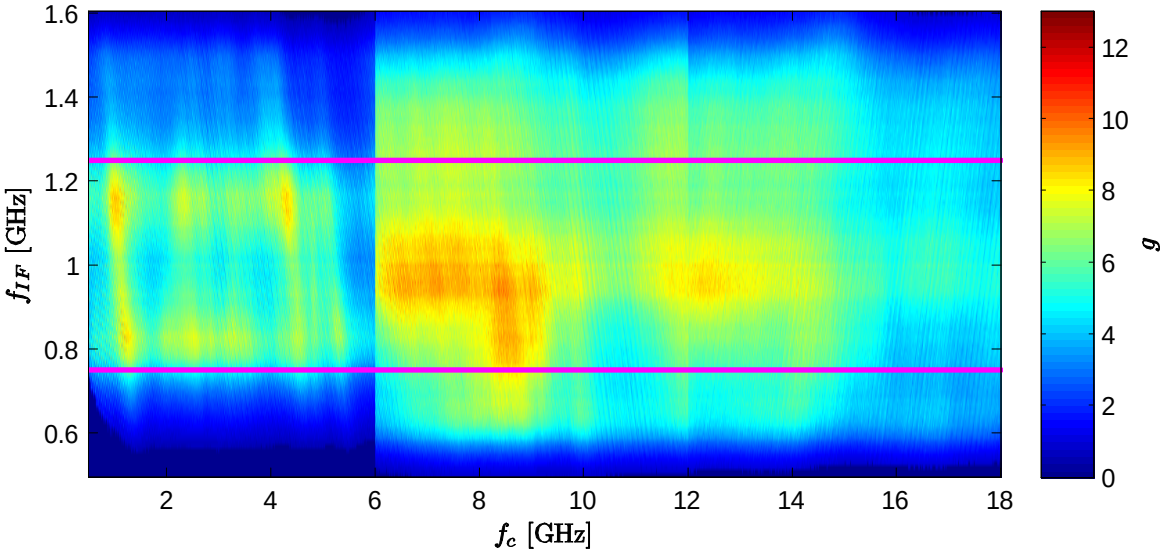

Figure 4.14 Tuner 6 gain at 50°C (linear scale).

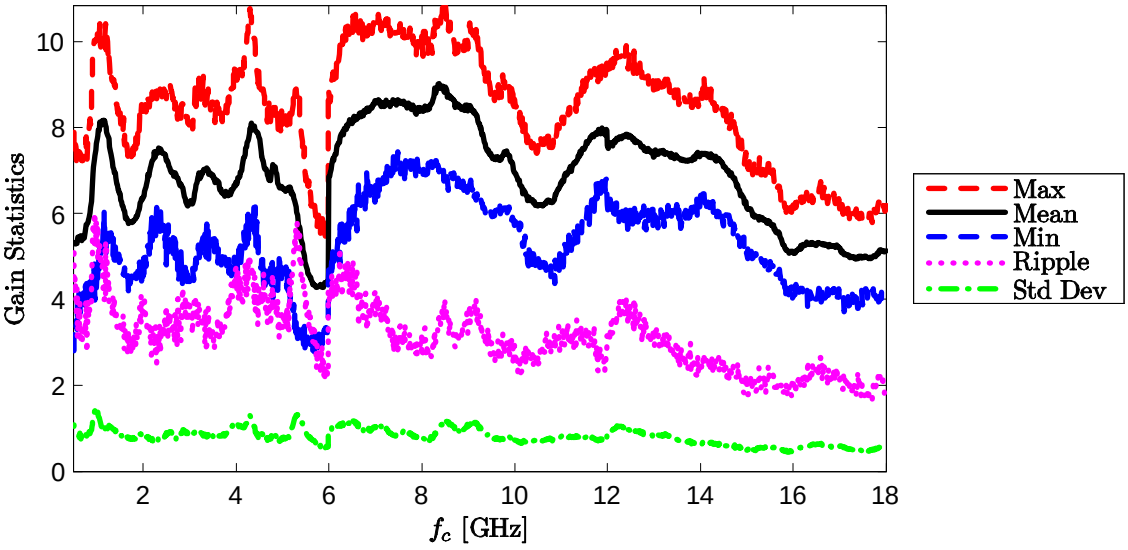

Figure 4.15 Tuner 6 gain statistics at 22°C, within the passband (linear scale).

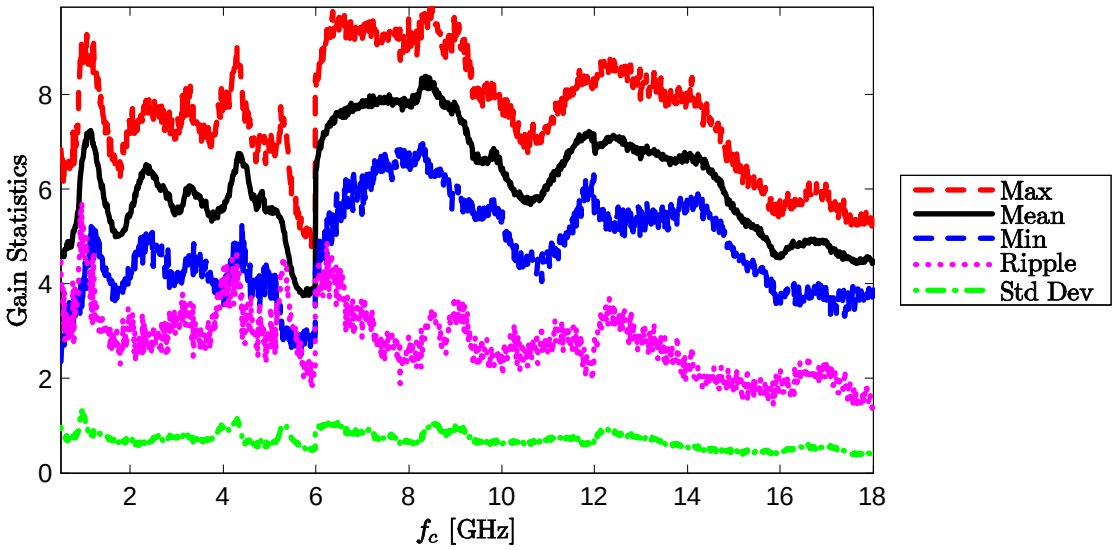

Figure 4.16 Tuner 6 gain statistics at 50°C, within the passband (linear scale).

Table 4.9 Measured voltage gain, within the passband, for Tuner 7.

	Linear Scale					Decibels				
f_c [GHz]	Max	Mean	Min	Ripple	Std Dev	Max	Mean	Min	Ripple	Std Dev
0.5	10.05	8.02	5.13	4.93	1.10	10.02	9.00	7.10	2.93	0.64
1	10.71	8.08	5.27	5.43	1.20	10.30	9.03	7.22	3.08	0.66
2	7.86	6.43	4.17	3.68	0.87	8.95	8.04	6.21	2.75	0.63
3	7.09	5.29	3.69	3.40	0.77	8.51	7.19	5.67	2.84	0.63
4	8.62	6.43	4.15	4.47	1.08	9.35	8.02	6.18	3.17	0.74
5	8.53	6.15	4.07	4.46	0.96	9.31	7.84	6.10	3.21	0.70
5.99	5.25	4.24	3.02	2.23	0.55	7.20	6.24	4.79	2.40	0.57
6	12.33	10.11	7.29	5.04	1.18	10.91	10.02	8.63	2.28	0.53
7	14.16	12.45	10.93	3.22	0.95	11.51	10.94	10.39	1.12	0.33
8	14.99	12.93	11.13	3.85	1.05	11.76	11.10	10.47	1.29	0.35
9	13.86	11.87	10.10	3.76	1.07	11.42	10.73	10.04	1.37	0.39
10	12.22	10.71	9.42	2.80	0.78	10.87	10.29	9.74	1.13	0.31
11	12.36	10.97	9.15	3.21	0.88	10.92	10.39	9.62	1.31	0.35
12	13.22	11.57	9.83	3.39	0.98	11.21	10.62	9.93	1.29	0.37
13	13.03	11.57	10.06	2.97	0.86	11.15	10.62	10.02	1.12	0.33
14	12.01	10.29	8.71	3.30	0.74	10.80	10.11	9.40	1.40	0.31
15	8.17	7.04	5.78	2.39	0.61	9.12	8.46	7.62	1.50	0.38
16	7.29	6.20	5.16	2.13	0.52	8.63	7.91	7.13	1.50	0.36
17	7.99	7.01	6.10	1.88	0.51	9.02	8.45	7.86	1.17	0.32
18	7.61	6.65	5.79	1.82	0.40	8.81	8.22	7.63	1.19	0.26

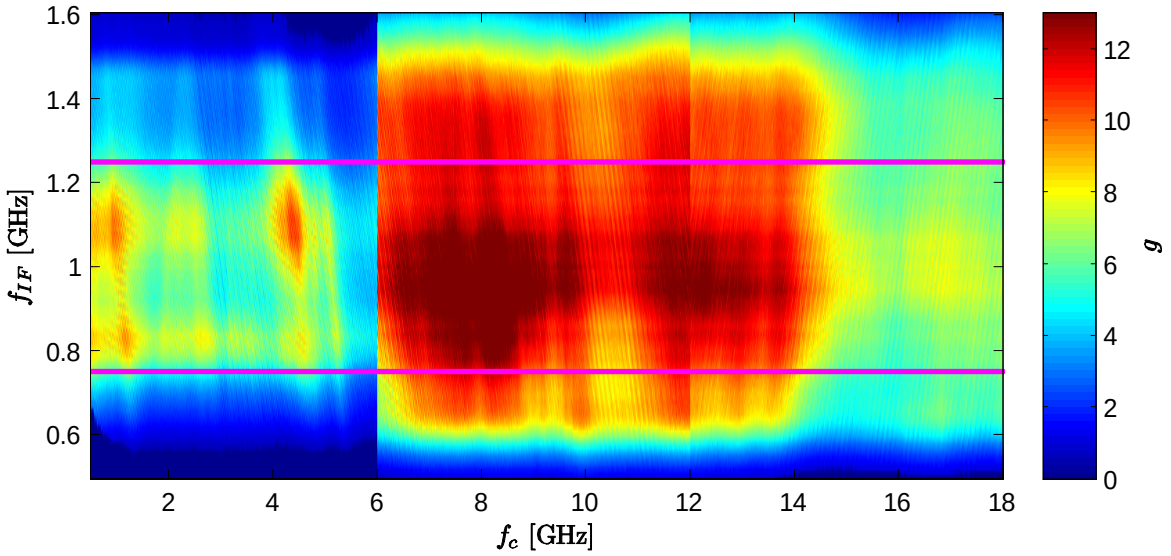

Figure 4.17 Tuner 7 gain (linear scale).

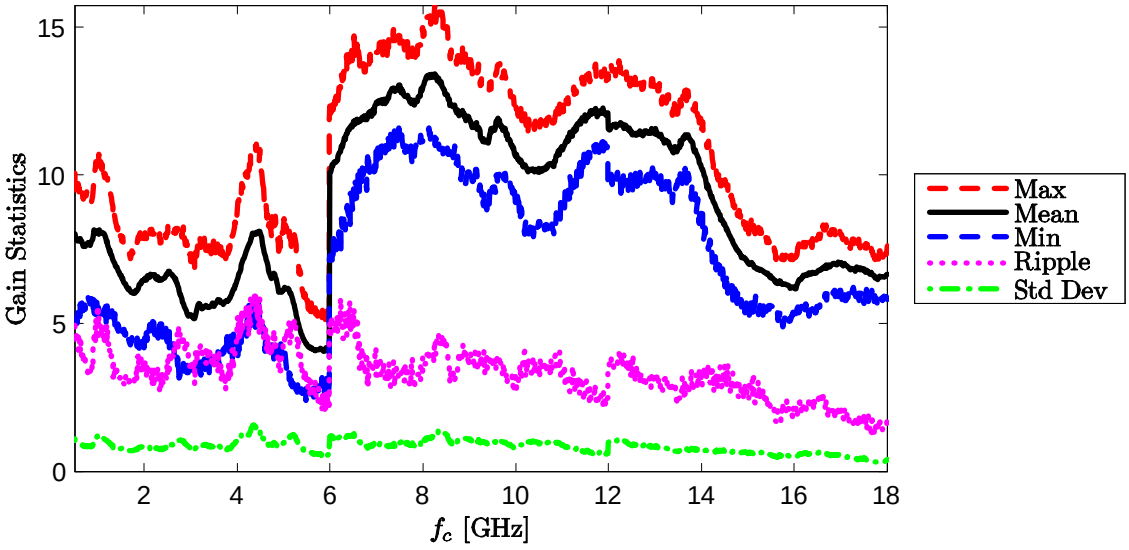

Figure 4.18 Tuner 7 gain statistics, within the passband (linear scale).

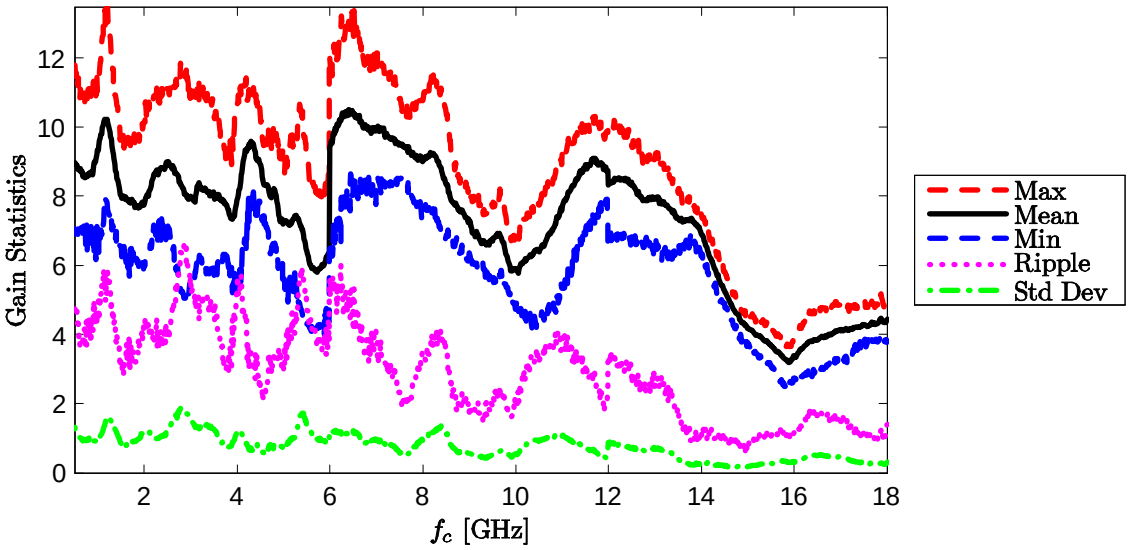

Figure 4.19 Tuner 8 gain statistics, within the passband (linear scale).

Table 4.10 Measured voltage gain, within the passband, for Tuner 8.

	Linear Scale					Decibels				
f_c [GHz]	Max	Mean	Min	Ripple	Std Dev	Max	Mean	Min	Ripple	Std Dev
0.5	11.78	8.97	7.04	4.74	1.32	10.71	9.48	8.48	2.23	0.63
1	11.01	9.33	6.36	4.65	0.97	10.42	9.68	8.04	2.38	0.47
2	10.14	7.73	6.01	4.13	1.18	10.06	8.83	7.79	2.27	0.65
3	11.24	7.98	5.58	5.67	1.51	10.51	8.95	7.46	3.05	0.81
4	10.48	7.88	5.31	5.16	1.15	10.20	8.92	7.25	2.95	0.63
5	8.78	7.25	5.83	2.95	0.69	9.43	8.58	7.66	1.78	0.42
5.99	8.39	6.35	4.60	3.79	0.89	9.24	7.98	6.62	2.61	0.61
6	12.09	9.44	6.49	5.60	1.23	10.82	9.71	8.12	2.70	0.59
7	12.13	9.91	8.20	3.93	0.93	10.84	9.94	9.14	1.70	0.40
8	10.76	9.01	7.42	3.34	0.93	10.32	9.52	8.70	1.61	0.45
9	8.11	7.27	6.36	1.75	0.55	9.09	8.60	8.04	1.05	0.33
10	6.86	5.90	4.90	1.96	0.55	8.36	7.69	6.91	1.46	0.40
11	8.91	7.56	5.34	3.57	1.05	9.50	8.74	7.28	2.22	0.65
12	9.92	8.32	6.70	3.22	0.89	9.96	9.18	8.26	1.70	0.46
13	9.23	7.92	6.58	2.65	0.69	9.65	8.97	8.18	1.47	0.38
14	7.52	6.91	6.27	1.25	0.31	8.76	8.39	7.97	0.79	0.20
15	4.59	4.17	3.72	0.88	0.19	6.62	6.20	5.70	0.92	0.20
16	3.87	3.33	2.69	1.19	0.32	5.88	5.21	4.29	1.59	0.43
17	4.86	4.11	3.24	1.61	0.46	6.86	6.12	5.11	1.76	0.49
18	5.19	4.45	3.79	1.40	0.31	7.15	6.47	5.78	1.37	0.31

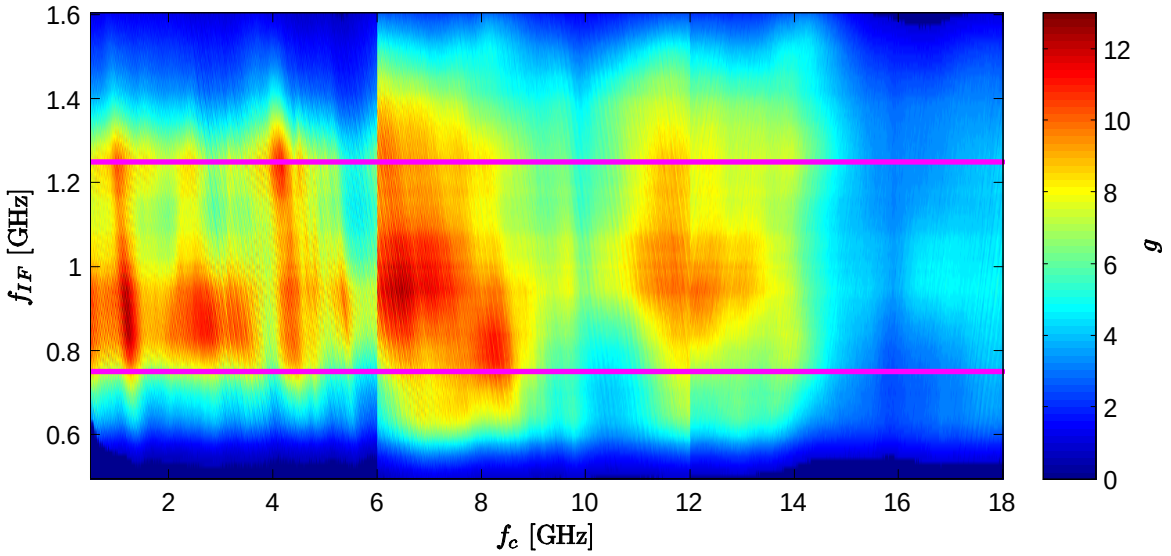

Figure 4.20 Tuner 8 gain (linear scale).

Table 4.11 Measured voltage gain, within the passband, for Tuner 9.

	Linear Scale					Decibels				
f_c [GHz]	Max	Mean	Min	Ripple	Std Dev	Max	Mean	Min	Ripple	Std Dev
0.5	7.85	5.24	3.02	4.82	0.97	8.95	7.11	4.80	4.14	0.85
1	6.39	5.04	3.05	3.34	0.83	8.05	6.96	4.84	3.21	0.76
2	7.43	6.02	3.94	3.49	0.88	8.71	7.75	5.95	2.76	0.67
3	6.11	4.85	3.09	3.02	0.73	7.86	6.81	4.91	2.96	0.68
4	5.81	4.69	3.26	2.55	0.62	7.64	6.67	5.13	2.51	0.60
5	5.04	3.94	2.48	2.56	0.67	7.02	5.89	3.94	3.08	0.78
5.99	4.63	3.35	1.96	2.67	0.60	6.66	5.17	2.92	3.74	0.81
6	6.80	5.82	4.87	1.93	0.44	8.32	7.64	6.87	1.45	0.33
7	7.51	6.47	5.48	2.03	0.42	8.76	8.10	7.39	1.37	0.28
8	7.65	6.88	6.14	1.51	0.43	8.84	8.37	7.88	0.96	0.27
9	7.95	7.22	6.53	1.43	0.40	9.01	8.58	8.15	0.86	0.24
10	7.85	7.11	6.07	1.78	0.50	8.95	8.51	7.83	1.12	0.31
11	7.60	6.62	6.00	1.60	0.37	8.81	8.20	7.78	1.03	0.24
12	6.26	5.62	4.99	1.27	0.31	7.97	7.49	6.98	0.98	0.24
13	6.81	6.08	5.13	1.68	0.37	8.33	7.83	7.10	1.23	0.27
14	7.02	6.30	5.53	1.48	0.37	8.46	7.99	7.43	1.03	0.25
15	5.89	5.27	4.42	1.47	0.38	7.70	7.20	6.45	1.25	0.32
16	4.52	4.07	3.39	1.13	0.27	6.55	6.09	5.31	1.24	0.29
17	4.24	3.69	3.19	1.05	0.22	6.27	5.66	5.03	1.24	0.26
18	4.47	3.85	2.80	1.68	0.41	6.51	5.83	4.46	2.04	0.48

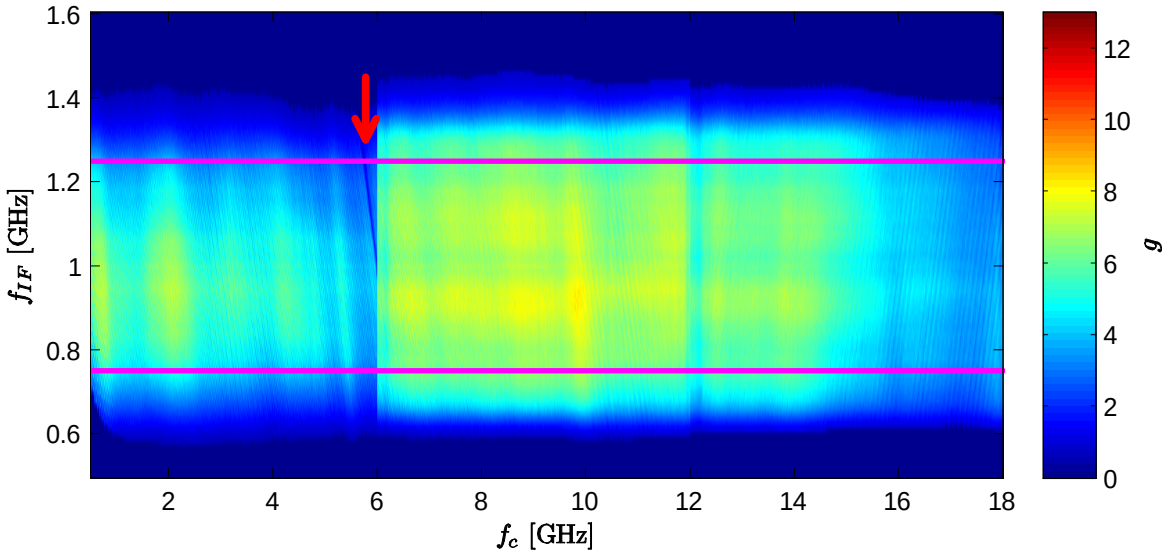

Figure 4.21 Tuner 9 gain (linear scale). The following defective area is highlighted: $5.99 \leq f_{in} \leq 6.01$ GHz, in the low band.

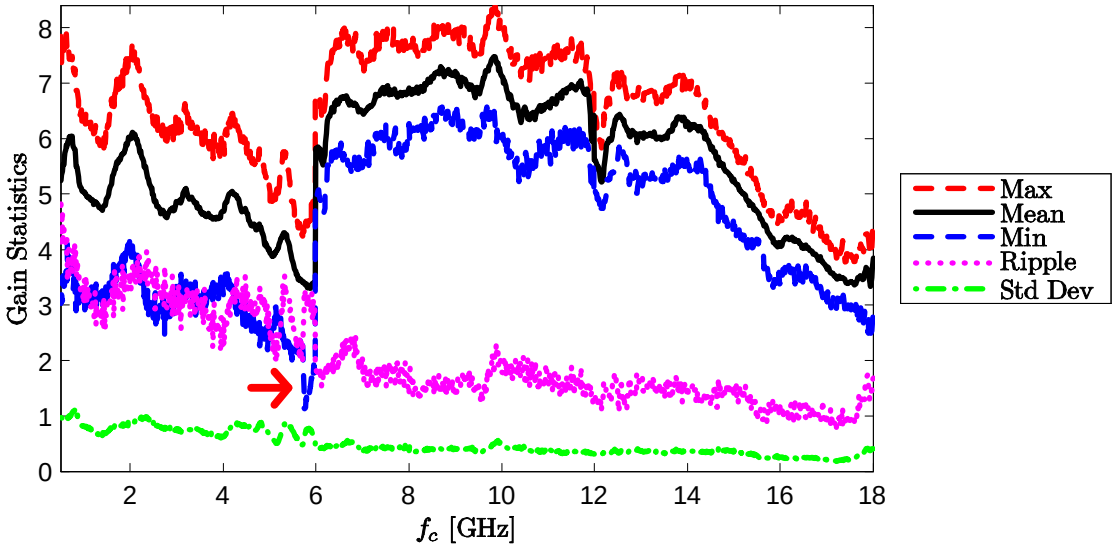

Figure 4.22 Tuner 9 gain statistics, within the passband (linear scale).

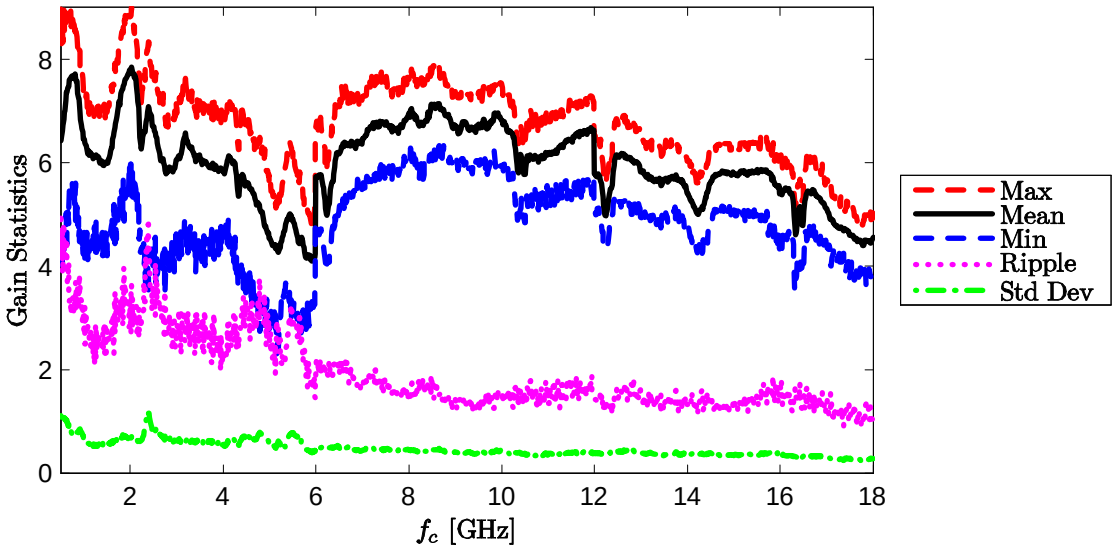

Figure 4.23 Tuner 10 gain statistics, within the passband (linear scale).

Table 4.12 Measured voltage gain, within the passband, for Tuner 10.

	Linear Scale					Decibels				
f_c [GHz]	Max	Mean	Min	Ripple	Std Dev	Max	Mean	Min	Ripple	Std Dev
0.5	8.97	6.42	4.04	4.92	1.11	9.53	8.01	6.07	3.46	0.78
1	7.44	6.45	4.23	3.21	0.72	8.71	8.07	6.26	2.45	0.53
2	8.81	7.76	5.47	3.34	0.69	9.45	8.88	7.38	2.07	0.41
3	6.95	6.06	4.22	2.73	0.62	8.42	7.80	6.26	2.16	0.46
4	6.76	5.84	4.41	2.35	0.55	8.30	7.64	6.44	1.85	0.42
5	5.52	4.53	3.00	2.53	0.58	7.42	6.52	4.77	2.66	0.58
5.99	5.04	4.23	3.59	1.45	0.42	7.03	6.25	5.55	1.48	0.43
6	6.67	5.72	4.77	1.89	0.50	8.24	7.56	6.79	1.45	0.39
7	7.27	6.46	5.58	1.69	0.44	8.62	8.09	7.47	1.15	0.30
8	7.63	6.94	6.16	1.47	0.45	8.83	8.40	7.90	0.93	0.28
9	7.37	6.69	5.92	1.45	0.40	8.67	8.25	7.73	0.95	0.26
10	7.45	6.80	5.95	1.50	0.42	8.72	8.31	7.74	0.98	0.27
11	6.90	6.15	5.46	1.44	0.34	8.39	7.88	7.37	1.02	0.24
12	6.52	5.79	5.08	1.44	0.38	8.14	7.61	7.06	1.08	0.29
13	6.49	5.82	4.93	1.55	0.41	8.12	7.64	6.93	1.19	0.31
14	6.03	5.40	4.71	1.32	0.37	7.80	7.31	6.73	1.07	0.30
15	6.36	5.78	5.08	1.28	0.34	8.04	7.61	7.06	0.98	0.26
16	6.14	5.44	4.50	1.64	0.37	7.88	7.35	6.53	1.35	0.31
17	5.66	5.11	4.33	1.33	0.31	7.53	7.07	6.36	1.17	0.27
18	5.10	4.55	3.87	1.23	0.28	7.07	6.57	5.87	1.20	0.27

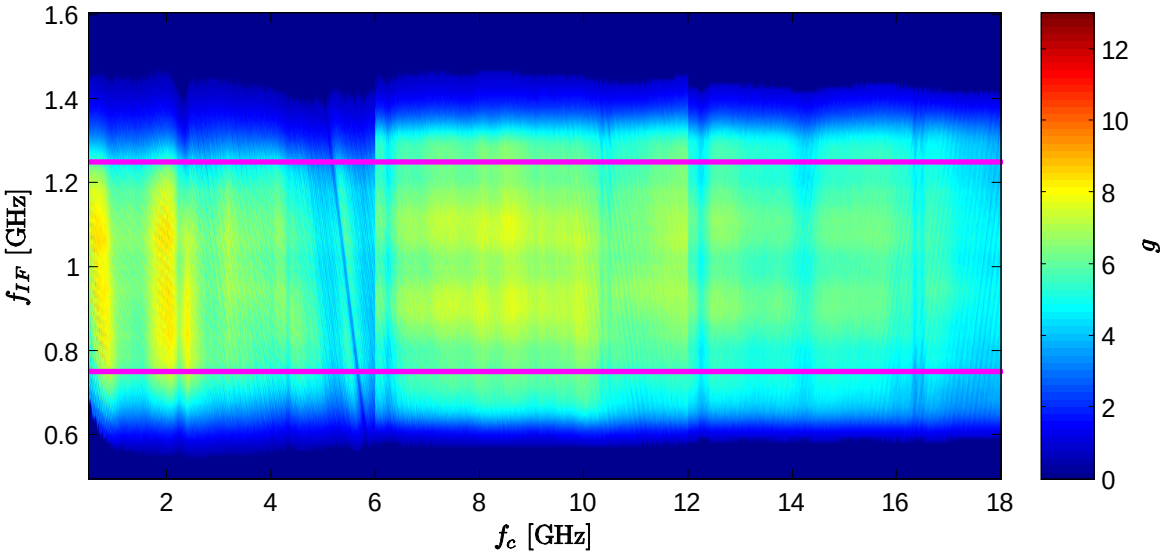

Figure 4.24 Tuner 10 gain (linear scale).

Table 4.13 Measured voltage gain, within the passband, for Tuner 11.

	Linear Scale					Decibels				
f_c [GHz]	Max	Mean	Min	Ripple	Std Dev	Max	Mean	Min	Ripple	Std Dev
0.5	9.88	6.65	4.72	5.16	1.00	9.95	8.18	6.74	3.21	0.65
1	8.51	6.96	4.14	4.37	1.12	9.30	8.37	6.17	3.13	0.76
2	9.73	7.87	4.87	4.86	1.12	9.88	8.91	6.88	3.00	0.66
3	7.95	6.39	4.20	3.75	0.90	9.00	8.01	6.24	2.77	0.64
4	7.56	6.43	4.52	3.04	0.68	8.79	8.06	6.55	2.24	0.48
5	6.34	5.01	2.99	3.34	0.85	8.02	6.93	4.76	3.26	0.79
5.99	5.94	4.25	2.37	3.57	0.84	7.74	6.20	3.75	3.99	0.89
6	8.08	6.51	4.87	3.21	0.75	9.07	8.11	6.88	2.19	0.52
7	8.80	7.35	5.69	3.11	0.73	9.45	8.64	7.55	1.89	0.44
8	8.92	7.71	6.16	2.76	0.74	9.50	8.85	7.89	1.61	0.43
9	8.76	7.72	6.40	2.37	0.63	9.43	8.86	8.06	1.37	0.37
10	9.33	8.36	7.08	2.25	0.51	9.70	9.22	8.50	1.20	0.27
11	9.07	8.24	6.72	2.35	0.60	9.57	9.15	8.27	1.30	0.33
12	7.58	6.65	5.50	2.07	0.54	8.79	8.21	7.41	1.39	0.36
13	7.58	6.70	5.44	2.14	0.61	8.79	8.24	7.35	1.44	0.41
14	7.16	6.30	4.91	2.25	0.63	8.55	7.97	6.91	1.64	0.45
15	6.23	5.38	4.25	1.98	0.54	7.94	7.29	6.29	1.66	0.46
16	5.37	4.85	3.87	1.50	0.35	7.30	6.85	5.88	1.42	0.33
17	5.14	4.63	3.71	1.43	0.30	7.11	6.64	5.69	1.42	0.29
18	6.42	5.79	4.84	1.58	0.43	8.07	7.61	6.85	1.23	0.33

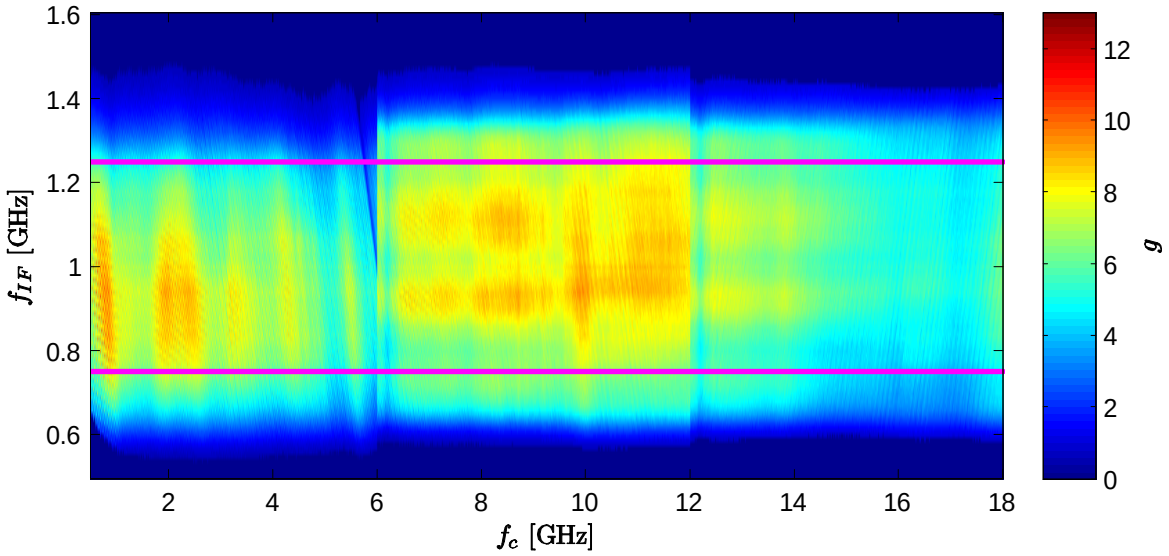

Figure 4.25 Tuner 11 gain (linear scale).

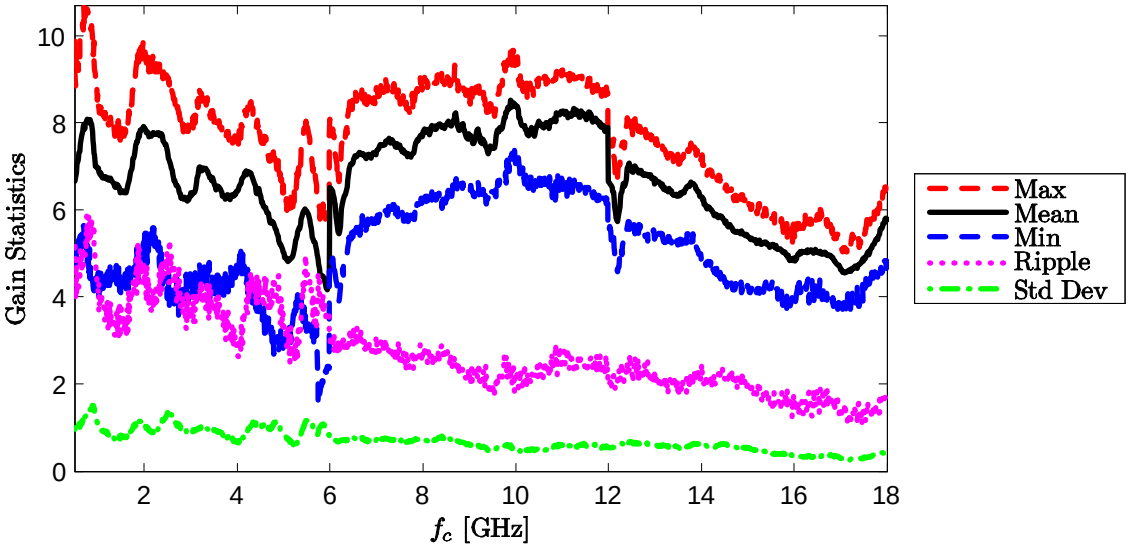

Figure 4.26 Tuner 11 gain statistics, within the passband (linear scale).

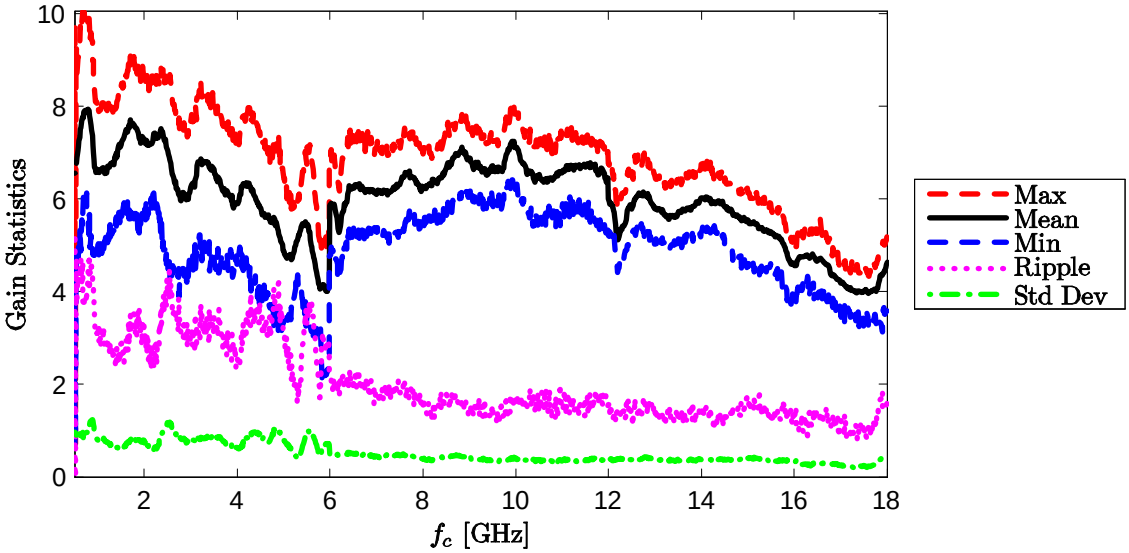

Figure 4.27 Tuner 12 gain statistics, within the passband (linear scale).

Table 4.14 Measured voltage gain, within the passband, for Tuner 12.

	Linear Scale					Decibels				
f_c [GHz]	Max	Mean	Min	Ripple	Std Dev	Max	Mean	Min	Ripple	Std Dev
0.5	9.69	6.55	4.55	5.14	0.97	9.86	8.12	6.58	3.28	0.64
1	7.95	6.64	4.83	3.12	0.82	9.01	8.19	6.84	2.16	0.55
2	8.83	7.29	5.57	3.26	0.79	9.46	8.60	7.46	2.00	0.48
3	7.65	6.25	4.64	3.01	0.77	8.84	7.93	6.67	2.17	0.55
4	7.16	5.89	4.59	2.56	0.64	8.55	7.68	6.62	1.93	0.48
5	6.42	4.87	3.36	3.06	0.81	8.08	6.81	5.26	2.82	0.74
5.99	5.19	4.13	2.43	2.76	0.68	7.15	6.10	3.85	3.30	0.78
6	6.93	5.86	4.79	2.14	0.50	8.41	7.66	6.80	1.61	0.37
7	7.08	6.09	5.28	1.79	0.44	8.50	7.84	7.23	1.27	0.32
8	7.09	6.21	5.60	1.49	0.39	8.51	7.92	7.48	1.02	0.27
9	7.51	6.88	6.15	1.36	0.41	8.76	8.37	7.89	0.87	0.26
10	7.84	7.12	6.31	1.53	0.39	8.94	8.52	8.00	0.95	0.24
11	7.32	6.56	5.74	1.57	0.35	8.64	8.17	7.59	1.05	0.23
12	6.76	5.99	5.21	1.56	0.38	8.30	7.77	7.17	1.14	0.28
13	6.43	5.78	5.04	1.39	0.39	8.08	7.61	7.02	1.06	0.29
14	6.75	6.02	5.28	1.47	0.38	8.29	7.79	7.23	1.07	0.27
15	6.12	5.55	4.60	1.52	0.42	7.87	7.43	6.63	1.24	0.34
16	5.07	4.57	3.80	1.27	0.32	7.05	6.59	5.80	1.25	0.31
17	4.66	4.18	3.57	1.09	0.26	6.69	6.20	5.53	1.16	0.27
18	5.20	4.63	3.58	1.61	0.35	7.16	6.65	5.54	1.61	0.34

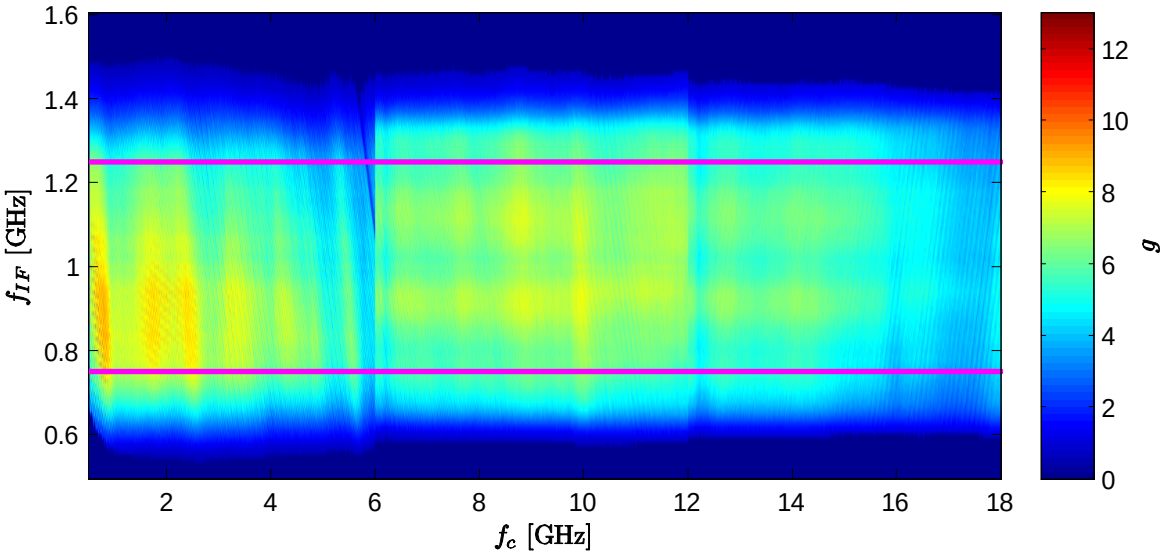

Figure 4.28 Tuner 12 gain (linear scale).

Table 4.15 Measured voltage gain, within the passband, for Tuner 13.

	Linear Scale					Decibels				
f_c [GHz]	Max	Mean	Min	Ripple	Std Dev	Max	Mean	Min	Ripple	Std Dev
0.5	9.33	7.04	5.00	4.33	0.95	9.70	8.44	6.99	2.71	0.60
1	8.64	7.07	5.22	3.41	0.90	9.36	8.46	7.18	2.18	0.57
2	8.35	7.28	5.57	2.78	0.75	9.22	8.60	7.46	1.76	0.46
3	8.60	7.11	5.51	3.09	0.78	9.34	8.49	7.41	1.93	0.48
4	7.82	6.23	4.69	3.14	0.78	8.93	7.91	6.71	2.22	0.55
5	6.55	4.74	3.24	3.31	0.88	8.17	6.68	5.11	3.06	0.80
5.99	4.96	4.27	3.58	1.38	0.38	6.96	6.29	5.54	1.42	0.38
6	7.93	6.56	5.26	2.67	0.65	8.99	8.15	7.21	1.78	0.44
7	7.96	6.80	5.72	2.24	0.52	9.01	8.31	7.57	1.43	0.33
8	7.51	6.51	5.59	1.92	0.47	8.76	8.12	7.47	1.28	0.32
9	8.80	7.93	6.64	2.16	0.63	9.45	8.98	8.22	1.23	0.36
10	8.31	7.35	6.66	1.65	0.45	9.19	8.66	8.23	0.96	0.26
11	8.07	7.16	6.23	1.84	0.46	9.07	8.54	7.95	1.12	0.28
12	6.76	6.08	5.00	1.76	0.46	8.30	7.82	6.99	1.31	0.34
13	6.92	6.07	5.20	1.71	0.47	8.40	7.82	7.16	1.24	0.34
14	7.17	6.27	5.29	1.88	0.46	8.55	7.96	7.23	1.32	0.32
15	6.60	5.79	4.43	2.17	0.64	8.20	7.60	6.46	1.73	0.51
16	4.98	4.51	3.50	1.48	0.41	6.97	6.53	5.45	1.53	0.41
17	4.24	3.78	3.12	1.12	0.24	6.28	5.77	4.94	1.34	0.28
18	5.61	4.79	3.87	1.74	0.41	7.49	6.79	5.88	1.61	0.38

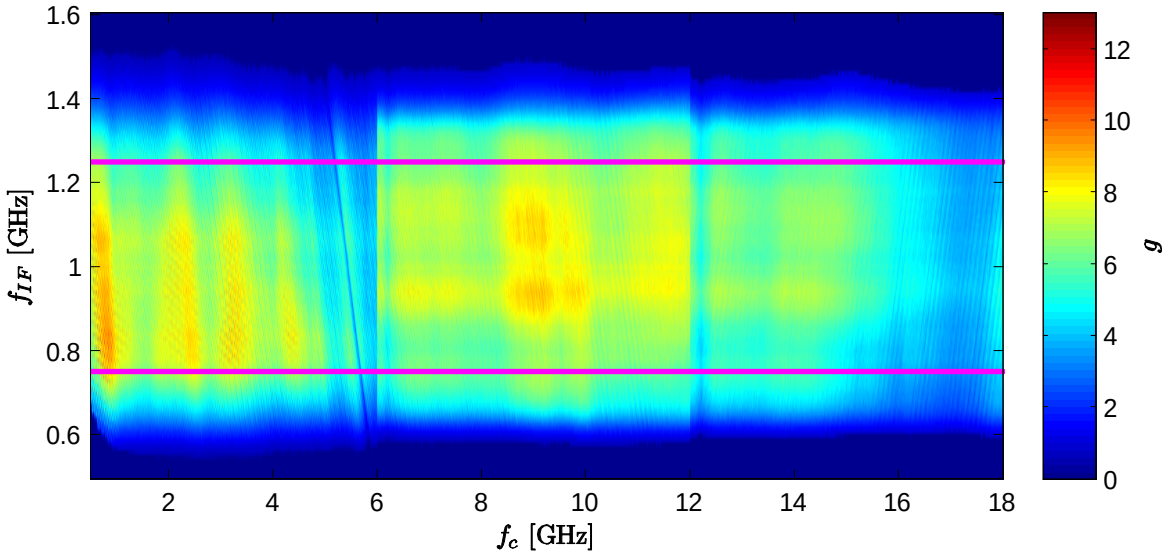

Figure 4.29 Tuner 13 gain (linear scale).

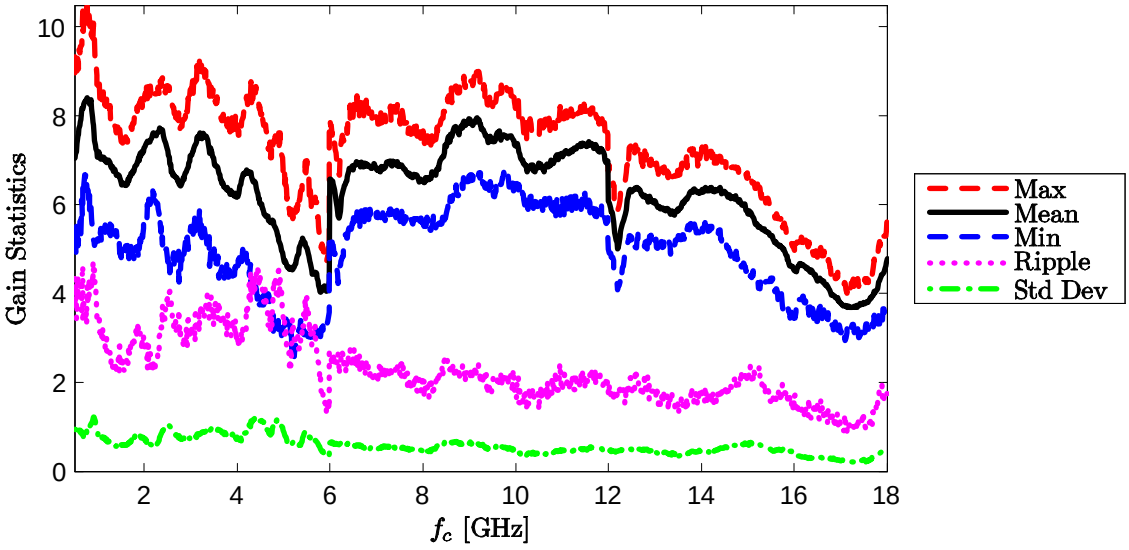

Figure 4.30 Tuner 13 gain statistics, within the passband (linear scale).

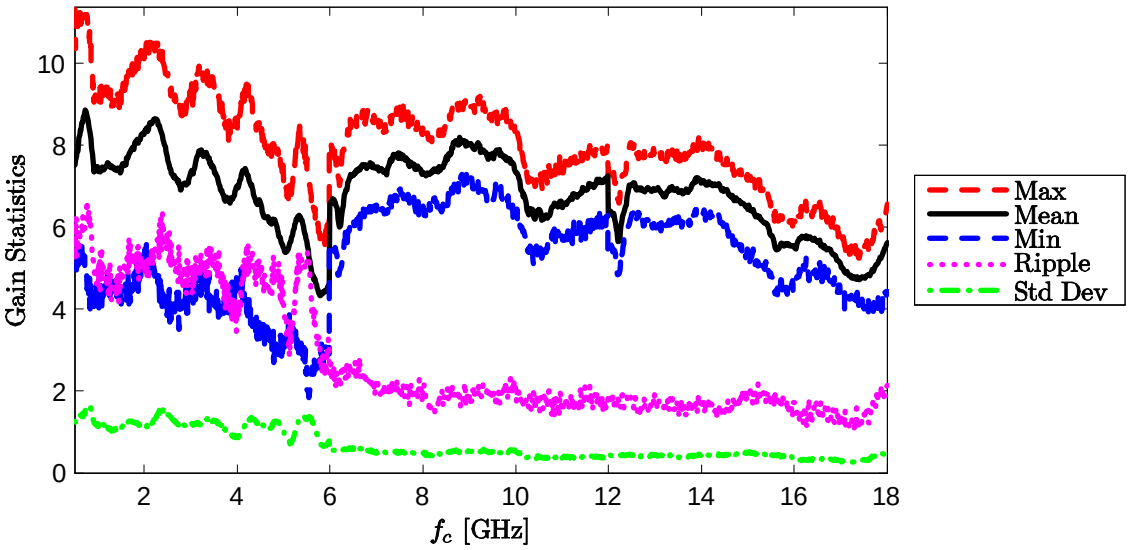

Figure 4.31 Tuner 14 gain statistics, within the passband (linear scale).

Table 4.16 Measured voltage gain, within the passband, for Tuner 14.

	Linear Scale					Decibels				
f_c [GHz]	Max	Mean	Min	Ripple	Std Dev	Max	Mean	Min	Ripple	Std Dev
0.5	11.29	7.51	5.09	6.20	1.25	10.53	8.70	7.07	3.46	0.73
1	9.18	7.48	4.14	5.04	1.20	9.63	8.67	6.17	3.46	0.78
2	10.10	8.26	5.07	5.04	1.15	10.04	9.12	7.05	3.00	0.66
3	8.97	7.34	4.21	4.76	1.19	9.53	8.59	6.24	3.29	0.77
4	8.66	6.99	4.50	4.17	0.88	9.38	8.41	6.53	2.85	0.58
5	7.11	5.47	3.06	4.05	1.01	8.52	7.30	4.86	3.66	0.87
5.99	5.95	4.60	2.90	3.04	0.78	7.74	6.56	4.63	3.11	0.78
6	7.92	6.54	5.48	2.44	0.57	8.99	8.14	7.39	1.60	0.38
7	8.57	7.44	6.52	2.05	0.49	9.33	8.71	8.14	1.19	0.28
8	8.42	7.33	6.39	2.02	0.49	9.25	8.64	8.06	1.19	0.29
9	8.92	8.03	7.05	1.87	0.53	9.50	9.04	8.48	1.02	0.29
10	8.28	7.32	6.31	1.97	0.51	9.18	8.64	8.00	1.18	0.31
11	7.46	6.48	5.90	1.57	0.36	8.73	8.11	7.71	1.02	0.23
12	7.31	6.33	5.38	1.93	0.45	8.64	8.01	7.31	1.33	0.30
13	7.79	6.89	5.99	1.80	0.44	8.91	8.38	7.77	1.14	0.28
14	7.88	7.06	6.28	1.60	0.43	8.97	8.48	7.98	0.99	0.27
15	7.13	6.42	5.37	1.77	0.48	8.53	8.07	7.30	1.23	0.33
16	6.14	5.51	4.42	1.72	0.39	7.88	7.40	6.46	1.43	0.32
17	5.76	5.09	4.33	1.43	0.30	7.61	7.06	6.37	1.24	0.26
18	6.55	5.62	4.42	2.13	0.45	8.16	7.48	6.45	1.71	0.36

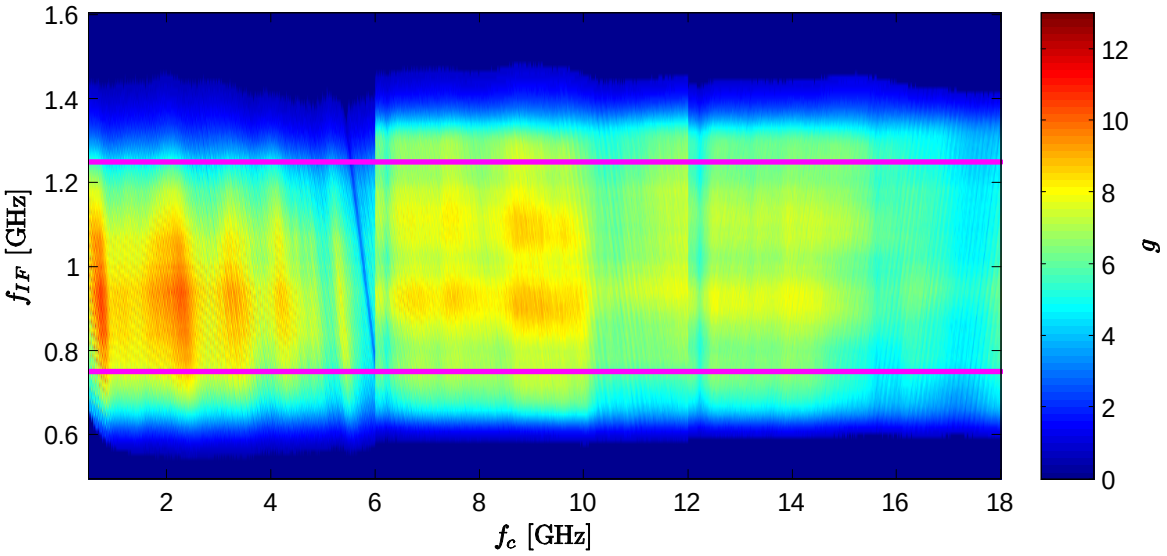

Figure 4.32 Tuner 14 gain (linear scale).

Table 4.17 Measured voltage gain, within the passband, for Tuner 15.

	Linear Scale					Decibels				
f_c [GHz]	Max	Mean	Min	Ripple	Std Dev	Max	Mean	Min	Ripple	Std Dev
0.5	10.26	7.60	5.60	4.66	1.11	10.11	8.76	7.48	2.63	0.64
1	8.35	7.01	4.65	3.69	0.91	9.21	8.42	6.68	2.54	0.60
2	8.67	7.04	4.97	3.70	0.83	9.38	8.44	6.97	2.41	0.53
3	8.00	6.60	4.38	3.62	0.91	9.03	8.15	6.41	2.62	0.63
4	7.56	6.33	4.67	2.90	0.63	8.79	7.99	6.69	2.10	0.44
5	6.58	5.15	3.36	3.22	0.76	8.18	7.07	5.26	2.92	0.67
5.99	5.71	4.75	3.86	1.84	0.47	7.56	6.75	5.87	1.70	0.43
6	7.78	6.54	5.36	2.42	0.65	8.91	8.14	7.29	1.62	0.44
7	7.85	6.87	5.80	2.05	0.57	8.95	8.35	7.64	1.31	0.37
8	7.65	6.64	5.82	1.83	0.52	8.84	8.21	7.65	1.19	0.34
9	7.96	7.06	6.03	1.93	0.55	9.01	8.48	7.80	1.21	0.34
10	8.01	7.21	6.18	1.83	0.47	9.03	8.57	7.91	1.12	0.29
11	8.06	7.23	5.99	2.07	0.51	9.06	8.58	7.77	1.29	0.32
12	7.01	6.21	5.19	1.82	0.50	8.46	7.91	7.15	1.31	0.35
13	6.81	6.00	5.04	1.77	0.49	8.33	7.77	7.02	1.31	0.36
14	7.03	6.28	5.20	1.83	0.53	8.47	7.96	7.16	1.31	0.38
15	5.78	5.13	4.17	1.61	0.47	7.62	7.09	6.20	1.42	0.41
16	5.07	4.54	3.72	1.35	0.31	7.05	6.56	5.71	1.34	0.30
17	4.95	4.38	3.57	1.38	0.32	6.94	6.41	5.53	1.42	0.32
18	5.60	4.94	4.07	1.53	0.41	7.48	6.92	6.10	1.38	0.37

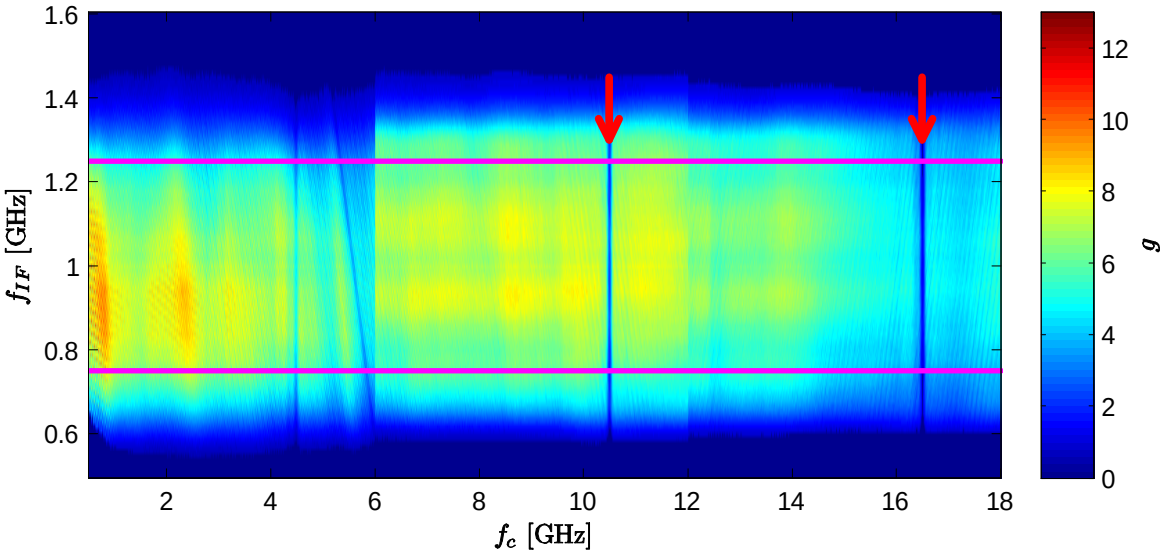

Figure 4.33 Tuner 15 gain (linear scale). The following defective areas are highlighted: $10.43 \leq f_c \leq 10.55$ GHz, and $16.32 \leq f_c \leq 16.55$ GHz.

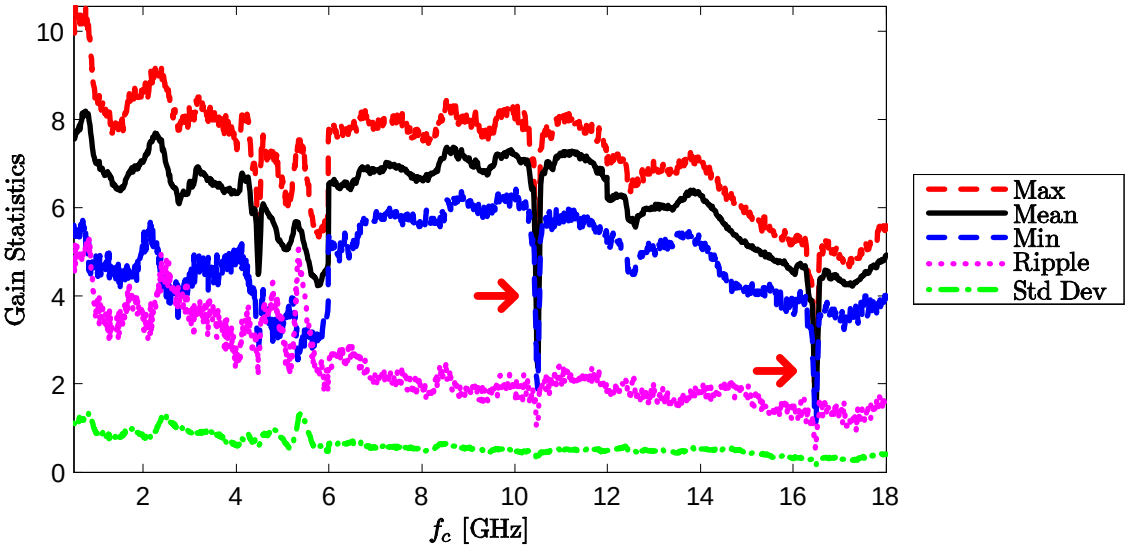

Figure 4.34 Tuner 15 gain statistics, within the passband (linear scale).

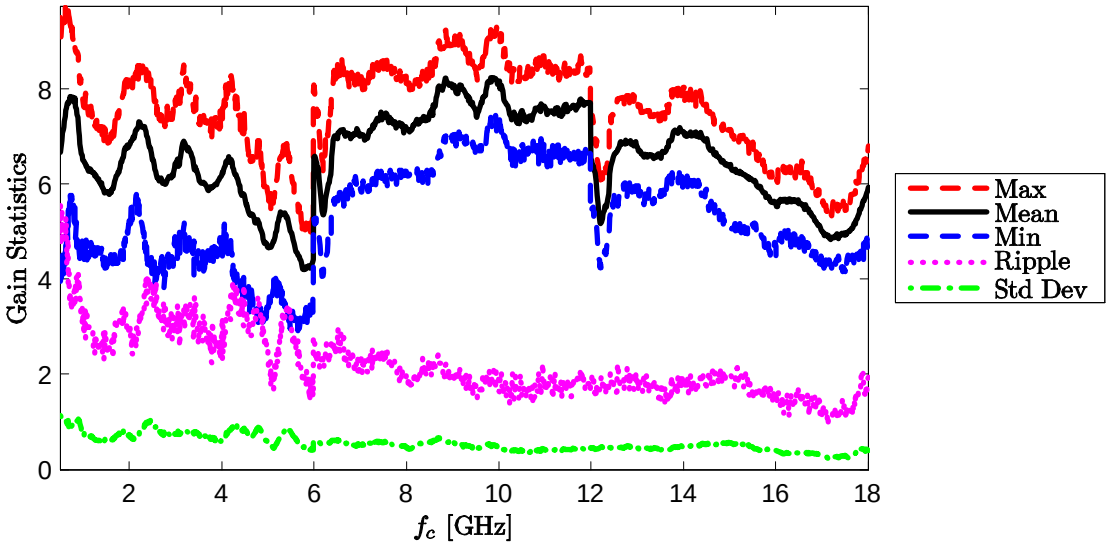

Figure 4.35 Tuner 16 gain statistics, within the passband (linear scale).

Table 4.18 Measured voltage gain, within the passband, for Tuner 16.

	Linear Scale					Decibels				
f_c [GHz]	Max	Mean	Min	Ripple	Std Dev	Max	Mean	Min	Ripple	Std Dev
0.5	9.50	6.67	3.96	5.54	1.14	9.78	8.17	5.97	3.80	0.79
1	7.87	6.51	4.47	3.40	0.81	8.96	8.10	6.50	2.46	0.57
2	8.03	6.81	5.14	2.89	0.74	9.04	8.31	7.11	1.94	0.49
3	7.65	6.45	4.62	3.03	0.75	8.84	8.06	6.65	2.19	0.52
4	7.29	6.17	4.66	2.63	0.61	8.63	7.88	6.68	1.95	0.44
5	5.76	4.66	3.36	2.40	0.55	7.60	6.65	5.27	2.34	0.52
5.99	5.11	4.42	3.59	1.52	0.42	7.08	6.43	5.55	1.53	0.41
6	8.08	6.56	5.28	2.80	0.63	9.07	8.15	7.22	1.85	0.42
7	8.26	7.06	5.93	2.33	0.53	9.17	8.47	7.73	1.44	0.33
8	8.26	7.18	6.28	1.99	0.47	9.17	8.55	7.98	1.19	0.28
9	8.93	8.02	6.90	2.02	0.56	9.51	9.03	8.39	1.12	0.31
10	8.99	8.16	7.36	1.63	0.48	9.54	9.11	8.67	0.87	0.25
11	8.55	7.64	6.88	1.67	0.41	9.32	8.82	8.38	0.94	0.23
12	7.43	6.55	5.51	1.93	0.47	8.71	8.15	7.41	1.30	0.31
13	7.77	6.76	5.85	1.92	0.47	8.90	8.29	7.67	1.23	0.30
14	8.03	7.11	6.04	1.99	0.51	9.05	8.50	7.81	1.24	0.32
15	7.13	6.39	5.17	1.96	0.57	8.53	8.04	7.14	1.39	0.40
16	6.14	5.57	4.69	1.44	0.40	7.88	7.45	6.72	1.16	0.32
17	5.56	5.01	4.41	1.15	0.29	7.45	6.99	6.44	1.01	0.26
18	6.80	5.93	4.87	1.94	0.40	8.33	7.72	6.87	1.45	0.30

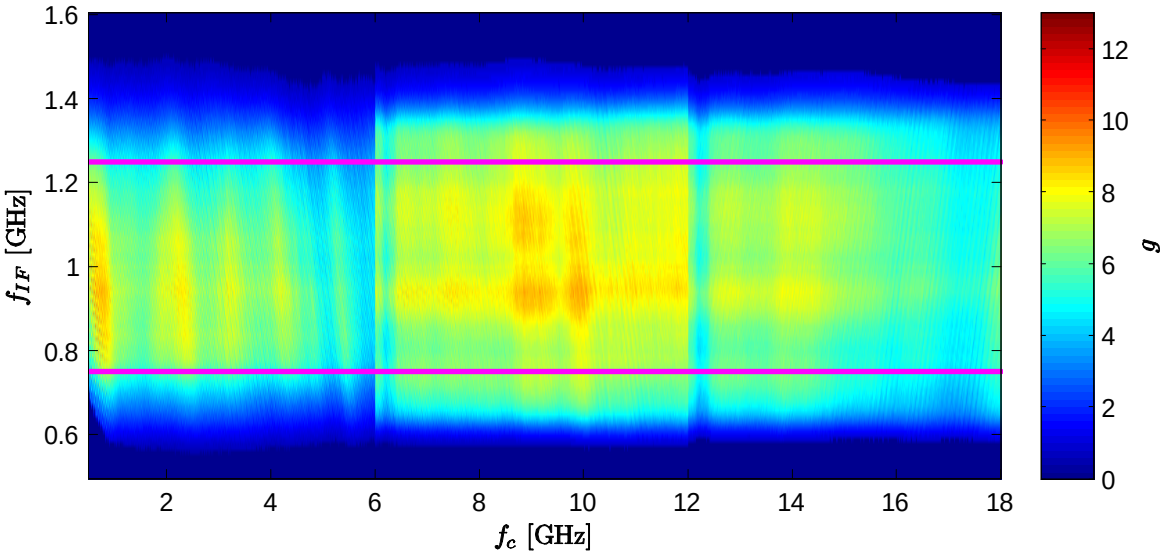

Figure 4.36 Tuner 16 gain (linear scale).

Table 4.19 Summary statistics for the tuner gain measurements at room temperature, within the passband.

	Linear Scale					Decibels				
f_c [GHz]	Max	Mean	Min	Range	Std Dev	Max	Mean	Min	Range	Std Dev
0.5	12.62	7.16	2.81	9.81	1.79	11.01	8.42	4.48	6.53	1.07
1	12.45	7.43	3.05	9.40	1.63	10.95	8.60	4.84	6.11	0.98
2	13.80	7.30	3.86	9.95	1.69	11.40	8.53	5.86	5.54	0.93
3	12.98	6.53	3.09	9.88	1.73	11.13	8.02	4.91	6.23	1.06
4	12.68	6.73	3.26	9.42	1.78	11.03	8.14	5.13	5.90	1.07
5	10.12	5.72	2.48	7.64	1.56	10.05	7.42	3.94	6.11	1.17
5.99	9.16	4.69	1.96	7.20	1.26	9.62	6.57	2.92	6.70	1.07
6	13.70	7.46	3.31	10.39	2.09	11.37	8.58	5.20	6.17	1.13
7	15.22	8.27	5.28	9.94	2.22	11.82	9.04	7.23	4.60	1.06
8	15.89	8.44	5.59	10.30	2.24	12.01	9.13	7.47	4.54	1.04
9	15.08	8.51	5.81	9.27	1.97	11.78	9.20	7.64	4.14	0.91
10	13.59	7.96	4.73	8.86	1.73	11.33	8.92	6.75	4.59	0.89
11	14.00	7.51	3.99	10.01	1.85	11.46	8.64	6.01	5.45	0.98
12	15.06	7.63	4.64	10.42	2.23	11.78	8.67	6.67	5.11	1.12
13	13.03	7.62	4.93	8.09	1.92	11.15	8.69	6.93	4.22	1.01
14	12.10	7.28	4.71	7.38	1.59	10.83	8.53	6.73	4.10	0.88
15	9.52	6.09	3.72	5.80	1.22	9.79	7.76	5.70	4.08	0.85
16	8.84	5.32	2.69	6.15	1.19	9.46	7.15	4.29	5.17	0.98
17	7.99	4.90	3.12	4.87	0.95	9.02	6.82	4.94	4.08	0.82
18	8.40	5.40	2.80	5.60	1.07	9.24	7.24	4.46	4.78	0.86

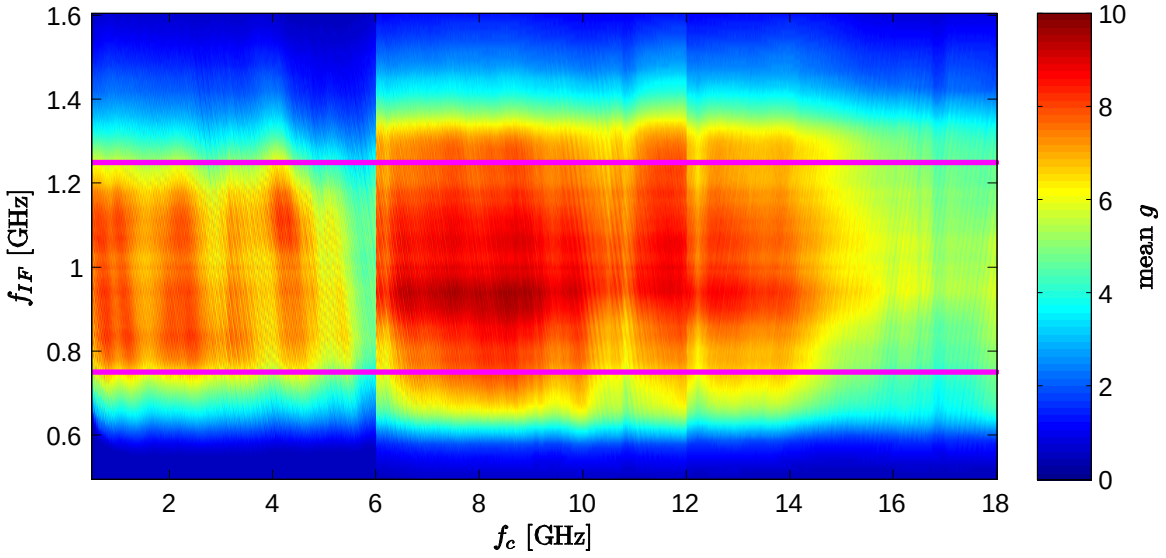

Figure 4.37 Average gain of the sixteen LCR400 tuners, at each point in the frequency spectrum.

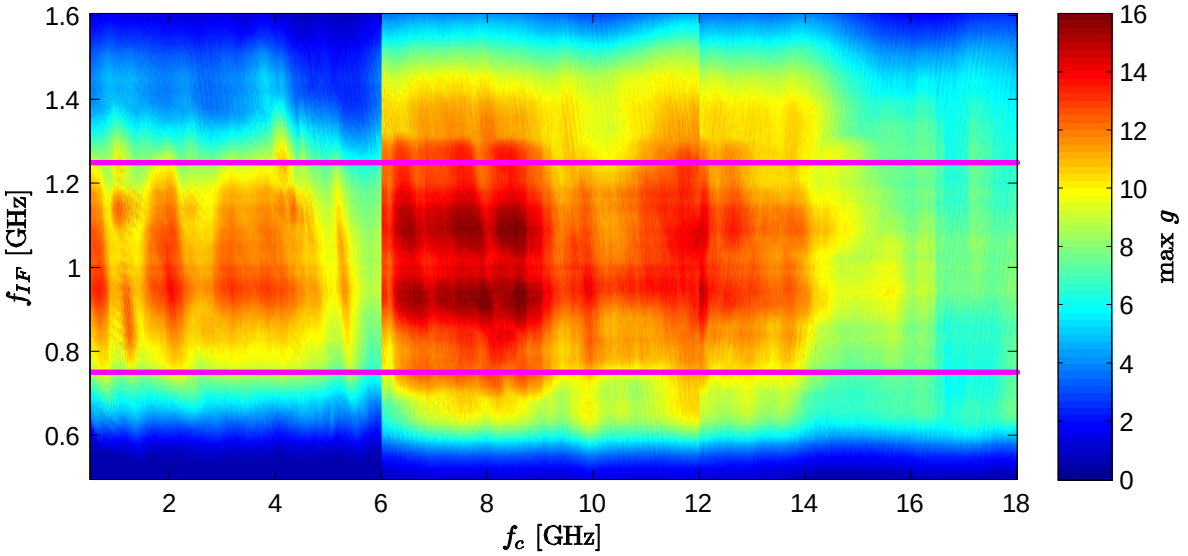

Figure 4.38 Maximum gain of the sixteen LCR400 tuners, at each point in the frequency spectrum.

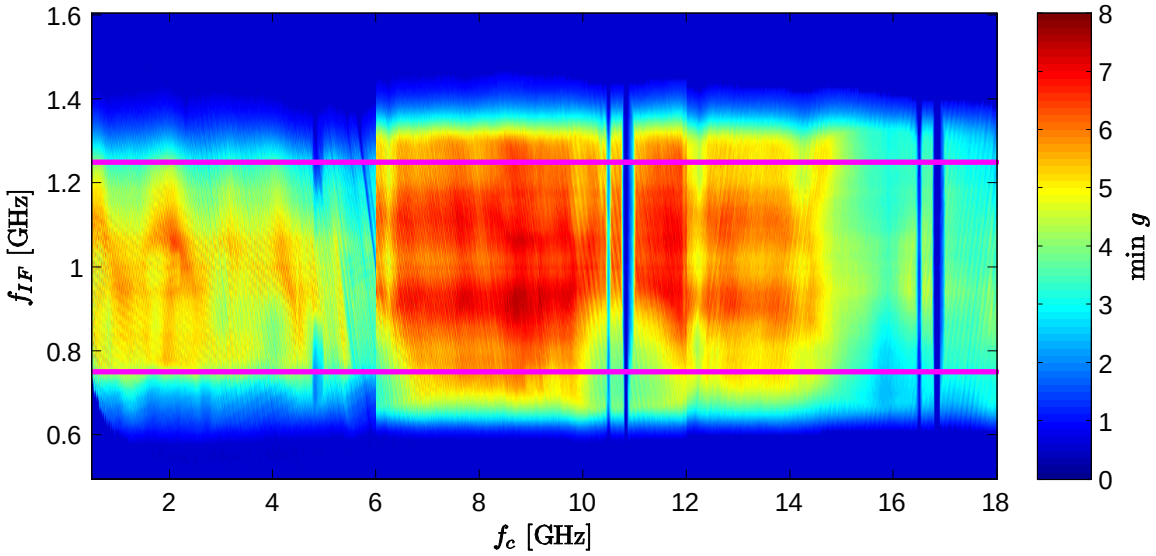

Figure 4.39 Minimum gain of the sixteen LCR400 tuners, at each point in the frequency spectrum.

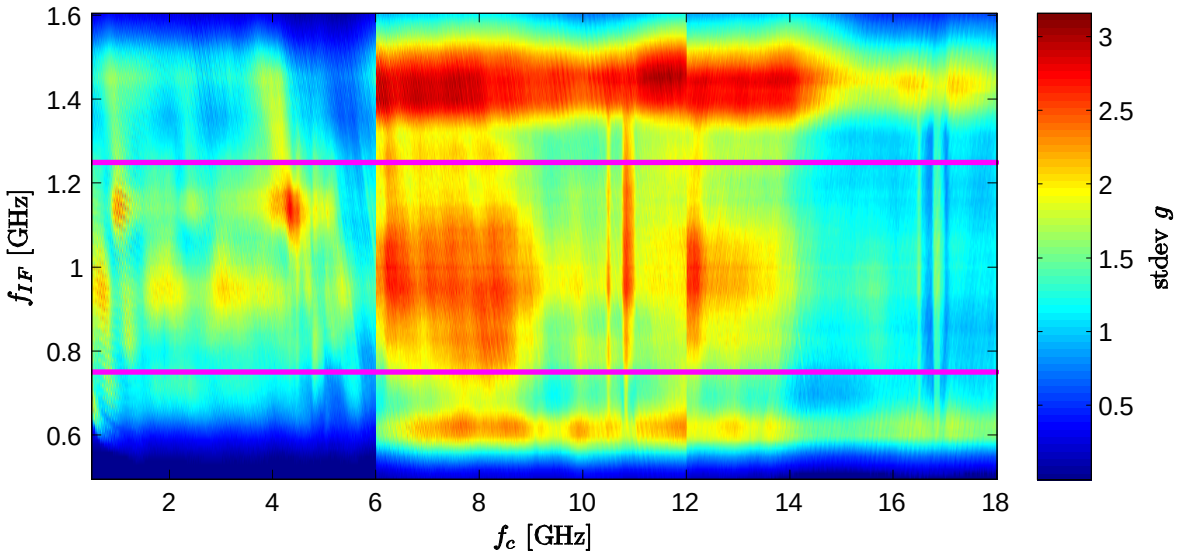

Figure 4.40 Standard deviation of the gains of the sixteen LCR400 tuners, at each point in the frequency spectrum.

4.2 Microwave Block Downconverter Gain

The results of the gain measurements for the downconverter section are shown in Tables 4.20-4.35 and Figs. 4.41-4.71, and summarized in Table 4.36 and Figs. 4.73-4.76. This takes into account the cable losses and the losses due to the power dividers within the downconverter block; however, the dominant effects come from the LCR400 tuners and the K&L anti-aliasing filters.

Table 4.20 Measured voltage gain, within the passband, for downconverter channel 1.

	Linear Scale					Decibels				
f_c [GHz]	Max	Mean	Min	Ripple	Std Dev	Max	Mean	Min	Ripple	Std Dev
0.5	6.24	4.94	3.44	2.79	0.65	7.95	6.90	5.37	2.58	0.59
1	6.30	4.90	3.57	2.73	0.71	8.00	6.86	5.53	2.47	0.63
2	5.15	4.56	3.06	2.09	0.46	7.12	6.56	4.85	2.26	0.47
3	4.94	4.05	2.81	2.13	0.41	6.94	6.05	4.49	2.45	0.46
4	6.30	4.63	3.08	3.21	0.87	7.99	6.58	4.89	3.10	0.82
5	5.02	4.23	2.35	2.67	0.70	7.01	6.19	3.72	3.29	0.80
5.99	3.90	3.19	2.26	1.65	0.32	5.92	5.02	3.54	2.38	0.45
6	6.30	5.47	3.86	2.44	0.58	7.99	7.35	5.86	2.13	0.48
7	8.00	6.93	5.21	2.80	0.79	9.03	8.38	7.16	1.87	0.51
8	8.61	7.51	5.40	3.22	0.94	9.35	8.72	7.32	2.03	0.57
9	7.92	6.80	5.24	2.68	0.69	8.99	8.31	7.19	1.79	0.45
10	7.48	6.35	4.72	2.76	0.70	8.74	8.00	6.74	2.00	0.49
11	7.64	6.48	4.38	3.26	0.78	8.83	8.08	6.42	2.41	0.54
12	7.70	6.65	4.73	2.97	0.72	8.87	8.20	6.75	2.12	0.49
13	6.98	6.16	4.67	2.31	0.61	8.44	7.87	6.69	1.75	0.44
14	6.19	5.37	4.01	2.18	0.59	7.92	7.27	6.03	1.89	0.49
15	5.68	4.73	3.52	2.16	0.50	7.54	6.72	5.46	2.08	0.48
16	5.76	4.83	3.48	2.28	0.54	7.61	6.81	5.42	2.19	0.50
17	5.19	4.43	2.98	2.22	0.58	7.15	6.42	4.74	2.42	0.61
18	4.81	4.13	3.12	1.69	0.43	6.82	6.14	4.94	1.88	0.46

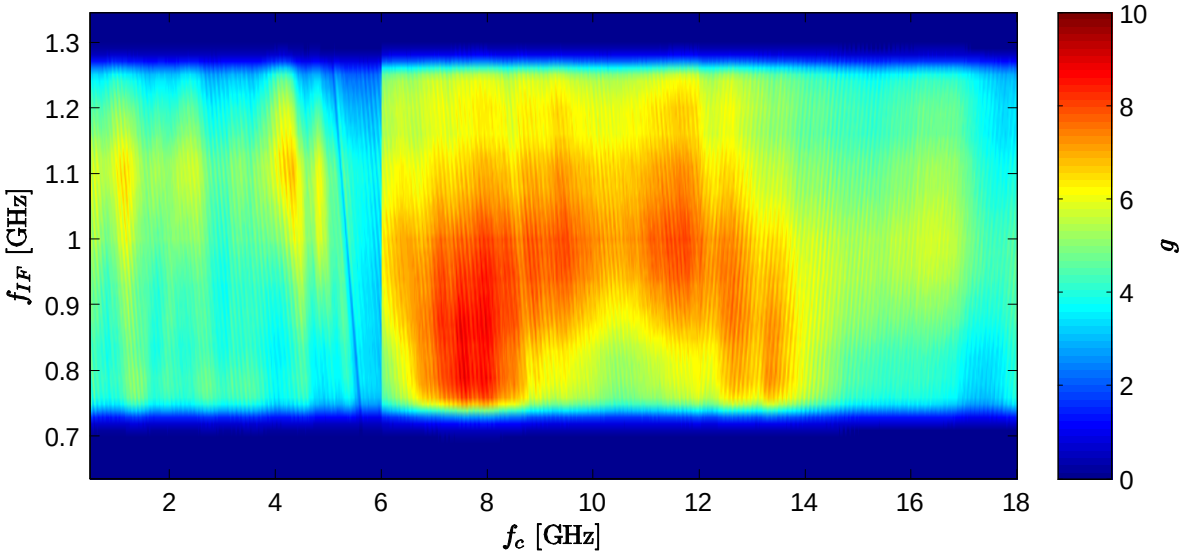

Figure 4.41 Downconverter channel 1 gain (linear scale).

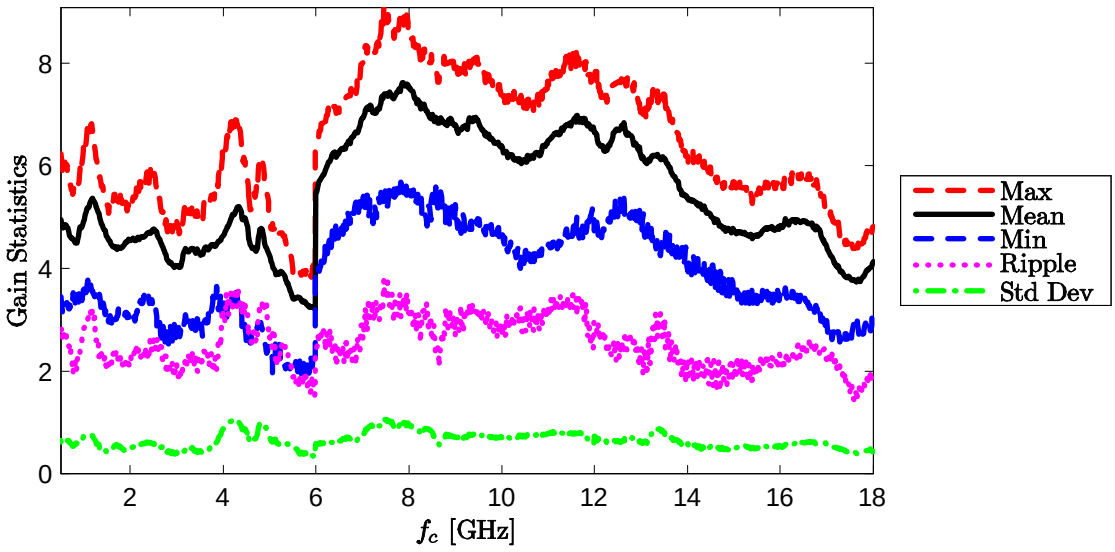

Figure 4.42 Channel 1 gain statistics, within the passband (linear scale).

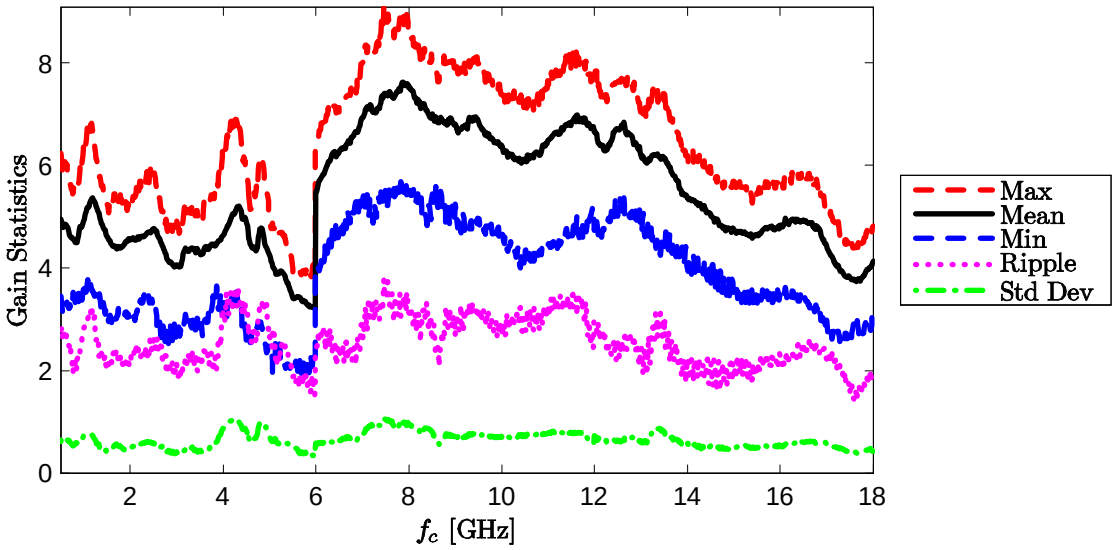

Figure 4.43 Channel 2 gain statistics, within the passband (linear scale).

Table 4.21 Measured voltage gain, within the passband, for downconverter channel 2.

	Linear Scale					Decibels				
f_c [GHz]	Max	Mean	Min	Ripple	Std Dev	Max	Mean	Min	Ripple	Std Dev
0.5	7.12	5.75	3.10	4.03	0.94	8.53	7.53	4.91	3.62	0.78
1	6.07	5.05	3.03	3.04	0.70	7.83	6.99	4.82	3.02	0.67
2	7.56	6.21	3.63	3.93	0.90	8.78	7.88	5.60	3.18	0.69
3	7.18	5.92	3.46	3.72	0.89	8.56	7.67	5.39	3.17	0.72
4	7.26	5.89	3.39	3.87	0.87	8.61	7.65	5.30	3.31	0.71
5	5.62	4.73	2.84	2.79	0.65	7.50	6.70	4.53	2.97	0.66
5.99	5.09	4.24	2.58	2.51	0.58	7.07	6.23	4.12	2.95	0.65
6	7.62	6.60	4.16	3.46	0.75	8.82	8.16	6.19	2.63	0.53
7	7.87	6.85	4.48	3.39	0.78	8.96	8.32	6.51	2.45	0.53
8	8.47	6.94	4.72	3.75	0.87	9.28	8.38	6.74	2.54	0.57
9	8.05	6.80	4.57	3.49	0.80	9.06	8.29	6.60	2.46	0.55
10	7.31	6.19	4.14	3.17	0.72	8.64	7.89	6.17	2.47	0.55
11	7.61	6.39	3.70	3.92	0.72	8.82	8.02	5.68	3.14	0.54
12	7.41	6.30	4.04	3.37	0.70	8.70	7.97	6.07	2.63	0.52
13	7.09	5.93	4.09	3.00	0.68	8.50	7.70	6.12	2.39	0.52
14	6.53	5.54	3.42	3.11	0.70	8.15	7.40	5.34	2.81	0.59
15	4.97	4.42	2.49	2.48	0.56	6.96	6.42	3.96	3.00	0.62
16	3.86	3.28	1.85	2.00	0.37	5.86	5.13	2.68	3.18	0.55
17	3.15	2.66	1.77	1.38	0.30	4.99	4.23	2.49	2.50	0.53
18	3.88	3.41	2.05	1.83	0.41	5.89	5.29	3.12	2.77	0.57

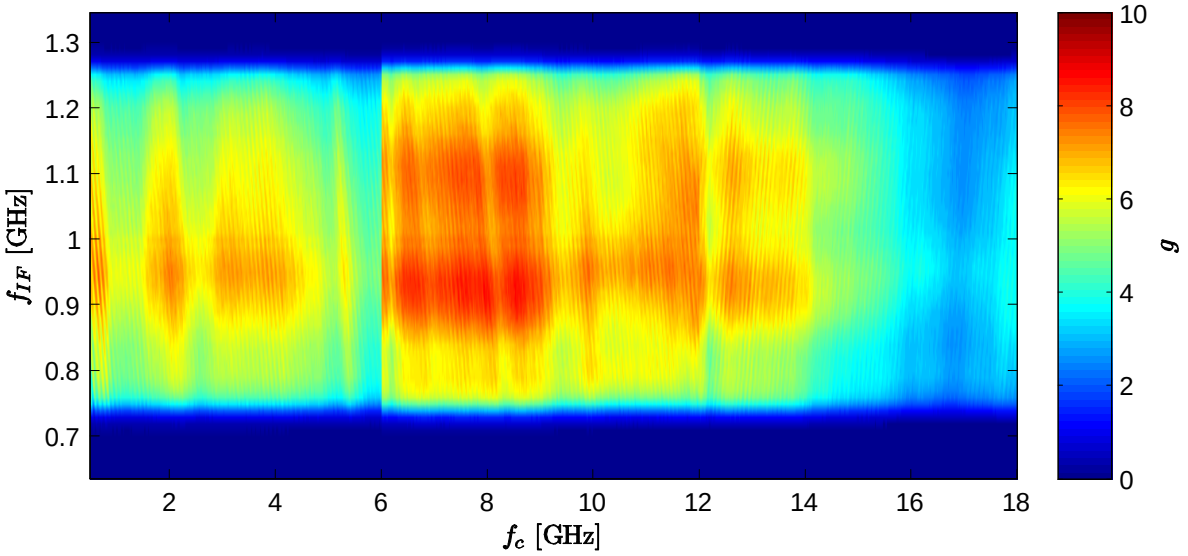

Figure 4.44 Downconverter channel 2 gain (linear scale).

Table 4.22 Measured voltage gain, within the passband, for downconverter channel 3.

	Linear Scale					Decibels				
f_c [GHz]	Max	Mean	Min	Ripple	Std Dev	Max	Mean	Min	Ripple	Std Dev
0.5	7.76	5.44	2.90	4.86	1.01	8.90	7.28	4.63	4.27	0.87
1	8.76	6.12	3.02	5.75	1.14	9.43	7.79	4.79	4.63	0.88
2	5.89	4.79	2.72	3.16	0.78	7.70	6.74	4.35	3.34	0.78
3	6.12	4.97	2.87	3.25	0.83	7.87	6.90	4.58	3.29	0.79
4	8.56	5.97	2.81	5.75	1.18	9.33	7.67	4.49	4.84	0.90
5	7.61	6.21	2.74	4.87	1.16	8.81	7.84	4.37	4.44	0.97
5.99	4.74	3.56	1.93	2.81	0.61	6.76	5.44	2.86	3.90	0.81
6	8.73	7.29	5.15	3.58	0.90	9.41	8.59	7.12	2.29	0.55
7	9.00	7.62	5.40	3.60	0.95	9.54	8.79	7.32	2.22	0.56
8	8.98	7.82	5.20	3.78	0.99	9.53	8.90	7.16	2.37	0.59
9	9.22	8.11	5.67	3.55	0.99	9.65	9.06	7.53	2.11	0.55
10	8.69	7.55	5.46	3.23	0.82	9.39	8.76	7.37	2.02	0.49
11	7.20	6.52	4.97	2.23	0.47	8.57	8.13	6.96	1.61	0.33
12	8.81	7.33	4.81	4.00	1.00	9.45	8.61	6.82	2.63	0.62
13	9.07	7.56	5.23	3.84	0.96	9.58	8.75	7.19	2.39	0.57
14	8.71	7.32	5.06	3.65	1.18	9.40	8.58	7.04	2.36	0.74
15	7.00	6.03	4.50	2.50	0.59	8.45	7.78	6.54	1.92	0.44
16	5.87	5.12	3.62	2.25	0.52	7.69	7.07	5.59	2.10	0.46
17	5.62	4.94	3.54	2.08	0.41	7.49	6.92	5.48	2.01	0.38
18	5.94	5.18	3.77	2.16	0.44	7.73	7.12	5.77	1.97	0.39

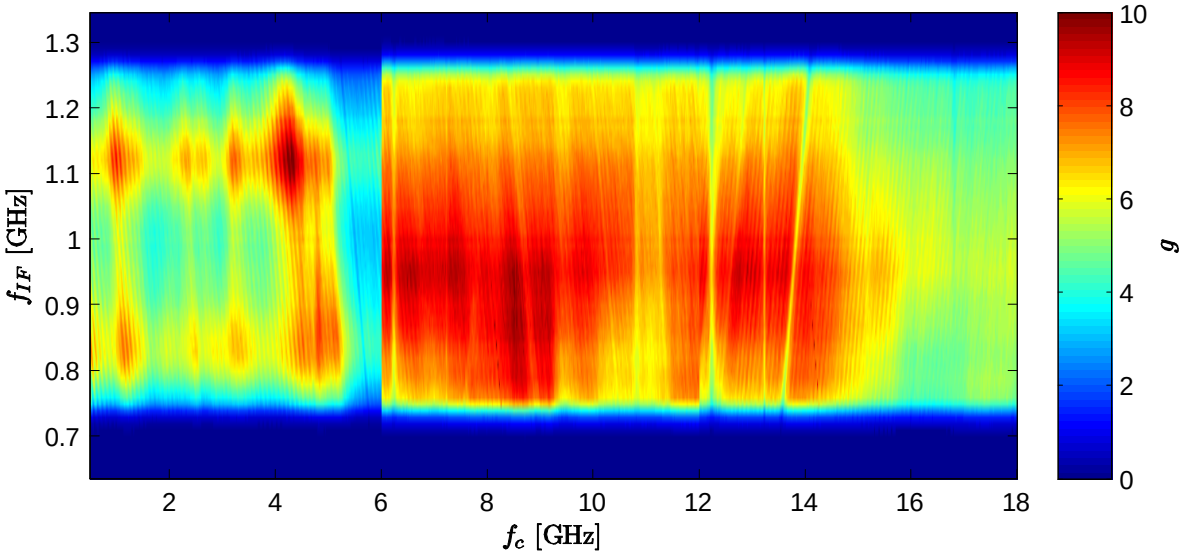

Figure 4.45 Downconverter channel 3 gain (linear scale).

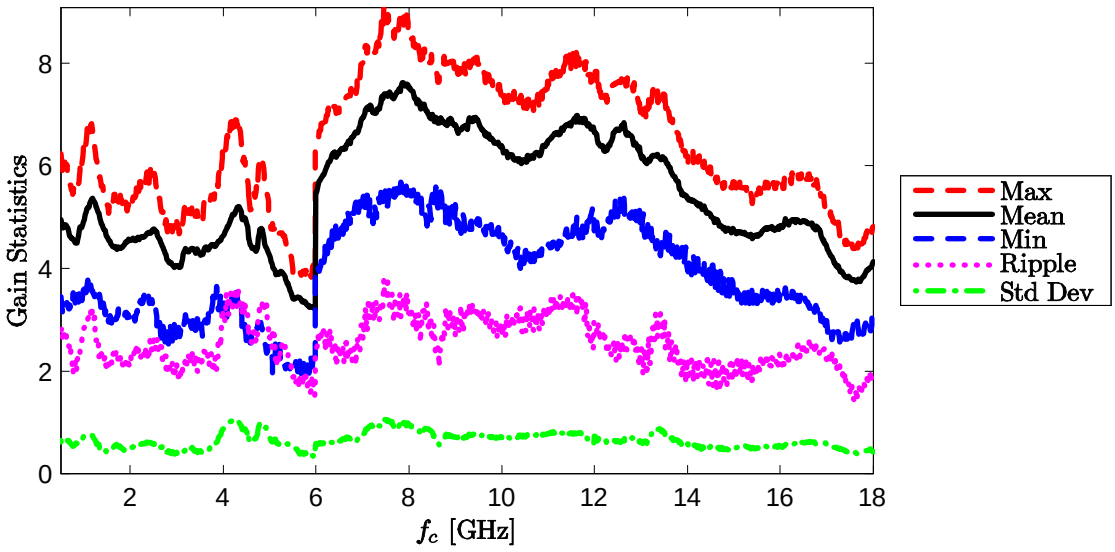

Figure 4.46 Channel 3 gain statistics, within the passband (linear scale).

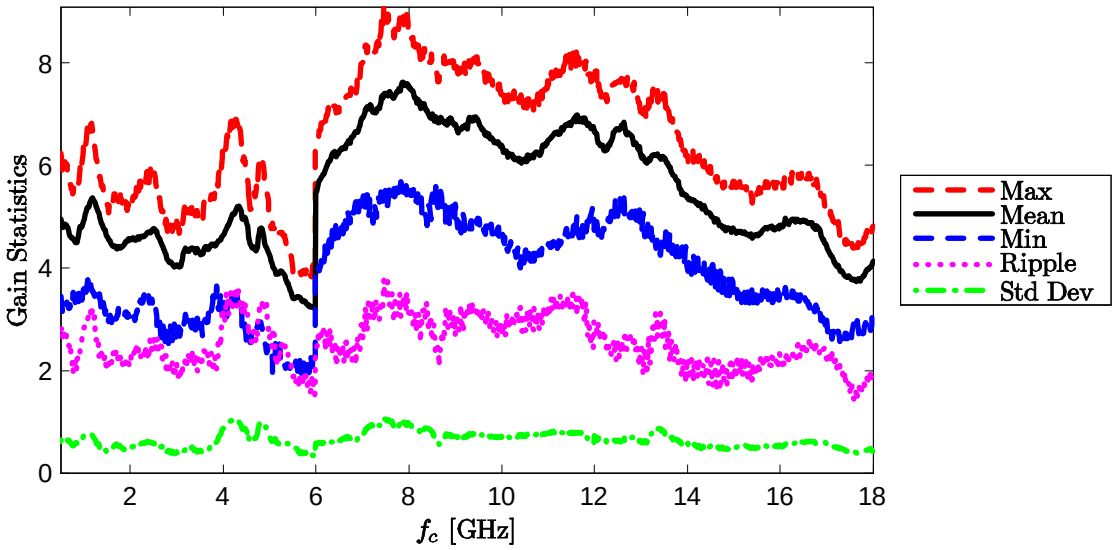

Figure 4.47 Channel 4 gain statistics, within the passband (linear scale).

Table 4.23 Measured voltage gain, within the passband, for downconverter channel 4.

	Linear Scale					Decibels				
f_c [GHz]	Max	Mean	Min	Ripple	Std Dev	Max	Mean	Min	Ripple	Std Dev
0.5	8.55	6.64	4.17	4.38	0.95	9.32	8.18	6.20	3.12	0.64
1	10.42	7.48	4.82	5.60	1.34	10.18	8.67	6.83	3.35	0.77
2	7.03	5.77	3.49	3.54	0.77	8.47	7.57	5.43	3.04	0.62
3	7.01	5.64	3.47	3.53	0.80	8.45	7.46	5.41	3.05	0.64
4	9.62	6.62	3.96	5.67	1.54	9.83	8.10	5.97	3.86	0.96
5	7.41	5.74	3.38	4.03	0.86	8.70	7.54	5.29	3.40	0.69
5.99	6.09	4.31	2.89	3.19	0.73	7.84	6.28	4.61	3.23	0.73
6	6.31	4.94	2.64	3.67	0.94	8.00	6.85	4.21	3.79	0.92
7	6.76	5.80	3.71	3.06	0.69	8.30	7.60	5.69	2.61	0.55
8	7.28	6.32	4.63	2.65	0.65	8.62	7.98	6.65	1.97	0.46
9	6.79	5.74	3.99	2.80	0.67	8.32	7.56	6.01	2.31	0.52
10	6.18	5.18	3.41	2.76	0.67	7.91	7.11	5.33	2.58	0.59
11	5.97	4.98	2.83	3.14	0.85	7.76	6.90	4.52	3.24	0.81
12	6.83	5.65	3.46	3.37	0.88	8.35	7.46	5.39	2.95	0.72
13	7.21	5.99	4.09	3.12	0.70	8.58	7.75	6.11	2.46	0.53
14	6.53	5.55	4.07	2.46	0.57	8.15	7.42	6.10	2.05	0.46
15	5.15	4.33	2.79	2.36	0.49	7.12	6.34	4.45	2.67	0.52
16	4.16	3.47	2.12	2.04	0.49	6.19	5.35	3.27	2.93	0.66
17	4.46	3.67	2.23	2.23	0.59	6.49	5.59	3.49	3.01	0.75
18	4.36	3.49	2.21	2.15	0.49	6.39	5.39	3.45	2.95	0.64

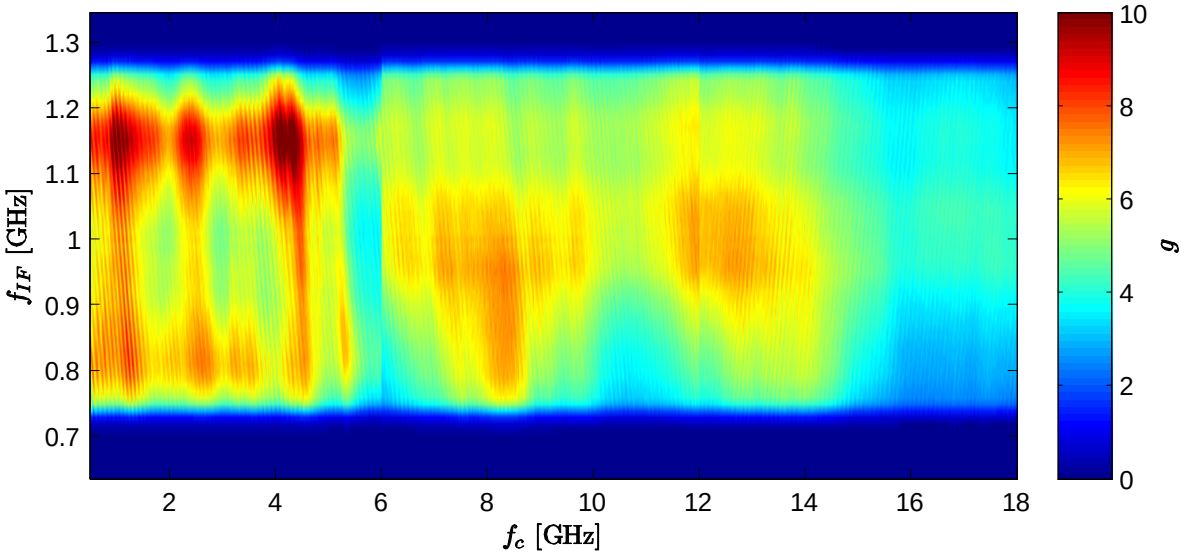

Figure 4.48 Downconverter channel 4 gain (linear scale).

Table 4.24 Measured voltage gain, within the passband, for downconverter channel 5.

	Linear Scale					Decibels				
f_c [GHz]	Max	Mean	Min	Ripple	Std Dev	Max	Mean	Min	Ripple	Std Dev
0.5	7.05	5.61	3.79	3.26	0.65	8.48	7.46	5.78	2.70	0.51
1	9.53	7.30	4.59	4.94	1.19	9.79	8.58	6.61	3.18	0.71
2	6.89	5.71	3.49	3.40	0.62	8.38	7.54	5.43	2.95	0.52
3	6.49	5.50	3.47	3.02	0.62	8.12	7.38	5.40	2.72	0.52
4	9.44	6.31	3.39	6.04	1.68	9.75	7.86	5.30	4.44	1.13
5	5.84	4.01	1.57	4.27	1.05	7.66	5.87	1.96	5.70	1.27
5.99	5.96	4.33	2.79	3.17	0.62	7.75	6.32	4.45	3.30	0.61
6	9.60	7.92	4.85	4.75	1.25	9.82	8.93	6.86	2.97	0.72
7	9.53	7.89	5.10	4.42	1.04	9.79	8.93	7.08	2.71	0.61
8	9.51	8.00	5.29	4.21	1.06	9.78	8.99	7.24	2.54	0.61
9	9.79	8.39	5.65	4.14	1.09	9.91	9.20	7.52	2.39	0.59
10	9.74	8.40	5.89	3.85	0.93	9.88	9.21	7.70	2.18	0.51
11	4.67	3.84	2.75	1.92	0.45	6.70	5.81	4.39	2.30	0.51
12	9.71	7.73	4.47	5.23	1.25	9.87	8.82	6.51	3.36	0.75
13	9.80	8.22	5.46	4.35	1.10	9.91	9.11	7.37	2.54	0.61
14	9.23	7.72	5.10	4.13	0.97	9.65	8.84	7.07	2.58	0.57
15	8.33	6.99	4.59	3.74	0.91	9.21	8.41	6.62	2.59	0.60
16	7.53	6.43	4.47	3.06	0.67	8.77	8.05	6.50	2.26	0.48
17	3.75	2.92	1.99	1.75	0.37	5.73	4.62	2.99	2.74	0.56
18	7.32	6.44	4.65	2.66	0.58	8.64	8.07	6.68	1.97	0.42

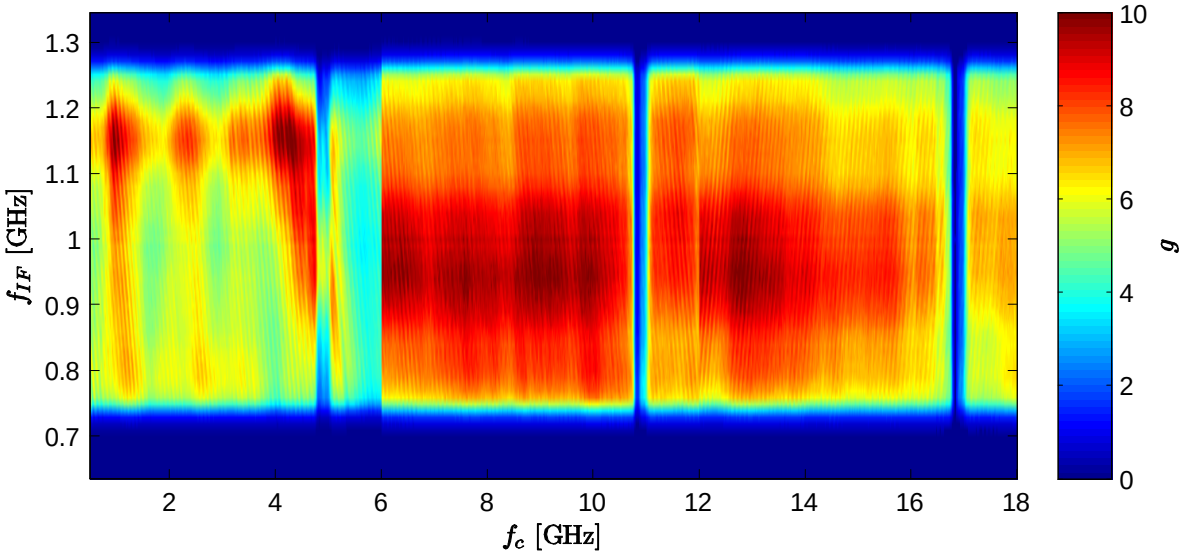

Figure 4.49 Downconverter channel 5 gain (linear scale).

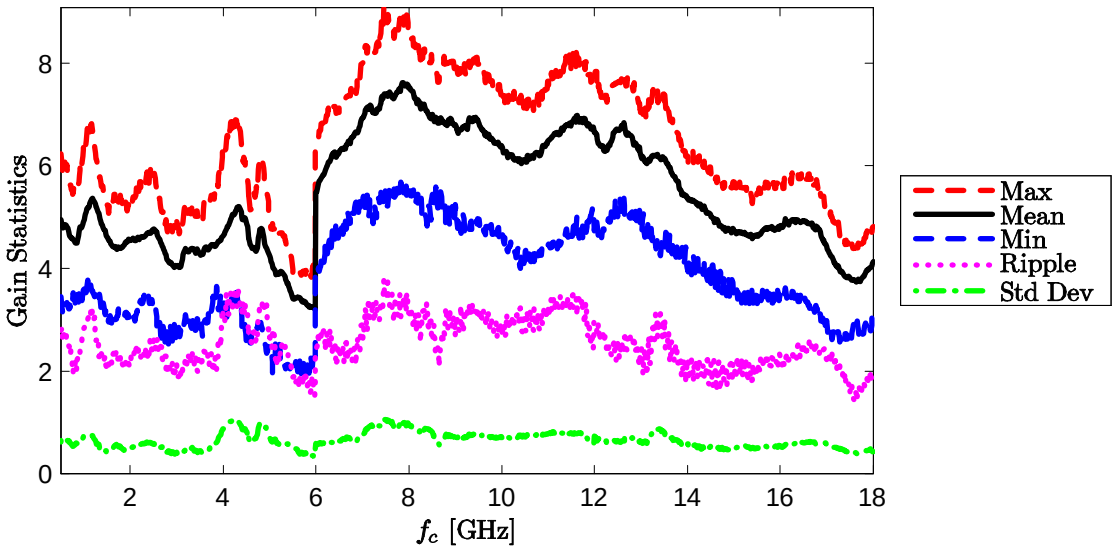

Figure 4.50 Channel 5 gain statistics, within the passband (linear scale).

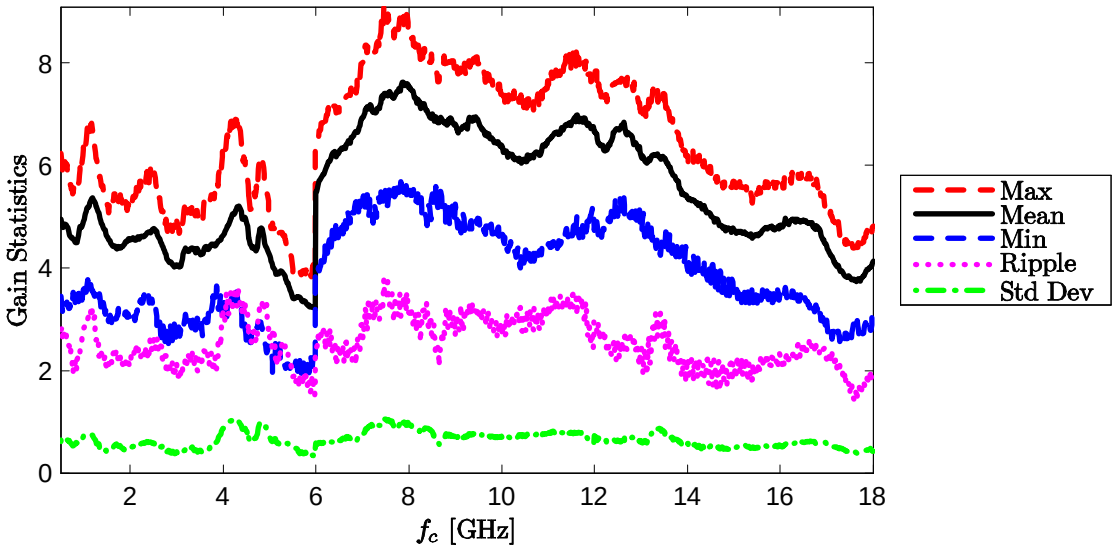

Figure 4.51 Channel 6 gain statistics, within the passband (linear scale).

Table 4.25 Measured voltage gain, within the passband, for downconverter channel 6.

	Linear Scale					Decibels				
f_c [GHz]	Max	Mean	Min	Ripple	Std Dev	Max	Mean	Min	Ripple	Std Dev
0.5	6.32	4.86	2.33	3.99	0.79	8.01	6.80	3.67	4.33	0.77
1	8.74	6.53	3.65	5.09	1.16	9.42	8.08	5.62	3.79	0.79
2	6.75	5.32	3.56	3.19	0.75	8.29	7.21	5.52	2.78	0.63
3	6.83	5.70	3.97	2.86	0.73	8.34	7.52	5.99	2.36	0.58
4	7.79	6.13	3.81	3.97	0.93	8.91	7.83	5.81	3.10	0.66
5	6.87	5.90	3.87	3.00	0.69	8.37	7.68	5.88	2.50	0.56
5.99	5.02	4.08	2.73	2.29	0.51	7.01	6.07	4.37	2.64	0.56
6	7.48	5.92	3.87	3.61	0.83	8.74	7.68	5.88	2.86	0.63
7	9.53	7.42	5.02	4.52	1.10	9.79	8.66	7.00	2.79	0.66
8	8.97	7.18	5.30	3.66	0.89	9.53	8.53	7.25	2.28	0.55
9	8.54	7.01	4.86	3.68	1.03	9.32	8.41	6.87	2.45	0.66
10	7.75	6.12	4.51	3.24	0.80	8.89	7.83	6.54	2.35	0.57
11	7.20	5.81	3.77	3.42	0.77	8.57	7.60	5.77	2.80	0.60
12	8.31	6.47	4.54	3.77	0.94	9.20	8.06	6.57	2.62	0.64
13	7.93	6.24	4.59	3.34	0.89	8.99	7.91	6.62	2.37	0.62
14	8.21	6.62	4.86	3.35	0.81	9.14	8.18	6.86	2.28	0.54
15	6.88	5.41	4.09	2.79	0.59	8.38	7.31	6.12	2.26	0.48
16	5.04	4.06	2.82	2.21	0.48	7.02	6.06	4.51	2.51	0.53
17	5.20	4.14	2.82	2.38	0.54	7.16	6.13	4.50	2.66	0.58
18	5.49	4.43	3.29	2.20	0.53	7.40	6.43	5.18	2.22	0.53

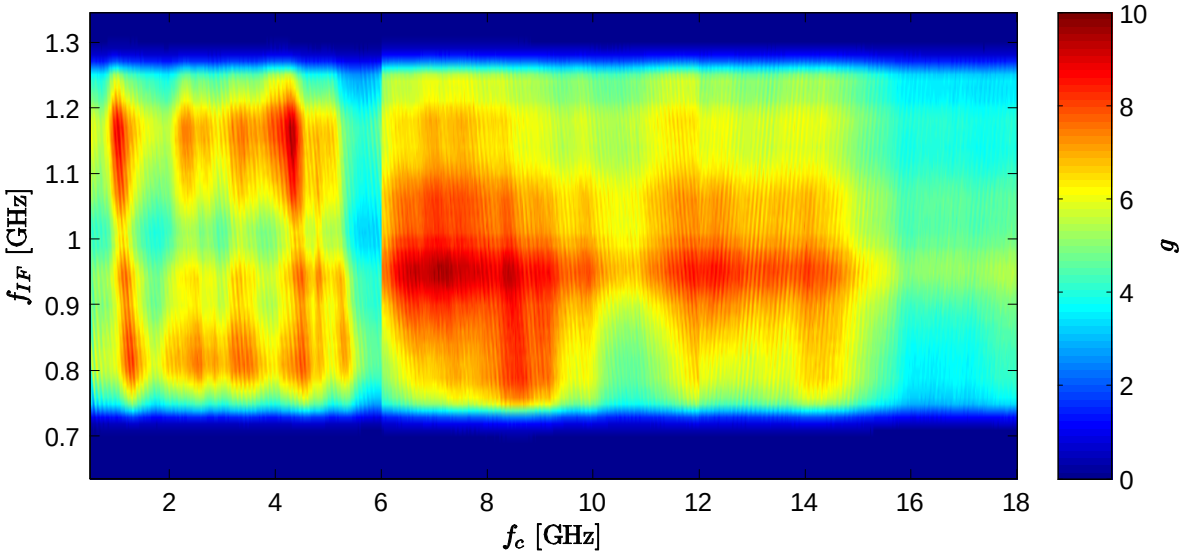

Figure 4.52 Downconverter channel 6 gain (linear scale).

Table 4.26 Measured voltage gain, within the passband, for downconverter channel 7.

	Linear Scale					Decibels				
f_c [GHz]	Max	Mean	Min	Ripple	Std Dev	Max	Mean	Min	Ripple	Std Dev
0.5	8.36	6.74	4.02	4.33	1.02	9.22	8.23	6.05	3.17	0.72
1	8.57	6.75	3.72	4.86	1.06	9.33	8.23	5.70	3.63	0.75
2	6.27	5.24	3.06	3.22	0.75	7.97	7.14	4.85	3.12	0.70
3	5.87	4.88	2.92	2.96	0.72	7.69	6.83	4.65	3.04	0.71
4	8.07	6.24	3.32	4.76	0.94	9.07	7.90	5.21	3.86	0.71
5	7.27	5.88	3.31	3.95	0.91	8.61	7.63	5.20	3.41	0.76
5.99	4.92	4.15	2.22	2.70	0.57	6.92	6.13	3.46	3.45	0.67
6	10.36	8.63	5.25	5.11	1.08	10.15	9.32	7.20	2.95	0.58
7	12.47	10.57	7.35	5.12	1.18	10.96	10.21	8.66	2.29	0.51
8	13.17	11.02	7.94	5.23	1.32	11.20	10.39	9.00	2.20	0.54
9	11.62	9.84	6.84	4.77	1.20	10.65	9.90	8.35	2.30	0.55
10	10.73	9.32	6.67	4.06	1.01	10.30	9.67	8.24	2.06	0.48
11	11.18	9.63	6.45	4.73	1.00	10.49	9.81	8.10	2.39	0.47
12	12.20	10.05	6.94	5.26	1.26	10.86	9.99	8.41	2.45	0.57
13	11.44	9.71	7.28	4.16	1.09	10.59	9.84	8.62	1.96	0.50
14	10.35	8.67	5.73	4.62	0.96	10.15	9.35	7.58	2.57	0.50
15	7.56	6.06	3.78	3.78	0.75	8.78	7.79	5.77	3.01	0.57
16	5.99	4.93	3.30	2.69	0.58	7.78	6.90	5.18	2.59	0.53
17	6.67	5.61	3.98	2.69	0.57	8.24	7.47	6.00	2.24	0.46
18	6.18	5.38	4.02	2.17	0.46	7.91	7.29	6.04	1.87	0.38

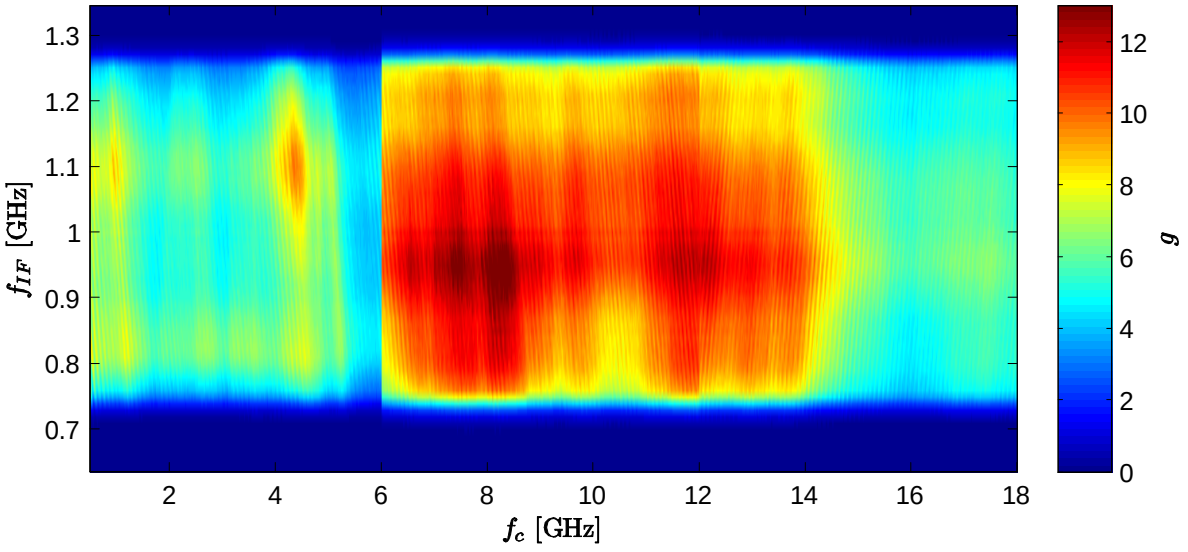

Figure 4.53 Downconverter channel 7 gain (linear scale).

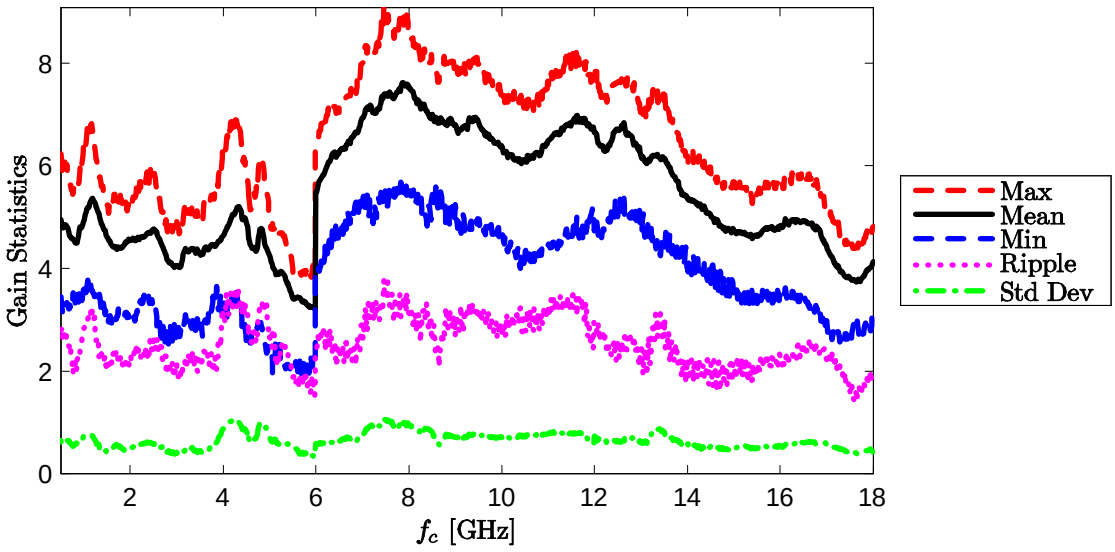

Figure 4.54 Channel 7 gain statistics, within the passband (linear scale).

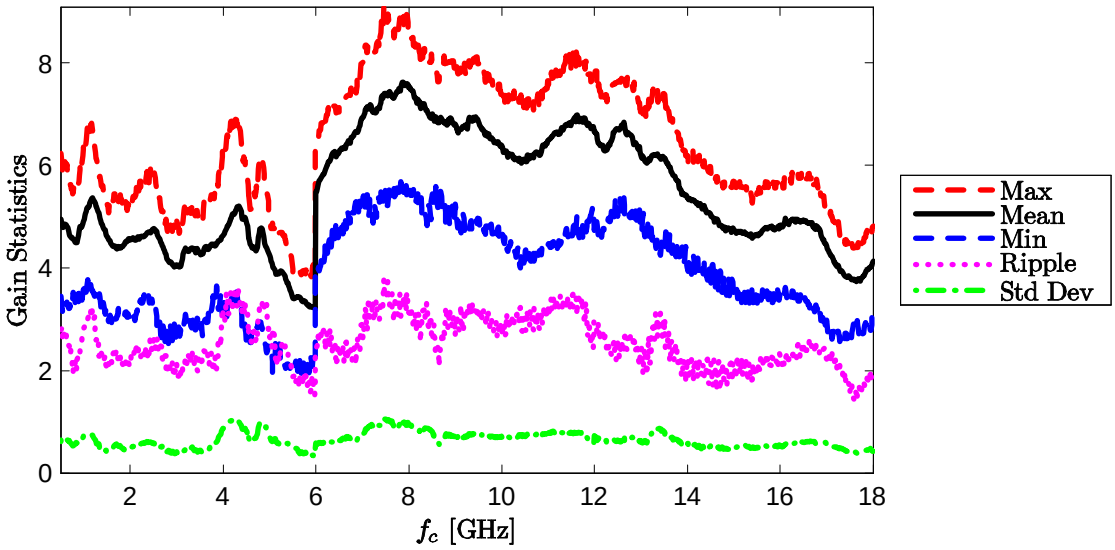

Figure 4.55 Channel 8 gain statistics, within the passband (linear scale).

Table 4.27 Measured voltage gain, within the passband, for downconverter channel 8.

	Linear Scale					Decibels				
f_c [GHz]	Max	Mean	Min	Ripple	Std Dev	Max	Mean	Min	Ripple	Std Dev
0.5	10.32	7.70	5.47	4.85	1.26	10.14	8.81	7.38	2.76	0.70
1	8.84	7.64	4.96	3.88	0.82	9.47	8.81	6.95	2.51	0.49
2	8.25	6.35	4.57	3.68	1.14	9.16	7.96	6.60	2.57	0.77
3	9.15	6.87	4.63	4.53	1.31	9.62	8.29	6.65	2.96	0.82
4	8.26	6.79	4.28	3.98	0.77	9.17	8.29	6.31	2.86	0.52
5	7.21	6.01	4.02	3.18	0.66	8.58	7.76	6.05	2.53	0.50
5.99	6.91	5.40	3.44	3.47	0.82	8.40	7.27	5.37	3.03	0.67
6	9.59	7.85	4.95	4.64	1.03	9.82	8.91	6.95	2.87	0.61
7	10.10	8.27	5.83	4.27	1.00	10.04	9.14	7.65	2.39	0.54
8	8.95	7.55	5.41	3.54	0.97	9.52	8.74	7.33	2.19	0.56
9	6.92	6.04	4.25	2.66	0.62	8.40	7.79	6.29	2.11	0.47
10	5.93	5.02	3.61	2.32	0.61	7.73	6.98	5.58	2.15	0.54
11	7.79	6.55	4.06	3.73	0.95	8.91	8.11	6.09	2.83	0.68
12	8.79	7.17	5.14	3.65	0.90	9.44	8.52	7.11	2.33	0.56
13	7.95	6.67	4.85	3.10	0.76	9.00	8.21	6.85	2.15	0.51
14	6.42	5.85	4.76	1.65	0.37	8.07	7.66	6.78	1.29	0.28
15	3.94	3.50	2.73	1.21	0.24	5.96	5.43	4.37	1.59	0.31
16	3.24	2.74	1.96	1.28	0.33	5.11	4.34	2.92	2.19	0.55
17	4.12	3.34	2.36	1.76	0.46	6.15	5.20	3.73	2.42	0.62
18	4.11	3.50	2.68	1.44	0.32	6.14	5.43	4.28	1.87	0.41

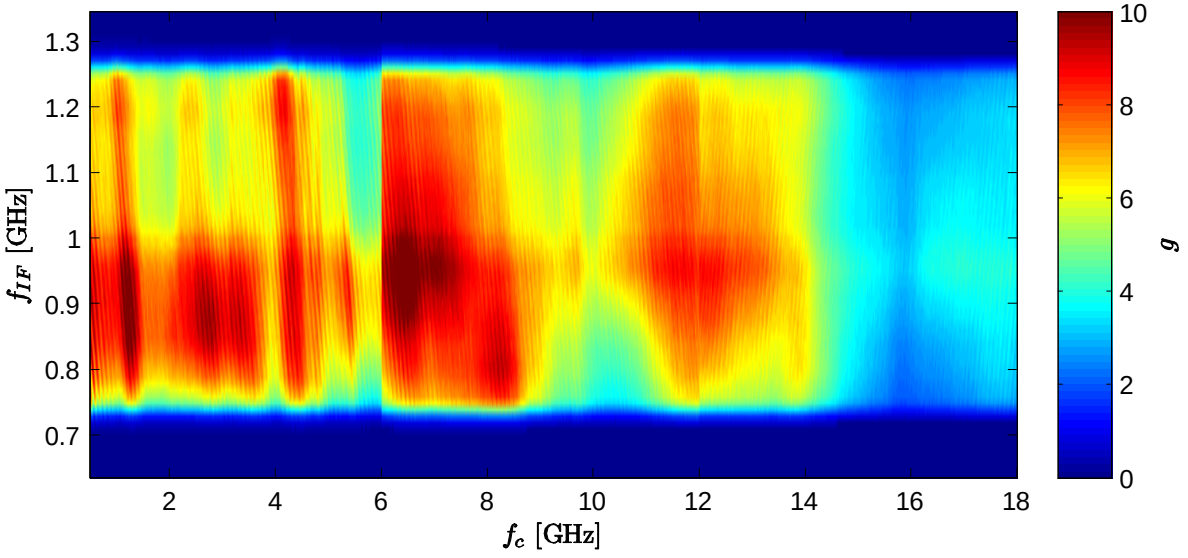

Figure 4.56 Downconverter channel 8 gain (linear scale).

Table 4.28 Measured voltage gain, within the passband, for downconverter channel 9.

	Linear Scale					Decibels				
f_c [GHz]	Max	Mean	Min	Ripple	Std Dev	Max	Mean	Min	Ripple	Std Dev
0.5	5.32	4.23	2.42	2.89	0.75	7.26	6.19	3.84	3.41	0.83
1	4.82	4.10	2.37	2.45	0.66	6.83	6.07	3.74	3.09	0.77
2	5.99	4.84	2.88	3.11	0.79	7.77	6.78	4.59	3.19	0.77
3	4.99	4.22	2.51	2.48	0.65	6.98	6.19	4.00	2.98	0.73
4	4.79	4.01	2.48	2.31	0.59	6.80	5.99	3.94	2.86	0.69
5	4.12	3.37	1.87	2.25	0.59	6.15	5.20	2.71	3.44	0.84
5.99	3.74	2.84	1.93	1.81	0.46	5.73	4.47	2.86	2.87	0.71
6	5.94	5.14	3.86	2.08	0.44	7.74	7.10	5.86	1.87	0.39
7	6.02	5.30	3.97	2.04	0.46	7.79	7.23	5.99	1.80	0.40
8	6.46	5.46	4.06	2.41	0.53	8.10	7.35	6.08	2.02	0.44
9	6.51	5.67	4.26	2.25	0.51	8.14	7.52	6.30	1.84	0.41
10	6.51	5.73	4.02	2.49	0.58	8.13	7.56	6.04	2.09	0.46
11	6.28	5.47	4.11	2.17	0.48	7.98	7.36	6.14	1.84	0.40
12	5.26	4.58	3.44	1.82	0.42	7.21	6.59	5.37	1.84	0.41
13	5.53	4.72	3.56	1.97	0.43	7.43	6.72	5.51	1.92	0.41
14	5.95	5.14	3.64	2.31	0.51	7.75	7.09	5.61	2.13	0.46
15	4.68	4.17	3.19	1.49	0.36	6.71	6.19	5.04	1.67	0.39
16	3.36	3.04	2.33	1.03	0.24	5.27	4.82	3.68	1.59	0.36
17	3.22	2.80	2.07	1.14	0.25	5.07	4.45	3.17	1.90	0.41
18	3.49	3.03	2.01	1.48	0.38	5.43	4.78	3.03	2.40	0.59

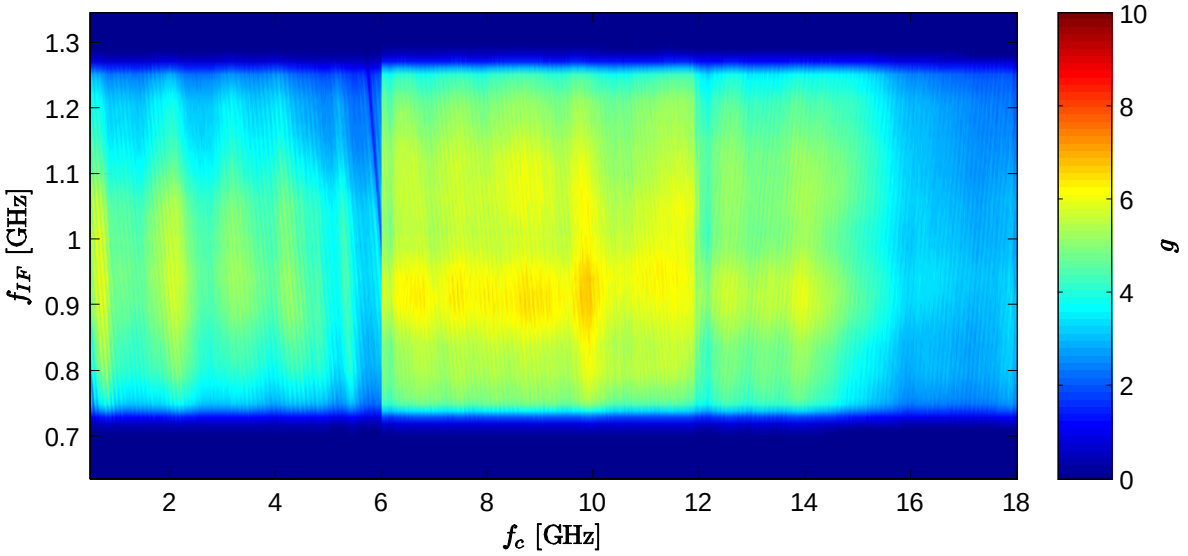

Figure 4.57 Downconverter channel 9 gain (linear scale).

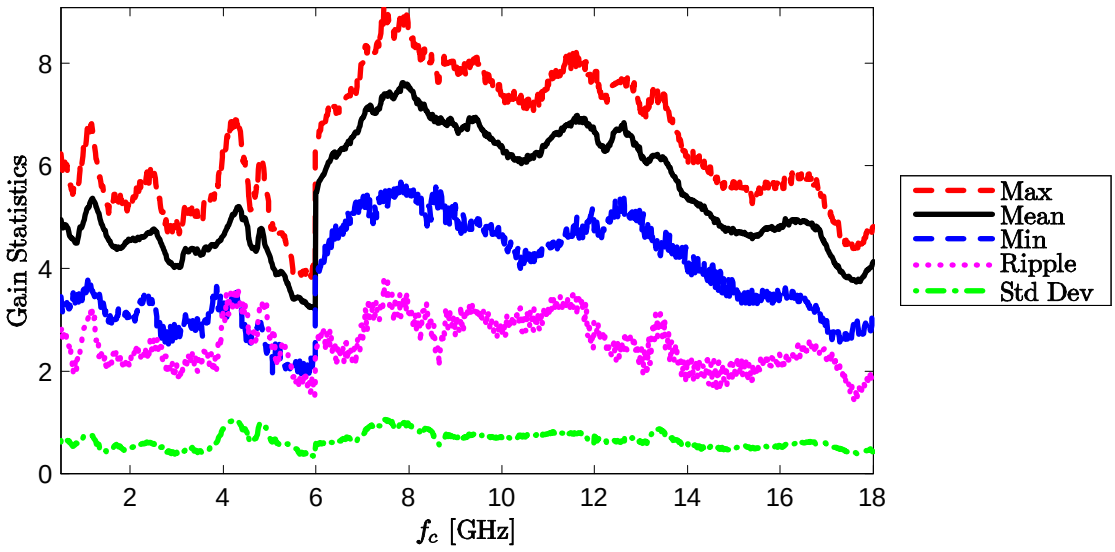

Figure 4.58 Channel 9 gain statistics, within the passband (linear scale).

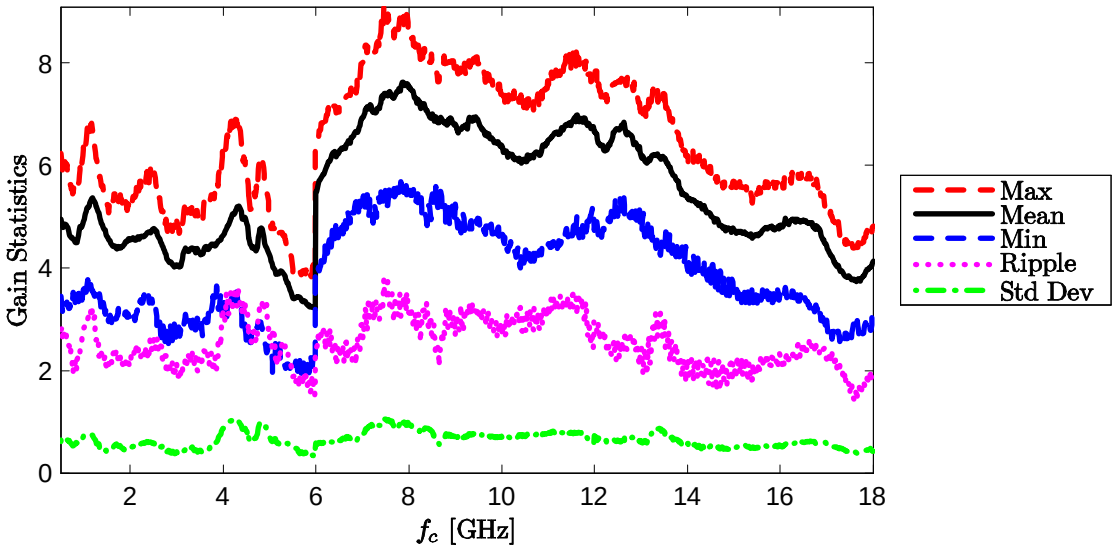

Figure 4.59 Channel 10 gain statistics, within the passband (linear scale).

Table 4.29 Measured voltage gain, within the passband, for downconverter channel 10.

	Linear Scale					Decibels				
f_c [GHz]	Max	Mean	Min	Ripple	Std Dev	Max	Mean	Min	Ripple	Std Dev
0.5	6.63	5.47	3.10	3.53	0.81	8.22	7.32	4.92	3.30	0.71
1	5.96	5.38	3.22	2.73	0.61	7.75	7.27	5.09	2.67	0.56
2	7.11	6.14	3.97	3.14	0.66	8.52	7.86	5.99	2.53	0.51
3	6.21	5.57	3.60	2.60	0.59	7.93	7.43	5.57	2.36	0.51
4	6.12	5.32	3.57	2.55	0.56	7.87	7.23	5.53	2.34	0.50
5	4.71	3.93	2.26	2.45	0.52	6.73	5.90	3.54	3.19	0.63
5.99	4.30	3.63	2.48	1.81	0.36	6.33	5.58	3.95	2.38	0.46
6	5.81	5.03	3.57	2.24	0.51	7.64	6.99	5.53	2.11	0.46
7	6.24	5.55	3.77	2.47	0.55	7.95	7.42	5.76	2.19	0.45
8	6.60	5.67	4.20	2.39	0.54	8.19	7.51	6.24	1.96	0.43
9	6.28	5.56	3.92	2.36	0.52	7.98	7.43	5.93	2.05	0.43
10	6.51	5.79	4.21	2.30	0.56	8.14	7.60	6.25	1.89	0.44
11	6.16	5.39	3.77	2.39	0.49	7.90	7.29	5.76	2.13	0.42
12	5.79	4.92	3.61	2.18	0.49	7.63	6.90	5.58	2.05	0.45
13	5.63	4.87	3.44	2.19	0.47	7.51	6.85	5.37	2.14	0.44
14	5.71	4.84	3.41	2.30	0.51	7.57	6.82	5.33	2.24	0.48
15	5.57	4.91	3.38	2.19	0.44	7.46	6.90	5.29	2.17	0.41
16	4.86	4.36	2.77	2.09	0.43	6.87	6.37	4.42	2.44	0.47
17	4.63	4.08	2.80	1.83	0.36	6.66	6.09	4.48	2.18	0.41
18	4.21	3.74	2.63	1.58	0.35	6.24	5.71	4.20	2.04	0.43

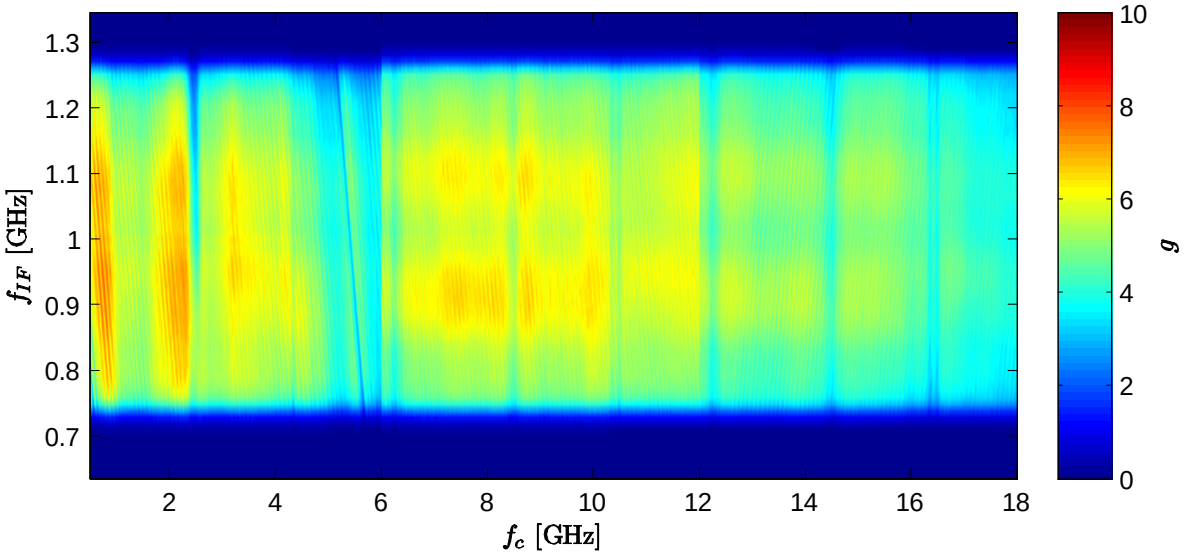

Figure 4.60 Downconverter channel 10 gain (linear scale).

Table 4.30 Measured voltage gain, within the passband, for downconverter channel 11.

	Linear Scale					Decibels				
f_c [GHz]	Max	Mean	Min	Ripple	Std Dev	Max	Mean	Min	Ripple	Std Dev
0.5	6.85	5.71	3.62	3.23	0.73	8.36	7.53	5.59	2.77	0.60
1	6.69	5.67	3.04	3.65	0.88	8.26	7.47	4.84	3.42	0.76
2	7.99	6.45	3.61	4.38	1.03	9.02	8.04	5.58	3.45	0.76
3	6.64	5.64	3.21	3.43	0.82	8.22	7.46	5.06	3.16	0.69
4	6.61	5.76	3.50	3.11	0.69	8.20	7.57	5.44	2.76	0.58
5	5.11	4.32	2.26	2.85	0.76	7.09	6.28	3.54	3.55	0.85
5.99	5.08	3.66	2.43	2.65	0.68	7.06	5.56	3.86	3.20	0.81
6	6.56	5.61	3.79	2.77	0.68	8.17	7.45	5.78	2.39	0.55
7	7.45	6.30	4.22	3.23	0.75	8.72	7.96	6.26	2.47	0.54
8	7.84	6.47	4.38	3.47	0.80	8.95	8.07	6.41	2.53	0.56
9	7.32	6.31	4.40	2.92	0.69	8.65	7.97	6.43	2.21	0.50
10	8.20	7.03	4.83	3.37	0.71	9.14	8.45	6.84	2.30	0.46
11	8.07	7.03	4.32	3.76	0.72	9.07	8.44	6.35	2.72	0.49
12	6.37	5.51	3.97	2.40	0.62	8.04	7.38	5.99	2.05	0.51
13	6.45	5.45	3.88	2.57	0.63	8.09	7.33	5.89	2.21	0.53
14	6.16	5.19	3.42	2.74	0.65	7.90	7.11	5.34	2.56	0.57
15	5.16	4.53	2.84	2.32	0.53	7.12	6.53	4.54	2.59	0.55
16	4.49	3.83	2.38	2.11	0.41	6.52	5.81	3.76	2.76	0.51
17	4.21	3.56	2.28	1.93	0.36	6.24	5.49	3.57	2.67	0.48
18	5.29	4.65	3.01	2.28	0.50	7.24	6.65	4.78	2.45	0.50

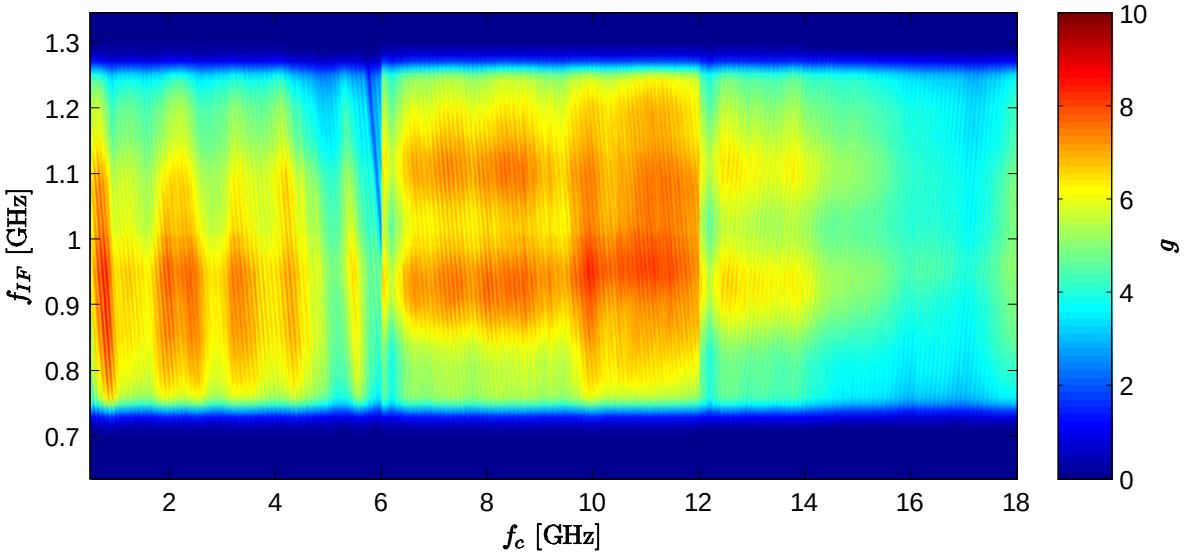

Figure 4.61 Downconverter channel 11 gain (linear scale).

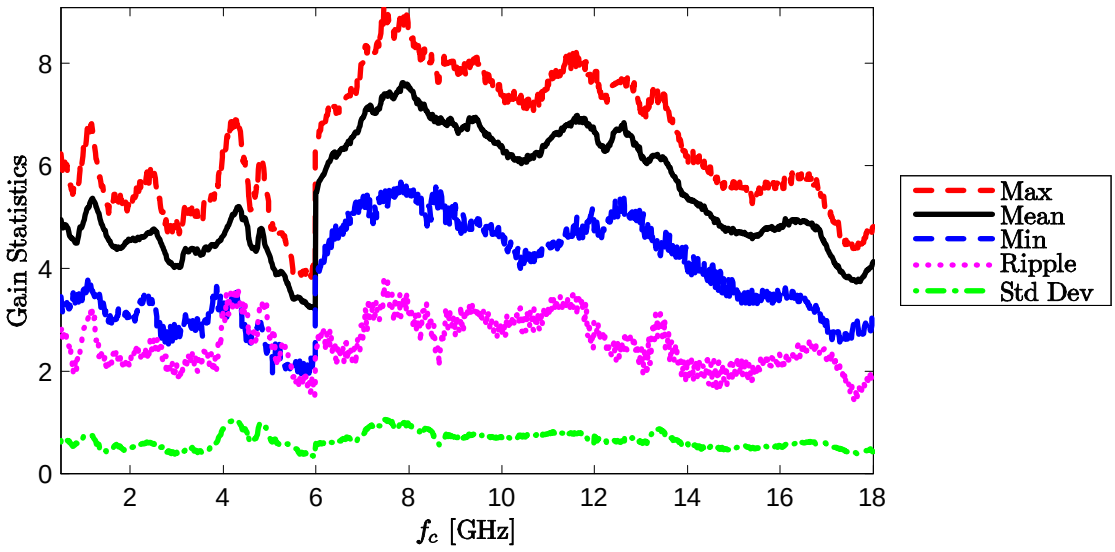

Figure 4.62 Channel 11 gain statistics, within the passband (linear scale).

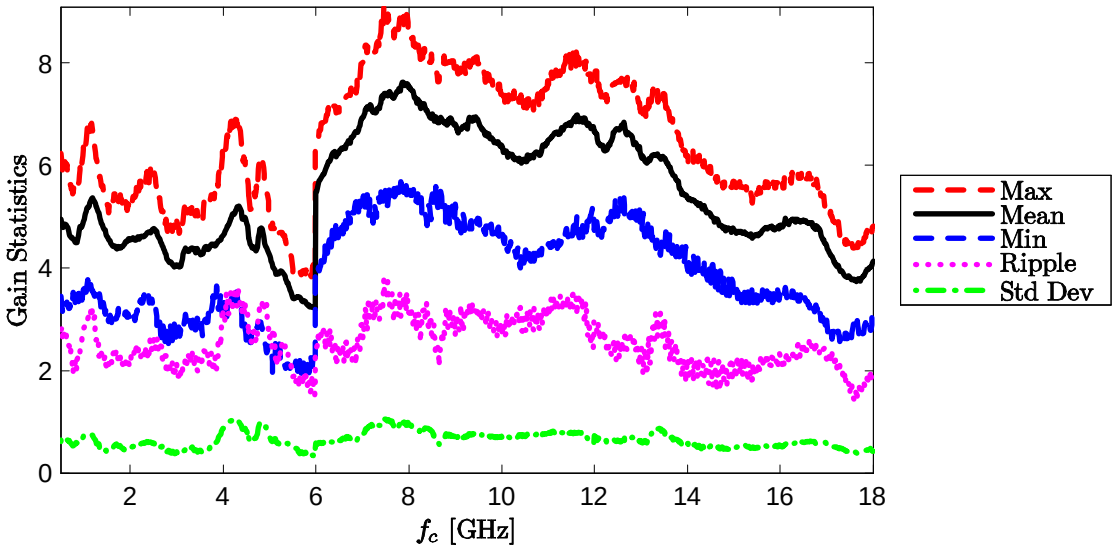

Figure 4.63 Channel 12 gain statistics, within the passband (linear scale).

Table 4.31 Measured voltage gain, within the passband, for downconverter channel 12.

	Linear Scale					Decibels				
f_c [GHz]	Max	Mean	Min	Ripple	Std Dev	Max	Mean	Min	Ripple	Std Dev
0.5	6.72	5.75	3.61	3.10	0.68	8.27	7.56	5.58	2.69	0.55
1	6.43	5.46	3.41	3.02	0.72	8.09	7.33	5.33	2.76	0.61
2	6.98	5.82	3.85	3.13	0.71	8.44	7.61	5.86	2.58	0.56
3	6.65	5.77	3.55	3.10	0.75	8.23	7.57	5.50	2.72	0.61
4	6.34	5.53	3.64	2.70	0.61	8.02	7.40	5.61	2.41	0.51
5	5.48	4.35	2.58	2.90	0.73	7.39	6.32	4.12	3.27	0.78
5.99	4.54	3.67	2.38	2.17	0.64	6.58	5.58	3.76	2.82	0.80
6	5.93	5.15	3.72	2.21	0.50	7.73	7.10	5.70	2.03	0.44
7	6.12	5.34	3.91	2.22	0.51	7.87	7.25	5.92	1.95	0.43
8	6.23	5.39	3.83	2.40	0.53	7.95	7.29	5.83	2.11	0.45
9	6.77	5.85	4.24	2.52	0.55	8.30	7.65	6.28	2.03	0.43
10	7.03	6.21	4.25	2.77	0.60	8.47	7.91	6.29	2.18	0.46
11	6.66	5.85	4.15	2.51	0.51	8.23	7.65	6.18	2.06	0.41
12	6.14	5.20	3.80	2.34	0.50	7.88	7.14	5.79	2.09	0.44
13	5.64	4.86	3.51	2.13	0.49	7.51	6.85	5.45	2.06	0.45
14	6.05	5.30	3.71	2.34	0.54	7.82	7.22	5.70	2.12	0.46
15	5.47	4.85	3.32	2.16	0.46	7.38	6.84	5.21	2.18	0.44
16	4.33	3.84	2.51	1.82	0.36	6.37	5.83	4.00	2.36	0.45
17	3.82	3.37	2.41	1.41	0.28	5.82	5.26	3.83	2.00	0.40
18	4.55	4.07	2.78	1.76	0.41	6.58	6.07	4.44	2.13	0.48

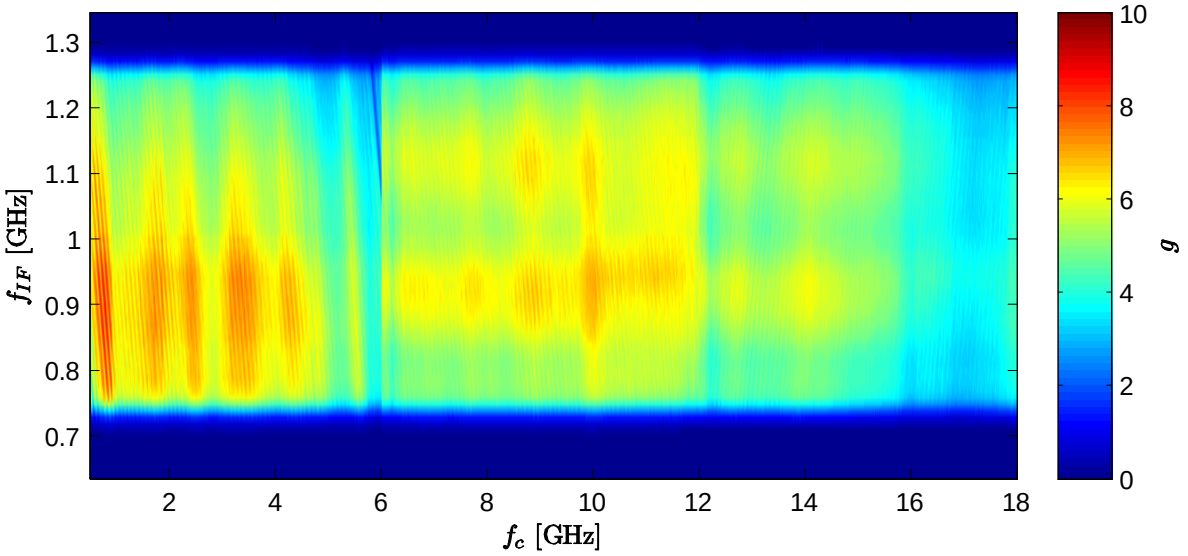

Figure 4.64 Downconverter channel 12 gain (linear scale).

Table 4.32 Measured voltage gain, within the passband, for downconverter channel 13.

	Linear Scale					Decibels				
f_c [GHz]	Max	Mean	Min	Ripple	Std Dev	Max	Mean	Min	Ripple	Std Dev
0.5	6.91	6.04	4.06	2.85	0.69	8.40	7.78	6.09	2.31	0.53
1	6.85	5.94	3.97	2.88	0.77	8.36	7.70	5.99	2.37	0.61
2	6.71	5.86	4.15	2.56	0.64	8.26	7.65	6.18	2.09	0.51
3	6.82	6.23	4.28	2.54	0.64	8.34	7.92	6.32	2.02	0.48
4	6.44	5.43	3.56	2.88	0.70	8.09	7.31	5.52	2.57	0.60
5	5.37	4.11	2.58	2.78	0.72	7.30	6.07	4.12	3.17	0.79
5.99	4.38	3.65	2.83	1.54	0.31	6.41	5.61	4.52	1.89	0.38
6	6.54	5.69	4.34	2.20	0.58	8.16	7.53	6.38	1.78	0.46
7	6.74	5.80	4.55	2.19	0.53	8.29	7.62	6.58	1.71	0.40
8	6.46	5.47	4.14	2.33	0.54	8.11	7.35	6.17	1.94	0.44
9	7.31	6.39	4.93	2.38	0.67	8.64	8.03	6.93	1.71	0.47
10	7.04	6.21	4.72	2.32	0.60	8.48	7.91	6.74	1.74	0.44
11	6.94	6.16	4.46	2.48	0.56	8.41	7.88	6.50	1.92	0.41
12	5.79	5.15	3.83	1.96	0.50	7.62	7.09	5.83	1.79	0.44
13	5.61	4.92	3.93	1.69	0.47	7.49	6.90	5.94	1.55	0.42
14	6.06	5.27	3.93	2.13	0.53	7.82	7.20	5.94	1.88	0.46
15	5.56	4.93	3.25	2.31	0.58	7.45	6.90	5.12	2.33	0.56
16	4.01	3.56	2.29	1.72	0.39	6.03	5.49	3.60	2.43	0.52
17	3.54	3.06	2.24	1.31	0.28	5.49	4.84	3.50	2.00	0.41
18	4.62	4.05	2.94	1.68	0.46	6.65	6.04	4.69	1.96	0.52

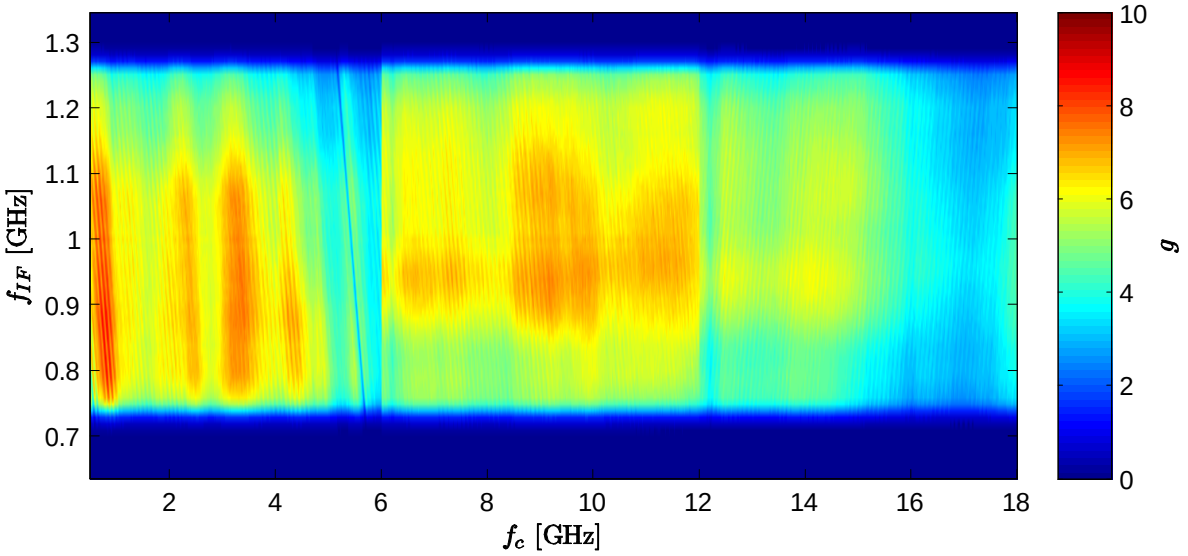

Figure 4.65 Downconverter channel 13 gain (linear scale).

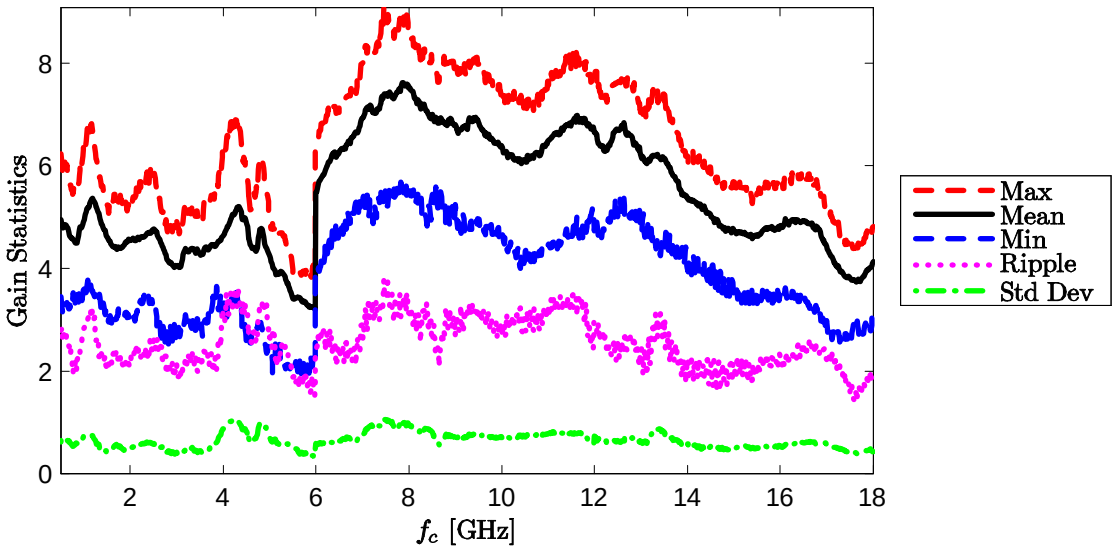

Figure 4.66 Channel 13 gain statistics, within the passband (linear scale).

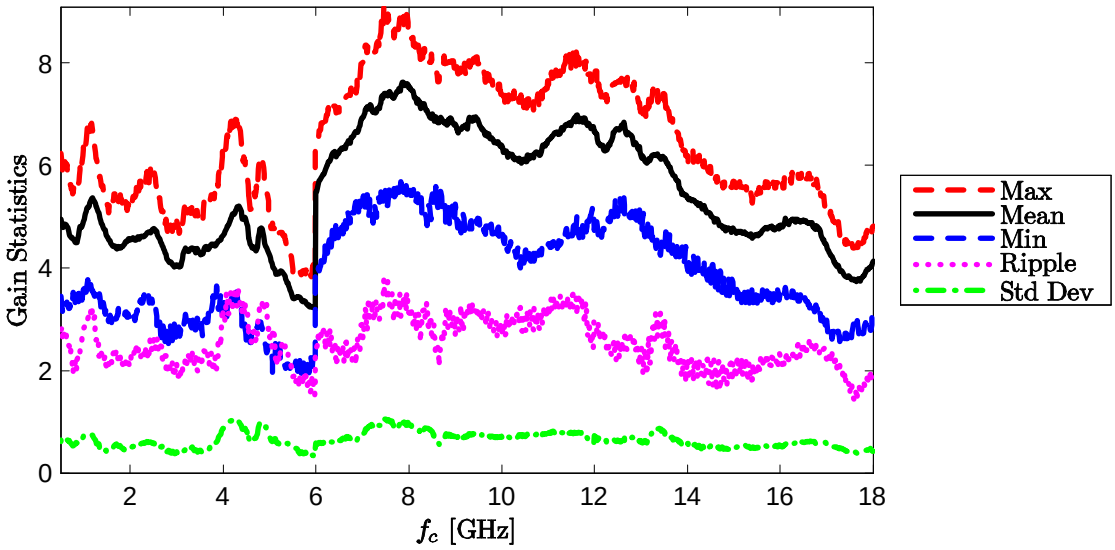

Figure 4.67 Channel 14 gain statistics, within the passband (linear scale).

Table 4.33 Measured voltage gain, within the passband, for downconverter channel 14.

	Linear Scale					Decibels				
f_c [GHz]	Max	Mean	Min	Ripple	Std Dev	Max	Mean	Min	Ripple	Std Dev
0.5	7.83	6.47	3.94	3.89	1.04	8.94	8.05	5.95	2.98	0.77
1	7.32	6.12	2.87	4.45	1.07	8.64	7.79	4.58	4.07	0.89
2	8.63	6.76	3.49	5.14	1.12	9.36	8.23	5.43	3.93	0.81
3	7.76	6.48	3.10	4.66	1.13	8.90	8.04	4.91	3.99	0.87
4	7.41	6.09	3.19	4.22	0.90	8.70	7.79	5.04	3.66	0.73
5	5.93	4.72	2.21	3.72	0.92	7.73	6.64	3.45	4.28	0.97
5.99	4.90	3.92	2.25	2.66	0.73	6.91	5.84	3.52	3.39	0.91
6	6.64	5.63	4.08	2.56	0.58	8.22	7.49	6.10	2.12	0.46
7	7.42	6.37	4.73	2.68	0.61	8.70	8.02	6.75	1.95	0.43
8	7.40	6.19	4.38	3.03	0.66	8.69	7.89	6.41	2.28	0.48
9	7.74	6.61	4.96	2.78	0.67	8.89	8.18	6.95	1.93	0.46
10	7.44	6.34	4.51	2.93	0.72	8.72	7.99	6.55	2.17	0.52
11	6.66	5.63	4.11	2.55	0.52	8.23	7.49	6.14	2.10	0.42
12	6.61	5.51	3.85	2.76	0.59	8.20	7.39	5.86	2.35	0.49
13	6.83	5.74	4.16	2.66	0.59	8.34	7.56	6.19	2.15	0.46
14	7.06	6.07	4.24	2.82	0.64	8.49	7.81	6.27	2.21	0.48
15	6.13	5.57	3.86	2.27	0.53	7.87	7.43	5.87	2.01	0.45
16	4.76	4.31	2.88	1.89	0.42	6.78	6.32	4.59	2.19	0.46
17	4.81	4.07	2.92	1.89	0.39	6.82	6.08	4.66	2.16	0.43
18	5.51	4.70	3.17	2.33	0.51	7.41	6.70	5.02	2.39	0.50

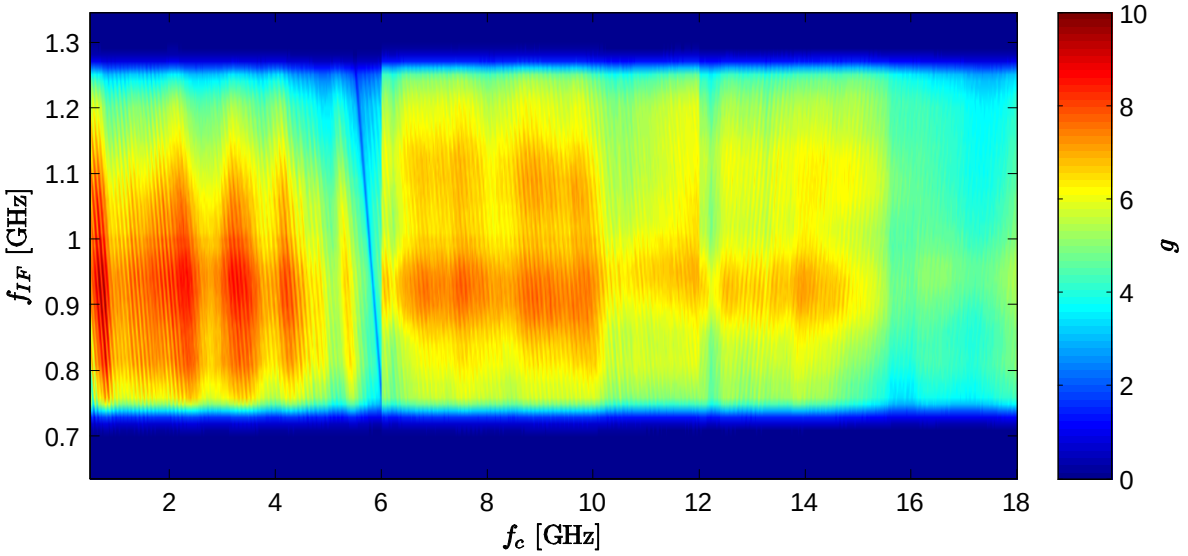

Figure 4.68 Downconverter channel 14 gain (linear scale).

Table 4.34 Measured voltage gain, within the passband, for downconverter channel 15.

	Linear Scale					Decibels				
f_c [GHz]	Max	Mean	Min	Ripple	Std Dev	Max	Mean	Min	Ripple	Std Dev
0.5	7.54	6.45	4.68	2.86	0.80	8.77	8.06	6.70	2.07	0.58
1	6.65	5.73	3.55	3.09	0.73	8.23	7.54	5.51	2.72	0.61
2	6.97	5.81	3.84	3.13	0.73	8.43	7.60	5.84	2.59	0.58
3	7.03	5.92	3.61	3.42	0.84	8.47	7.68	5.57	2.89	0.67
4	6.61	5.74	3.86	2.75	0.59	8.20	7.57	5.86	2.34	0.48
5	5.39	4.54	2.73	2.66	0.66	7.32	6.52	4.37	2.95	0.69
5.99	4.81	4.13	2.95	1.86	0.44	6.82	6.14	4.70	2.12	0.48
6	6.29	5.55	4.40	1.89	0.58	7.99	7.42	6.44	1.55	0.46
7	6.74	5.76	4.56	2.19	0.60	8.29	7.58	6.59	1.70	0.47
8	6.85	5.64	4.30	2.55	0.62	8.36	7.49	6.34	2.02	0.49
9	6.77	5.84	4.51	2.27	0.59	8.31	7.64	6.54	1.77	0.46
10	7.17	6.22	4.78	2.39	0.60	8.55	7.91	6.79	1.76	0.44
11	7.19	6.29	4.65	2.54	0.56	8.57	7.97	6.67	1.90	0.40
12	6.02	5.25	4.17	1.85	0.54	7.79	7.18	6.20	1.59	0.46
13	5.53	4.69	3.70	1.83	0.48	7.43	6.69	5.68	1.74	0.46
14	6.18	5.34	4.23	1.95	0.55	7.91	7.25	6.26	1.64	0.46
15	5.15	4.43	3.25	1.90	0.47	7.12	6.44	5.12	2.00	0.48
16	4.32	3.64	2.62	1.70	0.38	6.35	5.59	4.18	2.17	0.47
17	4.05	3.45	2.61	1.44	0.33	6.07	5.36	4.16	1.91	0.43
18	4.63	4.14	3.13	1.51	0.40	6.66	6.15	4.95	1.71	0.44

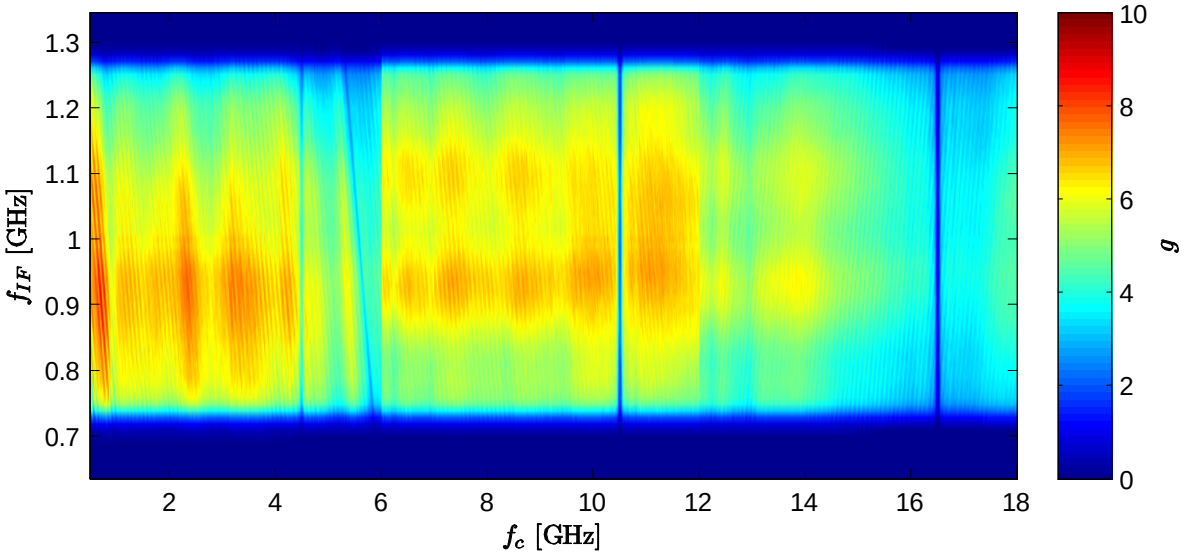

Figure 4.69 Downconverter channel 15 gain (linear scale).

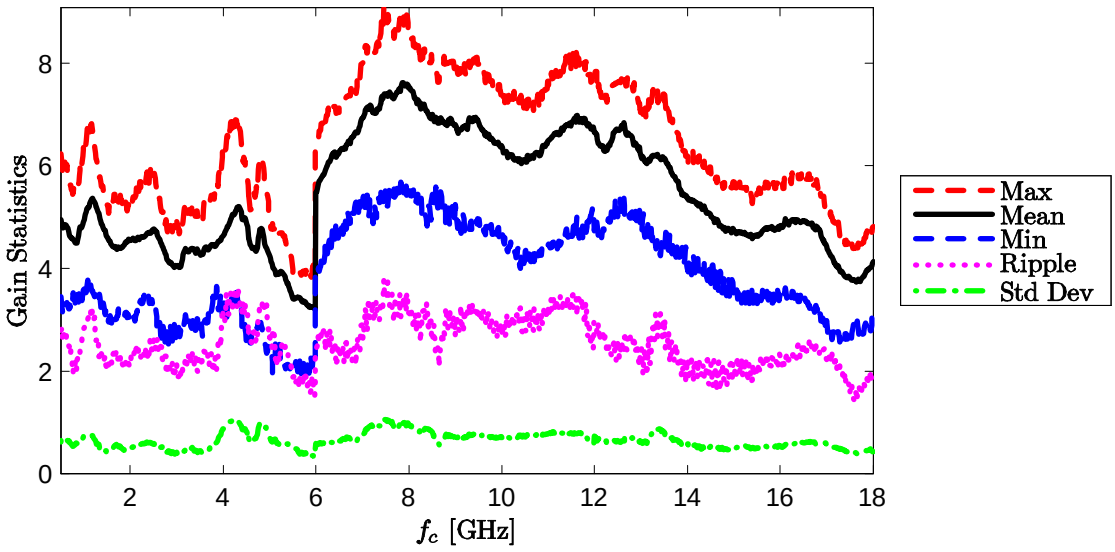

Figure 4.70 Channel 15 gain statistics, within the passband (linear scale).

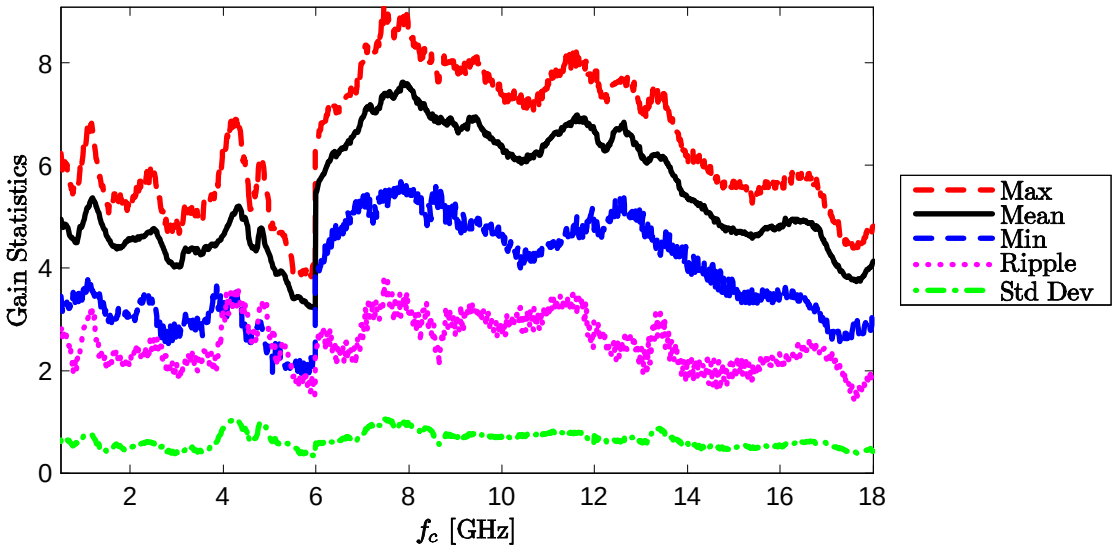

Figure 4.71 Channel 16 gain statistics, within the passband (linear scale).

Table 4.35 Measured voltage gain, within the passband, for downconverter channel 16.

	Linear Scale					Decibels				
f_c [GHz]	Max	Mean	Min	Ripple	Std Dev	Max	Mean	Min	Ripple	Std Dev
0.5	7.11	6.06	3.62	3.48	0.89	8.52	7.77	5.59	2.93	0.70
1	6.43	5.63	3.61	2.82	0.69	8.09	7.47	5.58	2.51	0.58
2	6.85	5.81	4.06	2.79	0.68	8.36	7.61	6.09	2.27	0.54
3	7.03	6.02	4.13	2.90	0.73	8.47	7.76	6.16	2.31	0.56
4	7.14	5.86	4.07	3.07	0.70	8.54	7.65	6.10	2.44	0.55
5	4.91	4.22	2.96	1.95	0.48	6.91	6.22	4.71	2.20	0.53
5.99	4.55	3.91	2.90	1.65	0.39	6.58	5.90	4.62	1.96	0.46
6	6.66	5.65	4.50	2.16	0.52	8.23	7.50	6.53	1.71	0.40
7	7.01	6.01	5.01	2.00	0.50	8.46	7.78	7.00	1.46	0.37
8	7.12	5.98	4.82	2.31	0.51	8.53	7.75	6.83	1.70	0.37
9	7.60	6.62	5.47	2.14	0.59	8.81	8.19	7.38	1.43	0.39
10	8.05	6.88	5.57	2.48	0.60	9.06	8.36	7.46	1.60	0.39
11	7.61	6.57	5.14	2.48	0.52	8.82	8.16	7.11	1.71	0.35
12	6.34	5.49	4.59	1.75	0.48	8.02	7.38	6.62	1.40	0.38
13	6.43	5.50	4.57	1.86	0.49	8.08	7.38	6.60	1.48	0.39
14	7.06	5.94	4.58	2.48	0.54	8.49	7.72	6.61	1.88	0.41
15	6.01	5.40	4.26	1.75	0.51	7.79	7.30	6.29	1.50	0.43
16	5.14	4.45	3.36	1.77	0.39	7.11	6.47	5.27	1.84	0.40
17	4.37	3.85	3.28	1.10	0.28	6.41	5.84	5.16	1.25	0.32
18	5.51	4.84	3.77	1.74	0.42	7.41	6.83	5.77	1.64	0.39

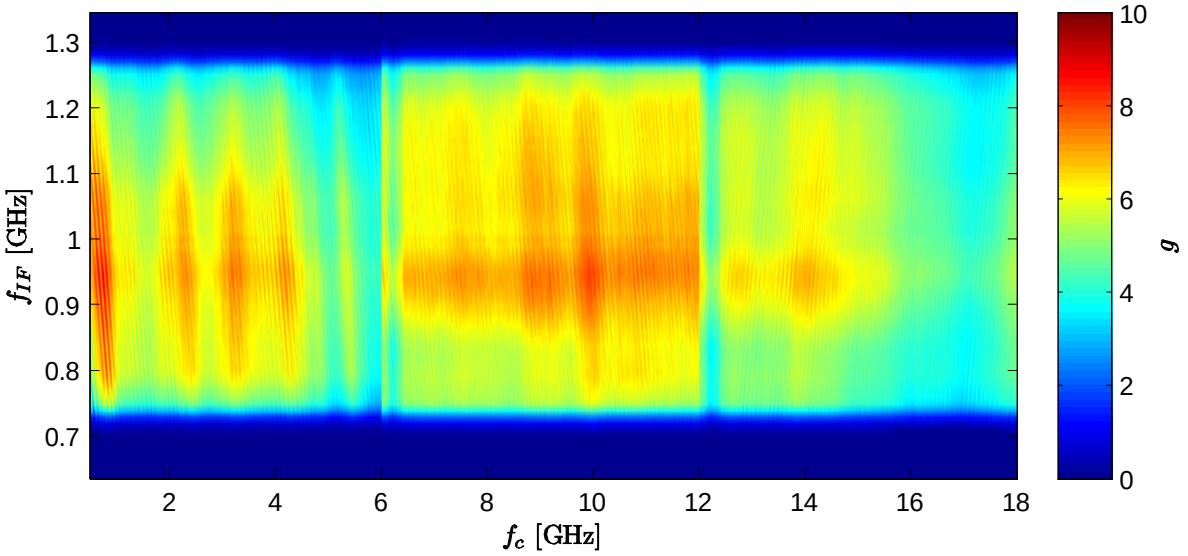

Figure 4.72 Downconverter channel 16 gain (linear scale).

Table 4.36 Summary statistics for the microwave block downconverter gain measurements, within the passband.

	Linear Scale					Decibels				
f_c [GHz]	Max	Mean	Min	Range	Std Dev	Max	Mean	Min	Range	Std Dev
0.5	10.32	5.87	2.33	7.99	1.18	10.14	7.59	3.67	6.46	0.92
1	10.42	5.99	2.37	8.05	1.31	10.18	7.67	3.74	6.44	0.98
2	8.63	5.71	2.72	5.90	1.00	9.36	7.50	4.35	5.01	0.80
3	9.15	5.59	2.51	6.64	1.08	9.62	7.38	4.00	5.61	0.88
4	9.62	5.77	2.48	7.15	1.15	9.83	7.52	3.94	5.90	0.89
5	7.61	4.77	1.57	6.04	1.15	8.81	6.65	1.96	6.86	1.10
5.99	6.91	3.92	1.93	4.98	0.79	8.40	5.84	2.86	5.54	0.89
6	10.36	6.13	2.64	7.72	1.36	10.15	7.77	4.21	5.94	0.93
7	12.47	6.74	3.71	8.76	1.55	10.96	8.18	5.69	5.26	0.93
8	13.17	6.79	3.83	9.34	1.61	11.20	8.21	5.83	5.36	0.95
9	11.62	6.72	3.92	7.70	1.36	10.65	8.20	5.93	4.72	0.83
10	10.73	6.53	3.41	7.31	1.29	10.30	8.07	5.33	4.97	0.84
11	11.18	6.16	2.75	8.44	1.34	10.49	7.80	4.39	6.09	0.95
12	12.20	6.18	3.44	8.76	1.55	10.86	7.79	5.37	5.50	1.00
13	11.44	6.08	3.44	8.00	1.53	10.59	7.72	5.37	5.22	1.01
14	10.35	5.98	3.41	6.94	1.25	10.15	7.68	5.33	4.82	0.85
15	8.33	5.02	2.49	5.85	1.00	9.21	6.92	3.96	5.25	0.86
16	7.53	4.12	1.85	5.67	0.99	8.77	6.03	2.68	6.08	1.03
17	6.67	3.75	1.77	4.90	0.87	8.24	5.62	2.49	5.75	0.99
18	7.32	4.33	2.01	5.31	0.95	8.64	6.26	3.03	5.62	0.95

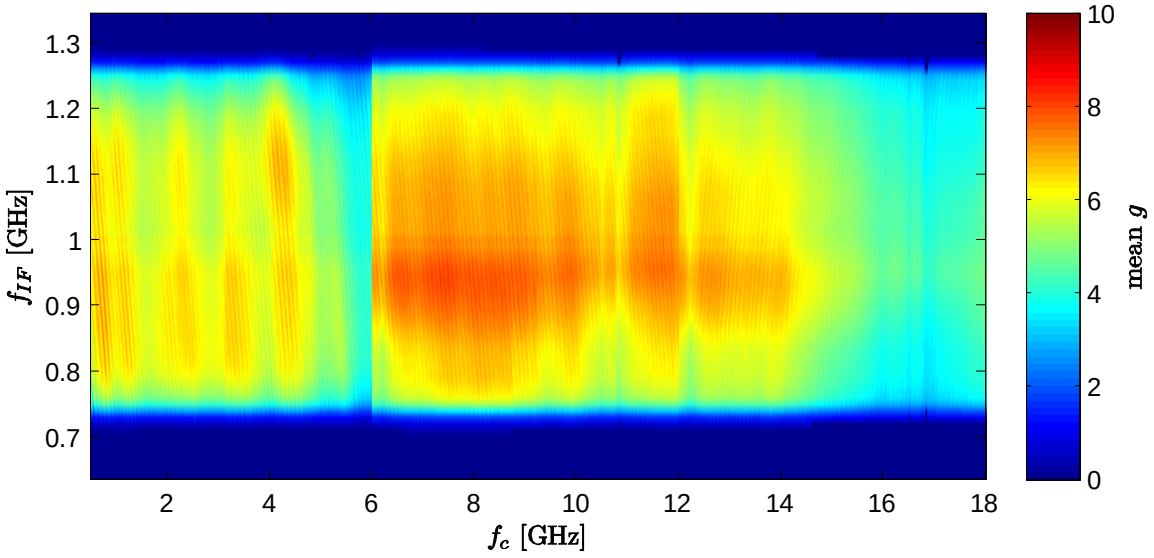

Figure 4.73 Average gain of the sixteen downconverter channels, at each point in the frequency spectrum.

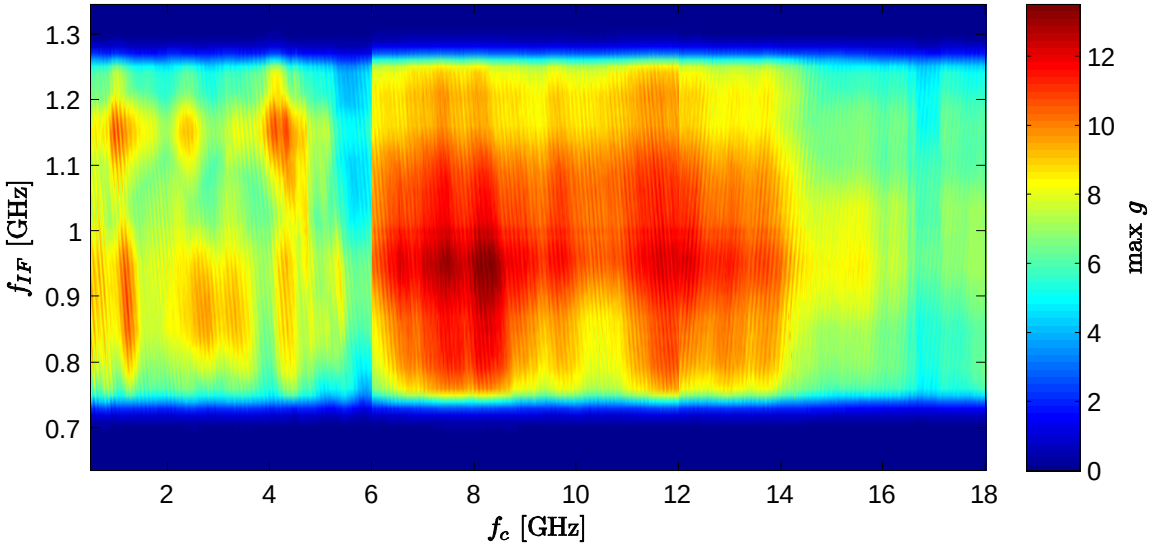

Figure 4.74 Maximum gain of the sixteen downconverter channels, at each point in the frequency spectrum.

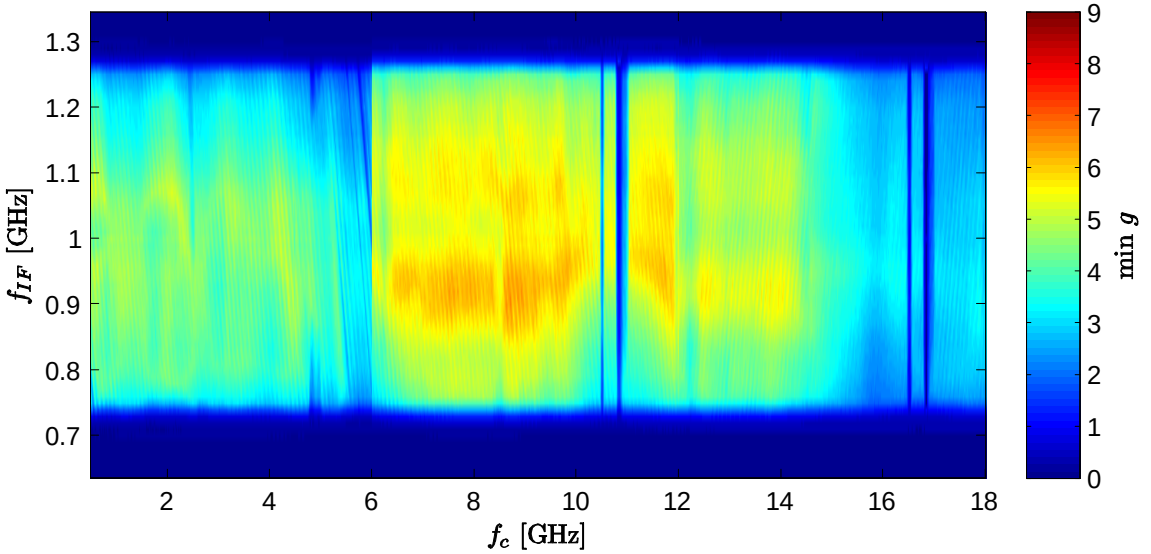

Figure 4.75 Minimum gain of the sixteen downconverter channels, at each point in the frequency spectrum.

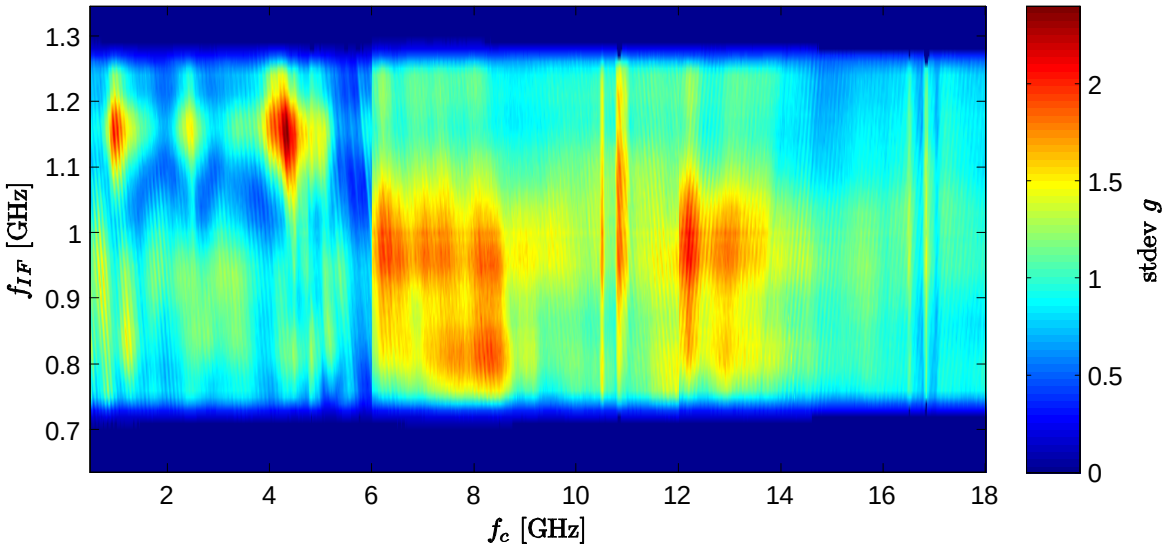

Figure 4.76 Standard deviation of the gains of the sixteen downconverter channels, at each point in the frequency spectrum.

4.3 Antenna Patterns

4.3.1 Array Columns Individually. A total of 1824 antenna patterns were measured for each of the sixteen columns, two polarizations, and 57 frequencies from 2.6 to 8.2 GHz. Typical examples are illustrated in Figs. 4.77-4.79 (note transposition of axes). The test setup was as shown in Fig. 3.8. In all cases, the transmitted signal was linearly polarized, and co-polarized with the the MCWESS antenna. All antenna patterns A_k are presented in dBi, meaning dB power gain relative to an isotropic antenna; recall that the comparison with the standard gain horn described in Section 3.4.1 makes knowledge of the absolute gain possible. Under this test setup, the NSI2000 did not collect enough data to show the entire beamwidth along the azimuth axis; the superelements were designed to have a 120° beamwidth in azimuth. Clearly, the beamwidth along the elevation axis is strongly dependent on the frequency f_{in}.

There are several observations we can use to characterize the measured antenna patterns. The antenna gain $A_{k,max}$ is defined as

$$A_{k,max} \equiv \max_{\phi,\theta} A_k(\phi,\theta)\,. \tag{4.1}$$

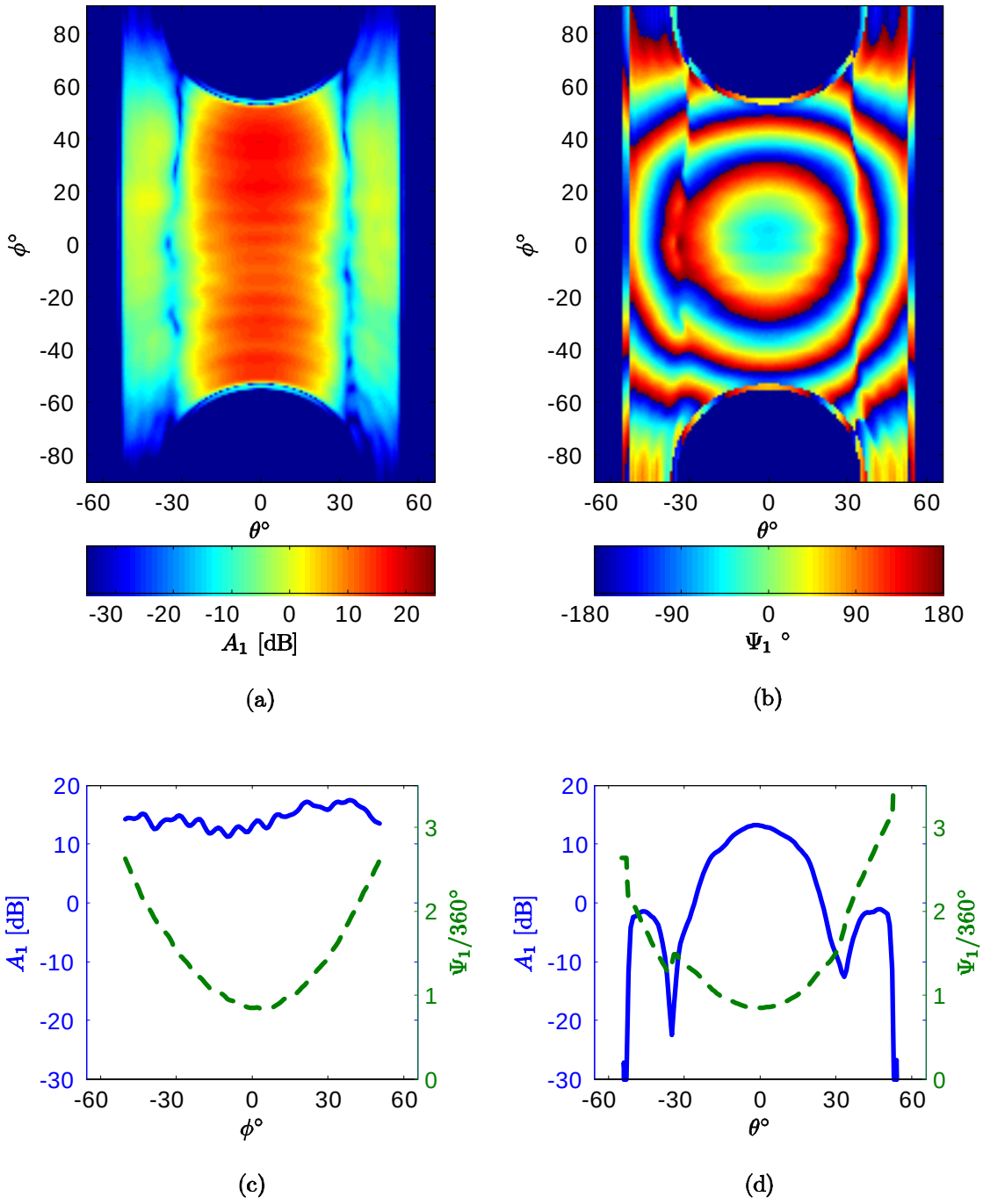

Figure 4.77 (a) Measured antenna directivity A_1 in dBi for column #1 of the MCWESS at 3 GHz (horizontally polarized). (b) Phase pattern Ψ_1. (c) Azimuth cut, $\theta = 0$, and $\psi_1 = \Psi_1(0,0) = 305°$. (d) Elevation cut, $\phi = 0$. Measurements were conducted using OEWG probe WR284.

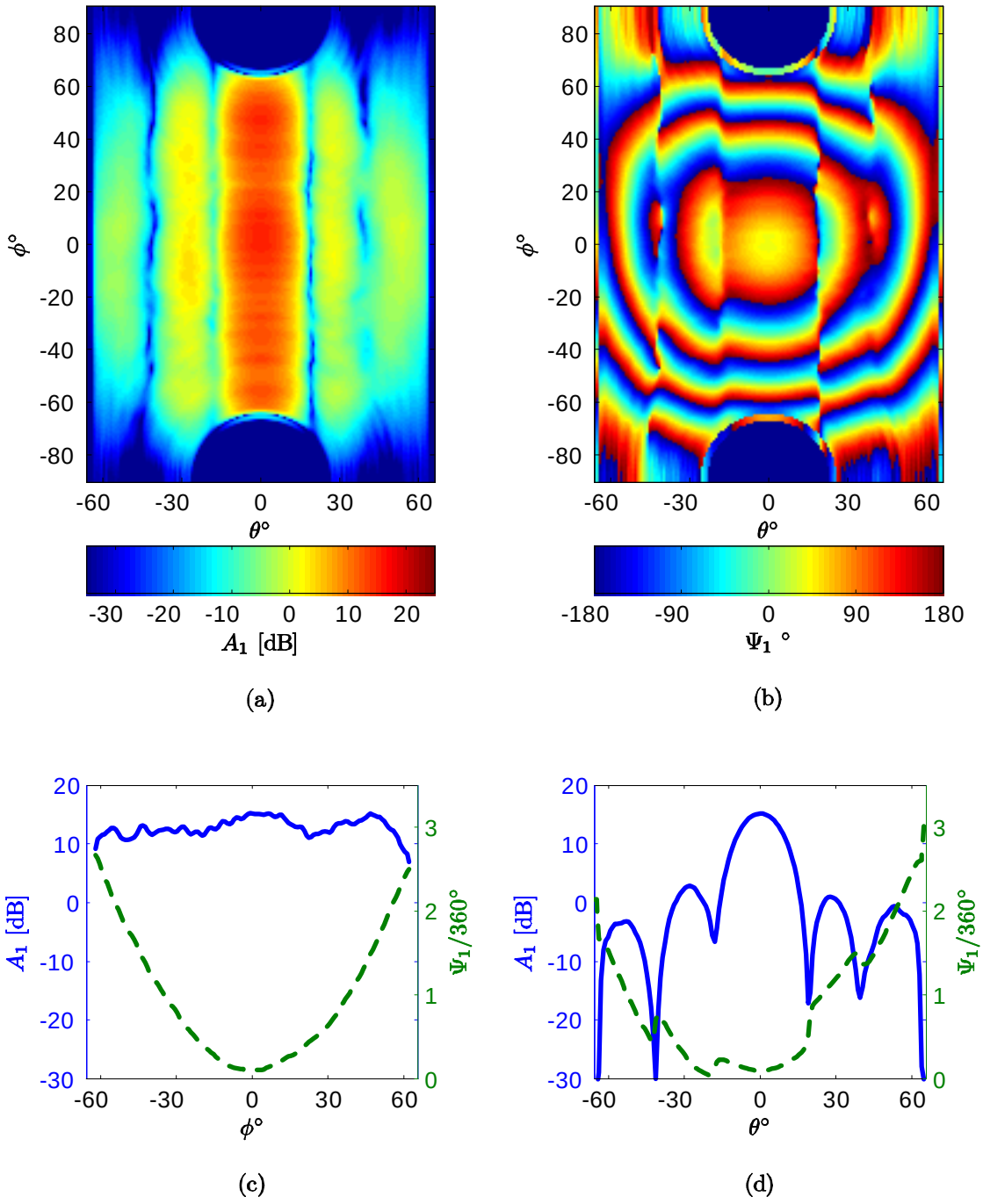

Figure 4.78 (a) Measured antenna directivity A_1 in dBi for column #1 of the MCWESS at 5 GHz (horizontally polarized). (b) Phase pattern Ψ_1. (c) Azimuth cut, $\theta = 0$, and $\psi_1 = \Psi_1(0,0) = 37°$. (d) Elevation cut, $\phi = 0$. Measurements were conducted using OEWG probe WR187.

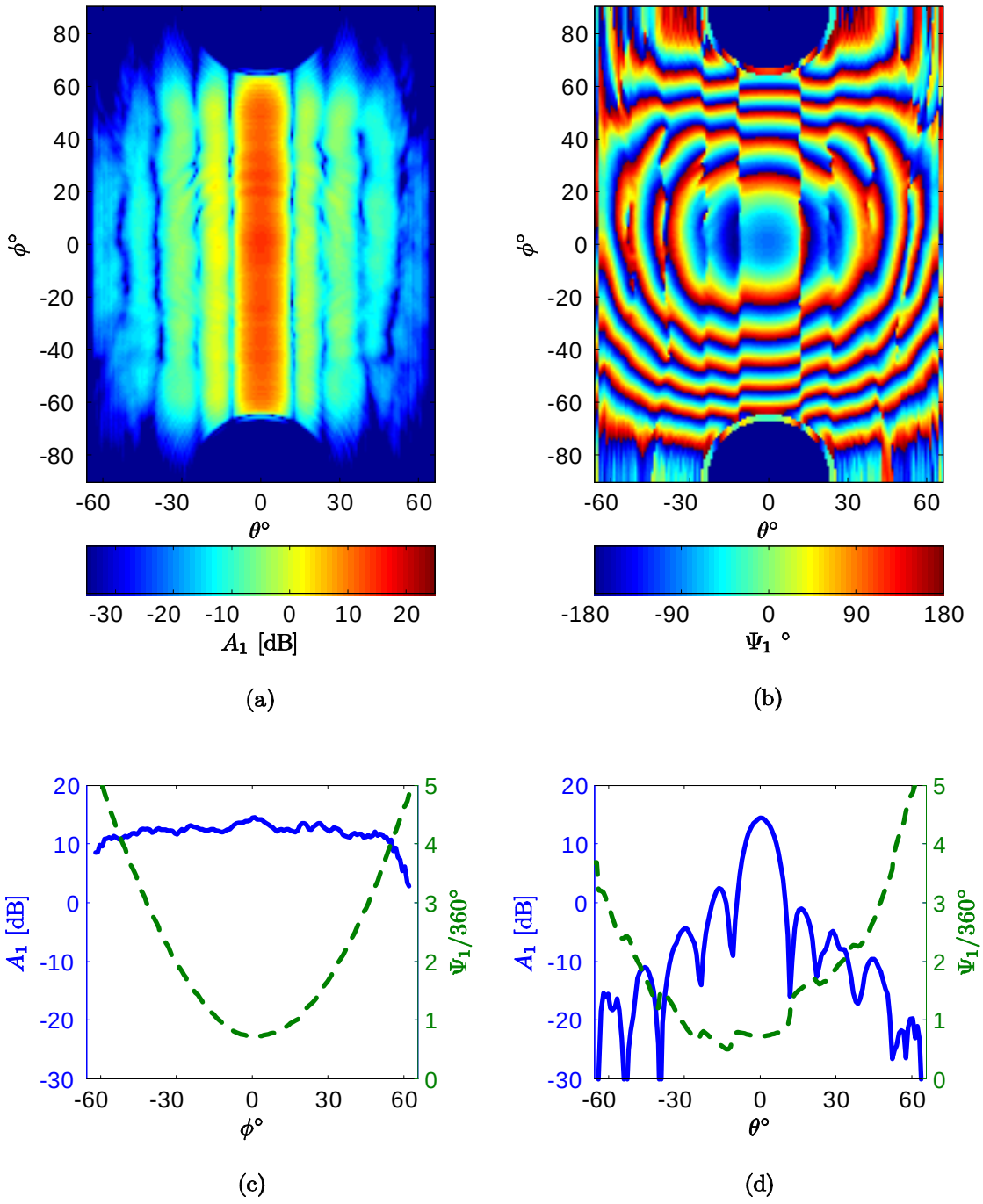

Figure 4.79 (a) Measured antenna directivity A_1 in dBi for column #1 of the MCWESS at 8 GHz (horizontally polarized). (b) Phase pattern Ψ_1. (c) Azimuth cut, $\theta = 0$, and $\psi_1 = \Psi_1(0,0) = 262°$. (d) Elevation cut, $\phi = 0$. Measurements were conducted using OEWG probe WR137.

The azimuth squint angle ξ_ϕ is the value of ϕ when $A_k = A_{k,max}$; the elevation squint angle ξ_θ is the value of θ when $A_k = A_{k,max}$. The First Null Beamwidth (FNBW) is the angular width of the main beam between the first nulls along a particular axis: the value FNBW_ϕ is the beamwidth, along the azimuth axis, between the first nulls; and FNBW_θ is the first-null beamwidth along the elevation axis. The half-power beamwidth (HPBW) is the width of the main beam, along a particular axis, such that $A_k \geq A_{k,max} - 3$ dB: the value HPBW_ϕ is the beamwidth, along the azimuth axis, between the half-power points; and HPBW_θ is the half-power beamwidth along the elevation axis. In the case of HPBW_ϕ, the main beam ripple for the *superelement pattern* (not the entire array pattern shown later) is usually so great that we need to modify the definition of HPBW_ϕ a little bit. Here, we let HPBW_ϕ be the azimuth angle difference between the two main-beam half-power points *which are closest to the first nulls*, and Φ_{main} is the set of all azimuth angles between those half-power points. The main beam ripple $\Delta A_{k,\phi}$ is the amount of variability in A_k within the main beam, along the azimuth axis:

$$\Delta A_{k,\phi} \equiv \frac{A_{k,max}}{\min\limits_{\phi} A_k \left(\phi \in \Phi_{main}, \xi_\theta\right)}. \tag{4.2}$$

Ideally, $\Delta A_{k,\phi}$ would always be 3 dB, but for the measured superelement patterns, it is never the case. The Sidelobe Level (SLL) is the ratio of the antenna gain $A_{k,max}$ to the value of A_k at the strongest sidelobe. The azimuth sidelobe level SLL_ϕ considers the only the sidelobes along the azimuth axis; SLL_θ is the sidelobe level along the elevation axis. For the individual column data sets, values for HPBW_ϕ, FNBW_ϕ, SLL_ϕ, and ξ_ϕ are generally not available from the NSI2000 measurements; however, from the design specifications we know that HPBW_ϕ is approximately 120° in each case. Also, the NSI2000 gave sufficient data to give us a good idea of the value of $\Delta A_{k,\phi}$. The phase ψ_k is defined in Section 3.4.2. The phase delay $\tau_{\psi,k}$ is defined as

$$\tau_{\psi,k} \equiv -\frac{\psi_k}{\omega_{in}}, \tag{4.3}$$

where ω_{in} is the radian frequency corresponding to f_{in}. The group delay $\tau_{g,k}$ is defined as

$$\tau_{g,k} \equiv -\frac{d\psi_k}{d\omega_{in}}. \tag{4.4}$$

Measured values for these statistics are given in Table 4.37 and Figs. 4.80-4.81 for column 8; additional data are provided in Appendix A. The ripple $\Delta A_{k,\phi}$ is particularly poor for some columns—as high as 11 dB in a few cases. On average, the main beam ripple is about 4.0 dB for all the measured patterns.

The antenna pattern measurements using the WR137 probe (for 5.9-8.2 GHz) were conducted in two separate test runs. As a result, the gain and phase measurements from the two runs are divergent. During the first run (4-8 June 2009), columns 1 and 8 were measured with horizontal polarization, and columns 1, 5, 6, 7, 8, 9, 10, 11, and 12 were measured with vertical polarization. During the second run (24-26 June 2009), columns 2, 3, 4, 5, 6, 7, 9, 10, 11, 12, 13, 14, 15, and 16 were measured with horizontal polarization, and columns 2, 3, 4, 13, 14, 15, and 16 were measured with vertical polarization. In between runs, the NSI2000 equipment apparently was reset or reconfigured in some way, as evidenced by Fig. 4.82. Below 5.9 GHz, the superelement gain and phase measurements expressed as $A_{k,max}e^{j\psi_k}$ appear in a farily tight distribution. At 5.9 GHz and above, the gain and particularly the phase measurements are clearly bimodal as in Fig. 4.82. To offset this apparent error, the following correction was applied to all data for the first run of the WR137 data:

$$A_{k,max}e^{j\psi_k} \rightarrow 0.8361 A_{k,max}e^{j(\psi_k - 16.34 f_{in})}, \tag{4.5}$$

where 16.34 is expressed in degrees per gigahertz. This formula was obtained by assuming that at each frequency, the geometric mean of all $A_{k,max}$ from the first run should equal the geometric mean of all $A_{k,max}$ from the second run, and likewise, the mean of all ψ_k from the first run should equal the mean of all ψ_k from the second run. A least squares fit was applied to the formula in (4.5), to force the two data sets to have the same average gain and phase. The correction is illustrated in Fig. 4.82.

Table 4.37 MCWESS measured antenna element pattern summary information for column $k = 8$.

Horizontal Polarization

f_{in}	$A_{k,max}$	$\Delta A_{k,\phi}$			SLL_θ			$\tau_{\psi,k}$	$\tau_{g,k}$
GHz	dBi	dB	$\text{HPBW}_\theta{}^\circ$	$\text{FNBW}_\theta{}^\circ$	dB	${\xi_\theta}^\circ$	${\psi_k}^\circ$	ps	ps
2.6	14.3	3.5	30.9	77	-	0.0	-46	49	2706
3.0	16.4	3.3	26.4	67	15.1	0.9	-377	349	2254
3.5	15.7	3.5	23.2	57	13.6	0.9	-733	582	1714
4.0	15.2	2.8	20.3	49	13.0	0.9	-1047	727	1082
4.5	13.6	2.7	18.2	41	11.3	0.0	-1230	759	664
5.0	15.6	3.6	16.7	39	11.6	0.0	-1360	756	831
5.5	15.6	2.8	15.3	34	11.4	0.0	-1473	744	850
6.0	16.8	3.5	13.7	32	10.9	0.0	-1545	715	849
6.5	15.6	2.9	12.6	29	11.4	0.0	-1659	709	481
7.0	14.9	4.1	11.7	27	12.1	0.0	-1758	698	499
7.5	15.3	6.2	10.9	24	10.6	0.0	-1863	690	717
8.0	15.0	6.3	10.4	23	11.6	0.0	-1965	682	663
8.2	14.5	3.8	10.4	23	11.8	0.0	-2008	680	561

Vertical Polarization

f_{in}	$A_{k,max}$	$\Delta A_{k,\phi}$			SLL_θ			$\tau_{\psi,k}$	$\tau_{g,k}$
GHz	dBi	dB	$\text{HPBW}_\theta{}^\circ$	$\text{FNBW}_\theta{}^\circ$	dB	${\xi_\theta}^\circ$	${\psi_k}^\circ$	ps	ps
2.6	13.1	2.7	30.4	80	-	-0.9	-71	76	2480
3.0	14.3	2.5	28.6	68	14.2	0.0	-379	351	2088
3.5	14.5	2.2	24.7	57	12.1	-0.9	-749	595	1839
4.0	14.2	2.5	21.7	48	11.5	-1.8	-1073	745	978
4.5	14.1	2.9	19.0	41	10.6	-1.8	-1247	770	806
5.0	15.0	4.6	16.8	38	11.1	-0.9	-1387	771	804
5.5	15.3	4.5	15.1	34	10.9	0.0	-1505	760	779
6.0	16.0	5.7	13.8	32	10.0	-0.9	-1567	725	802
6.5	15.0	2.9	12.9	30	11.1	-0.9	-1692	723	581
7.0	14.1	5.4	11.8	28	10.6	-1.8	-1791	711	484
7.5	14.1	3.8	10.8	25	10.1	-0.9	-1893	701	670
8.0	14.7	4.7	10.3	24	10.2	-0.9	-1996	693	662
8.2	14.1	3.0	10.1	23	12.5	-0.9	-2045	693	732

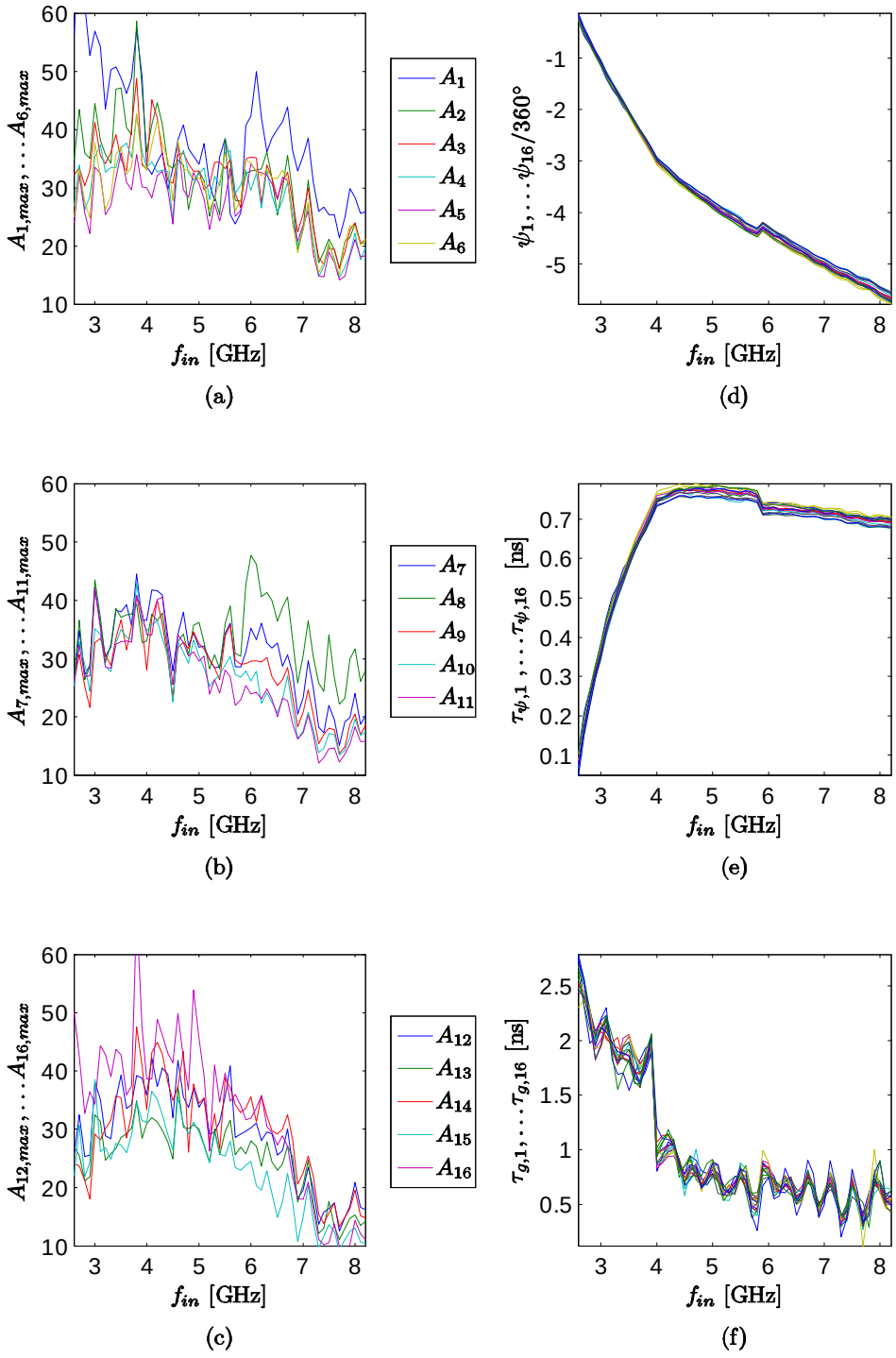

Figure 4.80 Measured antenna directivity, phase, phase delay, and group delay, for the horizontally polarized superelements. Directivity is in linear scale (not decibels). Discontinuities at 4.0 and 5.9 GHz are due to swapping the instrumentation probe.

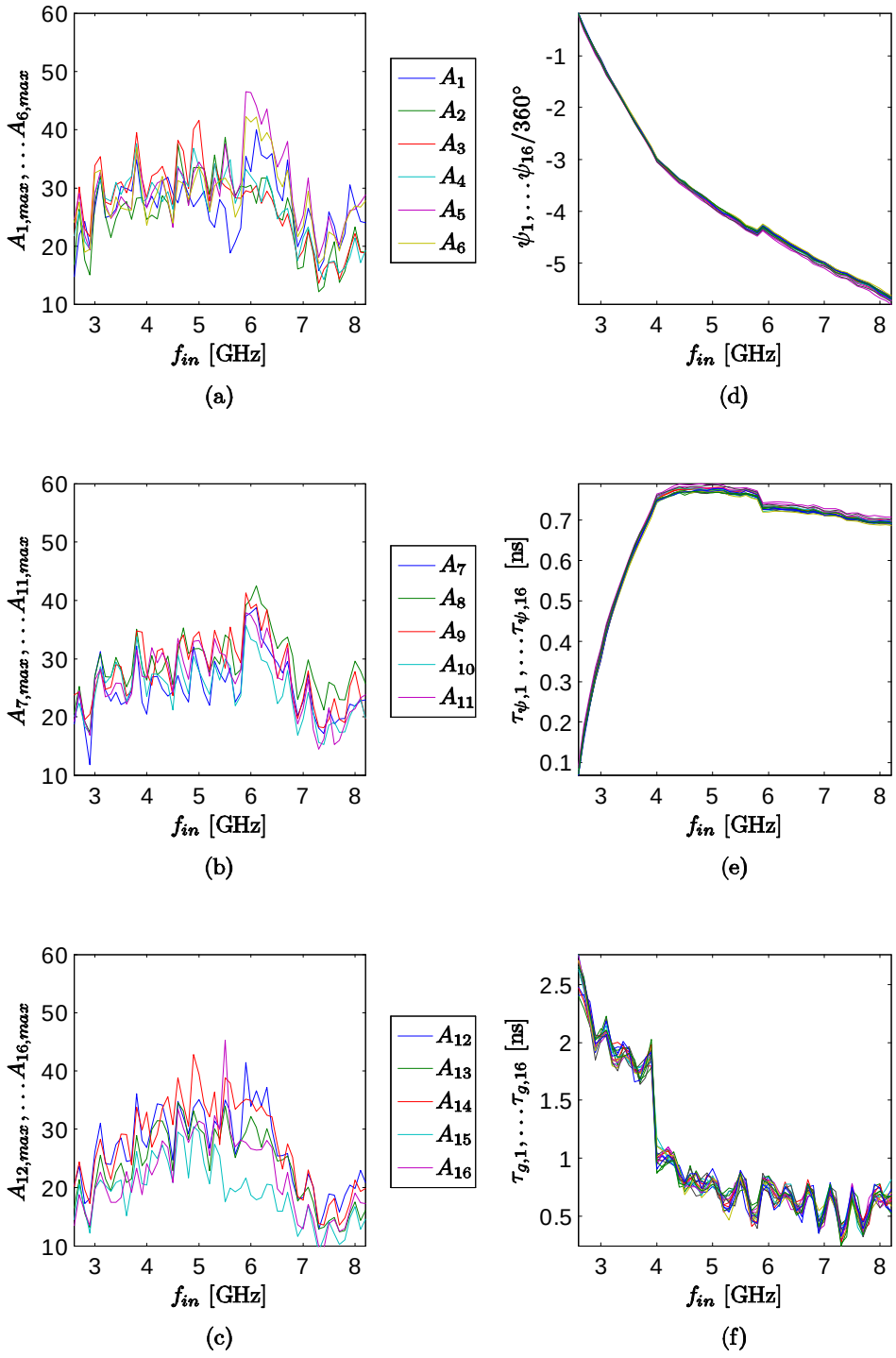

Figure 4.81 Measured antenna directivity, phase, phase delay, and group delay, for the vertically polarized superelements. Directivity is in linear scale (not decibels). Discontinuities at 4.0 and 5.9 GHz are due to swapping the instrumentation probe.

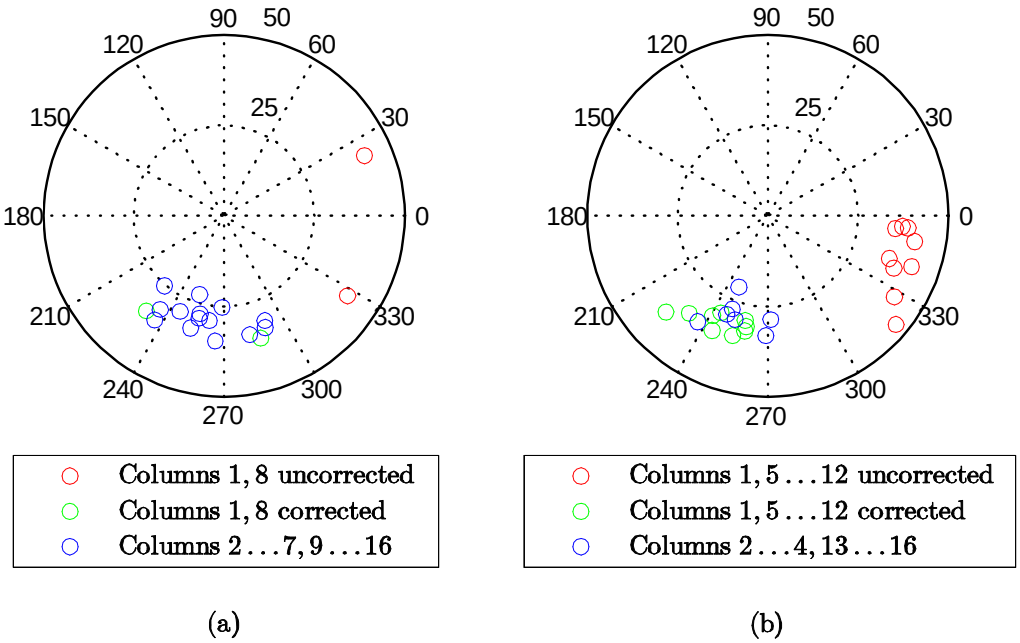

Figure 4.82 Polar plot of antenna superelement gain and phase $A_{k,max}e^{j\psi_k}$, for all sixteen columns at 5.9 GHz, with (a) horizontal polarization and (b) vertical polarization. The red circles show the uncorrected gain and phase for the superelements from the first test run, and the green circles show the same data after being corrected as per (4.5).

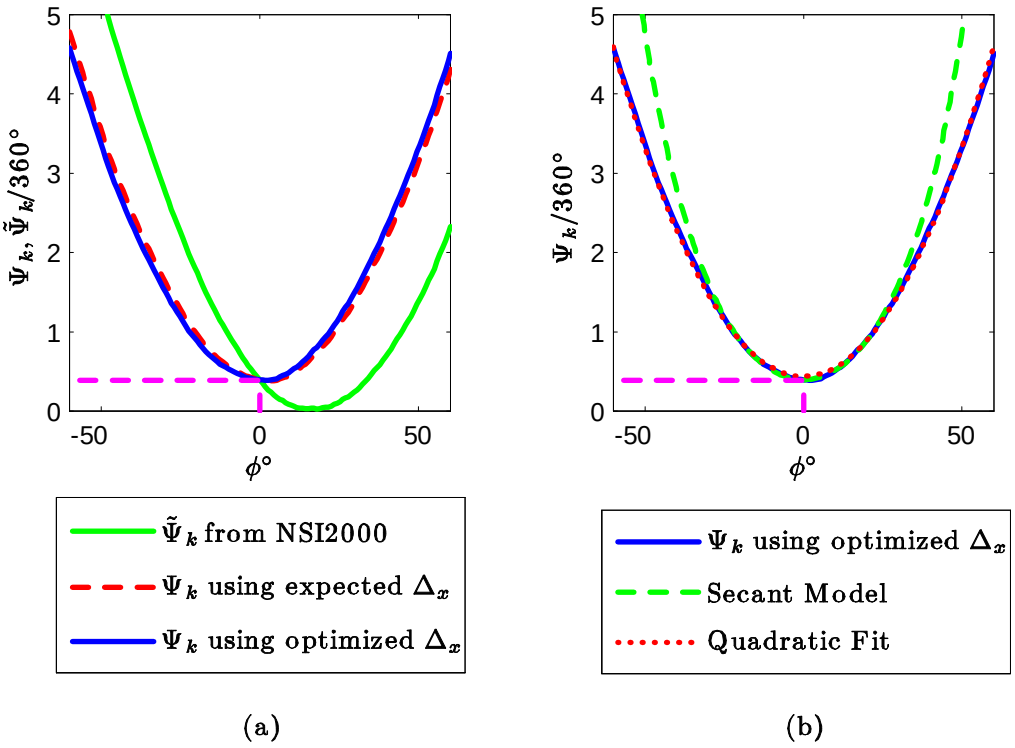

Figure 4.83 MCWESS antenna phase plots for column $k = 16$, horizontally polarized, at 8 GHz. (a) $\tilde{\Psi}_k(\phi, 0)$ reported by NSI2000, and $\Psi_k(\phi, 0)$ computed using (3.5) versus $\Psi_k(\phi, 0)$ optimized for symmetry. (b) Secant model from (3.12) versus actual $\Psi_k(\phi, 0)$, and quadratic fit to $\Psi_k(\phi, 0)$.

From (3.12) we expect $\Psi_k(\phi, 0)$ to be symmetric about $\phi = 0$, and we expect its minimum to be at $\phi = 0$. From this perspective, using (3.5) and (3.10) to transform $\tilde{\Psi}_k(\phi, 0)$ to $\Psi_k(\phi, 0)$ sometimes fails to give good results. Note the slight asymmetry of the dashed red line in Fig. 4.83a. This seems to be due to a slight bias in Δ_x on the order of about 5 mm, meaning the chamber coordinate system may be displaced slightly along the x axis; and with the WR137 data there seems to be a slight dependence on frequency as well, perhaps due to an imperfect knowledge of the wavelength. Nonetheless, in each case there is an optimal value of Δ_x which makes $\Psi_k(\phi, 0)$ centered about its minimum at $\phi = 0$; it is just sometimes a little different from what we expect from (3.5). Therefore, $\tilde{\Psi}_k(0, 0)$ still equals $\Psi_k(0, 0)$, and we can still use (3.15) to determine the phase ψ_k of the kth channel of the CSA/BFN assembly.

The secant model for $\Psi_k(\phi, 0)$ suggested in (3.12) is a fairly poor fit for the measured data beyond $|\phi| > 30^\circ$, as illustrated in Fig. 4.83b. The reason for this is unknown, but we speculate that the NSI2000 may be using a second-order Taylor series (i.e. quadratic) approximation to the various trigonometric functions. In fact, a second-order polynomial of ϕ is an excellent fit for $\Psi_k(\phi, 0)$ derived from measured $\tilde{\Psi}_k(\phi, 0)$ using (3.10), but there is no theoretical justification for it. However, since we are only interested in $\Psi_k(0, 0)$, we can still use (3.15) to determine ψ_k.

4.3.2 Entire Array. A total of 114 antenna patterns were measured for the entire array, using the setup shown in Fig. 3.9—two polarizations, and 57 frequencies from 2.6 to 8.2 GHz. Some examples are shown in Figs. 4.84-4.86; the results are summarized in Table 4.38 and Appendix A. The array pattern is denoted by $A(\phi, \theta)$; its peak A_{max} is the overall array gain. The array phase pattern is denoted by $\Psi(\phi, \theta)$.

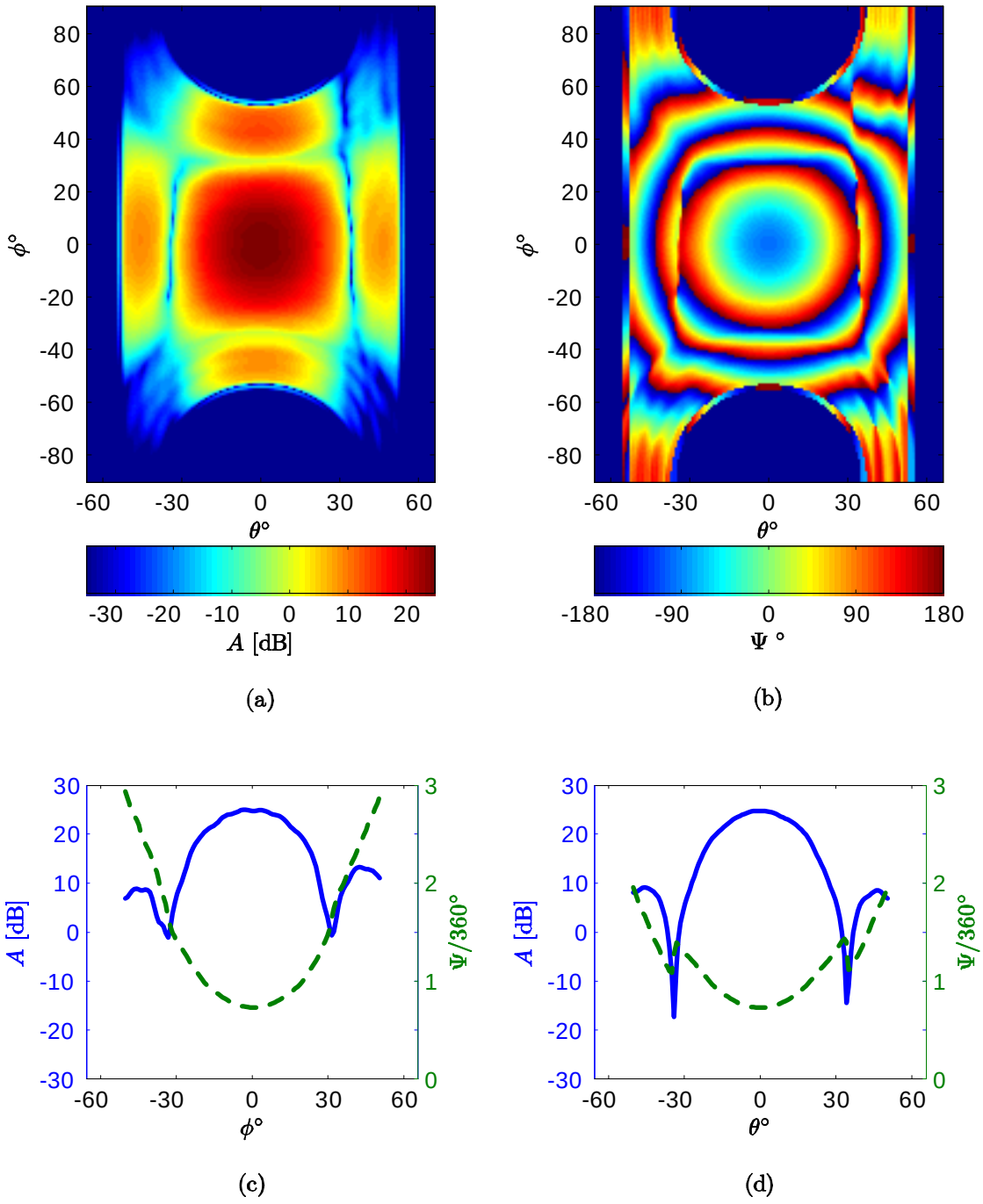

Figure 4.84 (a) Measured antenna directivity A in dBi for the entire MCWESS array at 3 GHz (horizontally polarized). (b) Phase pattern Ψ. (c) Azimuth cut, $\theta = 0$. (d) Elevation cut, $\phi = 0$. Measurements were conducted using OEWG probe WR284.

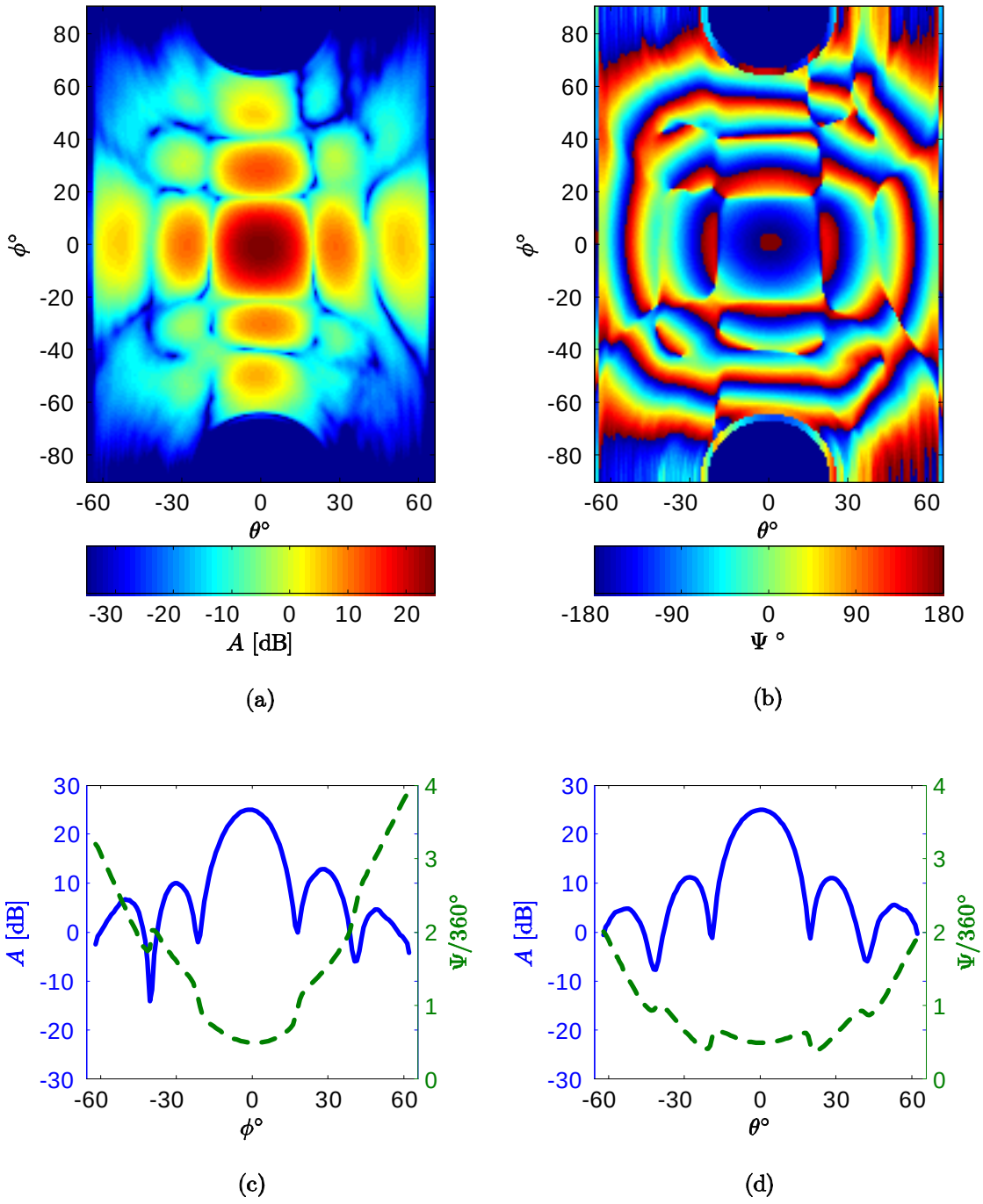

Figure 4.85 (a) Measured antenna directivity A in dBi for the entire MCWESS array at 5 GHz (horizontally polarized). (b) Phase pattern Ψ. (c) Azimuth cut, $\theta = 0$. (d) Elevation cut, $\phi = 0$. Measurements were conducted using OEWG probe WR187.

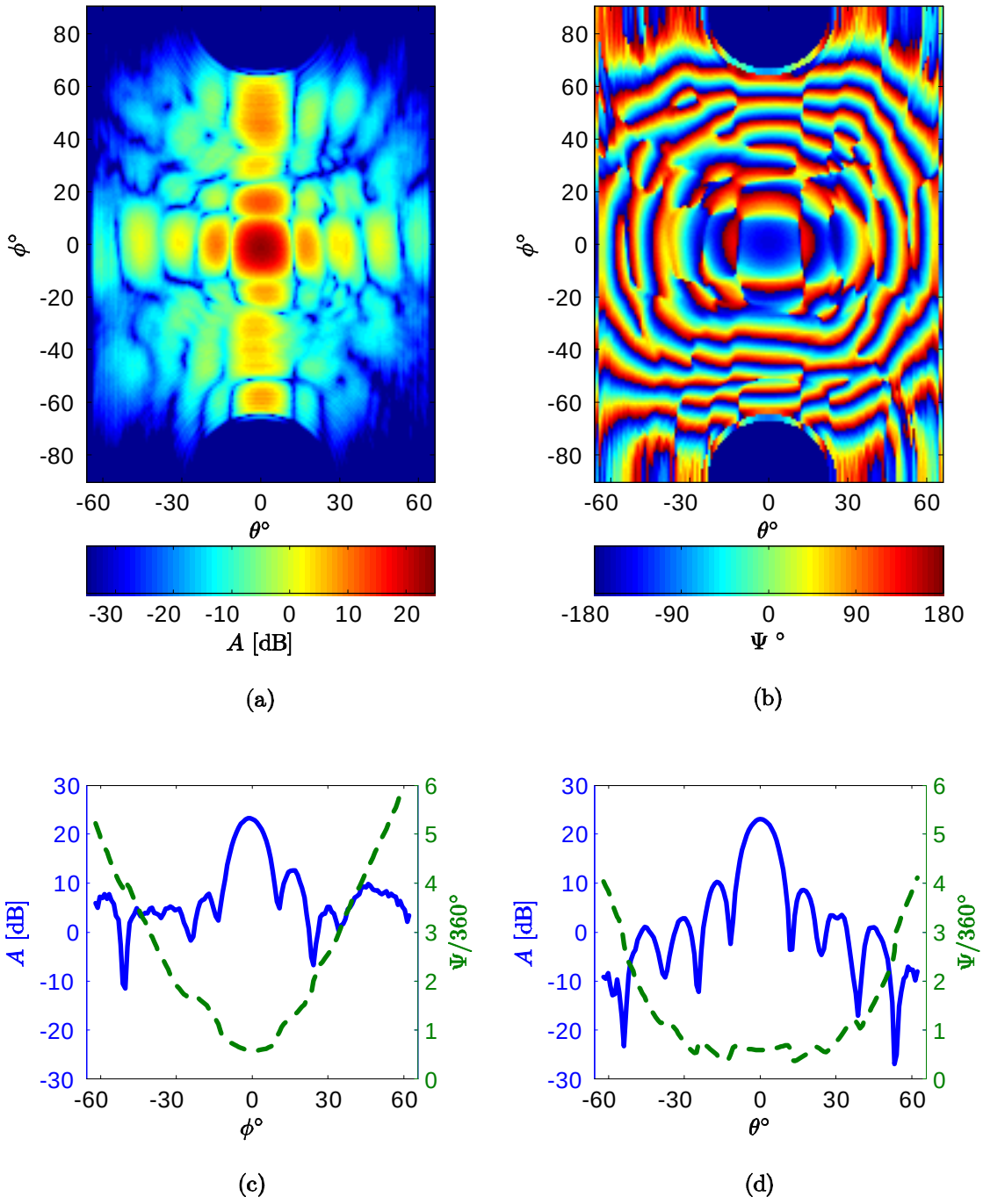

Figure 4.86 (a) Measured antenna directivity A in dBi for the entire MCWESS array at 8 GHz (horizontally polarized). (b) Phase pattern Ψ. (c) Azimuth cut, $\theta = 0$. (d) Elevation cut, $\phi = 0$. Measurements were conducted using OEWG probe WR137.

Table 4.38 MCWESS antenna pattern summary information for the array measured as a whole.

Horizontal Polarization

f_{in}	A_{max}					SLL_ϕ	SLL_θ		
GHz	dBi	$HPBW_\phi{}^\circ$	$FNBW_\phi{}^\circ$	$HPBW_\theta{}^\circ$	$FNBW_\theta{}^\circ$	dB	dB	$\xi_\phi{}^\circ$	$\xi_\theta{}^\circ$
2.6	24.0	37.0	75	31.3	79	-	-	0.0	0.0
3.0	25.0	28.8	65	27.1	68	11.7	15.9	-3.6	-0.9
3.5	25.3	26.1	56	23.0	57	12.6	15.0	0.0	0.0
4.0	24.9	19.8	49	20.3	50	12.8	14.0	-0.9	0.0
4.5	24.3	16.6	43	18.4	42	11.9	13.2	-0.9	0.0
5.0	25.1	16.1	40	17.3	39	12.2	13.9	-0.9	0.0
5.5	24.5	24.5	34	15.2	34	10.6	13.1	-0.9	0.0
6.0	25.6	25.6	32	13.9	32	10.6	13.2	-1.8	0.0
6.5	24.5	24.5	30	12.5	30	11.0	13.7	-1.8	0.0
7.0	24.0	24	27	11.7	28	11.0	14.2	-0.9	0.0
7.5	22.9	22.9	26	11.3	25	10.7	13.3	-0.9	0.0
8.0	23.3	23.3	24	10.6	24	10.7	13.1	-1.8	0.0
8.2	22.3	22.3	23	10.2	23	11.2	14.0	-0.9	0.0

Vertical Polarization

f_{in}	A_{max}					SLL_ϕ	SLL_θ		
GHz	dBi	$HPBW_\phi{}^\circ$	$FNBW_\phi{}^\circ$	$HPBW_\theta{}^\circ$	$FNBW_\theta{}^\circ$	dB	dB	$\xi_\phi{}^\circ$	$\xi_\theta{}^\circ$
2.6	25.3	30.2	80	29.3	80	-	-	0.0	0.0
3.0	25.8	27.0	68	29.5	67	14.5	13.8	-1.8	-2.7
3.5	25.9	24.1	57	25.4	55	13.5	13.3	-0.9	0.0
4.0	24.6	22.2	48	22.0	47	13.9	13.2	-0.9	0.0
4.5	24.2	18.6	43	18.7	42	12.9	12.8	-0.9	0.0
5.0	25.2	16.7	40	16.6	38	12.9	13.7	-0.9	0.0
5.5	25.1	14.7	35	14.3	36	13.4	13.4	-0.9	0.0
6.0	24.0	14.1	33	13.5	32	13.4	12.9	-0.9	0.0
6.5	23.0	13.0	30	12.5	29	13.3	12.4	-0.9	0.0
7.0	22.3	11.9	28	12.0	27	13.7	13.8	-0.9	0.0
7.5	21.7	11.3	25	11.1	25	13.7	13.0	-0.9	0.0
8.0	22.9	10.3	23	10.4	24	13.7	13.1	-0.9	0.0
8.2	22.0	10.0	23	10.3	23	13.8	14.8	-0.9	0.0

V. Curve Fitting/Modeling

5.1 Tuner Gain

5.1.1 Least Squares Fits Using Polynomial Models. The gain responses in Figs. 4.1-4.35 or 4.41-4.71 can be modeled using a regression model as follows [3] [5]:

$$\hat{g}\left(k, f_c, f_{IF}\right) = \sum_{i=1}^{q} \left(C_{c,i} f_c^i + C_{IF,i} f_{IF}^i\right) + \sum_{j=1}^{N-1} C_{cal,j} T_{k,j} + C_0, \tag{5.1}$$

where the coefficients $C_{c,i}$, $C_{IF,i}$, and C_0, and the calibration offsets $C_{cal,j}$, are computed using the least squares fit to the measured gain g, q is the degree of the polynomial, N is the number of tuners, $\mathbf{T}$ is a categorical variable representing each of the tuners, whose $N \times (N-1)$ elements $T_{k,j}$ are

$$T_{k,j} = \begin{cases} 1 & \text{for } j = k-1 \\ 0 & \text{otherwise.} \end{cases} \tag{5.2}$$

The quantity $\hat{g}\left(k, f_c, f_{IF}\right)$ is the gain model for the kth tuner, and

$$g\left(k, f_c, f_{IF}\right) = \hat{g}\left(k, f_c, f_{IF}\right) + \varepsilon\left(k, f_c, f_{IF}\right), \tag{5.3}$$

where ε is the residual error of the model. The categorical variable results in each tuner having the same gain model, except for a constant offset $C_{cal,j}$, and tuner #1 by definition has no calibration offset.

The solution to the linear least squares problem is computed as follows:

$$\mathbf{C} = \left(\mathbf{F}^T \mathbf{F}\right)^{-1} \mathbf{F}^T \mathbf{g}, \tag{5.4}$$

where $\mathbf{F}$ is the matrix of frequency samples and categorical variables, where the jth row $\mathbf{F}_j$ of matrix $\mathbf{F}$ is determined by

$$\mathbf{F}_j = \left(1, T_{k,1}, \ldots T_{k,N-1}, f_{c,j_c}^1, \ldots f_{c,j_c}^q, f_{I,j_{IF}}^1, \ldots f_{I,j_{IF}}^q\right) \tag{5.5}$$

with

$$j = (n_c - 1)(n_{IF} - 1)k + (n_c - 1)j_{IF} + j_c, \tag{5.6}$$

g is the vector of gain samples:

$$\mathbf{g} = \begin{pmatrix} g_1 & g_2 & \cdots & g_{Nn_cn_{IF}} \end{pmatrix}^T, \tag{5.7}$$

C is the coefficient vector:

$$\mathbf{C} = \tag{5.8}$$

$$\begin{pmatrix} C_0 & C_{cal,1} & C_{cal,2} & \cdots & C_{cal,N-1} & C_{c,1} & C_{c,2} & \cdots & C_{c,q} & C_{IF,1} & C_{IF,2} & \cdots & C_{IF,q} \end{pmatrix}^T,$$

n_c is the sample size along the f_c axis, n_{IF} is the sample size along the f_{IF} axis, and indices j_c and j_{IF} represent the frequency samples such that $j_c \in [1, \ldots n_c]$ and $j_{IF} \in [1, \ldots n_{IF}]$. Since f_{IF} was sampled at 10 MHz intervals, $n_{IF} = 51$ for the passband $f_{IF} \in [0.75$ GHz, 1.25 GHz]. For the low band $f_c \in [0.5$ GHz, 6 GHz), $n_c = 367$, and with $N = 16$ tuners, the sample size was $Nn_cn_{IF} = 299472$. For the high band $f_c \in [6\,\text{GHz}, 18\,\text{GHz}]$, $n_c = 801$; with 16 tuners, there sample size was 653616. Equation (5.5) expands to (5.9) on the following page:

$$\mathbf{F} = \tag{5.9}$$

$$\begin{pmatrix}
1 & T_{1,1} & T_{1,2} & \cdots & T_{1,N-1} & f_{c,1} & f_{c,1}^2 & \cdots & f_{c,1}^q & f_{IF,1} & f_{IF,1}^2 & \cdots & f_{IF,1}^q \\
1 & T_{1,1} & T_{1,2} & \cdots & T_{1,N-1} & f_{c,2} & f_{c,2}^2 & \cdots & f_{c,2}^q & f_{IF,1} & f_{IF,1}^2 & \cdots & f_{IF,1}^q \\
\vdots & \vdots & \vdots & \ddots & \vdots & \vdots & \vdots & \ddots & \vdots & \vdots & \vdots & \ddots & \vdots \\
1 & T_{1,1} & T_{1,2} & \cdots & T_{1,N-1} & f_{c,n_c} & f_{c,n_c}^2 & \cdots & f_{c,n_c}^q & f_{IF,1} & f_{IF,1}^2 & \cdots & f_{IF,1}^q \\
1 & T_{1,1} & T_{1,2} & \cdots & T_{1,N-1} & f_{c,1} & f_{c,1}^2 & \cdots & f_{c,1}^q & f_{IF,2} & f_{IF,2}^2 & \cdots & f_{IF,2}^q \\
1 & T_{1,1} & T_{1,2} & \cdots & T_{1,N-1} & f_{c,2} & f_{c,2}^2 & \cdots & f_{c,2}^q & f_{IF,2} & f_{IF,2}^2 & \cdots & f_{IF,2}^q \\
\vdots & \vdots & \vdots & \ddots & \vdots & \vdots & \vdots & \ddots & \vdots & \vdots & \vdots & \ddots & \vdots \\
1 & T_{1,1} & T_{1,2} & \cdots & T_{1,N-1} & f_{c,n_c} & f_{c,n_c}^2 & \cdots & f_{c,n_c}^q & f_{IF,2} & f_{IF,2}^2 & \cdots & f_{IF,2}^q \\
\vdots & \vdots & \vdots & \ddots & \vdots & \vdots & \vdots & \ddots & \vdots & \vdots & \vdots & \ddots & \vdots \\
1 & T_{1,1} & T_{1,2} & \cdots & T_{1,N-1} & f_{c,n_c} & f_{c,n_c}^2 & \cdots & f_{c,n_c}^q & f_{IF,n_{IF}} & f_{IF,n_{IF}}^2 & \cdots & f_{IF,n_{IF}}^q \\
1 & T_{2,1} & T_{2,2} & \cdots & T_{2,N-1} & f_{c,1} & f_{c,1}^2 & \cdots & f_{c,1}^q & f_{IF,1} & f_{IF,1}^2 & \cdots & f_{IF,1}^q \\
1 & T_{2,1} & T_{2,2} & \cdots & T_{2,N-1} & f_{c,2} & f_{c,2}^2 & \cdots & f_{c,2}^q & f_{IF,1} & f_{IF,1}^2 & \cdots & f_{IF,1}^q \\
\vdots & \vdots & \vdots & \ddots & \vdots & \vdots & \vdots & \ddots & \vdots & \vdots & \vdots & \ddots & \vdots \\
1 & T_{2,1} & T_{2,2} & \cdots & T_{2,N-1} & f_{c,n_c} & f_{c,n_c}^2 & \cdots & f_{c,n_c}^q & f_{IF,1} & f_{IF,1}^2 & \cdots & f_{IF,1}^q \\
1 & T_{2,1} & T_{2,2} & \cdots & T_{2,N-1} & f_{c,1} & f_{c,1}^2 & \cdots & f_{c,1}^q & f_{IF,2} & f_{IF,2}^2 & \cdots & f_{IF,2}^q \\
1 & T_{2,1} & T_{2,2} & \cdots & T_{2,N-1} & f_{c,2} & f_{c,2}^2 & \cdots & f_{c,2}^q & f_{IF,2} & f_{IF,2}^2 & \cdots & f_{IF,2}^q \\
\vdots & \vdots & \vdots & \ddots & \vdots & \vdots & \vdots & \ddots & \vdots & \vdots & \vdots & \ddots & \vdots \\
1 & T_{2,1} & T_{2,2} & \cdots & T_{2,N-1} & f_{c,n_c} & f_{c,n_c}^2 & \cdots & f_{c,n_c}^q & f_{IF,2} & f_{IF,2}^2 & \cdots & f_{IF,2}^q \\
\vdots & \vdots & \vdots & \ddots & \vdots & \vdots & \vdots & \ddots & \vdots & \vdots & \vdots & \ddots & \vdots \\
1 & T_{2,1} & T_{2,2} & \cdots & T_{2,N-1} & f_{c,n_c} & f_{c,n_c}^2 & \cdots & f_{c,n_c}^q & f_{IF,n_{IF}} & f_{IF,n_{IF}}^2 & \cdots & f_{IF,n_{IF}}^q \\
\vdots & \vdots & \vdots & \ddots & \vdots & \vdots & \vdots & \ddots & \vdots & \vdots & \vdots & \ddots & \vdots \\
1 & T_{N,1} & T_{N,2} & \cdots & T_{N,N-1} & f_{c,n_c} & f_{c,n_c}^2 & \cdots & f_{c,n_c}^q & f_{IF,n_{IF}} & f_{IF,n_{IF}}^2 & \cdots & f_{IF,n_{IF}}^q
\end{pmatrix}.$$

A fourth-degree polynomial model for the sixteen tuners is given in Table 5.1 and Fig. 5.1.

5.1.2 Residual Errors. The residual errors ε of the model shown in Fig. 5.1 are shown in Figs. 5.2-5.17. In each figure, the green areas indicate the best fits, while the red and blue areas indicate the greatest amounts of error.

Table 5.1 Polynomial models for the Mid-Atlantic LCR400 tuners.

	Low Band ($0.5 \leq f_c < 6$ GHz)	High Band ($6 \leq f_c \leq 18$ GHz)
q	4	4
C_0	-515.699	136.294
$C_{cal,1}$	5.119	3.686
$C_{cal,2}$	1.126	1.017
$C_{cal,3}$	2.014	-1.015
$C_{cal,4}$	1.647	1.522
$C_{cal,5}$	1.333	-0.101
$C_{cal,6}$	1.119	2.970
$C_{cal,7}$	2.921	-0.268
$C_{cal,8}$	-0.397	-1.251
$C_{cal,9}$	0.780	-1.178
$C_{cal,10}$	1.302	-0.478
$C_{cal,11}$	1.101	-1.299
$C_{cal,12}$	1.260	-0.969
$C_{cal,13}$	1.829	-0.460
$C_{cal,14}$	1.173	-1.098
$C_{cal,15}$	0.864	-0.391
$C_{c,1}$	0.115	-0.388
$C_{c,2}$	-0.408	0.146
$C_{c,3}$	0.152	-0.0133
$C_{c,4}$	-0.0172	0.000327
$C_{IF,1}$	2139.443	-605.603
$C_{IF,2}$	-3272.579	1017.617
$C_{IF,3}$	2215.559	-730.918
$C_{IF,4}$	-560.440	190.556

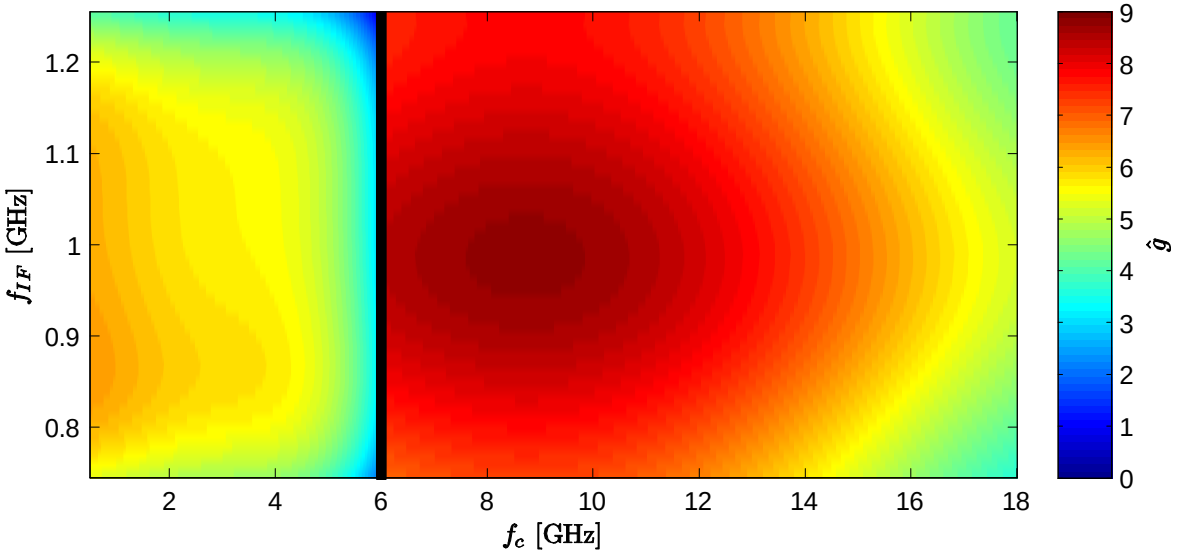

Figure 5.1 Fourth-degree polynomial voltage gain models for tuner #1. There is a different model for 0-6 GHz than for 6-18 GHz. The models for the other tuners have the same contour shape, but are shifted up or down according to their calibration offsets.

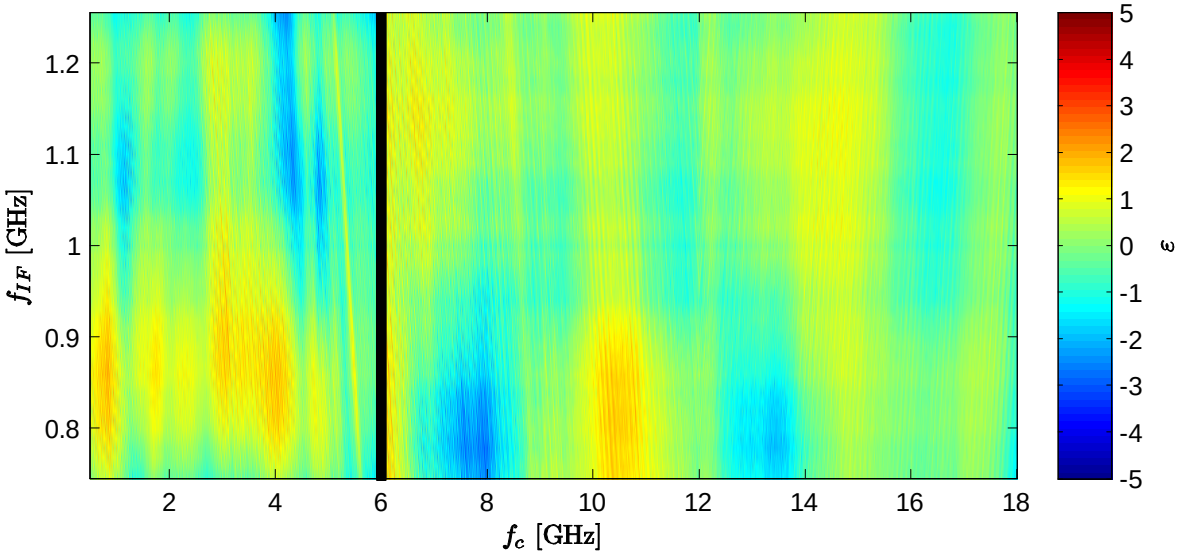

Figure 5.2 Residual errors of the model in Fig. 5.1, for tuner #1.

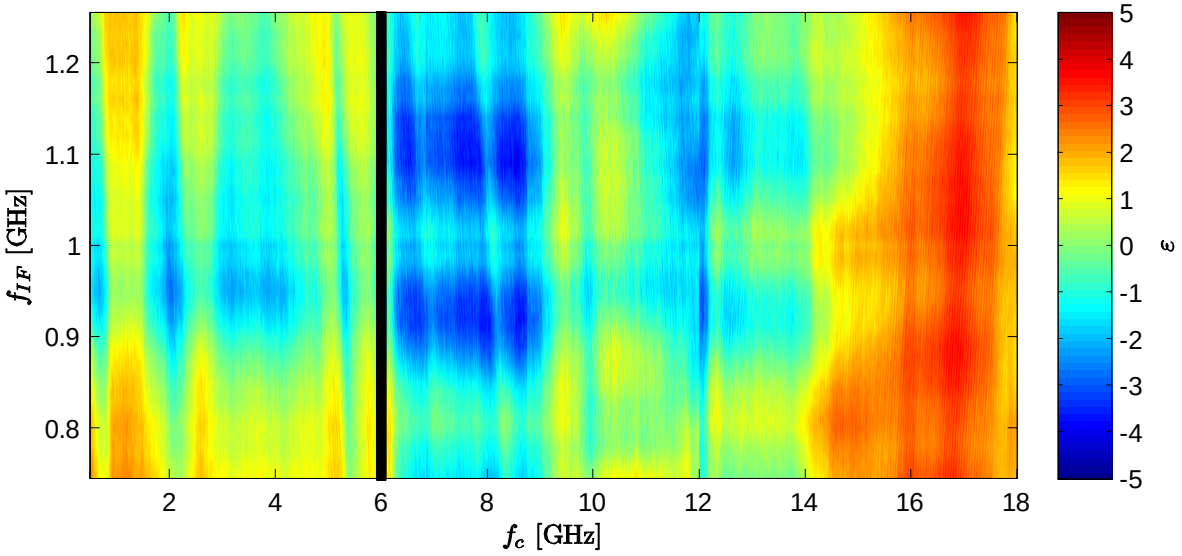

Figure 5.3 Residual errors of the model in Fig. 5.1, for tuner #2.

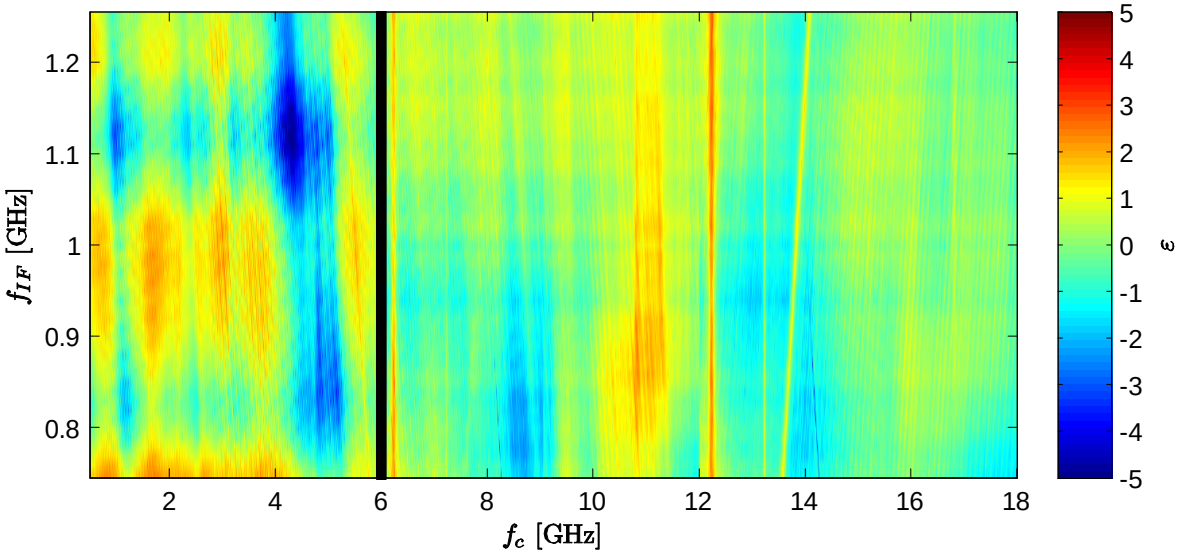

Figure 5.4 Residual errors of the model in Fig. 5.1, for tuner #3.

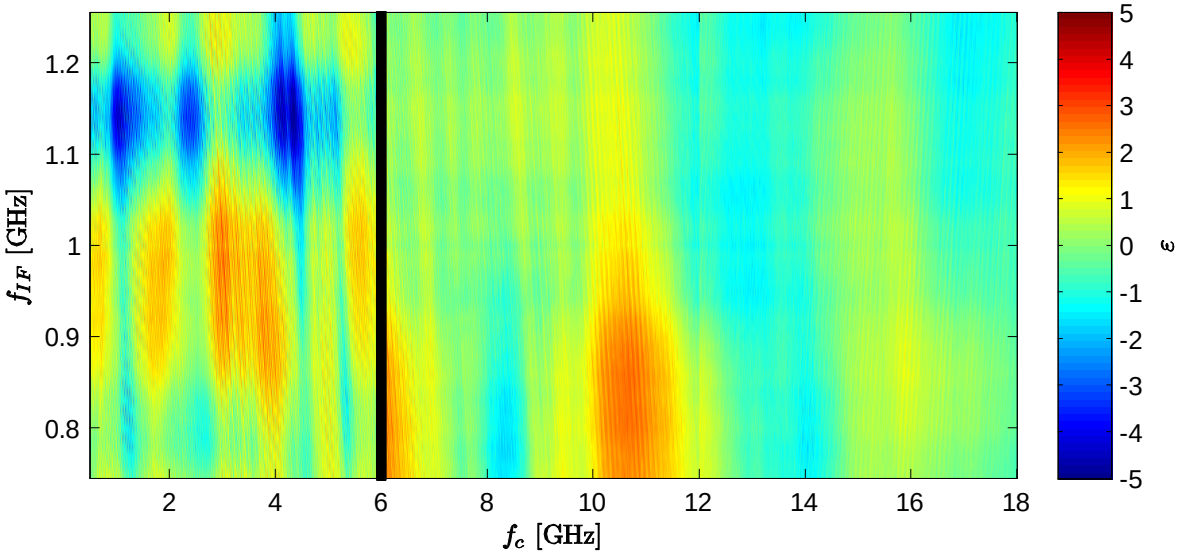

Figure 5.5 Residual errors of the model in Fig. 5.1, for tuner #4.

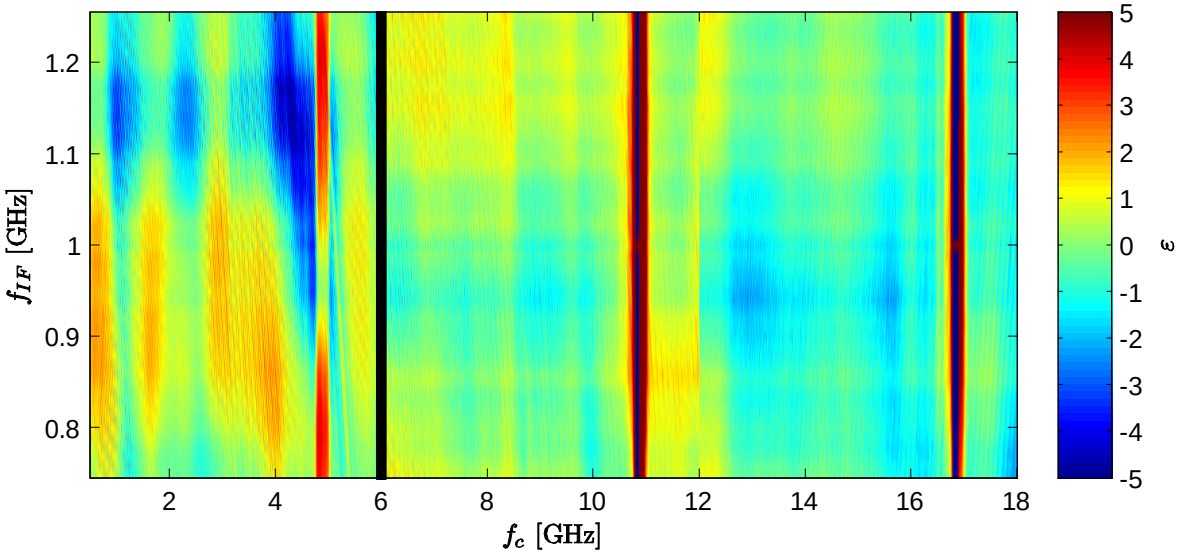

Figure 5.6 Residual errors of the model in Fig. 5.1, for tuner #5.

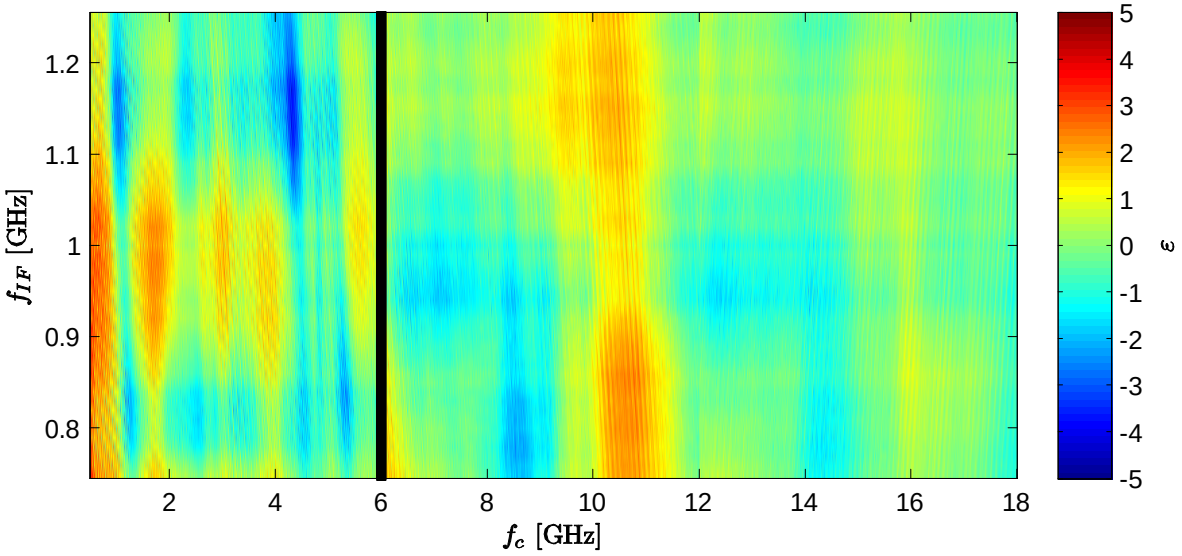

Figure 5.7 Residual errors of the model in Fig. 5.1, for tuner #6.

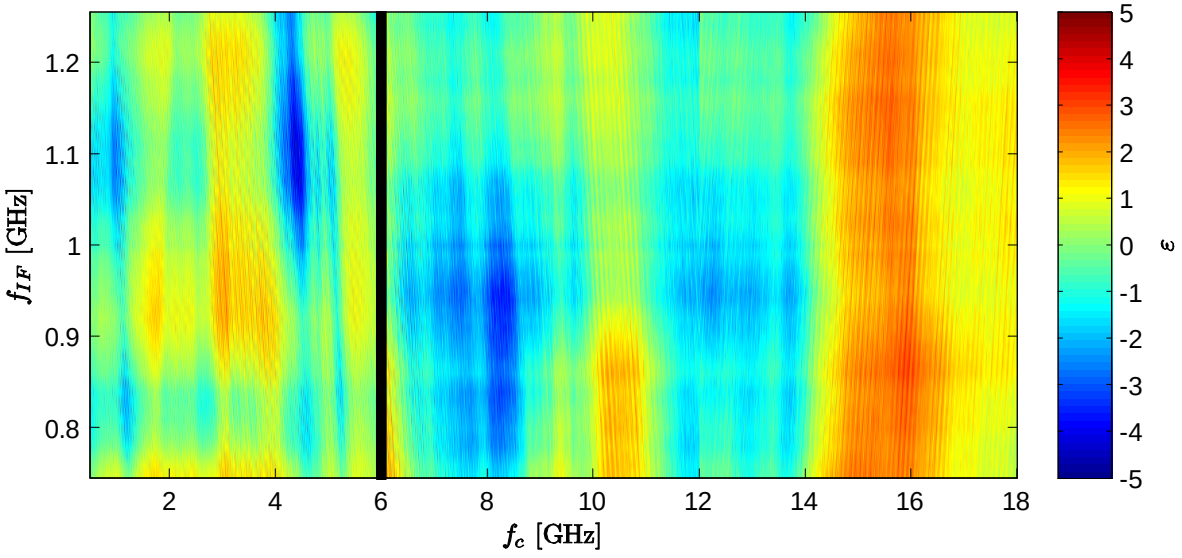

Figure 5.8 Residual errors of the model in Fig. 5.1, for tuner #7.

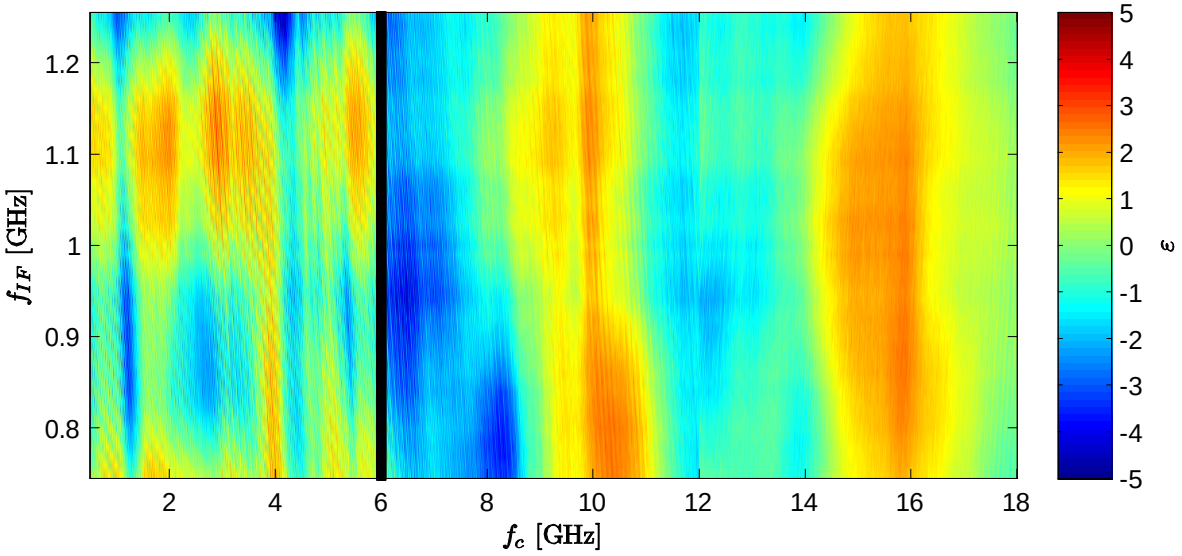

Figure 5.9 Residual errors of the model in Fig. 5.1, for tuner #8.

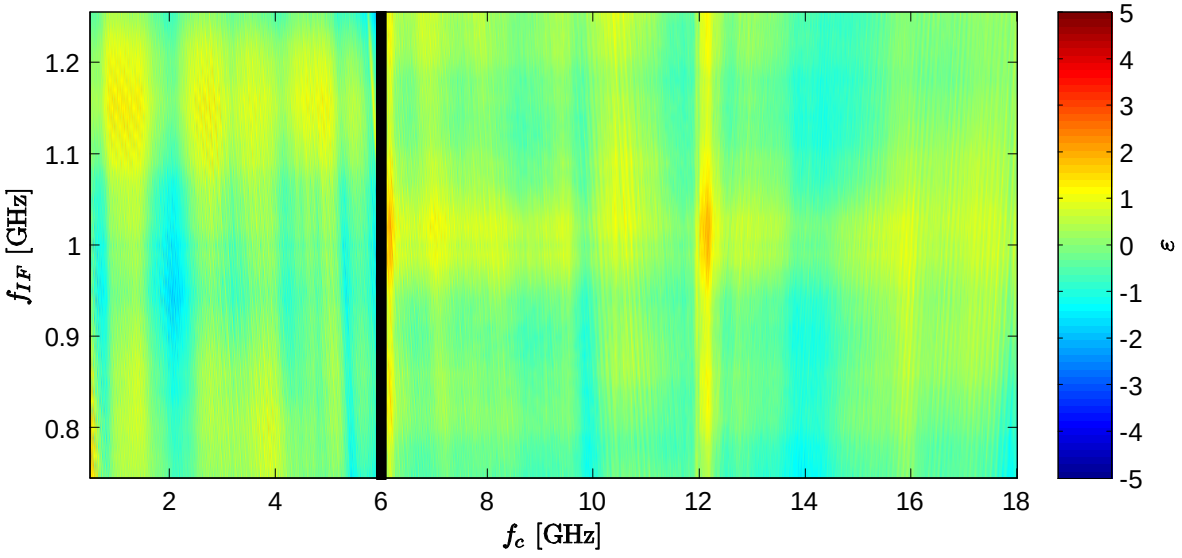

Figure 5.10 Residual errors of the model in Fig. 5.1, for tuner #9.

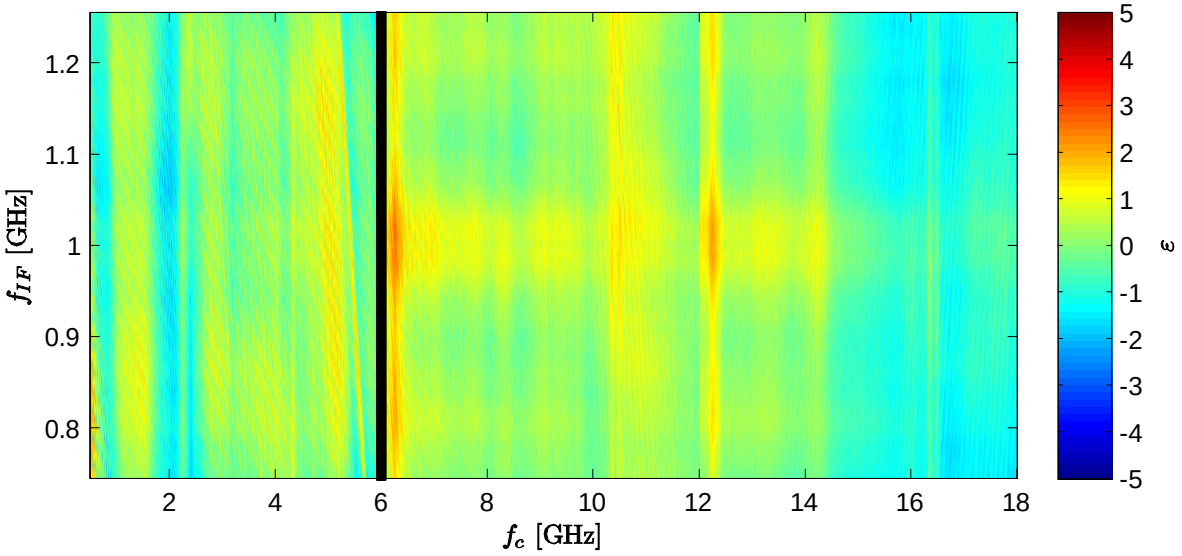

Figure 5.11 Residual errors of the model in Fig. 5.1, for tuner #10.

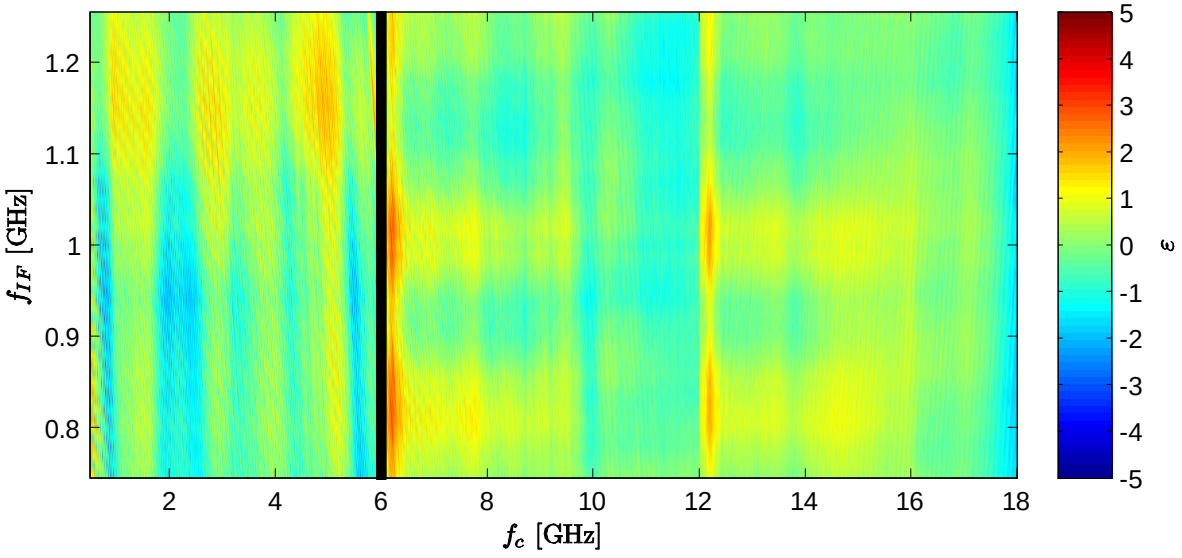

Figure 5.12 Residual errors of the model in Fig. 5.1, for tuner #11.

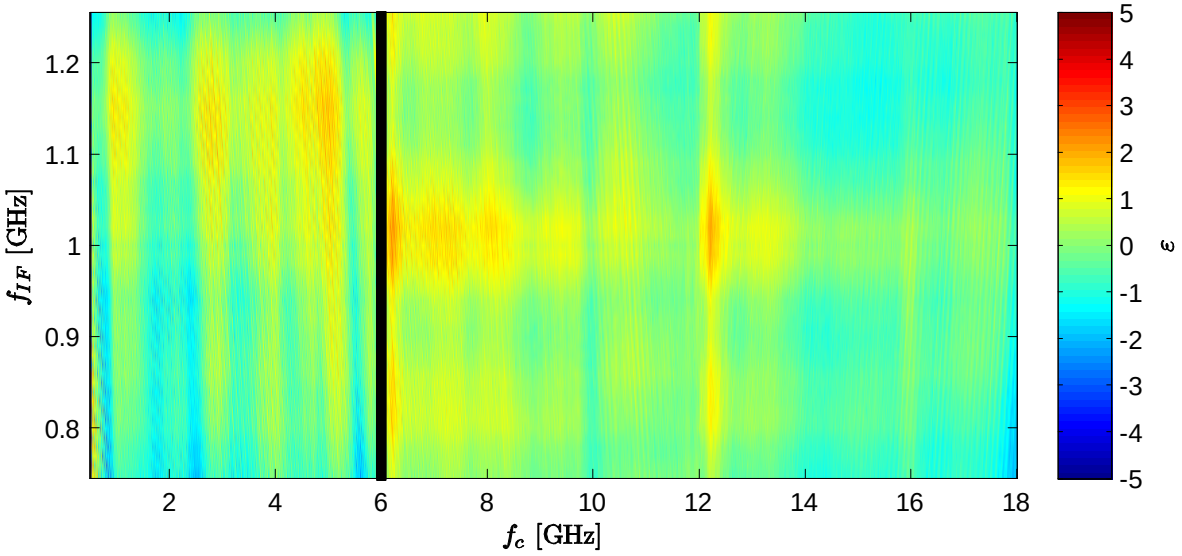

Figure 5.13 Residual errors of the model in Fig. 5.1, for tuner #12.

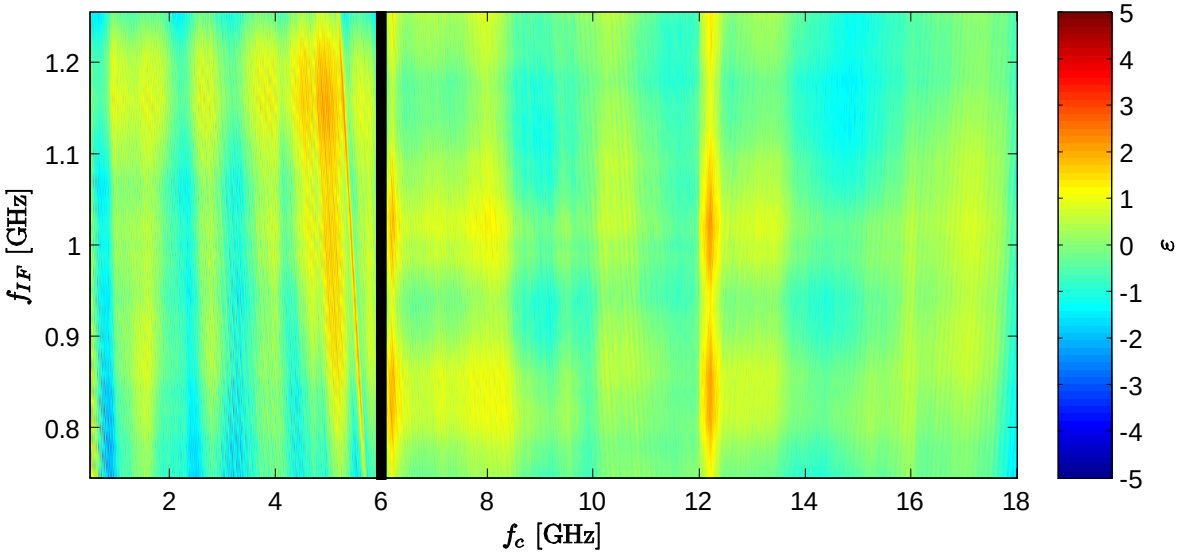

Figure 5.14 Residual errors of the model in Fig. 5.1, for tuner #13.

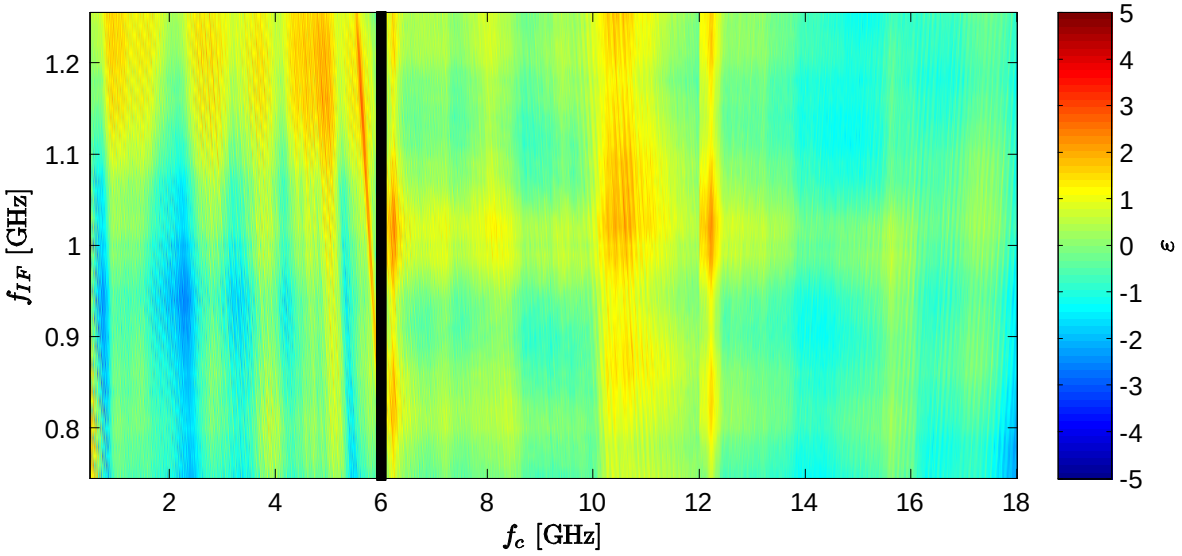

Figure 5.15 Residual errors of the model in Fig. 5.1, for tuner #14.

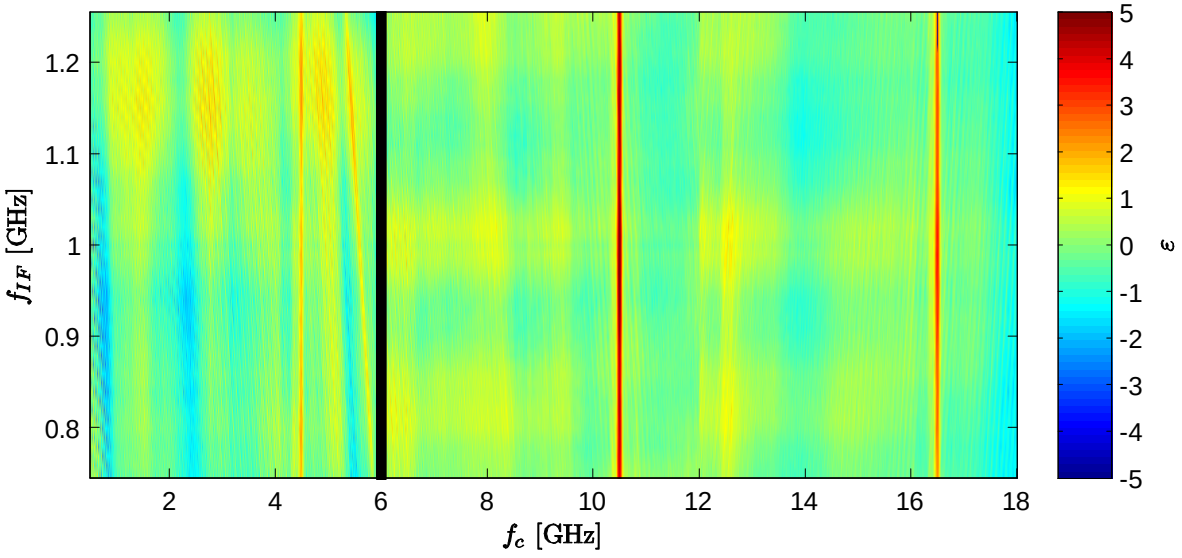

Figure 5.16 Residual errors of the model in Fig. 5.1, for tuner #15.

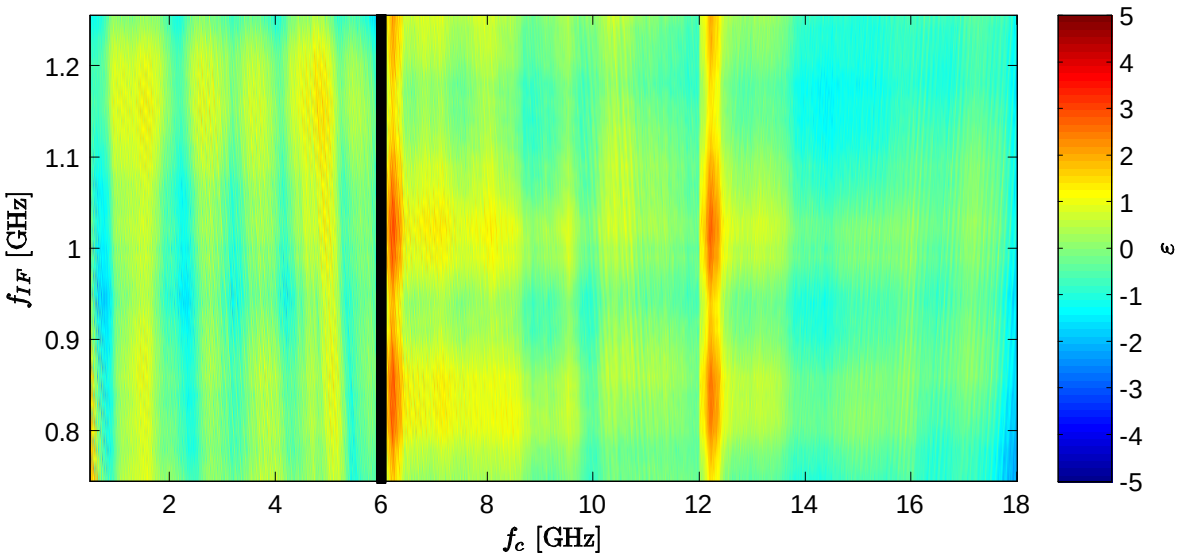

Figure 5.17 Residual errors of the model in Fig. 5.1, for tuner #16.

5.1.3 Statistical Distribution of Residual Errors. The residual errors in Figs. 5.2-5.17 are summarized in Figs. 5.18-5.19 and Table 5.2. The least squares method ensures that the residual errors will have a mean of zero; this is apparent in the histograms. For each model, three different hypothetical statistical distributions were fit to the set of residual errors: a Gaussian, a lognormal, and a t distribution [5], such that:

$$H_0 \quad : \quad \varepsilon \sim \mathcal{N}\left(\mu_\varepsilon, \sigma_\varepsilon^2\right) \tag{5.10}$$

$$H_1 \quad : \quad (\varepsilon - \Delta\varepsilon_L) \sim \text{Log-}\mathcal{N}\left(\mu_{\varepsilon,L}, \sigma_{\varepsilon,L}^2\right) \tag{5.11}$$

$$H_2 \quad : \quad \varepsilon \sim t\left(\mu_{\varepsilon,t}, \sigma_{\varepsilon,t}, \nu_{\varepsilon,t}\right), \tag{5.12}$$

where μ_ε and σ_ε^2 are the mean and variance of the Gaussian distribution; $\mu_{\varepsilon,L}$ and $\sigma_{\varepsilon,L}^2$ are the parameters of the lognormal distribution; the t distribution has location $\mu_{\varepsilon,t}$, scale factor $\sigma_{\varepsilon,t}$, and $\nu_{\varepsilon,t}$ degrees of freedom; and the correction $\Delta\varepsilon_L$ is allowed to create the optimum lognormal fit. The three distributions were evaluated according to the likelihood Λ of the fit, such that

$$\Lambda = \prod_{i=1}^{Nn_c n_{IF}} f_\varepsilon\left(\varepsilon_i\right) \tag{5.13}$$

and the log-likelihood is

$$\ln \Lambda = \sum_{i=1}^{N n_c n_{IF}} \ln f_\varepsilon \left(\varepsilon_i \right) \tag{5.14}$$

for all residuals ε_i, and f_ε is the Probability Density Function (PDF) of the hypothetical distribution. The three hypothetical PDFs are [1]:

$$\text{Gaussian} \quad : \quad f_\varepsilon \left(\varepsilon \right) = \frac{1}{\sqrt{2\pi}\sigma_\varepsilon} \exp\left(-\frac{\left(\varepsilon - \mu_\varepsilon \right)^2}{2\sigma_\varepsilon^2} \right) \tag{5.15}$$

$$\text{Lognormal} \quad : \quad f_\varepsilon \left(\varepsilon \right) = \frac{1}{\left(\varepsilon - \Delta\varepsilon_L \right)\sqrt{2\pi}\sigma_{\varepsilon,L}} \exp\left(-\frac{\left(\ln\left(\varepsilon - \Delta\varepsilon_L \right) - \mu_{\varepsilon,L} \right)^2}{2\sigma_{\varepsilon,L}^2} \right) \tag{5.16}$$

$$t \text{ Location-Scale} \quad : \quad f_\varepsilon \left(\varepsilon \right) = \frac{\Gamma\left(\frac{\nu_{\varepsilon,t}+1}{2} \right)}{\sqrt{\nu_{\varepsilon,t}\pi}\Gamma\left(\frac{\nu_{\varepsilon,t}}{2} \right)} \left(1 + \frac{\left(\varepsilon - \mu_{\varepsilon,t} \right)^2}{\nu_{\varepsilon,t}\sigma_{\varepsilon,t}^2} \right)^{-\left(\frac{\nu_{\varepsilon,t}+1}{2} \right)}, \tag{5.17}$$

where Γ is the gamma function defined as

$$\Gamma\left(z \right) \equiv \int_0^\infty x^{z-1} e^{-x} dx. \tag{5.18}$$

In each case, the residual errors are not normally distributed; in fact, the t distribution is the best fit, as seen in Figs. 5.18-5.19 and Table 5.2.

The t distribution arises when we try to characterize a normally-distributed population using a small sample size. It is expected that neighboring samples within Figs. 4.1-4.35 and 4.41-4.71 will be correlated with each other. The model in 5.1 contains 24 coefficients. In the low band, the residual error t distribution has only 9 degrees of freedom, and yet it was formed from hundreds of thousands of samples. This means that the samples are extremely highly correlated. By comparison, consider an arbitrary data set containing 34 independent samples from 16 tuners. If it were modeled using 5.1 with $q = 4$ as in Fig. 5.1, the t distribution of residuals would have $34 - 24 - 1 = 9$ degrees of freedom. Since there are 16 tuners in the MCWESS, on average each one contributes the equivalent of only $34/16 = 2.1$ independent samples throughout the low band data set.

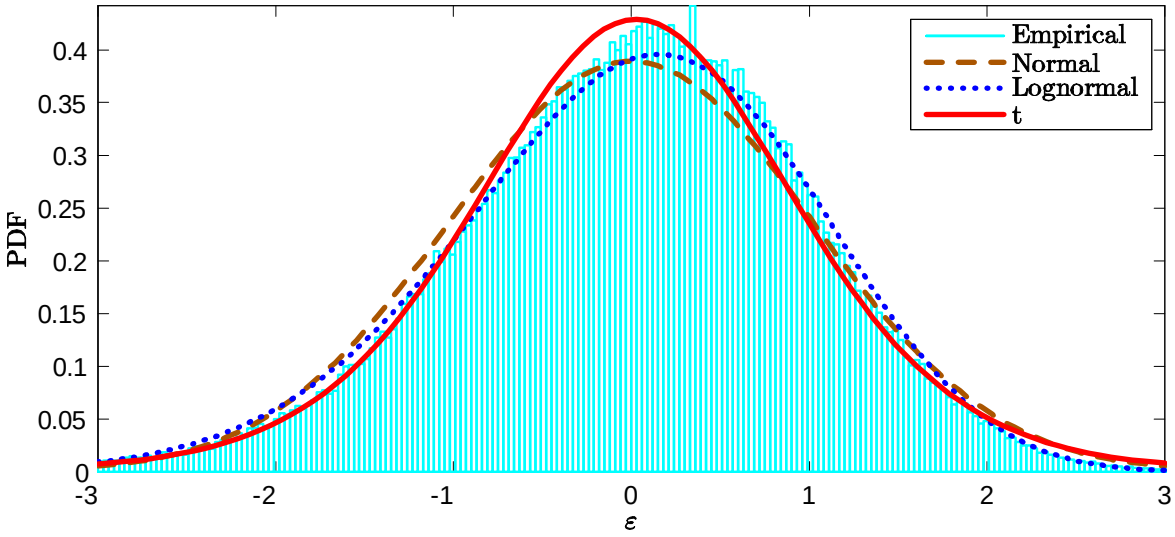

Figure 5.18 Histogram of the residual errors in Figs. 5.2-5.17, for the low band ($0.5 \leq f_c < 6$ GHz). Three hypothetical distributions are also shown: normal, lognormal, and t.

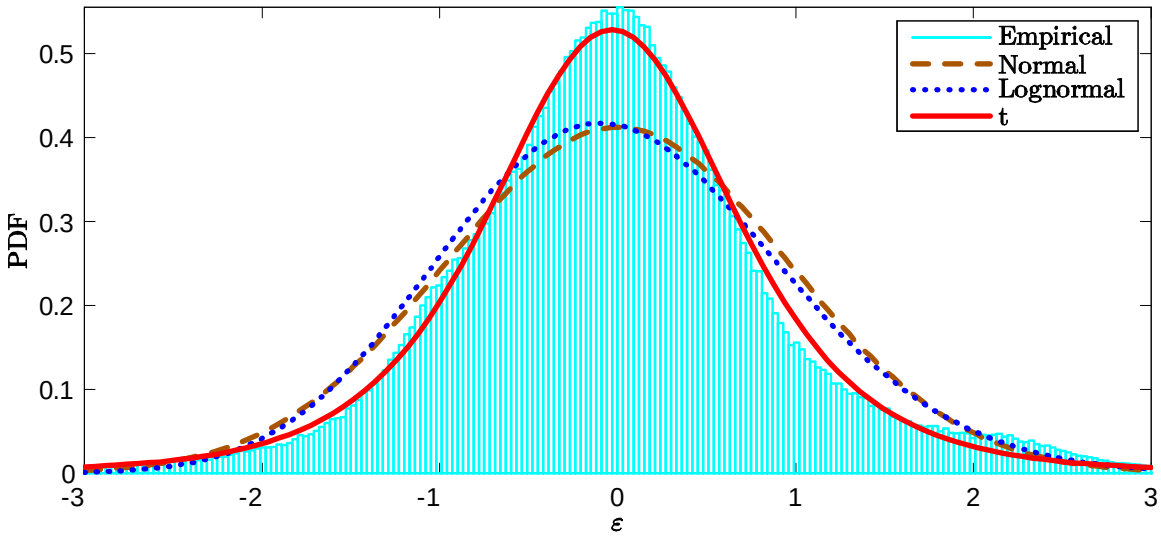

Figure 5.19 Histogram of the residual errors in Figs. 5.2-5.17, for the high band ($6 \leq f_c \leq 18$ GHz). Three hypothetical distributions are also shown: normal, lognormal, and t.

Table 5.2 Summary of the residual errors for the polynomial models for the Mid-Atlantic LCR400 tuners.

	Low Band ($0.5 \leq f_c < 6$ GHz)	High Band ($6 \leq f_c \leq 18$ GHz)
Sample Size	299422	653052
q	4	4
Residual Errors		
Mean	0.000	0.000
Std Dev	1.025	0.967
Skewness	-0.463	0.609
Kurtosis	4.187	7.576
Normal Dist.		
μ_ε	0.000	0.000
σ_ε	1.025	0.967
Log-Likelihood	-4.32×10^{-5}	-9.05×10^{-5}
Lognormal Dist.		
$\mu_{\varepsilon,L}$	2.298	2.650
$\sigma_{\varepsilon,L}$	0.102	0.068
$\Delta\varepsilon_L$	-10.007	14.192
Log-Likelihood	-4.29×10^{-5}	-8.99×10^{-5}
t Location-Scale		
$\mu_{\varepsilon,t}$	0.029	-0.032
$\sigma_{\varepsilon,t}$	0.905	0.711
$\nu_{\varepsilon,t}$	9.146	4.158
Log-Likelihood	-4.28×10^{-5}	-8.69×10^{-5}

5.1.4 Normality Test of Tuner Gain Performance. This section addresses the question of whether tuner gain is normally distributed from one channel to the next, holding f_c, f_{in}, and f_{IF} constant. If a tuner breaks, and we replace it with another tuner of the same make and model, how would we expect the replacement tuner to perform, based on data from the other tuners? What is the statistical distribution of channel mismatches caused by tuner gain issues?

Any statistical distribution is characterized by parameters such as the mean, median, standard deviation, skewness, and kurtosis. For any random variable X, the skewness quantifies the degree of asymmetry of the distribution, and is defined as

$$\text{Skew}\,[X] \equiv \frac{\mu_3}{\sigma^3}, \tag{5.19}$$

where μ_3 is the third moment about the mean, and σ is the standard deviation. If $\{x_1, \ldots x_n\}$ is a sample taken from X, the sample skewness γ_1 is computed by

$$\gamma_1 = \frac{\frac{1}{n}\sum_{i=1}^{n}(x_i - \bar{x})^3}{\left(\frac{1}{n}\sum_{i=1}^{n}(x_i - \bar{x})^2\right)^{3/2}}, \tag{5.20}$$

where n is the sample size, and $\bar{x}$ is the sample mean. The kurtosis quantifies how outlier-prone the distribution is, and is defined as

$$\text{Kurt}\,[X] \equiv \frac{\mu_4}{\sigma^4}, \tag{5.21}$$

where μ_4 is the fourth moment about the mean. For any random sample $\{x_1, \ldots x_n\}$, the sample kurtosis γ_2 is computed by

$$\gamma_2 = \frac{\frac{1}{n}\sum_{i=1}^{n}(x_i - \bar{x})^4}{\left(\frac{1}{n}\sum_{i=1}^{n}(x_i - \bar{x})^2\right)^2}. \tag{5.22}$$

It is known that *for any real-valued Gaussian distribution, the skewness is zero, and the kurtosis is three.*

To evaluate the question of normality, we can compute the sample skewness and kurtosis of the gain $g\left(K, f_c, f_{IF}\right)$, for a single value of (f_c, f_{IF}), where the tuner ID number K is a nominal random variable with a discrete uniform Probability Mass Function (PMF). We can then repeat that calculation for all values of f_c and f_{IF}. Equations (5.20) and (5.22) are then rewritten as

$$\gamma_1\left(f_{c,j_c}, f_{IF,j_{IF}}\right) = \frac{\frac{1}{N}\sum_{k=1}^{N}\left(g\left(k, f_{c,j_c}, f_{IF,j_{IF}}\right) - \overline{g\left(f_{c,j_c}, f_{IF,j_{IF}}\right)}\right)^3}{\left(\frac{1}{N}\sum_{k=1}^{N}\left(g\left(k, f_{c,j_c}, f_{IF,j_{IF}}\right) - \overline{g\left(f_{c,j_c}, f_{IF,j_{IF}}\right)}\right)^2\right)^{3/2}} \tag{5.23}$$

and

$$\gamma_2\left(f_{c,j_c}, f_{IF,j_{IF}}\right) = \frac{\frac{1}{N}\sum_{k=1}^{N}\left(g\left(k, f_{c,j_c}, f_{IF,j_{IF}}\right) - \overline{g\left(f_{c,j_c}, f_{IF,j_{IF}}\right)}\right)^4}{\left(\frac{1}{N}\sum_{k=1}^{N}\left(g\left(k, f_{c,j_c}, f_{IF,j_{IF}}\right) - \overline{g\left(f_{c,j_c}, f_{IF,j_{IF}}\right)}\right)^2\right)^2}, \tag{5.24}$$

where the sample mean $\overline{g\left(f_{c,j_c}, f_{IF,j_{IF}}\right)}$ is computed as

$$\overline{g\left(f_{c,j_c}, f_{IF,j_{IF}}\right)} = \frac{1}{N}\sum_{k=1}^{N} g\left(k, f_{c,j_c}, f_{IF,j_{IF}}\right). \tag{5.25}$$

We can improve the calculation of γ_1 and γ_2 by creating a window of $(2u_c+1)\times(2u_{IF}+1)$ samples centered about (j_c, j_{IF}), where u_c and u_{IF} determine the number of gain samples along the f_c and f_{IF} axes. This increases the sample size to $N\left(2u_c+1\right)\left(2u_{IF}+1\right)$. Thus

(5.23-5.25) are rewritten as

$$\gamma_1\left(f_{c,j_c}, f_{IF,j_{IF}}\right) = \tag{5.26}$$
$$\frac{\frac{1}{N(2u_c+1)(2u_{IF}+1)}\sum_{k=1}^{N}\sum_{m=-u_c}^{u_c}\sum_{n=-u_{IF}}^{u_{IF}}\left(g\left(k, f_{c,(j_c+m)}, f_{IF,(j_{IF}+n)}\right) - \overline{g\left(f_{c,j_c}, f_{IF,j_{IF}}\right)}\right)^3}{\left(\frac{1}{N(2u_c+1)(2u_{IF}+1)}\sum_{k=1}^{N}\sum_{m=-u_c}^{u_c}\sum_{n=-u_{IF}}^{u_{IF}}\left(g\left(k, f_{c,(j_c+m)}, f_{IF,(j_{IF}+n)}\right) - \overline{g\left(f_{c,j_c}, f_{IF,j_{IF}}\right)}\right)^2\right)^{3/2}},$$

$$\gamma_2\left(f_{c,j_c}, f_{IF,j_{IF}}\right) = \tag{5.27}$$
$$\frac{\frac{1}{N(2u_c+1)(2u_{IF}+1)}\sum_{k=1}^{N}\sum_{m=-u_c}^{u_c}\sum_{n=-u_{IF}}^{u_{IF}}\left(g\left(k, f_{c,(j_c+m)}, f_{IF,(j_{IF}+n)}\right) - \overline{g\left(f_{c,j_c}, f_{IF,j_{IF}}\right)}\right)^4}{\left(\frac{1}{N(2u_c+1)(2u_{IF}+1)}\sum_{k=1}^{N}\sum_{m=-u_c}^{u_c}\sum_{n=-u_{IF}}^{u_{IF}}\left(g\left(k, f_{c,(j_c+m)}, f_{IF,(j_{IF}+n)}\right) - \overline{g\left(f_{c,j_c}, f_{IF,j_{IF}}\right)}\right)^2\right)^{2}},$$

and

$$\overline{g\left(f_{c,j_c}, f_{IF,j_{IF}}\right)} = \frac{1}{N\left(2u_c+1\right)\left(2u_{IF}+1\right)}\sum_{k=1}^{N}\sum_{m=-u_c}^{u_c}\sum_{n=-u_{IF}}^{u_{IF}} g\left(k, f_{c,(j_c+m)}, f_{IF,(j_{IF}+n)}\right). \tag{5.28}$$

The tuner serial numbers in Table 3.1 indicate that the MCWESS tuners were produced in three different lots: tuners $\{1, 3, \ldots 8\}$ are lot 0649, tuners $\{9, \ldots 16\}$ are lot 0732, and tuner 2 alone is lot 0831. For the purpose of normality testing, we will treat these three sets as samples of three different populations; lot 0831 will not be considered, because the sample size is too small. Using (5.26-5.28) on tuners $\{9, \ldots 16\}$ with a 3×3 window size (i.e. $u_c = 1$ and $u_{IF} = 1$) give the skewnesses and kurtoses shown in Figs. 5.20-5.21; the sample size at each point on the plot is $8 \cdot 3 \cdot 3 = 72$. The green areas on both of these plots indicate that the tuner gain might be normally distributed among tuners, at those points in the frequency spectrum, i.e. $\gamma_1\left(f_{c,j_c}, f_{IF,j_{IF}}\right) = 0$ and $\gamma_2\left(f_{c,j_c}, f_{IF,j_{IF}}\right) = 3$ for some particular values of (j_c, j_{IF}). Fig. 5.22 shows histograms of the same data for three different frequency bands: $0.5 \le f_c < 6\,\text{GHz}$, $6 \le f_c < 12\,\text{GHz}$, and $12 \le f_c \le 18\,\text{GHz}$.

From Figs. 5.20-5.22 it seems clear that tuner gain in general is not normally distributed. But how do we test it? Although (5.26-5.28) improve the accuracy of γ_1 and γ_2, we can not simply perform a Jarque-Bera or Lilliefors test for normality using a sample size of $N\left(2u_c+1\right)\left(2u_{IF}+1\right)$, because the samples which come from a single tuner are not

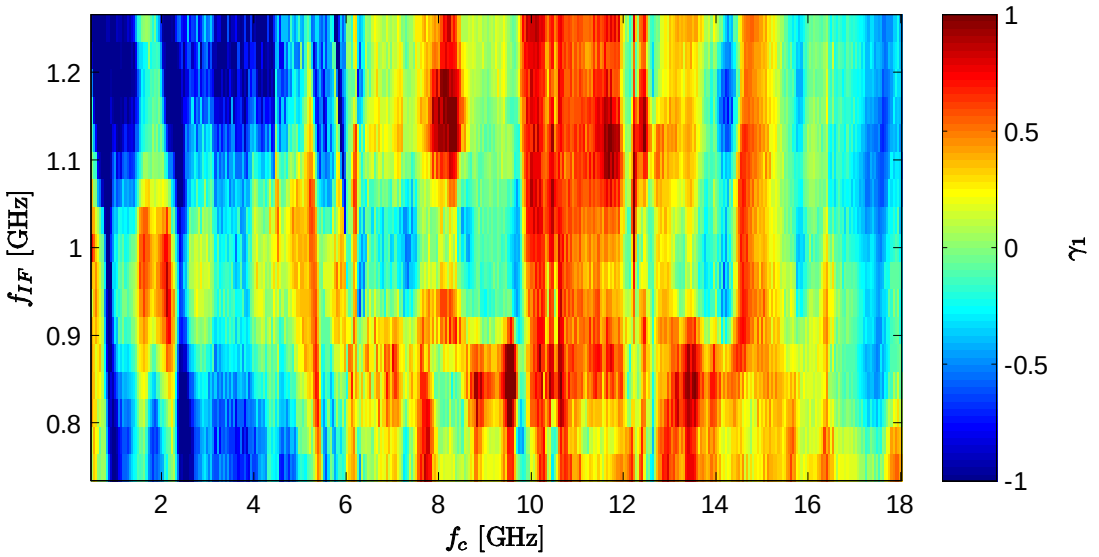

Figure 5.20 Skewness of the voltage gain of tuners $\{9, \ldots 16\}$, with respect to each other, at each point in the frequency spectrum. (Voltage gain is in linear scale.)

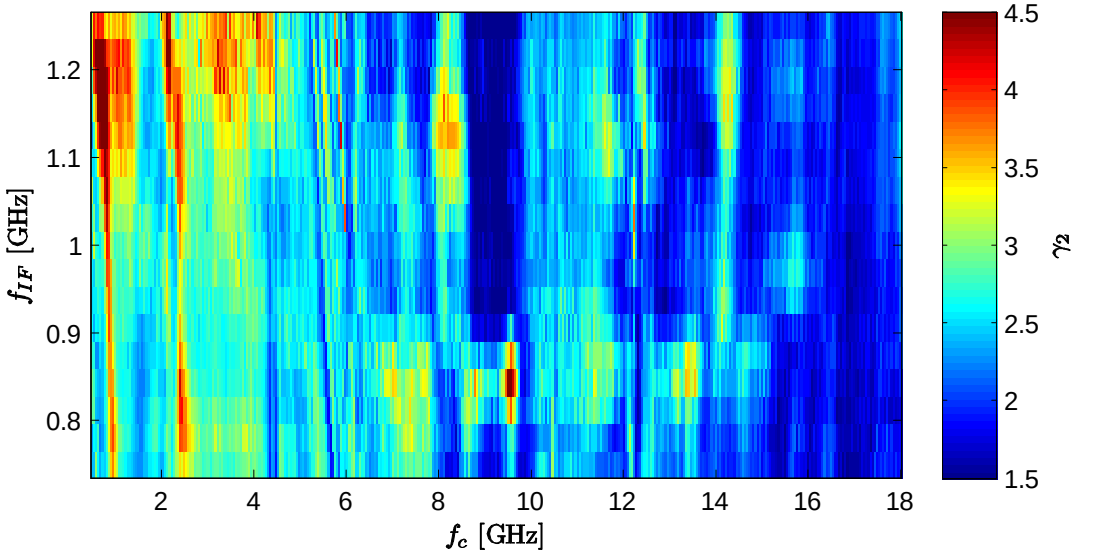

Figure 5.21 Kurtosis of the voltage gain of tuners $\{9, \ldots 16\}$, with respect to each other, at each point in the frequency spectrum. (Voltage gain is in linear scale.)

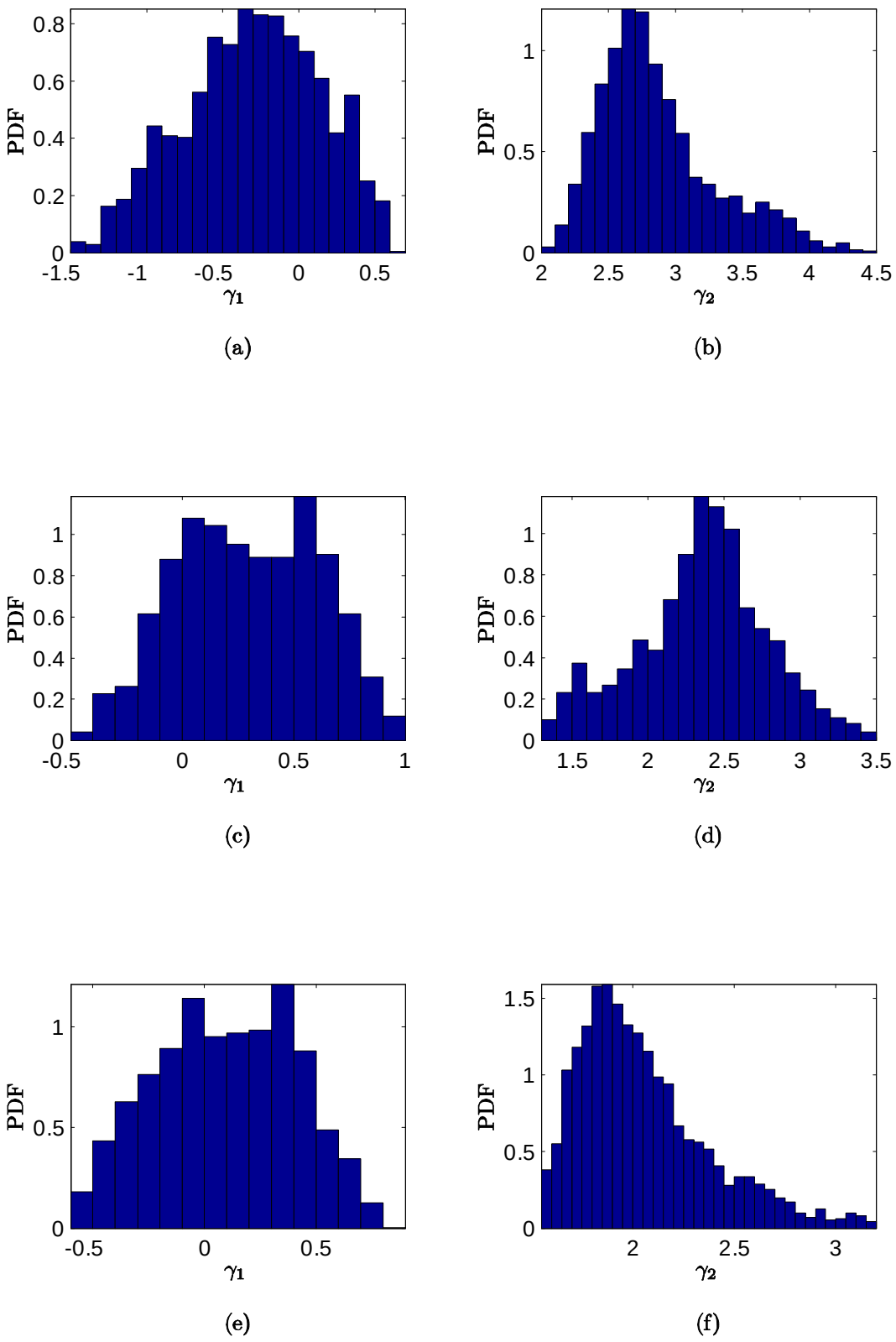

Figure 5.22 Histograms of the skewnesses γ_1 and kurtoses γ_2 shown in Figs. 5.20-5.21. (a,b) $0.5 \leq f_c < 6\,\text{GHz}$. (c,d) $6 \leq f_c < 12\,\text{GHz}$. (e,f) $12 \leq f_c \leq 18\,\text{GHz}$.

independent; in fact, they are very strongly correlated. To test normality at each point in the spectrum, we can perform a one-sample Wilcoxon signed rank test [2]. Regardless of the shape of the distribution, the Wilcoxon test allows us to determine the likelihood that the samples came from a zero-median population. Consider a random variable X, from which we obtain M nonzero samples $\{x_1, \ldots x_M\}$. Our null hypothesis H_0 is

$$H_0 : \text{Median}\,[X] = 0, \tag{5.29}$$

and the alternatives H_1 and H_2 are

$$\begin{aligned} H_1 &: \text{Median}\,[X] \neq 0 \\ H_2 &: \text{Median}\,[X] > 0. \end{aligned} \tag{5.30}$$

The Wilcoxon signed rank statistic W^+ is computed as

$$W^+ = \sum_{i=1}^{M} \xi_i R_i, \tag{5.31}$$

where

$$\xi_i = \begin{cases} 1 & \text{if } x_i > 0 \\ 0 & \text{otherwise,} \end{cases} \tag{5.32}$$

and the ranks $R_i \in \{1, \ldots M\}$ are the indices obtained by sorting the magnitudes of the samples $\{|x_1|, \ldots |x_M|\}$ in order from least to greatest. If H_0 is true and M is large, then

$$W^* = \frac{W^+ - \text{E}\,[W^+]}{\sqrt{\text{Var}\,[W^+]}} = \frac{W^+ - M\,(M+1)\,/4}{\sqrt{M\,(M+1)\,(2M+1)\,/24}}, \tag{5.33}$$

(where E[$\cdot$] means expected value and Var[$\cdot$] means variance) has the standard normal distribution. Therefore, we can test H_0 versus H_2 using:

$$\begin{aligned} \text{accept } H_0 \quad &\text{if} \quad W^* < z_{(\alpha)} \\ \text{accept } H_2 \quad &\text{if} \quad W^* \geq z_{(\alpha)}, \end{aligned} \tag{5.34}$$

where $\left(1 - z_{(\alpha)}\right)$ is the inverse Cumulative Distribution Function (CDF) of the standard Gaussian distribution, and α is the statistical significance level of the test. This can be

rewritten as

$$\begin{aligned} &\text{accept } H_0 \quad \text{if} \quad P_{W^*} > \alpha \\ &\text{accept } H_2 \quad \text{if} \quad P_{W^*} \leq \alpha, \end{aligned} \tag{5.35}$$

where the p-value P_{W^*} is defined as

$$P_{W^*} = \mathrm{P}\left[\text{Median}\left[X\right] \geq W^*\right], \tag{5.36}$$

where P[·] means probability, and P_{W^*} tells us the likelihood that the population median could be greater than or equal to W^*, given the sample. Equations (5.34)-(5.35) are a one-sided test; instead, what we really need is a two-sided test. The two-sided test is:

$$\begin{aligned} &\text{accept } H_0 \quad \text{if} \quad |W^*| < z_{(\alpha)} \\ &\text{accept } H_1 \quad \text{if} \quad |W^*| \geq z_{(\alpha)}. \end{aligned} \tag{5.37}$$

or

$$\begin{aligned} &\text{accept } H_0 \quad \text{if} \quad 2P_{W^*} > \alpha \\ &\text{accept } H_1 \quad \text{if} \quad 2P_{W^*} \leq \alpha. \end{aligned} \tag{5.38}$$

To test the normality of the gain, we set up the following hypotheses:

$$\begin{aligned} H_{\gamma_1,0} &: \text{Median}[\text{Skew}\left[g\left(K, f_c, f_{IF}\right)\right]] = 0 \\ H_{\gamma_1,1} &: \text{Median}[\text{Skew}\left[g\left(K, f_c, f_{IF}\right)\right]] \neq 0 \end{aligned} \tag{5.39}$$

and

$$\begin{aligned} H_{\gamma_2,0} &: \text{Median}[\text{Kurt}\left[g\left(K, f_c, f_{IF}\right)\right] - 3] = 0 \\ H_{\gamma_2,1} &: \text{Median}[\text{Kurt}\left[g\left(K, f_c, f_{IF}\right)\right] - 3] \neq 0 \end{aligned} \tag{5.40}$$

where $g\left(K, f_c, f_{IF}\right)$ represents the population of gains of all tuners at a fixed value of (f_c, f_{IF}). Once again, we will look at the data from Figs. 5.20-5.21, which was computed using (5.26)-(5.28). Similarly to the way we used a window to sample the gain in (5.26)-(5.28), we will use a larger window of size $(2v_c + 1) \times (2v_{IF} + 1)$ to sample the skewnesses and kurtoses shown in Figs. 5.20-5.21, where v_c and v_{IF} determine the number of skewness or kurtosis samples along the f_c and f_{IF} axes. Thus the samples used to test $H_{\gamma_1,0}$ and

$H_{\gamma_2,0}$ are

$$S_{\gamma_1} = \left\{ \left\{ \gamma_1 \left(f_{c,(j_c+m)}, f_{IF,(j_{IF}+n)} \right) \right\}_{n=-v_{IF}}^{v_{IF}} \right\}_{m=-v_c}^{v_c} \tag{5.41}$$

$$S_{\gamma_2} = \left\{ \left\{ \gamma_2 \left(f_{c,(j_c+m)}, f_{IF,(j_{IF}+n)} \right) \right\}_{n=-v_{IF}}^{v_{IF}} \right\}_{m=-v_c}^{v_c}, \tag{5.42}$$

where γ_1 and γ_1 are computed from (5.26)-(5.28), and so the actual tests we will perform are:

$$\begin{aligned} H_{\gamma_1,0} &: \text{Median}\big[S_{\gamma_1}\big] = 0 \\ H_{\gamma_1,1} &: \text{Median}\big[S_{\gamma_1}\big] \neq 0 \end{aligned} \tag{5.43}$$

and

$$\begin{aligned} H_{\gamma_2,0} &: \text{Median}\big[S_{\gamma_2} - 3\big] = 0 \\ H_{\gamma_2,1} &: \text{Median}\big[S_{\gamma_2} - 3\big] \neq 0. \end{aligned} \tag{5.44}$$

At any given point (f_c, f_{IF}), samples S_{γ_1} and S_{γ_2} are therefore computed from $N\,(2u_c+1)\,(2u_{IF}+1)\,(2v_c+1)\,(2v_{IF}+1)$ of the original gain samples. Note that (5.41)-(5.44) tolerate some local variation around (f_c, f_{IF}), as long as within that neighborhood, the median skewness is zero and the median kurtosis is three.

Letting $u_c = 3$ and $u_{IF} = 2$ gives a 5×7 window of skewnesses and a 5×7 window of kurtoses at each point in the frequency spectrum; the sample size is 35, and we will use the large-sample Wilcoxon statistic defined in (5.33). From (5.37), given W^*, we can calculate the significance level α at which we can reject the null hypothesis H_0. Equivalently, we can compute the p-value $2P_{W^*}$ which tells us the likelihood that H_0 could be true, given the sample. Now define $W^+_{\gamma_1}, W^+_{\gamma_2}, W^*_{\gamma_1}$, and $W^*_{\gamma_2}$ as the Wilcoxon statistics for γ_1 and γ_2, and $2P_{W^*_{\gamma_1}}$ and $2P_{W^*_{\gamma_2}}$ as the associated two-sided p-values. Using (5.41)-(5.44) on the data in Figs. 5.20-5.21 gives the two-sided p-values shown in Figs. 5.23-5.24. These plots tell us that it is plausible that the gain skewness is zero, or the gain kurtosis is three, in certain isolated parts of the spectrum. However, in general it is clearly not the case; and the joint likelihood of $\gamma_1 = 0$ and $\gamma_2 = 3$ is practically nil everywhere. Therefore, we can conclude that, at any fixed frequency, *tuner gain is definitely not normally distributed among devices*. Performing the same normality test on the power gain g^2, the decibel

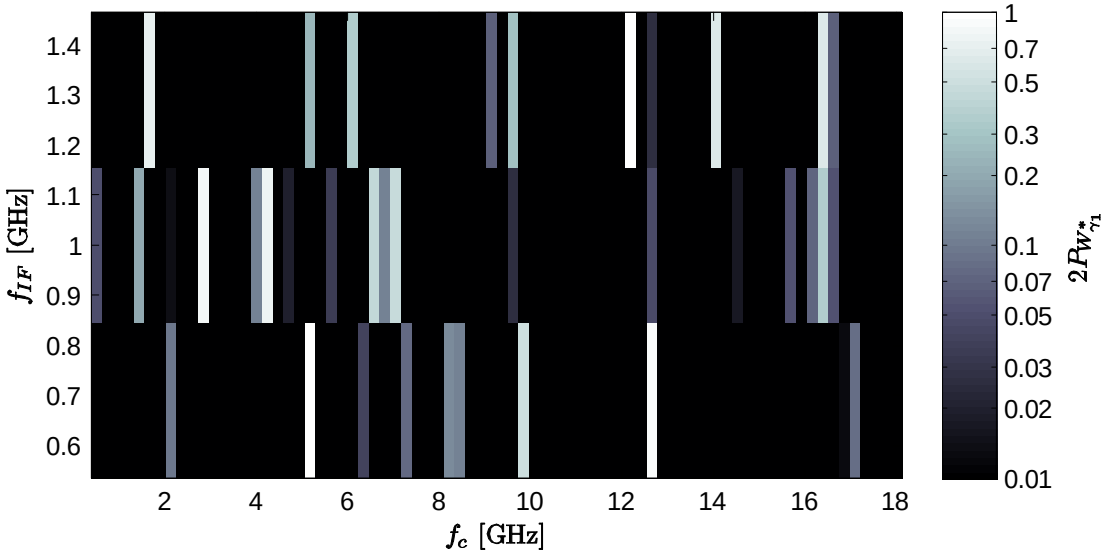

Figure 5.23 Two-sided p-values of the hypothesis $H_{\gamma_1,0}$ that the gain skewness is zero, at each point in the frequency spectrum.

gain $10\log_{10} g$, or the gain of tuners $\{1, 3, \ldots 8\}$ (the other production lot), yields similar results.

5.2 Antenna Pattern

5.2.1 Superelement Model. The antenna pattern of a single superelement of the MCWESS can be modeled as follows:

$$\hat{A}_{col}(\phi,\theta) = \begin{cases} \hat{A}_{col,max}\cos^2\frac{\phi}{\beta_\phi}\operatorname{sinc}^2\frac{\sin\theta}{\beta_\theta} & \text{for } |\phi| \le \beta_\phi \\ 0.032 \quad (-30 \text{ dBi}) & \text{otherwise,} \end{cases} \tag{5.45}$$

where $\hat{A}_{col,max}, \beta_\phi$, and β_θ are parameters of the model, computed from measured data at a particular frequency. This model represents the directivity pattern $A_k(\phi,\theta)$ in linear scale (not decibels). A generalized illustration is shown in Fig. 5.25. Note that this model is dependent on f_{in}, but not on the column number k. Ideally, the superelement gain $\hat{A}_{col,max}$ would equal each measured $A_{k,max}$ presented earlier, but in practice this is not the case. Here, $|\phi| = \pm\beta_\phi$ and $|\sin\theta| = \pm\beta_\theta$ are the locations of the first nulls. We have seen that each antenna superelement pattern has significant ripple, so there will always be error in this model.

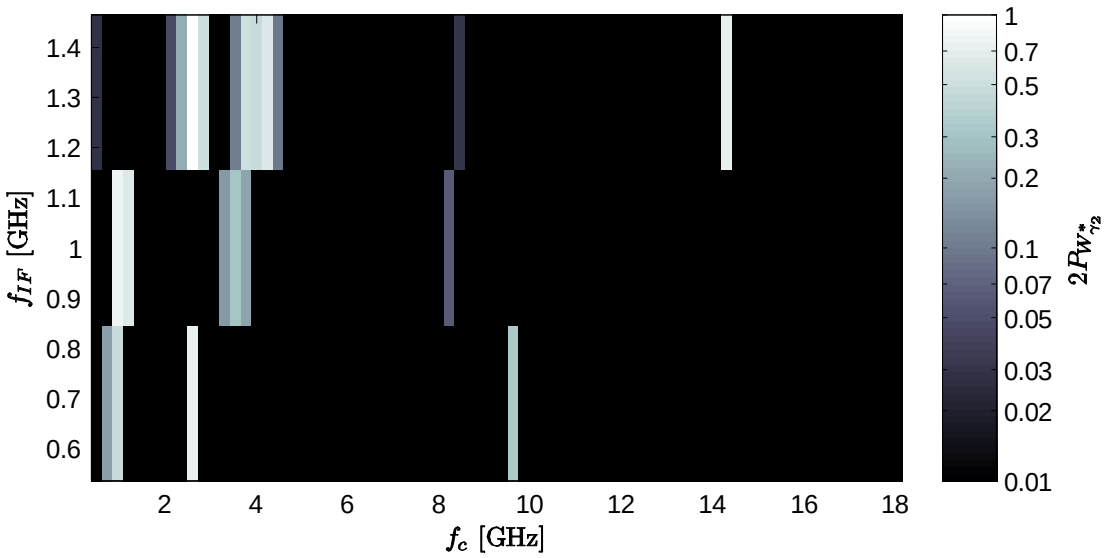

Figure 5.24 Two-sided p-values of the hypothesis $H_{\gamma_2,0}$ that the gain kurtosis is three, at each point in the frequency spectrum.

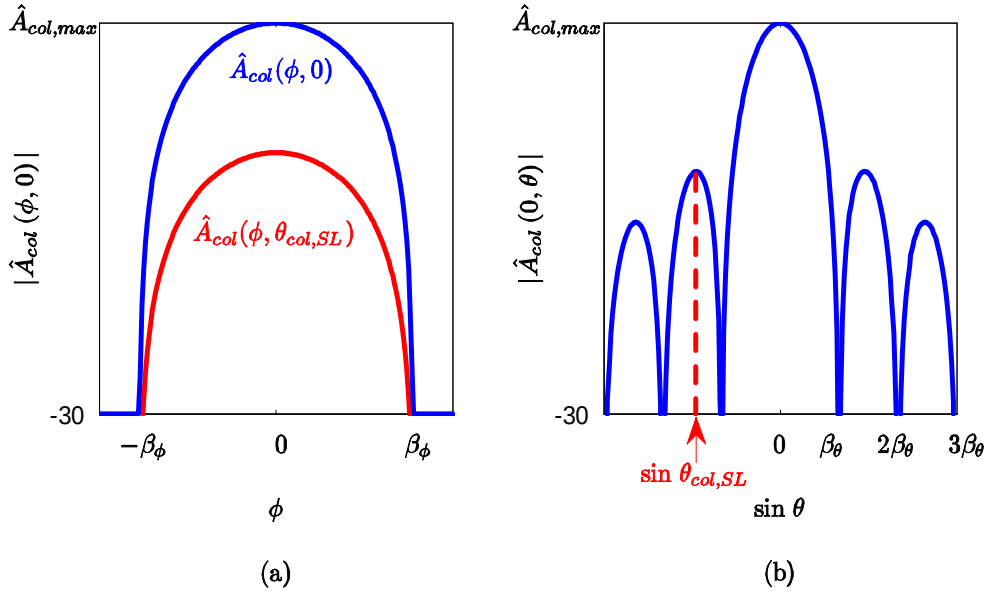

Figure 5.25 (a) Azimuth and (b) elevation cuts of the antenna superelement model in (5.45). Figure (a) shows the sidelobe at $\theta = \theta_{col,SL}$ superimposed with the mainlobe.

To create the model, first we define $\overline{A_{col}(\phi_i, \theta_j)}$ as the geometric mean of all sixteen measured voltage patterns:

$$\overline{A_{col}(\phi_i, \theta_j)} \equiv \left| \prod_{k=1}^{N} A_k(\phi_i, \theta_j) \right|^{1/N}, \tag{5.46}$$

where $N = 16$ is the number of superelements, and ϕ_i is the ith sample of $A_k(\phi_i, \theta_j)$ along the ϕ axis, and θ_j is the jth sample of $A_k(\phi_i, \theta_j)$ along the θ axis. Now $\overline{A_{col}(0, \theta)}$ is the average elevation cut for all sixteen columns. Given this average pattern, which is sinc-shaped, it is easy to locate the first nulls. We compute β_θ by solving

$$\sin^{-1}\beta_\theta = \frac{\mathrm{FNBW}_\theta}{2}. \tag{5.47}$$

Next, we wish to compute β_ϕ. Unfortunately, as seen in Figs. 4.77-4.79, the NSI2000 did not provide the location of the first null along the ϕ axis. However, from the contour plots, it seems apparent that in each case, the main beam has the same width along the ϕ axis as the *sidelobes*, and for the sidelobes, we can see the complete shape. We compute β_ϕ from the measured sidelobe data. To do this, we define Θ_{meas} as the set of all elevation angles for which measured antenna pattern data was available across the complete domain of $|\phi_i| \leq 90°$, as seen in Figs. 4.77a-4.79a. For example, in Fig. 4.79, $\Theta_{meas} = \{\pm 26.1°, \pm 27.0°, \ldots, \pm 66.6°\}$, and for other antenna patterns, Θ_{meas} is nearly the same. A further illustration of this is given in Fig. 5.26. Then $\theta_{col,SL} = \theta_{j_{max}}$, where

$$(i_{max}, j_{max}) = \arg\max_{i,j} \overline{A_{col}(\phi_i, \theta_j \in \Theta_{meas})}. \tag{5.48}$$

Note that in most cases $\theta_{col,SL}$ is on the first sidelobe along the elevation cut, i.e. $\theta_{col,SL} \approx \pm\sin^{-1}(1.43\beta_\theta)$; however, by definition it is the location of the peak of $\overline{A_{col}(\phi_i, \theta_j)}$ within Θ_{meas}, and at lower frequencies it is actually on the skirt of the main lobe. Now $\overline{A_{col}(\phi, \theta_{col,SL})}$ is the average azimuth cut for all sixteen columns, but it is off boresight, and usually on a sidelobe. In many cases, the first null of the azimuth cut is easy to see from the sidelobe pattern. In other cases, the sidelobe does not have a well-defined null. In the easy cases, FNBW_ϕ is on average about 162°, and does not vary from this by more

Table 5.3 MCWESS antenna superelement model parameters, horizontally polarized. Frequency is in GHz, gain is in linear scale.

f_{in}	$\hat{A}_{col,max}$	$\beta_\phi{}^\circ$	β_θ	$\theta_{col,SL}{}^\circ$	f_{in}	$\hat{A}_{col,max}$	$\beta_\phi{}^\circ$	β_θ	$\theta_{col,SL}{}^\circ$
2.6	5.01	77	0.6314	35	5.5	6.56	83	0.2940	-24
2.7	5.86	77	0.6129	33	5.6	6.94	80	0.2903	-23
2.8	5.08	81	0.5814	-46	5.7	6.20	82	0.2865	-26
2.9	5.13	81	0.5750	-48	5.8	5.94	82	0.2865	-26
3.0	6.35	81	0.5686	-46	5.9	7.35	81	0.2714	-23
3.1	6.07	81	0.5490	-44	6.0	7.87	78	0.2714	-24
3.2	5.74	81	0.5090	-43	6.1	7.96	78	0.2714	-23
3.3	5.58	81	0.5023	-44	6.2	7.79	78	0.2714	-23
3.4	5.89	81	0.4886	-43	6.3	7.59	78	0.2639	24
3.5	5.90	81	0.4818	42	6.4	7.44	78	0.2639	-23
3.6	5.78	81	0.4540	-41	6.5	7.19	78	0.2487	23
3.7	5.62	81	0.4540	-39	6.6	6.98	80	0.2487	25
3.8	6.35	81	0.4470	-39	6.7	7.21	80	0.2487	24
3.9	5.94	81	0.4115	-37	6.8	6.75	80	0.2411	23
4.0	6.06	81	0.4115	-35	6.9	5.72	80	0.2373	25
4.1	6.06	81	0.4187	-34	7.0	6.40	80	0.2411	24
4.2	6.20	81	0.3899	32	7.1	6.83	80	0.2296	23
4.3	6.58	81	0.3754	-32	7.2	5.69	86	0.2258	35
4.4	6.10	81	0.3754	-33	7.3	5.25	81	0.2258	33
4.5	5.38	81	0.3608	-29	7.4	5.04	80	0.2258	23
4.6	6.68	81	0.3608	-32	7.5	5.67	81	0.2181	34
4.7	6.61	81	0.3535	30	7.6	5.17	81	0.2143	33
4.8	6.19	81	0.3387	-29	7.7	4.68	84	0.2105	-32
4.9	6.44	81	0.3313	-28	7.8	5.04	81	0.2105	-32
5.0	6.42	81	0.3313	-28	7.9	5.38	81	0.2105	-32
5.1	6.21	81	0.3239	-27	8.0	5.91	81	0.2028	32
5.2	5.74	81	0.3090	-26	8.1	5.24	81	0.2028	-30
5.3	6.08	81	0.3090	27	8.2	4.87	87	0.2028	28
5.4	5.96	86	0.3015	-25					

than a few degrees, and it does not seem to correlate with frequency. In the more difficult cases, we assume $\text{FNBW}_\phi \approx 162^\circ$. We then compute β_ϕ as

$$\beta_\phi = \frac{\text{FNBW}_\phi}{2}. \tag{5.49}$$

Finally, given β_ϕ, we compute the overall gain $\hat{A}_{col,max}$ via a least squares curve fit, in the log domain, of the main beam azimuth cut $\overline{A_{col}(\phi, 0)}$ to

$$\overline{A_{col}(\phi, 0)} \approx \begin{cases} \hat{A}_{col,max} \cos^2 \frac{\phi}{\beta_\phi} & \text{for } |\phi| \le \beta_\phi \\ 0 & \text{otherwise,} \end{cases} \tag{5.50}$$

which assumes the azimuth cut is a cosine shape with no sidelobes. The computed model parameters $\hat{A}_{col,max}, \beta_\phi, \beta_\theta$, and $\theta_{col,SL}$ are given in Tables 5.3-5.4.

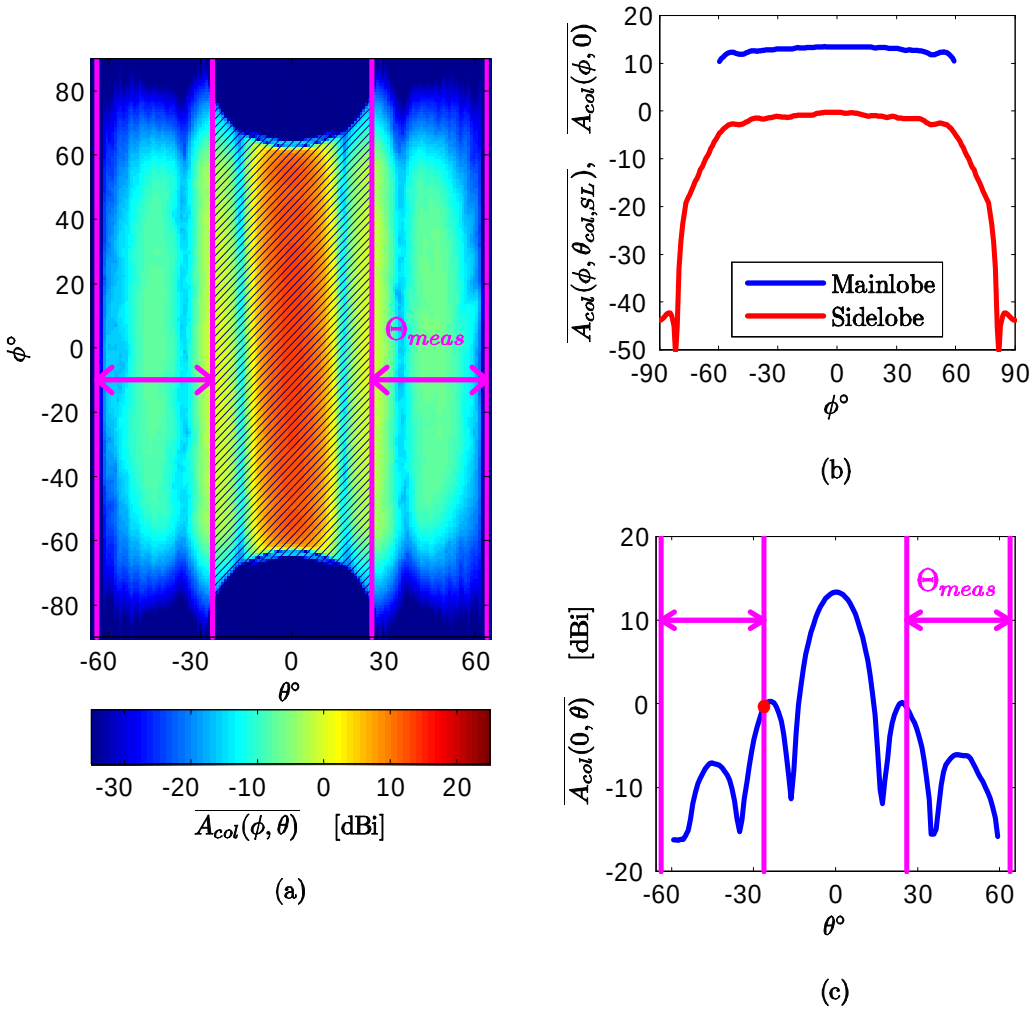

Figure 5.26 Illustration of how Θ_{meas} is used to find FNBW$_\phi$.by looking at a sidelobe. (a) Plot of $\overline{A_{col}(\phi,\theta)}$. We can not determine FNBW$_\phi$ from the main lobe, because no data are available at those angles. (b) Azimuth cut, showing the main lobe $\overline{A_{col}(\phi,0)}$ and the sidelobe $\overline{A_{col}(\phi,\theta_{col,SL})}$. The first nulls of the sidelobe are *sometimes* well-shaped, as in this figure. In all such cases, FNBW$_\phi \approx 162°$, regardless of frequency. (c) Elevation cut. The angle $\theta_{col,SL}$ is highlighted with the red dot. Remember that none of these plots are of a single antenna pattern, but rather are the *average* of all sixteen superelement patterns.

Table 5.4 MCWESS antenna superelement model parameters, vertically polarized. Frequency is in GHz, gain is in linear scale.

f_{in}	$\hat{A}_{col,max}$	$\beta_\phi{}^\circ$	β_θ	$\theta_{col,SL}$	f_{in}	$\hat{A}_{col,max}$	$\beta_\phi{}^\circ$	β_θ	$\theta_{col,SL}$
2.6	4.64	78	0.6554	35	5.5	6.14	86	0.3090	-25
2.7	5.30	77	0.6129	-33	5.6	5.86	87	0.2940	-25
2.8	4.62	81	0.5814	-46	5.7	5.35	82	0.2865	26
2.9	4.46	81	0.5490	44	5.8	5.48	82	0.2865	-26
3.0	5.37	81	0.5358	-45	5.9	6.59	84	0.2790	-24
3.1	5.75	81	0.5292	-44	6.0	6.71	78	0.2714	24
3.2	5.36	81	0.5090	-42	6.1	6.93	78	0.2714	23
3.3	5.30	81	0.4818	-43	6.2	6.57	78	0.2639	23
3.4	5.65	81	0.4818	-42	6.3	6.56	78	0.2639	24
3.5	5.56	81	0.4610	-41	6.4	6.24	78	0.2563	23
3.6	5.42	81	0.4610	-40	6.5	5.90	78	0.2525	23
3.7	5.54	81	0.4329	-37	6.6	5.57	80	0.2487	25
3.8	6.27	80	0.4258	-36	6.7	5.88	80	0.2487	24
3.9	5.51	81	0.4115	-35	6.8	5.74	80	0.2411	23
4.0	5.65	81	0.4043	-33	6.9	4.80	81	0.2334	34
4.1	6.17	81	0.3971	-32	7.0	5.03	81	0.2334	-35
4.2	5.96	81	0.3827	-32	7.1	5.66	80	0.2334	23
4.3	6.11	81	0.3827	-32	7.2	5.04	85	0.2181	35
4.4	6.35	81	0.3681	-31	7.3	4.56	81	0.2181	-34
4.5	5.57	81	0.3681	-31	7.4	4.18	81	0.2220	-33
4.6	6.15	81	0.3608	-30	7.5	4.94	81	0.2181	-33
4.7	6.46	81	0.3535	-29	7.6	4.71	81	0.2143	-32
4.8	6.24	81	0.3461	-28	7.7	4.01	87	0.2181	-32
4.9	6.38	81	0.3387	-28	7.8	4.18	86	0.2105	-32
5.0	6.12	81	0.3313	-29	7.9	4.92	81	0.2028	-32
5.1	6.17	81	0.3239	-28	8.0	4.95	81	0.2028	-31
5.2	5.74	81	0.3090	-27	8.1	4.66	81	0.2028	-30
5.3	5.98	81	0.3165	-27	8.2	4.77	81	0.2028	-29
5.4	5.85	81	0.3090	-27					

5.2.2 Residual Errors. The model given in Equation (5.45) and Tables 5.3-5.4, compared with some actual antenna patterns, is illustrated in Figs. 5.27-5.29. The figures also include residual error data, where the residual error ε_k is computed as

$$\varepsilon_k(\phi,\theta) = \frac{\left|\hat{A}_{col}(\phi,\theta)\right|}{|A_k(\phi,\theta)|}. \tag{5.51}$$

Since this model places more emphasis on the mainlobe, we quantify the residual errors of the mainlobe separately from those of the sidelobes. Now the mainlobe is the domain $\mathcal{M} = \left(|\phi| \le \beta_\phi, |\sin\theta| \le \beta_\theta\right)$; the sidelobes are everywhere else ($\mathcal{M}^c$). Within the log domain, we compute the Mean Absolute Error (MAE) $\overline{\varepsilon_{ML,k}}$ of the residual errors within the mainlobe as

$$\overline{\varepsilon_{ML,k}} = \frac{1}{N_{\mathcal{M}}} \sum_i \sum_j 10\log_{10}|\varepsilon_k(\phi_i,\theta_j)| \quad \text{dB} \qquad \text{for all } (\phi_i,\theta_j) \in \mathcal{M}, \tag{5.52}$$

where $N_{\mathcal{M}}$ is the number of samples in $\mathcal{M}$. The average $\overline{\varepsilon_{ML}}$ is then the mean of $\overline{\varepsilon_{ML,k}}$ over all values of k:

$$\overline{\varepsilon_{ML}} = \frac{1}{N}\sum_{k=1}^{N} \overline{\varepsilon_{ML,k}} \quad \text{dB}. \tag{5.53}$$

Similarly, we compute the MAE $\overline{\varepsilon_{SL,k}}$ of the residuals within the sidelobes as

$$\overline{\varepsilon_{SL,k}} = \frac{1}{N_{\mathcal{M}^c}} \sum_i \sum_j 10\log_{10}|\varepsilon_k(\phi_i,\theta_j)| \quad \text{dB} \qquad \text{for all } (\phi_i,\theta_j) \in \mathcal{M}^c, \tag{5.54}$$

where $N_{\mathcal{M}^c}$ is the number of samples in $\mathcal{M}^c$, and the average $\overline{\varepsilon_{SL}}$ of $\overline{\varepsilon_{SL,k}}$ over all values of k is

$$\overline{\varepsilon_{SL}} = \frac{1}{N}\sum_{k=1}^{N} \overline{\varepsilon_{SL,k}} \quad \text{dB}. \tag{5.55}$$

Plots of $\overline{\varepsilon_{ML,k}}$ and $\overline{\varepsilon_{SL,k}}$ for each superelement, as a function of frequency, are given in Figs. 5.30-5.31, and summarized in Table 5.5. The overall residuals $\overline{\varepsilon_{ML}}$ and $\overline{\varepsilon_{SL}}$ are summarized in Table 5.6.

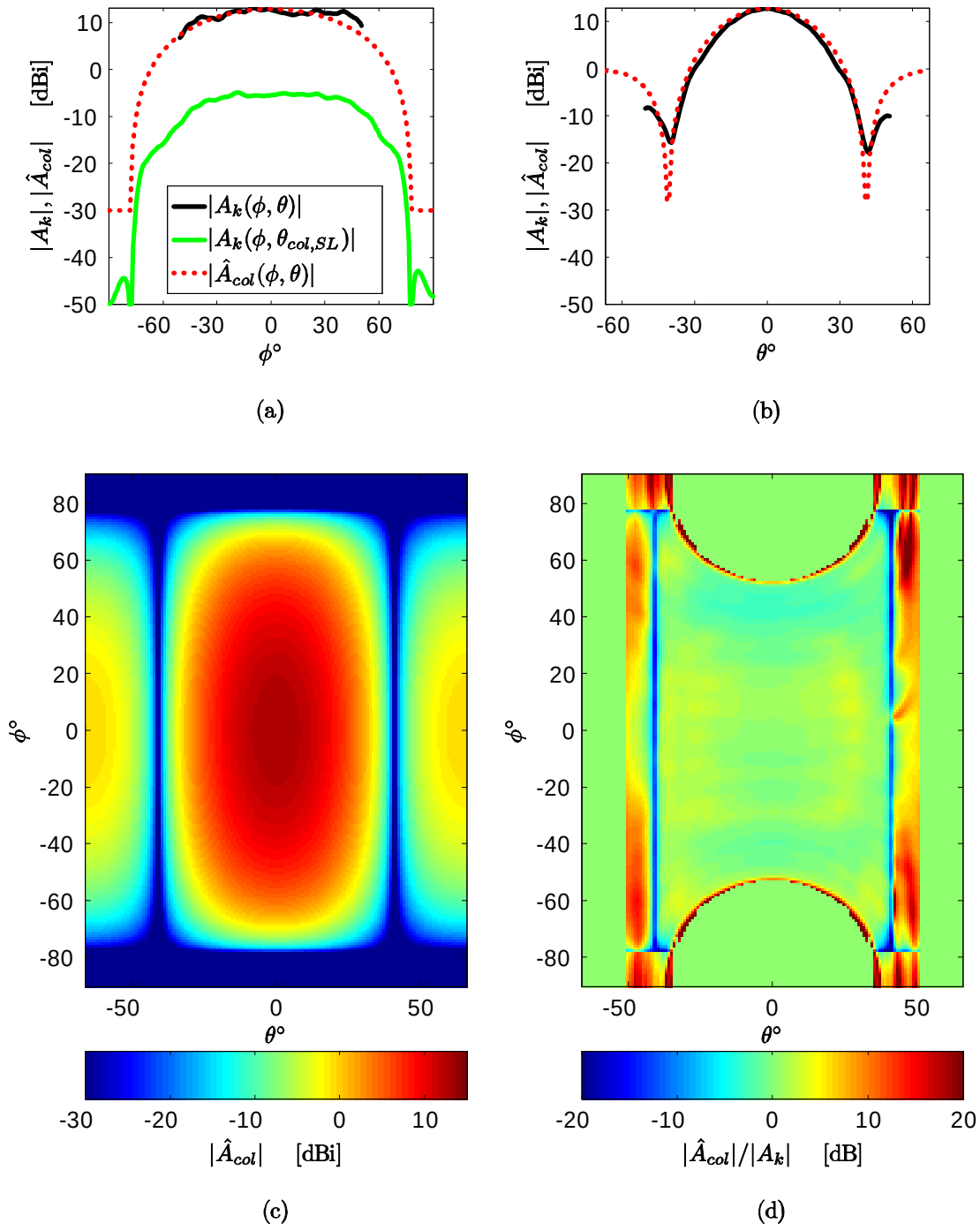

Figure 5.27 Superelement pattern model, compared with measured antenna pattern data for column $k = 12$, vertically polarized, at 2.6 GHz. (a) Azimuth cut, showing measured mainlobe (black), mainlobe model (dotted red), and sidelobe (green). (b) Elevation cut, showing measured mainlobe vs. model. (c) Entire superelement pattern model. (d) Residual error of the model, as a function of (ϕ, θ)—green is most desirable.

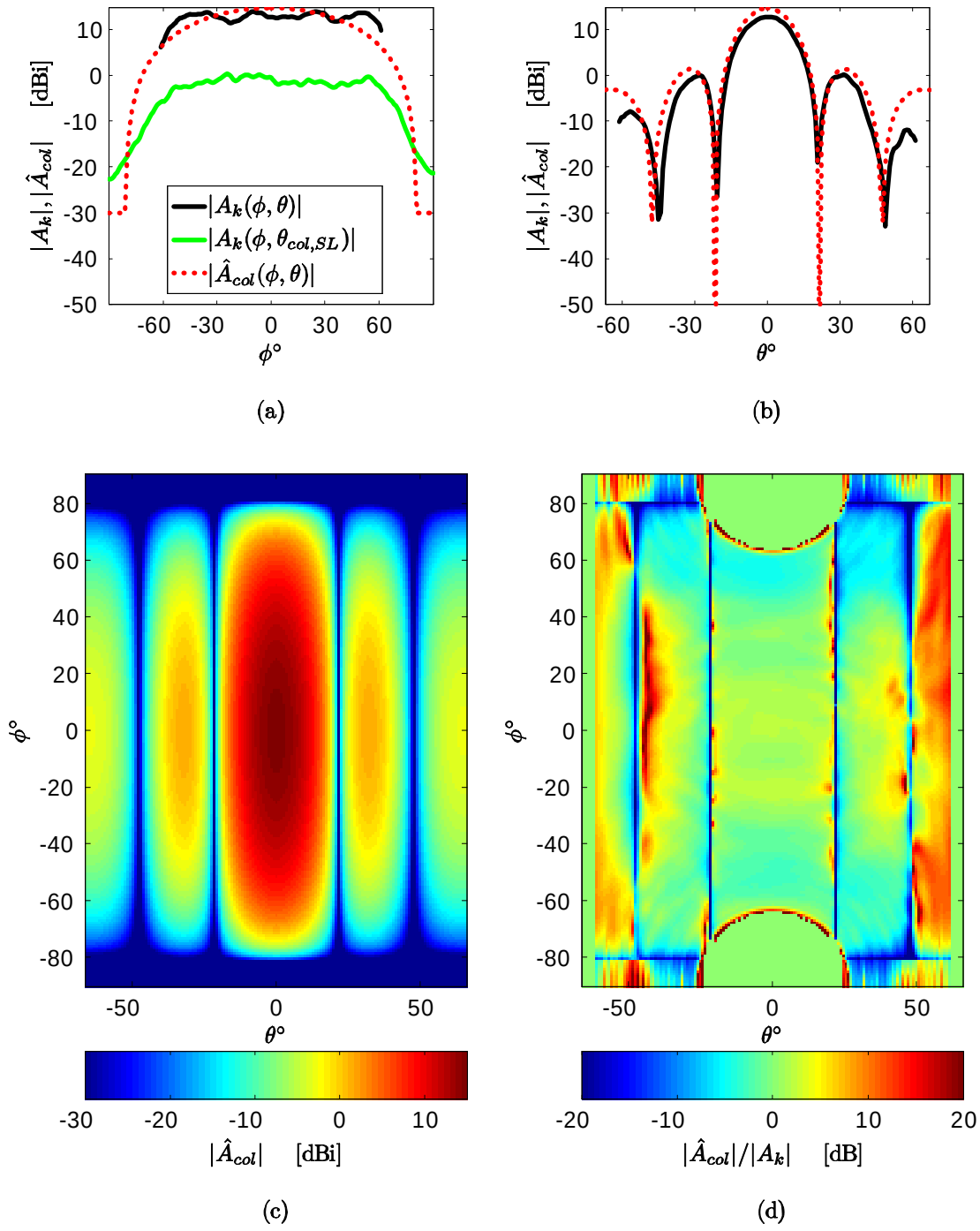

Figure 5.28 Superelement pattern model, compared with measured antenna pattern data for column $k = 12$, vertically polarized, at 4.5 GHz. (a) Azimuth cut, showing measured mainlobe (black), mainlobe model (dotted red), and sidelobe (green). (b) Elevation cut, showing measured mainlobe vs. model. (c) Entire superelement pattern model. (d) Residual error of the model, as a function of (ϕ, θ)—green is most desirable.

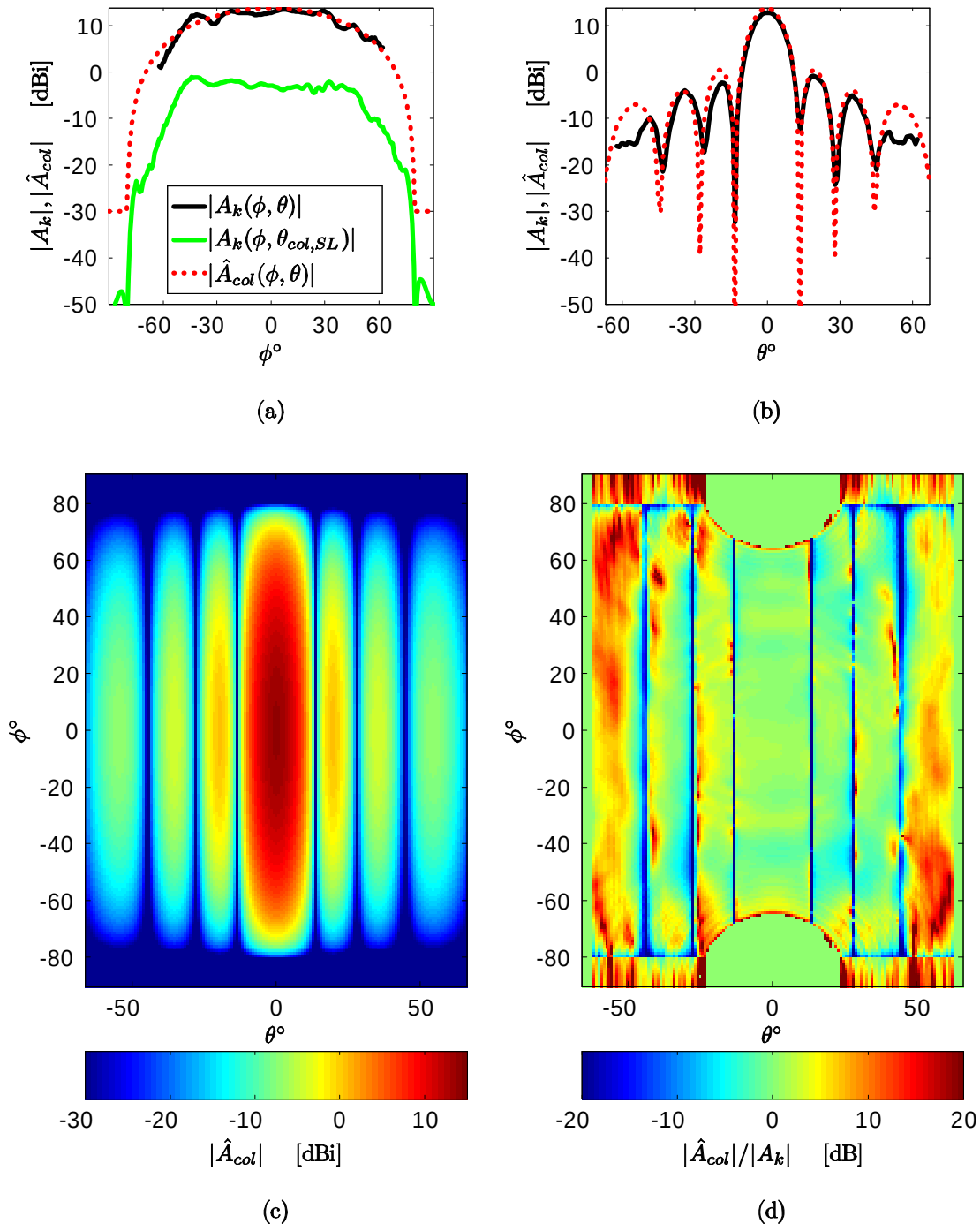

Figure 5.29 Superelement pattern model, compared with measured antenna pattern data for column $k = 12$, vertically polarized, at 7.1 GHz. (a) Azimuth cut, showing measured mainlobe (black), mainlobe model (dotted red), and sidelobe (green). (b) Elevation cut, showing measured mainlobe vs. model. (c) Entire superelement pattern model. (d) Residual error of the model, as a function of (ϕ, θ)—green is most desirable.

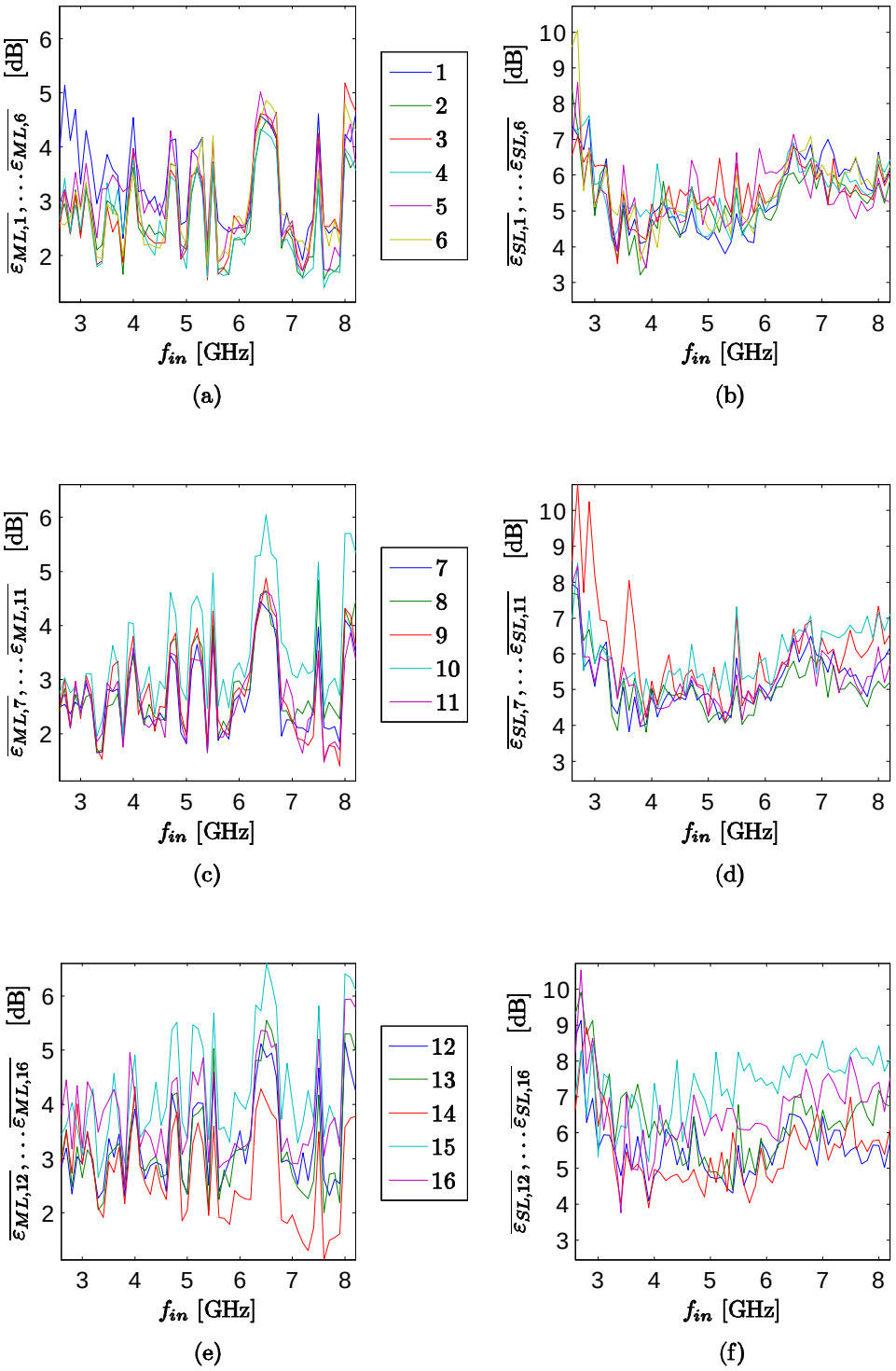

Figure 5.30 Average residual errors $\overline{\varepsilon_{ML,k}}$ for the mainlobe and $\overline{\varepsilon_{SL,k}}$ for the sidelobes of the antenna pattern model (horizontal polarization). (a,b) Superelements 1-6. (c,d) Superelements 7-11. (e,f) Superelements 12-16.

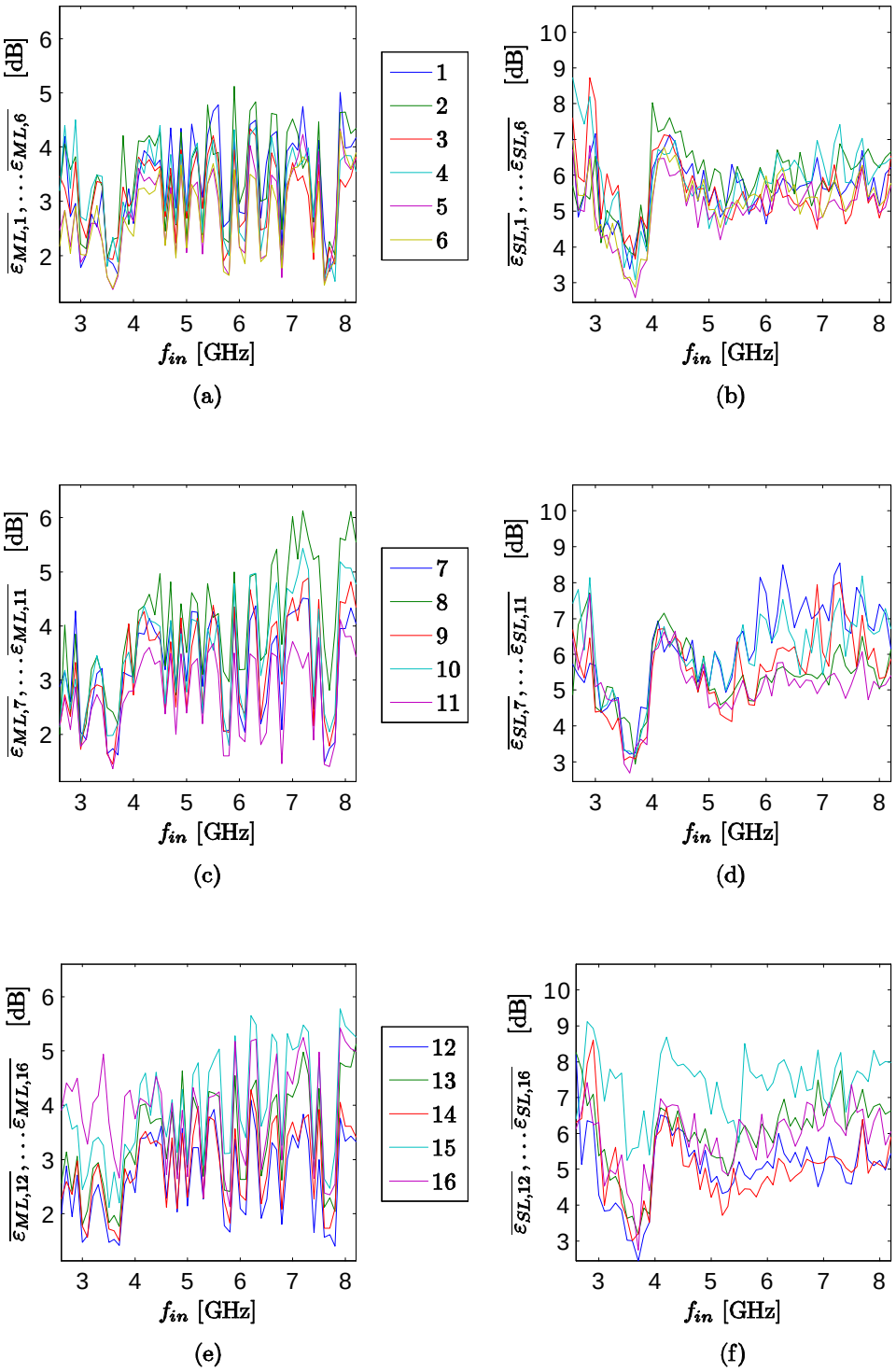

Figure 5.31 Average residual errors $\overline{\varepsilon_{ML,k}}$ for the mainlobe and $\overline{\varepsilon_{SL,k}}$ for the sidelobes of the antenna pattern model (vertical polarization). (a,b) Superelements 1-6. (c,d) Superelements 7-11. (e,f) Superelements 12-16.

Table 5.5 Summary of the residual errors of the antenna pattern model, over all frequencies and all superelements.

	H-Polarized		V-Polarized	
	$\overline{\varepsilon_{ML,k}}$ (Mainlobe)	$\overline{\varepsilon_{SL,k}}$ (Sidelobes)	$\overline{\varepsilon_{ML,k}}$ (Mainlobe)	$\overline{\varepsilon_{SL,k}}$ (Sidelobes)
Minimum [dB]	1.14	3.23	1.37	2.45
Mean [dB]	3.11	5.74	3.28	5.70
Maximum [dB]	6.60	10.74	6.13	9.12
Standard Deviation [dB]	0.99	1.11	1.00	1.14

Table 5.6 Residual errors of the antenna pattern model.

	H-Pol		V-Pol			H-Pol		V-Pol	
f_{in}	$\overline{\varepsilon_{ML}}$	$\overline{\varepsilon_{SL}}$	$\overline{\varepsilon_{ML}}$	$\overline{\varepsilon_{SL}}$	f_{in}	$\overline{\varepsilon_{ML}}$	$\overline{\varepsilon_{SL}}$	$\overline{\varepsilon_{ML}}$	$\overline{\varepsilon_{SL}}$
GHz	dB	dB	dB	dB	GHz	dB	dB	dB	dB
2.6	2.88	7.83	2.73	6.82	5.7	2.31	5.10	2.25	5.31
2.7	3.31	8.54	3.40	6.19	5.8	2.28	4.98	2.12	5.34
2.8	2.69	6.67	2.68	6.40	5.9	2.81	5.74	4.28	5.93
2.9	3.31	7.45	3.44	7.19	6.0	2.86	5.34	2.62	5.77
3.0	2.68	5.87	2.10	5.85	6.1	2.74	5.29	2.49	5.54
3.1	3.39	6.25	2.20	4.75	6.2	3.06	5.52	4.42	6.24
3.2	3.04	6.34	2.87	4.89	6.3	4.35	5.98	4.32	6.36
3.3	2.15	5.05	3.13	4.92	6.4	4.74	6.21	2.50	5.96
3.4	2.31	4.54	2.98	4.77	6.5	4.89	6.69	2.91	5.80
3.5	3.12	5.73	1.94	3.67	6.6	4.65	6.40	4.06	5.78
3.6	3.17	5.16	1.95	3.59	6.7	4.45	6.42	4.09	5.97
3.7	3.17	5.43	1.95	3.32	6.8	2.62	6.57	2.36	5.85
3.8	2.20	4.65	3.10	4.28	6.9	2.81	6.00	3.96	6.09
3.9	3.41	4.37	3.13	4.02	7.0	2.58	6.46	4.21	5.81
4.0	3.95	5.14	2.91	6.13	7.1	2.27	5.97	4.11	5.88
4.1	2.92	5.04	3.79	6.73	7.2	2.25	6.20	4.44	6.43
4.2	2.66	5.30	3.86	6.85	7.3	2.35	5.87	4.22	6.50
4.3	2.73	5.35	3.81	6.58	7.4	2.60	5.97	2.57	5.69
4.4	2.63	5.21	3.75	6.66	7.5	4.22	6.18	4.14	5.93
4.5	2.67	5.07	3.87	6.21	7.6	2.16	6.07	1.97	6.14
4.6	2.56	5.04	2.67	5.78	7.7	2.34	5.84	1.99	6.79
4.7	3.96	5.87	3.79	6.04	7.8	2.43	5.78	2.19	5.83
4.8	3.90	5.26	2.49	5.36	7.9	2.21	5.87	4.54	6.06
4.9	2.43	5.04	3.97	5.87	8.0	4.65	6.48	4.28	5.87
5.0	2.30	4.94	2.61	5.06	8.1	4.56	5.91	4.31	5.95
5.1	3.76	5.15	3.86	5.46	8.2	4.36	6.30	4.24	6.23
5.2	3.93	5.06	3.90	5.00					
5.3	3.77	4.92	2.54	4.83	**Min**	**2.10**	**4.37**	**1.94**	**3.32**
5.4	2.10	4.85	3.95	5.18	**Mean**	**3.11**	**5.74**	**3.28**	**5.70**
5.5	4.20	6.12	4.07	5.65	**Max**	**4.89**	**8.54**	**4.54**	**7.19**
5.6	2.18	4.88	3.81	5.78	**Stdev**	**0.82**	**0.79**	**0.84**	**0.82**

VI. Applications

6.1 Receiver Operating Characteristic (ROC)

Consider the basic problem of a receiver attempting to detect a signal. The signal s has an amplitude of A_s volts, and a frequency of f_{in} GHz (ω_{in} rad/s), and is expressed as

$$s(t) = A_s \cos(\omega_{in} t). \tag{6.1}$$

The transmitted signal is mixed with Additive White Gaussian Noise (AWGN) $w(t)$ within the receiver band from ω_L to ω_U. Then the signal received at the front-end of the receiver is

$$\tilde{s}_R(t) = s(t) + w(t). \tag{6.2}$$

Assuming normalized impedance, the instantaneous signal power at the receiver is

$$\tilde{p}_R(t) = \tilde{s}_R^2(t), \tag{6.3}$$

and the average power within the sampling window from time T_1 to T_2 is

$$\tilde{P}_R = \frac{1}{T_2 - T_1} \int_{T_1}^{T_2} \tilde{p}_R(t)\, dt. \tag{6.4}$$

Using the receiver, we wish to test the hypothesis H_1 that a signal has been transmitted, versus the null hypothesis H_0, i.e.

$$\begin{aligned} H_0 &: \text{No signal is present} \\ H_1 &: \text{Signal is present.} \end{aligned}$$

If the received power $\tilde{P}_R$ exceeds a threshold τ_R, then we reject the null hypothesis [8]:

$$\tilde{P}_R \underset{H_0}{\overset{H_1}{\gtrless}} \tau_R. \tag{6.5}$$

The presence of noise complicates the detection problem. If, using (6.5), the receiver incorrectly tells us a signal is present, when in fact one is not, this is called a *false alarm*.

If the receiver correctly tells us a signal is present, when in fact one is, this is called a *detection*. The probabilities P_D of a detection and P_F of a false alarm depend primarily on the detection threshold τ_R and the Signal-to-Noise Ratio (SNR). It is desirable to have high P_D and low P_F, but these are competing objectives. The relationship between P_D and P_F is called the Receiver Operating Characteristic (ROC).

Now consider an N-channel receiver. Mismatches in gain and phase can also complicate the detection problem. To take advantage of the multiple channels, suppose we now let $\tilde{s}_R$ be the sum of the signals received in all channels:

$$\tilde{s}_R(t) = \sum_{k=1}^{N} (s(t) + w_k(t)) g_k, \tag{6.6}$$

where g_k is the gain of the kth channel, and w_k is the noise received in the kth channel. This greatly increases P_D while decreasing P_F. Equation (6.6) also accounts for gain mismatches among channels. If the channels are also mismatched in phase, then (6.6) becomes

$$\tilde{s}_R(t) = \sum_{k=1}^{N} \left(s\left(t + \frac{\psi_k}{\omega_{in}}\right) + w_k(t) \right) g_k, \tag{6.7}$$

where ψ_k is the phase response of each channel in the receiver. Equations (6.2)-(6.5) were simulated using Matlab, including the signal model in (6.1) and an AWGN model. A weak SNR of -10.5 dB was chosen to highlight the limits of system performance. Fig. 6.1 shows the resulting ROC plot (in black), using various values of the parameter τ_R. For each value of τ_R, (6.2)-(6.4) were simulated 10,000 times to compute P_D and P_F. The same simulation was repeated, using Equation (6.7) with various mismatched sets of channel gains, and then again with various mismatched sets of channel phases, given in Table 6.1. The gain values $\{g_k\}_{k=1}^{N}$ for Simulation 2 of Table 6.1 are taken from the tuner gain experiments at 4.5 GHz, and have a mean of 7.45 and a standard deviation of 1.74 (linear scale); normalized, it becomes a mean of 1 and a standard deviation of 0.23. The gain and phase values for Simulations 3-9 are normally distributed as shown in the table. By comparison, the phase values $\{\psi_k\}_{k=1}^{N}$ from the antenna pattern measurements have a standard deviation of 10.5 degrees. The results of these simulations are shown in Fig. 6.1.

Table 6.1 Gain and phase mismatches used in ROC simulations.

Simulation 1:	$g_k = 1$	$\psi_k = 0^\circ$
Simulation 2:	$g_k =$ Tuner Gain at 4.5 GHz	$\psi_k = 0^\circ$
Simulations 3-5:	$g_k \sim \mathcal{N}(1, \sigma_g^2)$	$\psi_k = 0^\circ$
Simulations 6-9:	$g_k = 1$	$\psi_k \sim \mathcal{N}(0, \sigma_\psi^2)$

	Simulation #							
	2	3	4	5	6	7	8	9
k	g_k	g_k	g_k	g_k	$\psi_k{}^\circ$	$\psi_k{}^\circ$	$\psi_k{}^\circ$	$\psi_k{}^\circ$
1	6.71	3.26	1.86	0.46	-38	-56	-84	-113
2	11.26	4.50	3.51	2.52	-26	-40	-60	-79
3	8.20	5.19	4.43	3.68	-20	-30	-46	-61
4	8.77	5.71	5.13	4.55	-16	-23	-35	-47
5	9.84	6.16	5.72	5.29	-12	-17	-26	-35
6	7.82	6.55	6.25	5.95	-8	-12	-18	-24
7	8.77	6.92	6.74	6.57	-5	-7	-11	-14
8	8.94	7.28	7.22	7.16	-2	-2	-4	-5
9	5.33	7.63	7.69	7.75	2	2	4	5
10	5.75	7.98	8.16	8.34	5	7	11	14
11	7.10	8.35	8.65	8.96	8	12	18	24
12	5.98	8.75	9.18	9.62	12	17	26	35
13	6.21	9.19	9.77	10.35	16	23	35	47
14	7.24	9.72	10.47	11.23	20	30	46	61
15	5.22	10.41	11.40	12.38	26	40	60	79
16	6.10	11.65	13.05	14.45	38	56	84	113
	σ_g	σ_g	σ_g	σ_g	$\sigma_\psi{}^\circ$	$\sigma_\psi{}^\circ$	$\sigma_\psi{}^\circ$	$\sigma_\psi{}^\circ$
	0.23	0.3	0.4	0.5	20	30	45	60
(normalized to mean)								

As shown in the figure, there is degradation in receiver performance due to the mismatches, and performance worsens as gain and phase mismatches increase.

Clearly, the channels must be matched in phase to achieve optimal signal detection. Phase mismatches greater than $\pm 90^\circ$ negate the benefits of having multiple channels. For example, from Table 6.1, in Simulation 8, channels 1 and 16 are $84 - (-84) = 168^\circ$ out of phase, and destructively interfere with each other. In our 16-channel simulations using (6.7) and (6.3)-(6.5) at 4.5 GHz with SNR= -10.5 dB, detection performance is severely degraded when $\sigma_\psi > 45^\circ$, as shown in Fig. 6.1b.

Gain mismatches degrade detection performance, by diminishing the benefits of multichannel signal integration. If the gain of one channel is much stronger than the others, it defeats the purpose of having multiple channels. The strongest channel amplifies its own

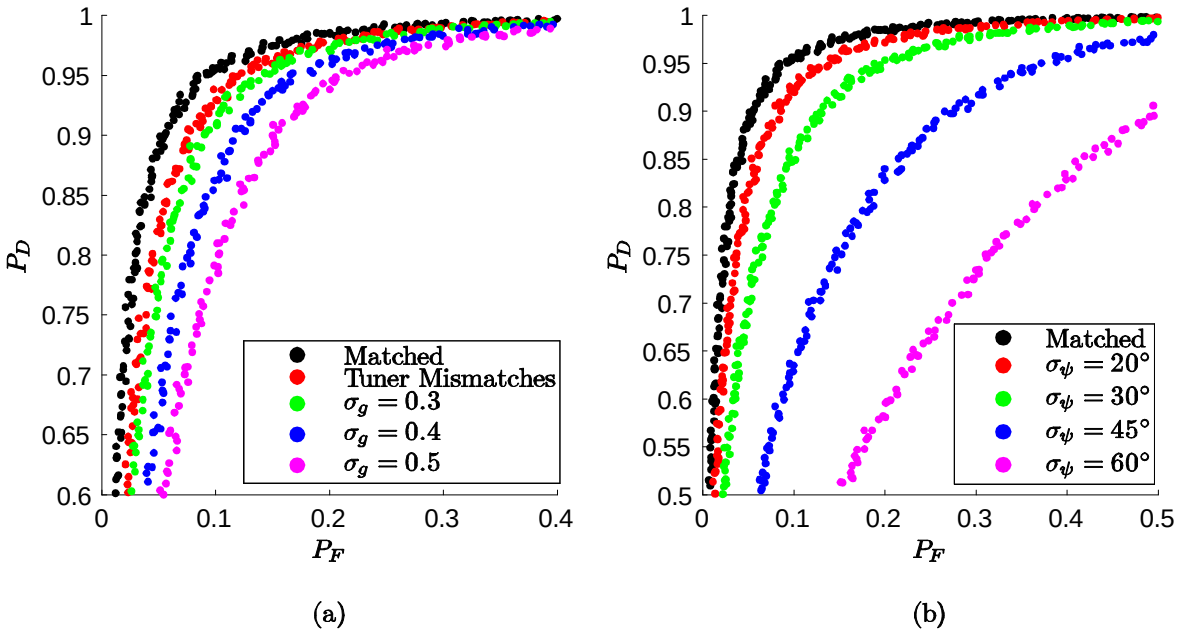

Figure 6.1 Simulated ROC curves for a 16-channel receiver, with $A_s = 3$ μV, $f_{in} = 4.5$ GHz, $\sigma_w = 10$ μV, $T_2 - T_1 = 2.2$ ns, SNR=0.09 (-10.5 dB), and noise bandwidth from 1-8 GHz. (a) Results of Simulations 1-5 (gain mismatches). (b) Results of Simulations 1 and 6-9 (phase mismatches). The simulation parameters are given in Table 6.1. Combined effects of gain and phase mismatches are not shown.

noise without taking advantage of signal integration from the other channels. Having one channel whose gain is infinitely higher than the others, is just like having only one channel. However, in our simulations, the significant gain mismatches caused by the LCR400 tuners have only a slight effect on the ROC, as shown in Fig. 6.1a.

These simulations are very limited in scope, and are meant to demonstrate possible effects of gain and phase mismatches. A comprehensive analysis would include many different values of f_{in}, N, and SNR. Also, for the MCWESS, an end-to-end phase response characterization of the system is needed before its detection capability can be thoroughly analyzed.

6.2 Antenna Array Beamforming

Given an antenna element far-field radiation pattern model, it is possible to construct a model for the antenna pattern of an array of such elements, by means of *steering vectors*. Consider a uniform rectangular array with N columns and P rows, in the x-z plane. The elements are spaced at an interval of d_x inches in the x direction, and d_z inches in the z direction. The corner element, located at $(x, z) = (0, 0)$, is the *reference element*. The vector $\mathbf{d}_{n,p}$ defines the physical location of the (n, p)th element relative to the reference element, and

$$\mathbf{d}_{n,p} = nd_x\hat{\mathbf{x}} + pd_z\hat{\mathbf{z}}, \tag{6.8}$$

where $\hat{\mathbf{x}}$ and $\hat{\mathbf{z}}$ are the unit vector along the x and z axes. Next, we define the *normalized spatial angle* ϑ as

$$\vartheta \equiv \frac{\mathbf{k}\,(\phi, \theta) \cdot \mathbf{d}_{n,p}}{2\pi} = \frac{\hat{\mathbf{k}}\,(\phi, \theta) \cdot \mathbf{d}_{n,p}}{\lambda}, \tag{6.9}$$

where λ is the wavelength, $\hat{\mathbf{k}}$ is the unit vector in the direction of travel of the wave, and $\mathbf{k}$ is the wave vector where $\mathbf{k} = \|\mathbf{k}\|\,\hat{\mathbf{k}}$ and $\|\mathbf{k}\| = 2\pi/\lambda$. The normalized spatial angle ϑ is unitless, and is a function of ϕ and θ, and the position of the particular antenna element in question. This expands to

$$\vartheta = \frac{nd_x \cos\theta \sin\phi + pd_z \sin\theta}{\lambda}. \tag{6.10}$$

The x and z components of ϑ are

$$\vartheta_x = \frac{d_x \cos\theta \sin\phi}{\lambda} \tag{6.11}$$

$$\vartheta_z = \frac{d_z \sin\theta}{\lambda}. \tag{6.12}$$

We next define the azimuth and elevation *steering vectors* $\mathbf{a}$ and $\mathbf{e}$ as

$$\mathbf{a}(\vartheta_x) = \begin{bmatrix} 1 & e^{j2\pi\vartheta_x} & \dots & e^{j2\pi(N-1)\vartheta_x} \end{bmatrix}^T \tag{6.13}$$

$$\mathbf{e}(\vartheta_z) = \begin{bmatrix} 1 & e^{j2\pi\vartheta_z} & \dots & e^{j2\pi(P-1)\vartheta_z} \end{bmatrix}^T. \tag{6.14}$$

Then the *array factor* AF is

$$\mathrm{AF}(\phi,\theta) = [\mathbf{e}(\vartheta_z) \otimes \mathbf{a}(\vartheta_x)]^T \mathbf{w} \tag{6.15}$$

$$= \sum_{p=0}^{P-1} \sum_{n=0}^{N-1} e^{j2\pi p\vartheta_z} e^{j2\pi n\vartheta_x} w_{n,p}, \tag{6.16}$$

where $\mathbf{w}$ is the matrix of element weights, $w_{n,p}$ is the (n,p)th element of $\mathbf{w}$, and $\otimes$ is the Kronecker product operator. If the array elements are perfectly matched and steered to boresight, then all elements of $\mathbf{w}$ are ones, denoted by $\mathbf{w} = \mathbf{1}$; otherwise, the elements of $\mathbf{w}$ are complex values. If we have an antenna element directivity model $\hat{A}_{elem}(\phi,\theta)$ which is common to all NP elements, then the predicted directivity pattern $\hat{A}$ of the array is

$$\hat{A}(\phi,\theta) = |\mathrm{AF}(\phi,\theta)|^2 \hat{A}_{elem}(\phi,\theta). \tag{6.17}$$

This model neglects mutual coupling between antenna elements.

For the MCWESS, we measured each column of sixteen elements as a superelement, with $d_x = 0.45$ in $= 1.14$ cm, $N = 16$, $P = 1$, $\hat{A}_{elem} = \hat{A}_{col}$, and d_z is not applicable because there is only one row. In our array pattern measurements, according to the test configuration the array was designed to be steered to boresight, i.e. $\mathbf{w} = \mathbf{1}$. We are interested in looking at the effects of mismatches among elements. As such, we can use the weights $\mathbf{w}$ to simulate the undesired gain and phase mismatches among antenna

elements. As such, we let

$$w_k = A_{k,max}^{1/2} e^{j\psi_k} \tag{6.18}$$

be the weight for the kth antenna superelement. Using (5.50) with the parameters in Tables 5.3-5.4, and applying the gain and phase mismatches from Appendix A, we obtain the results shown in Figs. 6.2-6.4. According to Fig. 6.2c, the model does not seem to reflect the sidelobe level very well; however, this may be due to the limited amount of measured data available at that frequency.

Gain mismatches affect antenna array beam shape as shown in Fig. 6.5. To simulate this, we let each weight w_k be a positive real value randomly chosen from a normally-distributed population with a mean of 1 and a standard deviation $\sigma_g \leq 0.4$. This was done similarly to the methodology of the detector simulations in Table 6.1, except with multiple random permutations of the same sixteen weights. Since each weight is a positive real value, the phases are matched. For an array with only one row, the gain and phase mismatches do not seem to affect the main-beam elevation cut at all. However, there are significant effects along the azimuth axis, as shown in the figure. The gain mismatches increase the beamwidth and reduce the sidelobe level, while making the nulls shallower. Fig. 6.5 shows the results of various amounts of mismatch, reflected by σ_g. By comparison, the MCWESS tuners at 4.5 GHz have a mean voltage gain of 7.45 with a standard deviation of 1.74; this normalizes to a mean of 1 and a standard deviation of 0.23, roughly equivalent to Fig. 6.5b, where the sidelobe level is shown to decrease by about 2.4 dB. The MCWESS tuner gain mismatches could affect digital beamforming in this manner. These values at 4.5 GHz are typical; however, at certain points in the frequency spectrum, our measured gain is much more greatly mismatched. As we have shown, the tuner gain is not normally distributed, but this simulation provides a basis for comparison.

Phase mismatches affect the array pattern as shown in Fig. 6.6. For this simulation, we let each w_k take a complex value along the unit circle, where the phase ψ_k is randomly chosen from a normally-distributed population with a mean of 0 and a standard deviation σ_ψ. The effects of worsening phase mismatches are shown in the figure. The mismatches cause squint and decreased sidelobe level, and in the worst case the various elements begin

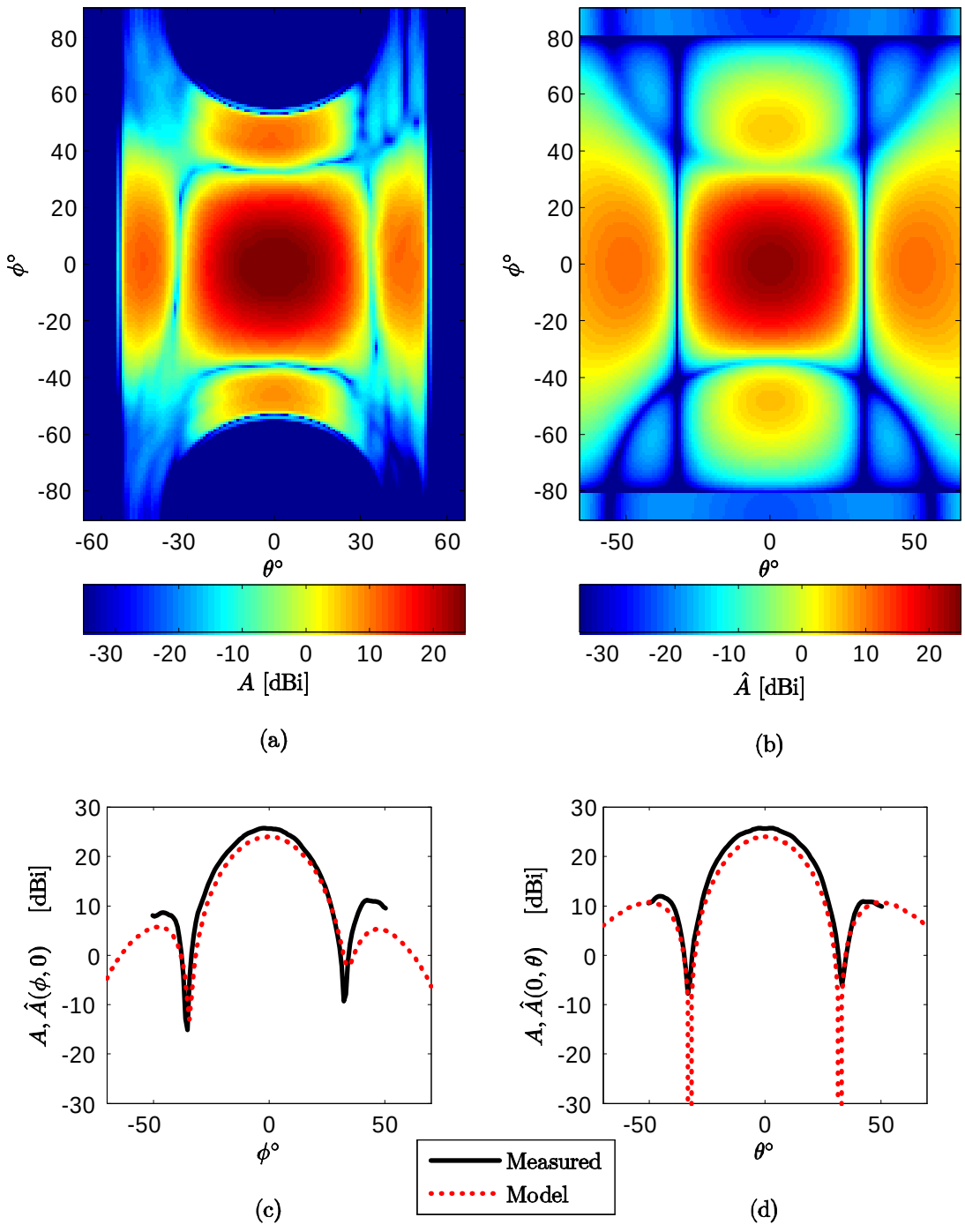

Figure 6.2 (a) Measured antenna pattern data $A(\phi, \theta)$ at 3.0 GHz, vertically polarized. (b) Model $\hat{A}(\phi, \theta)$ from (5.45) and (6.11)-(6.18). (c) Azimuth cut of A and $\hat{A}$. (d) Elevation cut.

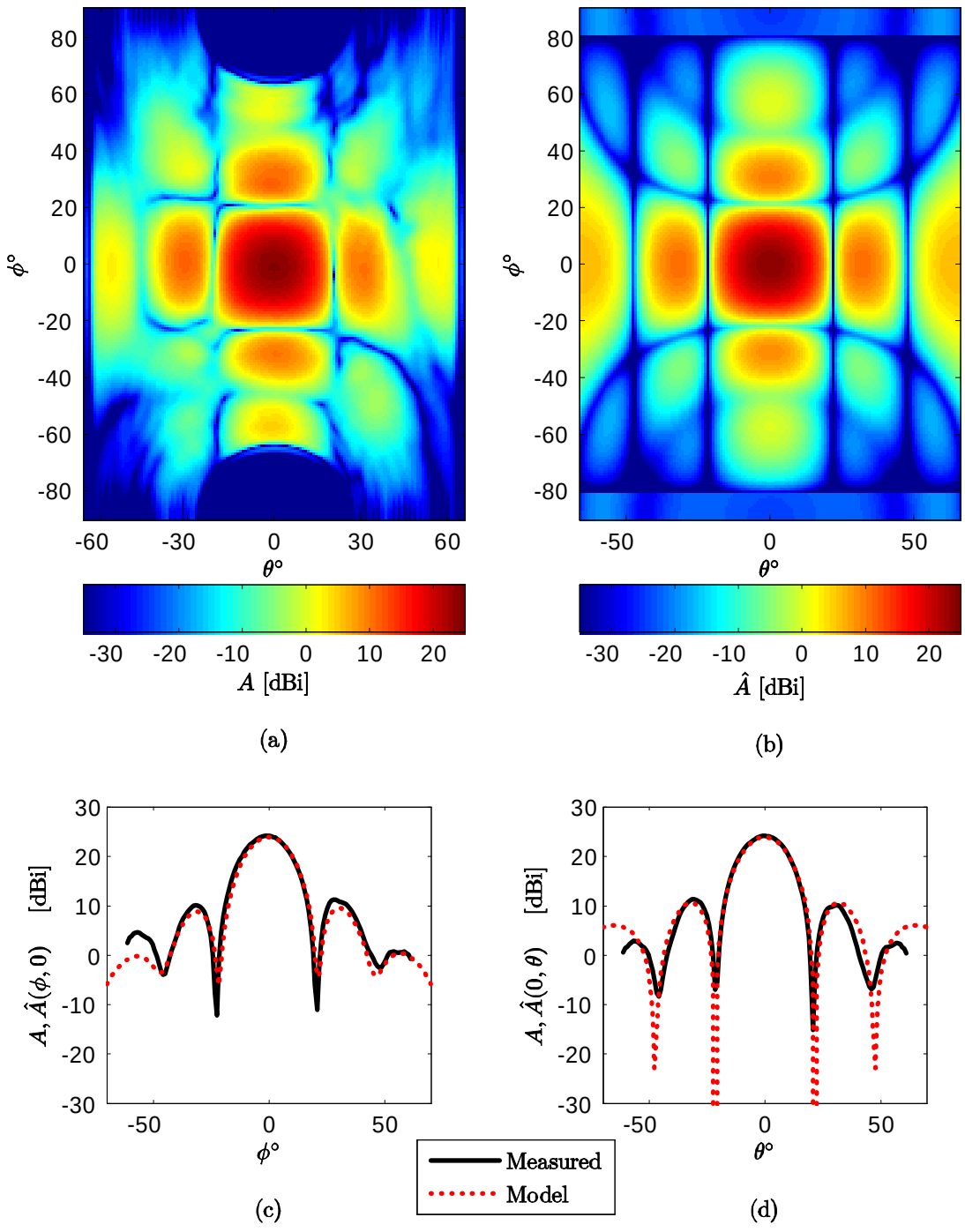

Figure 6.3 (a) Measured antenna pattern data $A(\phi, \theta)$ at 4.5 GHz, vertically polarized. (b) Model $\hat{A}(\phi, \theta)$ from (5.45) and (6.11)-(6.18). (c) Azimuth cut of A and $\hat{A}$. (d) Elevation cut.

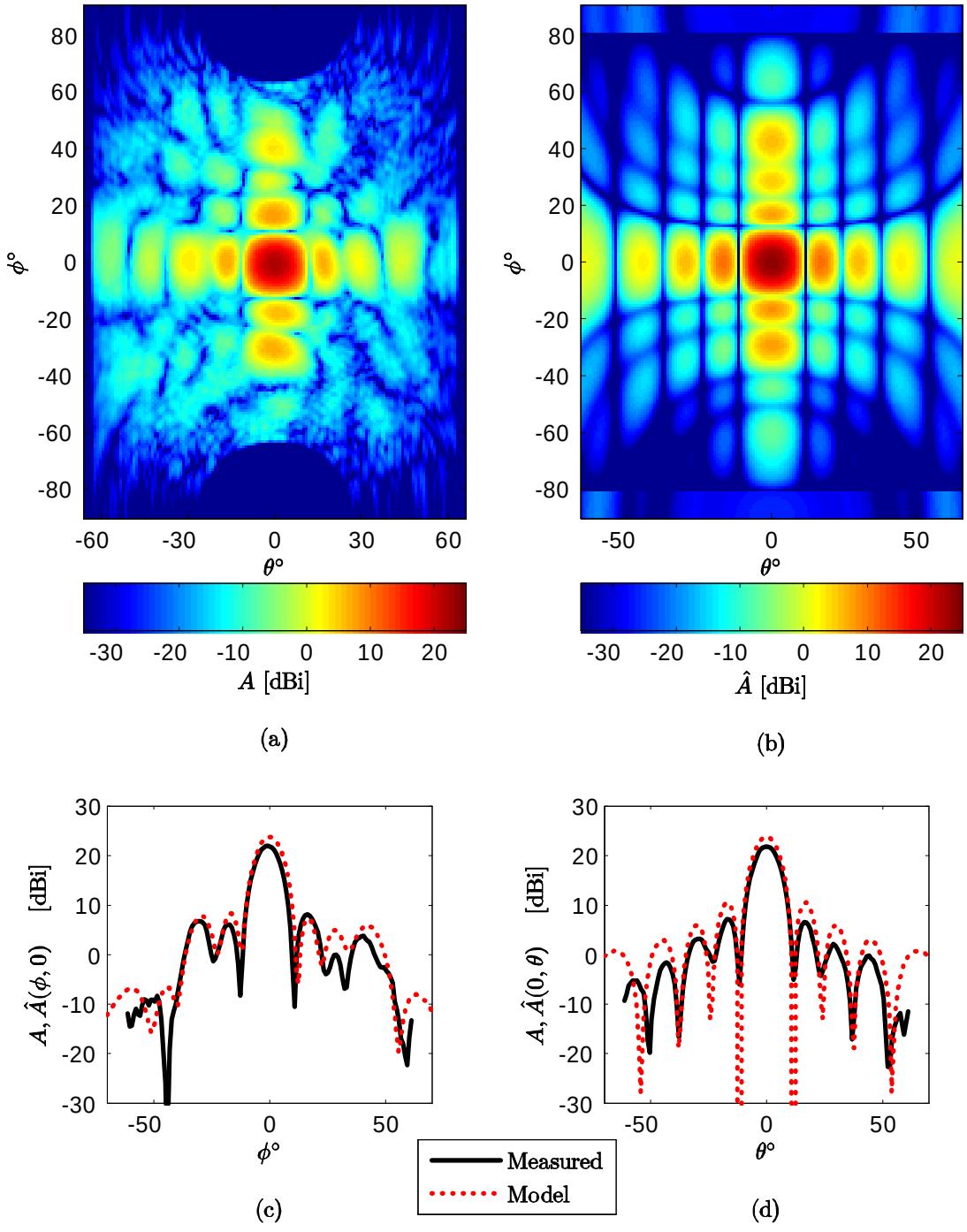

Figure 6.4 (a) Measured antenna pattern data $A(\phi, \theta)$ at 8.2 GHz, vertically polarized. (b) Model $\hat{A}(\phi, \theta)$ from (5.45) and (6.11)-(6.18). (c) Azimuth cut of A and $\hat{A}$. (d) Elevation cut.

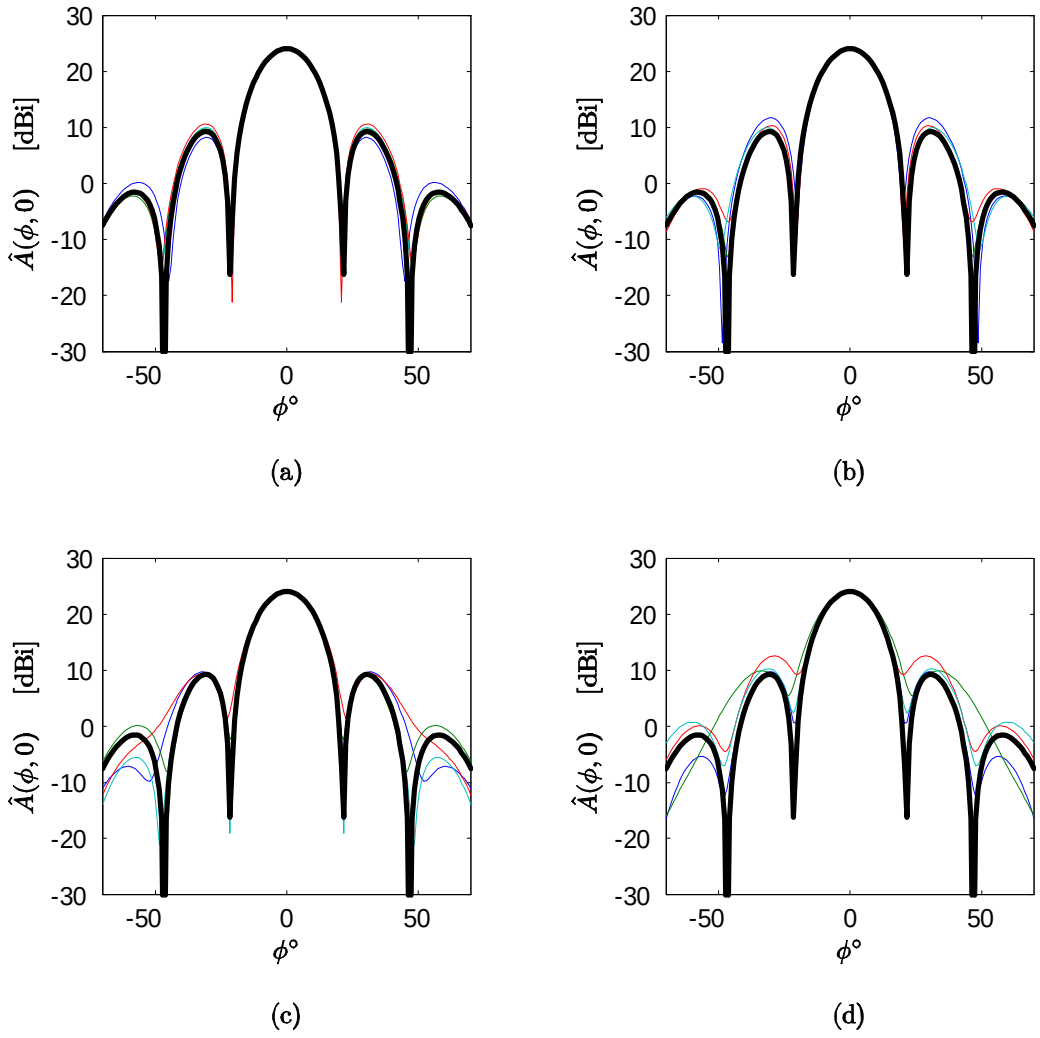

Figure 6.5 Effects of hypothetical gain mismatches on array pattern at 4.5 GHz. The real-valued weight $w_k \sim \mathcal{N}\left(1, \sigma_g^2\right)$. (a) $\sigma_g = 0.1$. (b) $\sigma_g = 0.2$. (c) $\sigma_g = 0.3$. (d) $\sigma_g = 0.4$. Ideal (matched) array pattern is shown in black; other patterns are from simulations with gain mismatches.

cancelling each other out, and cause the beam to lose its shape altogether, as in Fig. 6.6d. At 4.5 GHz, the MCWESS antenna assembly and its cables have a σ_ψ value of about 10.5°. The MCWESS has very long RF cables, and the tuner phase response has yet to be measured or characterized. These unknown phase mismatches could significantly impact digital beamforming.

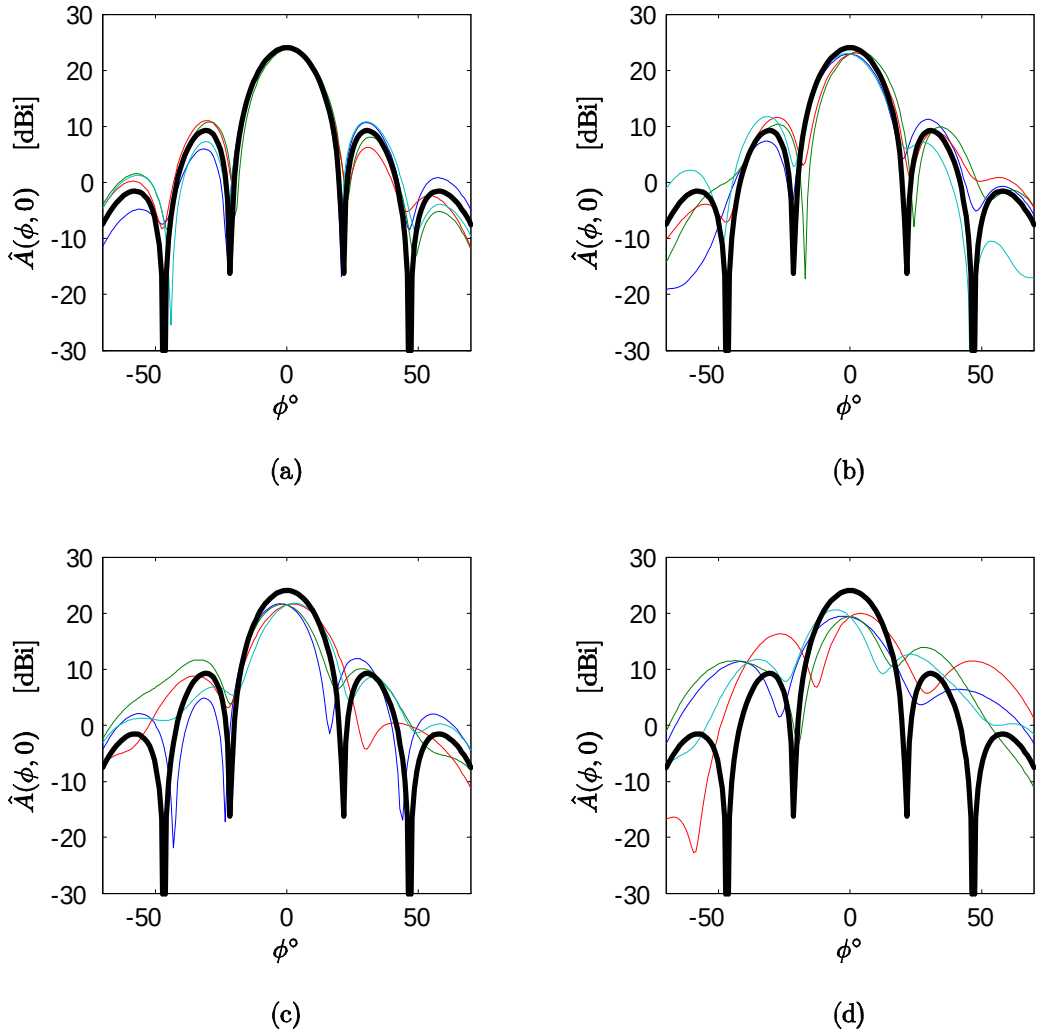

Figure 6.6 Effects of hypothetical phase mismatches on array pattern at 4.5 GHz. The complex-valued weight $w_k = e^{j\psi_k}, \psi_k \sim \mathcal{N}\left(0, \sigma_\psi^2\right)$. (a) $\sigma_\psi = 15°$. (b) $\sigma_\psi = 30°$. (c) $\sigma_\psi = 45°$. (d) $\sigma_\psi = 60°$. Ideal (matched) array pattern is shown in black; other patterns are from simulations with phase mismatches.

VII. Conclusions and Future Work

We have conducted thorough conversion gain measurements on sixteen units of the Mid-Atlantic LCR series tuners. Although these devices have a nominal voltage gain of 10 dB, there is great variation from one unit to the next. We have seen that the gain of these tuners varies anywhere from 12 dB down to 3 dB within the passband, and even down to -2 dB in a few defective devices. Out-of-band performance is poor; the additional anti-aliasing filters are necessary.

We have computed a linear regression model of the tuner gain using a fourth-degree polynomial in (f_c, f_{IF}), with a calibration offset for each individual channel. We have attempted to characterize tuner gain via statistical distributions, and found it very challenging. For each tuner, the gain $g(f_c, f_{IF})$ is very strongly autocorrelated, as evidenced by the extremely small number of degrees of freedom of the resulting t distribution despite the large sample size. In effect, this drastically reduces our sample size and limits our ability to characterize the data. There does not seem to be any simple distribution that can predict the tuner gain of an untested device from the same population. This means that if a tuner breaks and has to be replaced, there is no simple way to predict how the replacement will perform. Tuner gain is definitely *not* normally distributed from one channel to the next. Therefore, strictly speaking, it is not correct to assume that steering vector errors are normally distributed.

Future work should include thorough phase response measurement and characterization for the Mid-Atlantic tuners, as this could greatly impact digital beamforming and signal detection performance. Even greater impact could come from phase mismatches due to mismatched RF cable lengths, as these cables are very long. An end-to-end phase characterization of the entire MCWESS system is highly desirable.

We have conducted extensive antenna pattern measurements of each column of the MCWESS array, including directivity pattern and phase. The main beam ripple is poor in some cases. The phase is fairly consistent, except with the high-band data (using the WR137 probe) the chamber seemed to have been reconfigured, resulting in two divergent data sets, which had to be corrected. The phase patterns were not centered the antenna

element under test; instead they appeared to be centered on a point about 5 mm left of the center of the array, which slightly complicates analysis. We have provided a model for the antenna superelement pattern, and applied steering vectors to construct a model for the entire array. Better antenna pattern models could be developed if additional measurements were conducted to cover the domain ($60° < |\phi| < 90°, |\theta| < 30°$), as this region contains part of the mainlobe of the superelement patterns. This could be done in the near-field chamber at AFRL, by testing the array with it offset 60° in azimuth.

We conducted simulations to see how channel gain and phase mismatches could affect digital beamforming. For the MCWESS, if the channel phases are normally distributed with $\sigma_\psi \leq 45°$, the array pattern reasonably holds its shape; greater mismatches cause the pattern to fall apart. Significant gain variations, such as those seen in our tuners, cause only slight degradation in the array pattern.

Finally, we conducted simulations to demonstrate how channel gain and phase mismatches could degrade signal detection performance. Again, we found that if the channel phases are normally distributed with $\sigma_\psi \leq 45°$, the detector performed reasonably well even with a low SNR; greater mismatches caused poor performance. Gain mismatches slightly degraded detector performance. More research could be done in this area.

Appendix A. Measured Antenna Pattern Summary Data

Tables A.1-A.2 contain measured antenna pattern data for the entire MCWESS array, collected as shown in Fig. 3.9. Tables A.3-A.34 contain measured antenna pattern data for individual superelements, collected as shown in Fig. 3.8. Plots of all 1938 measured antenna patterns are available upon request from [12].

Table A.1 Antenna pattern of entire array, horizontally polarized.

f_{in} GHz	A_{max} dBi	HPBW$_\phi{}^\circ$	FNBW$_\phi{}^\circ$	HPBW$_\theta{}^\circ$	FNBW$_\theta{}^\circ$	SLL$_\phi$ dB	SLL$_\theta$ dB	$\xi_\phi{}^\circ$	$\xi_\theta{}^\circ$
2.6	24.0	37.0	75	31.3	79	-	-	0.0	0.0
2.7	25.0	34.1	73	30.9	77	-	-	0.0	0.0
2.8	23.9	33.7	69	28.6	70	-	-	0.9	0.0
2.9	23.5	33.6	66	27.6	70	-	-	-3.6	0.0
3.0	25.0	28.8	65	27.1	68	11.7	15.9	-3.6	-0.9
3.1	25.3	30.0	65	26.5	65	12.3	14.1	-2.7	-1.8
3.2	24.9	28.8	62	25.2	63	12.1	14.7	-1.8	0.0
3.3	24.9	27.3	59	24.1	61	12.2	14.5	0.0	0.0
3.4	25.4	27.0	56	23.8	57	12.1	13.6	0.0	0.0
3.5	25.3	26.1	56	23.0	57	12.6	15.0	0.0	0.0
3.6	24.5	24.9	53	22.3	54	12.1	13.7	-0.9	0.0
3.7	24.7	23.5	53	21.9	54	12.4	14.8	0.0	0.0
3.8	25.9	22.6	51	21.5	51	12.7	14.6	-0.9	0.0
3.9	25.6	20.5	50	20.6	49	12.5	14.1	-0.9	0.0
4.0	24.9	19.8	49	20.3	50	12.8	14.0	-0.9	0.0
4.1	25.3	18.3	49	20.2	49	12.4	15.2	-0.9	0.0
4.2	25.7	18.0	47	19.4	47	12.6	14.1	0.0	0.0
4.3	25.6	18.1	46	19.4	45	12.6	13.7	-0.9	0.0
4.4	24.8	17.7	46	19.5	44	12.3	13.2	-1.8	0.0
4.5	24.3	16.6	43	18.4	42	11.9	13.2	-0.9	0.0
4.6	25.5	16.7	43	18.7	43	12.5	13.7	-0.9	0.0
4.7	25.4	16.5	41	18.2	41	12.0	13.8	-0.9	0.0
4.8	25.2	15.7	41	17.3	41	12.0	13.3	-0.9	0.0
4.9	25.5	16.1	40	17.2	40	12.2	13.7	-0.9	0.0
5.0	25.1	16.1	40	17.3	39	12.2	13.9	-0.9	0.0
5.1	24.9	15.7	38	16.7	38	12.0	13.1	-0.9	0.0
5.2	24.0	16.0	37	16.3	37	12.7	12.9	-0.9	0.0
5.3	24.4	15.9	37	16.4	36	12.2	13.5	-0.9	0.0
5.4	24.2	15.7	36	15.9	35	12.4	12.8	-1.8	0.0
5.5	24.5	15.6	34	15.2	34	10.6	13.1	-0.9	0.0
5.6	24.6	15.8	34	15.2	34	11.4	12.9	-1.8	0.0
5.7	23.8	15.3	33	14.7	33	11.5	12.9	-0.9	0.9
5.8	23.8	15.2	32	14.3	33	11.5	12.8	-0.9	0.0
5.9	25.7	14.9	32	14.3	32	11.1	13.2	-1.8	0.0
6.0	25.6	14.5	32	13.9	32	10.6	13.2	-1.8	0.0
6.1	25.5	14.4	31	13.7	32	11.1	13.3	-1.8	0.0
6.2	25.2	14.2	31	13.2	31	10.9	13.6	-0.9	0.0
6.3	25.7	13.8	31	13.4	31	10.8	14.0	-1.8	0.0
6.4	25.1	13.5	30	12.7	31	11.0	14.0	-0.9	0.0
6.5	24.5	13.2	30	12.5	30	11.0	13.7	-1.8	0.0
6.6	24.7	12.9	30	12.3	29	10.9	13.6	-1.8	0.0
6.7	25.4	12.5	29	12.2	29	10.8	13.9	-0.9	0.0
6.8	24.6	12.0	28	12.1	29	10.5	14.0	-0.9	0.0
6.9	23.1	11.8	27	11.9	28	10.8	13.3	-0.9	0.0
7.0	24.0	11.6	27	11.7	28	11.0	14.2	-0.9	0.0
7.1	24.7	11.5	27	11.7	27	10.8	13.6	-0.9	0.0
7.2	23.7	11.4	27	11.4	27	11.0	13.4	-1.8	0.0
7.3	22.5	11.3	27	11.7	27	10.7	14.1	-1.8	0.0
7.4	22.6	11.0	26	11.2	26	10.6	13.5	-0.9	0.0
7.5	22.9	11.0	26	11.3	25	10.7	13.3	-0.9	0.0
7.6	23.0	10.7	25	11.0	25	10.8	13.7	-0.9	0.0
7.7	21.4	10.8	25	11.2	25	10.4	13.5	-0.9	0.0
7.8	22.5	10.5	25	10.9	24	10.0	13.3	-1.8	0.0
7.9	23.1	10.6	24	10.7	24	10.9	13.5	-1.8	0.0
8.0	23.3	10.6	24	10.6	24	10.7	13.1	-1.8	0.0
8.1	22.5	10.6	24	10.4	23	11.2	13.4	-0.9	0.0
8.2	22.3	10.4	23	10.2	23	11.2	14.0	-0.9	0.0

Table A.2 Antenna pattern of entire array, vertically polarized.

f_{in} GHz	A_{max} dBi	HPBW$_\phi{}^\circ$	FNBW$_\phi{}^\circ$	HPBW$_\theta{}^\circ$	FNBW$_\theta{}^\circ$	SLL$_\phi$ dB	SLL$_\theta$ dB	$\xi_\phi{}^\circ$	$\xi_\theta{}^\circ$
2.6	25.3	30.2	80	29.3	80	-	-	0.0	0.0
2.7	26.2	28.2	76	27.5	74	-	-	0.0	0.0
2.8	25.1	28.1	74	28.0	70	-	-	0.0	0.0
2.9	24.4	27.7	71	29.3	66	-	-	0.0	-1.8
3.0	25.8	27.0	68	29.5	67	14.5	13.8	-1.8	-2.7
3.1	26.4	26.4	66	27.5	65	14.5	14.4	-1.8	-1.8
3.2	25.7	26.2	64	27.6	60	13.9	13.4	-1.8	0.0
3.3	25.6	25.4	61	26.3	58	14.1	13.3	-0.9	0.0
3.4	26.0	24.6	59	25.5	57	13.6	13.6	0.0	0.0
3.5	25.9	24.1	57	25.4	55	13.5	13.3	-0.9	0.0
3.6	25.4	23.3	55	24.1	53	13.6	13.6	-0.9	0.0
3.7	25.3	23.3	54	24.0	51	13.7	13.3	-0.9	0.0
3.8	26.5	23.2	52	23.5	50	13.6	13.6	-0.9	0.0
3.9	25.7	22.5	50	22.9	48	13.5	13.2	-0.9	0.0
4.0	24.6	22.2	48	22.0	47	13.9	13.2	-0.9	0.0
4.1	25.1	21.3	48	21.4	47	13.7	14.0	-0.9	0.0
4.2	25.4	20.7	47	20.2	45	14.2	13.5	-0.9	0.0
4.3	25.4	20.5	45	20.0	43	13.8	13.1	-0.9	0.0
4.4	24.7	19.7	44	20.1	42	13.5	12.9	-0.9	0.0
4.5	24.2	18.6	43	18.7	42	12.9	12.8	-0.9	0.0
4.6	25.4	18.5	42	18.0	41	13.6	13.4	-0.9	0.0
4.7	25.3	17.8	42	17.8	41	12.9	13.9	-0.9	0.0
4.8	25.0	16.9	41	16.8	40	12.8	13.5	-0.9	0.0
4.9	25.7	16.9	41	16.3	40	12.8	14.4	-0.9	0.0
5.0	25.2	16.7	40	16.6	38	12.9	13.7	-0.9	0.0
5.1	25.2	15.7	39	15.8	38	12.5	13.3	-0.9	0.0
5.2	24.6	15.8	38	15.3	36	13.3	13.4	-0.9	0.0
5.3	25.0	15.5	37	15.1	37	12.8	13.7	-0.9	0.0
5.4	24.8	15.2	37	14.8	36	13.0	13.5	-0.9	0.0
5.5	25.1	14.7	35	14.3	36	13.4	13.4	-0.9	0.0
5.6	24.9	15.2	35	14.4	34	13.4	12.7	-0.9	0.0
5.7	24.1	14.7	35	14.1	34	14.0	13.0	-0.9	0.0
5.8	24.5	14.5	33	13.7	34	14.1	13.6	-0.9	0.0
5.9	24.3	14.3	33	13.9	33	13.8	13.2	-0.9	0.0
6.0	24.0	14.1	33	13.5	32	13.4	12.9	-0.9	0.0
6.1	24.1	13.7	32	13.3	32	13.4	13.2	-0.9	0.0
6.2	23.8	13.6	32	13.2	31	13.5	13.0	-0.9	0.0
6.3	24.2	13.4	31	13.0	31	13.2	13.0	-0.9	0.0
6.4	23.8	13.1	30	12.7	30	13.2	13.2	-0.9	0.0
6.5	23.0	13.0	30	12.5	29	13.3	12.4	-0.9	0.0
6.6	23.1	12.7	30	12.3	29	13.5	13.0	-0.9	0.0
6.7	23.7	12.5	29	12.6	29	13.1	13.6	-0.9	0.0
6.8	22.9	12.3	28	12.3	29	13.2	13.2	-0.9	0.0
6.9	21.5	12.1	28	12.0	27	13.7	13.2	-0.9	0.0
7.0	22.3	11.9	28	12.0	27	13.7	13.8	-0.9	0.0
7.1	23.2	11.6	27	12.1	27	13.1	14.1	-0.9	0.0
7.2	22.2	11.5	27	11.7	26	12.8	12.7	-0.9	0.0
7.3	21.1	11.5	27	11.6	26	13.4	13.7	-0.9	0.0
7.4	21.4	11.4	26	11.3	25	13.5	13.1	-0.9	0.0
7.5	21.7	11.3	25	11.1	25	13.7	13.0	-0.9	0.0
7.6	21.9	11.1	25	11.1	25	13.3	13.2	-0.9	0.0
7.7	20.9	11.1	25	11.1	25	13.6	14.1	-0.9	0.0
7.8	21.8	10.9	25	10.9	25	13.4	14.0	-0.9	0.0
7.9	22.2	10.6	25	10.3	23	14.3	13.7	0.0	0.0
8.0	22.9	10.3	23	10.4	24	13.7	13.1	-0.9	0.0
8.1	22.5	10.3	23	10.4	23	13.9	13.5	-0.9	0.0
8.2	22.0	10.0	23	10.3	23	13.8	14.8	-0.9	0.0

Table A.3 Column $k = 1$, horizontally polarized.

f_{in}	$A_{k,max}$	$\Delta A_{k,\phi}$			SLL_θ			$\tau_{\psi,k}$	$\tau_{g,k}$
GHz	dBi	dB	$\text{HPBW}_\theta{}^\circ$	$\text{FNBW}_\theta{}^\circ$	dB	${\xi_\theta}^\circ$	${\psi_k}^\circ$	ps	ps
2.6	17.5	10.8	30.0	78	-	0.9	-99	106	2643
2.7	19.0	11.2	28.4	74	-	0.9	-194	200	2333
2.8	17.9	11.2	27.1	70	-	0.0	-267	265	2048
2.9	17.2	9.0	26.7	67	-	0.9	-342	327	2057
3.0	17.6	6.3	26.1	66	13.4	-0.9	-415	384	2186
3.1	17.3	6.6	25.3	61	12.2	0.9	-499	447	2104
3.2	16.4	6.2	24.7	64	12.7	0.0	-567	492	1845
3.3	17.0	6.8	24.1	59	12.5	0.0	-632	532	1722
3.4	17.1	8.6	23.1	53	10.6	-0.9	-691	564	1607
3.5	16.9	7.1	23.1	56	12.2	0.9	-747	593	1583
3.6	16.6	6.7	22.1	53	12.0	0.0	-805	621	1757
3.7	16.9	7.0	21.8	52	12.3	-0.9	-874	656	1931
3.8	17.6	6.8	21.5	51	11.6	0.0	-944	690	1949
3.9	16.9	7.6	20.3	48	9.2	0.0	-1014	722	1965
4.0	15.3	5.6	20.4	48	10.8	0.0	-1078	749	915
4.1	15.1	5.6	20.3	49	12.5	0.0	-1111	753	1035
4.2	15.4	5.4	19.0	44	9.5	0.0	-1153	762	1115
4.3	15.6	5.7	19.0	45	10.4	0.0	-1191	770	1010
4.4	14.7	5.1	19.0	44	10.7	0.9	-1225	774	779
4.5	15.2	5.1	17.9	41	9.3	0.9	-1247	770	759
4.6	15.8	4.7	18.0	41	9.3	0.0	-1280	773	934
4.7	16.1	4.9	17.4	40	10.3	0.0	-1315	777	925
4.8	15.7	5.0	17.2	39	9.8	0.0	-1347	779	838
4.9	15.5	5.2	16.9	40	11.1	0.0	-1375	779	787
5.0	15.3	4.7	16.3	37	9.1	0.0	-1403	780	871
5.1	15.8	5.7	16.1	37	8.9	0.0	-1438	783	869
5.2	14.9	4.7	15.9	36	9.6	0.0	-1466	783	629
5.3	14.4	6.3	15.5	35	8.9	0.0	-1483	777	634
5.4	15.5	4.9	15.3	34	9.5	0.0	-1512	778	775
5.5	15.8	4.7	15.2	35	9.7	0.0	-1539	777	743
5.6	14.1	4.6	14.8	33	8.9	0.0	-1565	776	576
5.7	13.8	4.6	14.6	32	10.0	0.0	-1580	770	457
5.8	14.1	4.6	14.3	32	10.1	0.0	-1598	765	490
5.9	16.1	4.3	14.2	32	9.8	0.0	-1569	739	877
6.0	16.3	3.8	13.7	31	9.4	0.0	-1601	741	808
6.1	17.0	4.4	13.8	32	10.1	0.0	-1627	741	694
6.2	16.2	4.8	13.4	30	9.9	0.0	-1651	740	596
6.3	15.6	4.1	13.1	30	9.5	0.0	-1670	737	655
6.4	15.9	3.3	12.9	30	9.8	0.0	-1698	737	665
6.5	16.0	4.5	12.6	30	10.1	0.0	-1718	734	548
6.6	16.2	4.5	12.3	28	9.5	0.0	-1737	731	527
6.7	16.4	4.2	12.4	30	9.2	0.0	-1756	728	618
6.8	15.6	4.0	12.1	28	8.4	0.0	-1782	728	558
6.9	15.2	4.7	11.8	27	8.2	0.0	-1796	723	432
7.0	15.5	4.2	11.8	28	9.3	0.0	-1813	719	606
7.1	15.9	4.4	11.4	26	8.4	0.0	-1840	720	684
7.2	14.9	6.3	11.1	26	8.8	0.0	-1862	718	561
7.3	14.1	5.9	11.1	26	9.0	0.0	-1880	716	419
7.4	14.3	5.4	10.8	24	8.9	0.0	-1893	710	529
7.5	14.1	4.6	10.8	24	7.8	0.9	-1919	711	713
7.6	14.1	3.8	10.7	25	8.0	0.0	-1944	710	516
7.7	13.3	3.7	10.5	24	8.8	0.0	-1956	706	393
7.8	14.0	3.7	10.5	24	9.8	0.0	-1972	702	563
7.9	14.8	3.8	10.4	24	10.3	0.0	-1996	702	780
8.0	14.5	3.9	10.3	23	9.9	0.0	-2028	704	740
8.1	14.1	3.5	10.1	23	10.2	0.0	-2049	703	618
8.2	14.1	4.2	10.1	23	10.3	0.0	-2073	702	648

Table A.4 Column $k = 1$, vertically polarized.

f_{in}	$A_{k,max}$	$\Delta A_{k,\phi}$			SLL_θ			$\tau_{\psi,k}$	$\tau_{g,k}$
GHz	dBi	dB	$\text{HPBW}_\theta{}^\circ$	$\text{FNBW}_\theta{}^\circ$	dB	$\xi_\theta{}^\circ$	$\psi_k{}^\circ$	ps	ps
2.6	11.7	2.6	29.9	85	-	0.0	-66	71	2422
2.7	13.4	3.9	28.3	75	-	0.0	-153	158	2424
2.8	13.8	3.5	27.8	76	-	0.0	-241	239	2356
2.9	13.0	3.1	28.1	68	-	-1.8	-323	309	2068
3.0	14.2	3.4	29.2	67	10.3	-0.9	-390	361	2062
3.1	15.1	3.9	26.7	64	12.1	-1.8	-471	422	2126
3.2	14.0	4.0	26.5	59	9.5	-2.7	-543	471	1921
3.3	14.0	3.6	25.8	59	10.1	0.9	-610	513	1920
3.4	14.2	3.8	24.4	55	7.6	-0.9	-681	556	1980
3.5	14.8	3.4	25.3	56	9.3	-1.8	-752	597	1914
3.6	14.8	3.5	23.9	52	10.0	0.0	-819	632	1783
3.7	14.7	3.3	23.2	50	8.2	0.0	-881	661	1750
3.8	15.4	3.4	22.9	50	9.5	0.0	-945	691	1856
3.9	14.4	3.4	21.9	48	8.7	-0.9	-1014	722	1931
4.0	14.3	2.8	21.9	48	9.6	0.0	-1083	752	1000
4.1	14.6	2.7	21.0	46	9.0	0.0	-1119	758	1015
4.2	14.2	2.8	19.9	43	9.0	0.0	-1156	765	1013
4.3	14.9	2.8	19.6	43	8.8	-0.9	-1192	770	1011
4.4	15.0	3.3	19.2	41	9.1	-0.9	-1229	776	863
4.5	14.6	3.2	18.7	41	9.7	-0.9	-1254	774	765
4.6	14.4	2.8	18.1	41	9.6	-0.9	-1284	776	778
4.7	14.9	2.8	17.8	40	9.8	-0.9	-1310	774	732
4.8	14.6	3.1	16.9	38	9.8	-0.9	-1337	774	710
4.9	14.3	3.1	16.6	38	11.0	-0.9	-1361	772	724
5.0	14.5	3.2	16.1	37	10.7	-0.9	-1389	772	767
5.1	14.7	4.2	15.8	36	9.8	-0.9	-1417	772	727
5.2	13.9	4.6	15.4	35	10.3	-0.9	-1441	770	675
5.3	13.7	3.6	15.1	35	11.0	-0.9	-1465	768	635
5.4	14.5	4.2	14.9	34	10.2	-0.9	-1487	765	726
5.5	14.2	4.2	15.1	35	10.4	-0.9	-1517	766	804
5.6	12.7	3.8	14.4	33	10.2	0.0	-1545	766	540
5.7	13.2	4.9	14.2	32	9.8	-0.9	-1556	758	442
5.8	13.6	5.2	14.2	32	10.0	-0.9	-1577	755	571
5.9	15.5	4.4	14.2	32	10.6	0.0	-1542	726	777
6.0	15.2	4.8	13.7	32	10.2	-0.9	-1570	727	834
6.1	16.0	4.4	13.5	32	10.9	-0.9	-1602	730	770
6.2	15.5	5.3	13.3	31	11.1	-0.9	-1626	728	639
6.3	15.4	5.1	12.9	30	9.9	-0.9	-1648	727	678
6.4	15.6	5.8	13.0	30	10.2	-0.9	-1674	727	668
6.5	14.7	5.4	12.6	30	10.6	-0.9	-1696	725	536
6.6	14.4	6.2	12.1	28	9.5	0.0	-1713	721	516
6.7	15.4	6.2	12.3	28	10.3	0.0	-1733	719	752
6.8	14.1	6.3	12.1	28	9.7	0.0	-1767	722	676
6.9	13.0	6.5	11.8	27	9.5	0.0	-1782	717	364
7.0	13.5	7.7	11.8	28	11.5	-0.9	-1793	712	518
7.1	14.2	7.2	11.6	26	10.2	-0.9	-1819	712	794
7.2	13.8	7.2	11.3	26	10.0	-0.9	-1850	714	595
7.3	12.0	8.5	11.0	25	10.6	-0.9	-1862	709	279
7.4	12.5	8.8	10.8	24	10.3	0.0	-1871	702	467
7.5	14.1	4.9	10.7	24	9.2	0.0	-1896	702	668
7.6	13.7	4.5	10.8	25	10.0	-0.9	-1919	701	490
7.7	12.9	5.3	10.4	24	11.1	0.0	-1931	697	316
7.8	13.5	4.4	10.3	23	10.3	0.0	-1941	691	502
7.9	14.9	3.5	10.4	24	10.6	0.0	-1967	692	768
8.0	14.3	3.5	10.2	23	10.7	-0.9	-1997	693	760
8.1	13.8	3.6	10.0	23	9.3	0.0	-2022	693	619
8.2	13.8	3.4	10.1	23	11.8	0.0	-2041	691	534

Table A.5 Column $k = 2$, horizontally polarized.

f_{in}	$A_{k,max}$	$\Delta A_{k,\phi}$			SLL_θ			$\tau_{\psi,k}$	$\tau_{g,k}$
GHz	dBi	dB	$\text{HPBW}_\theta{}^\circ$	$\text{FNBW}_\theta{}^\circ$	dB	$\xi_\theta{}^\circ$	$\psi_k{}^\circ$	ps	ps
2.6	15.4	4.2	31.1	82	-	-0.9	-65	69	2835
2.7	16.4	4.8	30.4	77	-	0.0	-167	171	2641
2.8	15.6	4.3	27.6	70	-	0.0	-255	253	2289
2.9	15.4	3.4	27.2	68	-	0.9	-331	317	1985
3.0	16.5	4.1	27.2	66	15.0	-0.9	-398	368	2007
3.1	15.8	3.1	26.1	63	13.3	0.0	-476	426	2068
3.2	15.5	3.8	24.9	62	13.1	1.8	-547	474	1921
3.3	15.3	4.1	24.1	58	13.0	0.9	-614	517	1906
3.4	16.7	3.3	23.4	57	13.3	0.0	-684	559	1962
3.5	16.7	3.5	23.5	59	13.8	0.0	-756	600	1888
3.6	16.1	3.9	22.2	54	12.0	0.0	-820	632	1650
3.7	15.9	4.2	22.0	54	12.0	0.0	-874	656	1598
3.8	17.7	4.4	21.8	53	12.0	0.0	-935	683	1795
3.9	16.7	4.7	21.0	51	11.9	0.0	-1004	715	1912
4.0	15.6	4.5	20.2	48	11.9	0.0	-1071	744	1109
4.1	16.1	4.7	20.1	48	13.1	0.0	-1111	753	1164
4.2	16.5	5.0	19.6	46	11.2	0.0	-1155	764	1149
4.3	16.1	4.9	18.8	45	11.4	0.0	-1194	771	1016
4.4	15.3	4.7	18.9	43	11.1	0.0	-1228	775	757
4.5	15.2	4.3	18.1	42	11.0	0.9	-1248	770	786
4.6	15.4	4.0	18.2	42	11.9	0.0	-1285	776	875
4.7	15.3	3.1	17.5	41	11.6	0.0	-1311	775	764
4.8	14.2	3.3	17.1	39	10.4	0.0	-1340	775	745
4.9	14.9	3.2	17.0	41	11.8	0.0	-1365	774	768
5.0	15.2	4.4	17.0	40	12.6	0.9	-1395	775	844
5.1	14.9	4.8	16.5	38	12.1	0.0	-1426	776	712
5.2	14.0	4.6	15.8	35	9.5	0.9	-1446	772	624
5.3	14.6	4.8	15.9	36	11.1	0.0	-1471	771	556
5.4	14.1	4.5	15.5	35	11.4	0.0	-1486	764	671
5.5	15.9	4.8	15.5	36	11.5	0.0	-1519	767	940
5.6	15.4	5.1	15.1	34	11.5	0.0	-1554	771	637
5.7	14.4	3.6	14.6	32	10.8	0.0	-1565	762	364
5.8	14.4	4.5	14.6	33	11.9	0.0	-1580	757	426
5.9	15.1	3.7	14.5	32	11.5	0.0	-1544	727	879
6.0	15.2	2.8	14.0	32	9.8	0.9	-1576	730	742
6.1	15.2	3.2	13.9	32	11.3	0.0	-1598	728	611
6.2	15.2	3.1	13.7	32	11.8	0.9	-1620	726	649
6.3	15.6	3.9	13.5	31	11.4	0.0	-1645	725	701
6.4	15.0	3.1	13.0	31	11.3	0.0	-1671	725	653
6.5	14.0	2.7	12.7	29	10.7	0.0	-1692	723	555
6.6	14.8	3.2	12.2	28	11.3	0.0	-1710	720	611
6.7	15.5	4.1	12.2	28	12.3	0.0	-1736	720	792
6.8	14.6	2.9	12.3	29	11.3	0.0	-1768	722	672
6.9	12.9	3.9	11.9	27	10.8	0.0	-1784	718	420
7.0	13.6	4.0	11.7	28	11.9	0.9	-1798	713	593
7.1	15.0	3.3	11.6	27	12.3	0.0	-1827	715	793
7.2	13.7	3.2	11.4	27	11.1	0.0	-1855	716	642
7.3	12.4	3.7	11.4	27	11.0	0.9	-1873	713	327
7.4	12.8	4.7	11.2	25	11.2	0.0	-1878	705	459
7.5	13.3	3.4	11.1	25	11.2	0.0	-1906	706	779
7.6	12.9	3.4	10.9	25	9.9	0.0	-1934	707	527
7.7	12.1	4.1	10.7	25	10.7	0.0	-1944	701	393
7.8	13.2	4.5	10.7	24	10.9	0.0	-1963	699	534
7.9	13.3	4.7	10.5	24	11.7	0.0	-1982	697	696
8.0	13.8	3.3	10.4	23	11.6	0.0	-2013	699	615
8.1	13.1	3.4	10.3	23	11.4	0.0	-2027	695	449
8.2	13.1	4.6	10.3	23	11.0	0.0	-2045	693	515

Table A.6 Column $k = 2$, vertically polarized.

f_{in}	$A_{k,max}$	$\Delta A_{k,\phi}$			SLL_θ			$\tau_{\psi,k}$	$\tau_{g,k}$
GHz	dBi	dB	$\text{HPBW}_\theta{}^\circ$	$\text{FNBW}_\theta{}^\circ$	dB	$\xi_\theta{}^\circ$	$\psi_k{}^\circ$	ps	ps
2.6	12.3	3.2	29.9	78	-	0.0	-65	70	2733
2.7	14.2	4.1	26.9	72	-	0.0	-164	168	2575
2.8	12.5	3.6	25.6	64	-	0.0	-251	249	2210
2.9	11.8	3.2	26.2	61	-	-2.7	-323	309	1926
3.0	14.4	3.8	28.9	64	8.4	2.7	-389	361	2084
3.1	15.0	3.3	26.5	61	10.2	-1.8	-473	424	2212
3.2	14.0	3.0	25.9	59	9.0	-0.9	-549	476	1918
3.3	13.3	3.0	24.4	53	8.1	-0.9	-611	514	1807
3.4	13.9	3.0	24.4	55	9.3	-0.9	-679	555	1985
3.5	14.3	3.1	23.6	52	8.2	0.0	-754	598	1968
3.6	14.4	3.3	22.9	50	8.4	0.0	-820	633	1783
3.7	13.9	3.1	22.3	48	8.1	-0.9	-882	662	1673
3.8	14.5	2.8	21.4	46	7.7	-0.9	-941	688	1691
3.9	14.5	3.1	21.8	47	10.1	-0.9	-1004	715	1750
4.0	13.9	3.1	20.5	43	7.2	-0.9	-1075	747	850
4.1	14.0	3.0	20.4	44	9.0	-0.9	-1106	749	919
4.2	13.9	2.6	19.5	42	8.4	0.9	-1141	755	980
4.3	14.6	3.2	19.2	42	8.3	0.9	-1176	760	1005
4.4	14.4	2.8	18.9	41	9.4	0.0	-1214	766	769
4.5	13.8	2.5	18.6	41	8.5	0.0	-1232	760	770
4.6	15.7	3.1	18.0	40	10.3	0.0	-1269	766	940
4.7	15.1	2.8	17.8	41	10.7	0.0	-1299	768	772
4.8	14.3	3.6	16.9	38	9.6	0.0	-1325	767	715
4.9	15.3	5.6	16.3	37	10.0	0.0	-1351	766	795
5.0	15.2	3.4	16.3	38	10.6	0.0	-1382	768	831
5.1	15.2	6.4	15.9	36	9.7	0.0	-1411	768	697
5.2	14.6	5.5	15.3	35	8.5	-0.9	-1432	765	683
5.3	15.5	5.4	15.2	35	9.8	0.0	-1460	765	731
5.4	14.8	5.2	14.5	33	8.5	0.0	-1485	764	730
5.5	15.9	4.1	15.0	35	9.4	0.0	-1512	764	838
5.6	15.1	3.8	14.3	33	10.0	0.0	-1545	766	744
5.7	14.6	4.3	14.2	33	9.4	0.0	-1566	763	537
5.8	14.8	4.8	13.9	32	9.9	0.0	-1584	758	493
5.9	14.8	4.5	13.5	31	7.8	0.0	-1547	728	823
6.0	14.8	4.7	13.2	30	7.6	0.9	-1577	730	655
6.1	14.4	4.6	13.0	30	7.5	0.0	-1594	726	614
6.2	15.0	5.4	13.0	29	8.1	0.9	-1621	726	673
6.3	15.0	5.7	13.0	30	8.6	0.0	-1643	724	666
6.4	14.6	6.1	12.4	28	7.4	0.0	-1669	724	691
6.5	14.0	6.0	12.5	28	8.2	0.0	-1693	723	579
6.6	13.9	7.1	12.1	28	8.0	0.0	-1711	720	533
6.7	14.5	6.9	12.0	27	8.4	0.0	-1731	718	757
6.8	14.0	7.2	11.7	27	8.9	0.0	-1765	721	705
6.9	12.1	7.4	11.5	26	7.7	0.0	-1782	717	403
7.0	12.2	8.2	11.3	25	8.2	0.0	-1794	712	489
7.1	13.6	9.3	11.4	26	9.4	0.0	-1817	711	715
7.2	12.7	10.3	11.0	25	8.5	0.0	-1846	712	640
7.3	10.8	3.5	10.8	25	7.9	0.0	-1863	709	254
7.4	11.1	3.7	10.6	24	8.2	0.9	-1864	700	297
7.5	12.5	3.8	10.5	23	8.7	0.0	-1884	698	755
7.6	13.2	3.5	10.6	24	8.2	0.0	-1918	701	672
7.7	11.4	3.2	10.4	23	8.8	0.0	-1933	697	415
7.8	12.0	3.7	10.3	23	9.0	0.0	-1948	694	489
7.9	12.9	3.4	10.3	23	8.6	0.0	-1968	692	756
8.0	13.7	4.1	10.1	23	8.8	0.0	-2003	695	749
8.1	12.8	3.9	10.0	23	9.3	0.0	-2022	693	523
8.2	12.8	4.1	9.9	23	10.0	0.0	-2040	691	511

Table A.7 Column $k = 3$, horizontally polarized.

f_{in}	$A_{k,max}$	$\Delta A_{k,\phi}$			SLL_θ			$\tau_{\psi,k}$	$\tau_{g,k}$
GHz	dBi	dB	$\text{HPBW}_\theta{}^\circ$	$\text{FNBW}_\theta{}^\circ$	dB	$\xi_\theta{}^\circ$	$\psi_k{}^\circ$	ps	ps
2.6	15.1	4.3	31.0	79	-	1.8	-70	75	2720
2.7	15.2	4.4	29.5	77	-	0.0	-168	173	2501
2.8	14.8	3.6	27.6	70	-	0.0	-250	248	2193
2.9	15.2	3.5	26.8	70	-	0.0	-326	312	1962
3.0	16.2	3.6	26.8	68	14.0	-0.9	-391	362	1936
3.1	15.5	2.8	25.7	64	12.5	0.9	-465	417	2057
3.2	15.3	2.9	25.2	62	13.6	0.0	-540	468	1962
3.3	15.6	4.2	24.7	61	13.9	2.7	-607	511	1935
3.4	15.9	3.4	23.2	59	12.2	0.0	-679	555	2009
3.5	15.4	4.0	23.1	58	12.2	0.0	-751	596	1872
3.6	15.2	5.2	22.3	54	12.1	0.0	-814	628	1689
3.7	16.0	5.4	21.9	54	12.1	0.0	-873	655	1631
3.8	16.9	4.9	21.5	52	12.5	0.0	-931	681	1727
3.9	15.3	3.9	20.5	49	11.2	0.9	-997	710	1837
4.0	15.2	3.5	20.3	50	12.5	0.9	-1068	742	1116
4.1	16.5	4.5	20.1	48	11.9	0.0	-1109	751	1137
4.2	16.2	4.0	19.3	46	10.4	0.0	-1150	761	1085
4.3	15.5	3.0	19.0	45	10.6	0.9	-1187	767	1011
4.4	14.9	2.9	18.9	43	10.5	0.0	-1223	772	901
4.5	14.9	3.6	18.1	41	9.6	0.0	-1252	773	739
4.6	15.5	2.7	18.3	42	11.0	0.0	-1276	771	765
4.7	15.6	3.9	17.5	41	10.1	0.0	-1307	772	801
4.8	15.3	4.2	17.2	40	9.8	0.0	-1334	772	684
4.9	15.2	4.8	17.1	40	11.4	0.0	-1356	769	721
5.0	15.2	4.7	16.7	37	10.4	0.0	-1386	770	788
5.1	14.7	3.6	16.2	37	10.3	0.9	-1413	769	695
5.2	14.9	4.1	16.2	38	10.8	0.9	-1436	767	522
5.3	15.4	3.8	15.6	35	9.8	0.9	-1450	760	596
5.4	15.4	3.5	15.5	35	10.4	0.0	-1479	761	692
5.5	15.2	3.5	15.4	35	10.8	0.0	-1500	758	836
5.6	15.4	3.4	14.9	33	10.1	0.9	-1539	763	804
5.7	14.6	3.3	14.7	33	10.8	0.9	-1558	759	486
5.8	14.3	4.3	14.5	32	11.0	0.0	-1574	754	445
5.9	15.4	4.1	14.4	32	11.6	0.9	-1533	722	850
6.0	15.5	3.9	13.8	32	10.4	0.9	-1563	724	789
6.1	15.5	3.8	13.8	32	11.0	0.0	-1590	724	670
6.2	14.4	3.7	13.4	30	10.9	0.9	-1612	722	620
6.3	15.3	3.8	13.3	30	11.5	0.9	-1634	721	730
6.4	15.0	3.3	13.0	30	11.6	0.9	-1664	722	727
6.5	14.5	3.2	12.7	30	10.7	0.9	-1687	721	618
6.6	14.9	3.3	12.2	28	10.7	0.9	-1709	719	687
6.7	15.1	3.5	12.3	28	11.4	0.9	-1736	720	760
6.8	14.4	3.6	12.2	28	10.2	0.9	-1764	720	651
6.9	13.5	3.2	11.9	28	9.9	0.9	-1783	718	493
7.0	14.1	4.0	11.8	28	12.0	0.9	-1799	714	569
7.1	14.8	3.0	11.5	26	10.6	0.9	-1824	714	665
7.2	13.7	3.0	11.2	26	9.8	0.9	-1847	713	574
7.3	12.6	3.4	11.4	26	10.7	0.9	-1865	710	331
7.4	12.3	3.6	11.1	25	10.7	0.9	-1871	702	355
7.5	12.9	4.0	10.8	24	9.9	0.9	-1891	700	710
7.6	12.9	2.9	10.9	25	11.2	0.9	-1922	702	532
7.7	12.1	3.3	10.8	24	10.6	0.9	-1929	696	334
7.8	12.8	3.8	10.7	24	10.4	0.9	-1946	693	557
7.9	13.6	3.0	10.5	23	10.5	0.0	-1969	692	739
8.0	13.8	3.0	10.4	23	11.2	0.9	-1999	694	597
8.1	13.1	3.8	10.5	23	11.3	0.9	-2012	690	400
8.2	13.3	3.9	10.3	23	11.2	0.9	-2028	687	440

Table A.8 Column $k = 3$, vertically polarized.

f_{in}	$A_{k,max}$	$\Delta A_{k,\phi}$			SLL_θ			$\tau_{\psi,k}$	$\tau_{g,k}$
GHz	dBi	dB	$\text{HPBW}_\theta{}^\circ$	$\text{FNBW}_\theta{}^\circ$	dB	${\xi_\theta}^\circ$	${\psi_k}^\circ$	ps	ps
2.6	13.4	3.0	30.2	91	-	0.9	-69	74	2719
2.7	14.8	3.1	28.0	77	-	0.0	-167	172	2550
2.8	13.6	3.0	28.3	77	-	0.0	-253	251	2305
2.9	13.4	3.1	27.9	70	-	-0.9	-333	319	2034
3.0	15.3	3.4	28.7	69	10.3	2.7	-399	370	2071
3.1	15.5	3.1	26.5	65	11.3	-1.8	-482	432	2092
3.2	14.4	2.8	26.2	61	10.2	0.9	-550	478	1822
3.3	14.3	2.5	25.4	59	10.2	0.9	-614	516	1843
3.4	14.9	3.0	25.3	58	11.5	0.9	-683	558	1979
3.5	14.9	2.8	24.3	54	10.0	0.0	-756	600	1943
3.6	14.7	3.2	23.8	54	10.5	0.0	-823	635	1763
3.7	15.0	3.8	23.2	51	11.0	0.0	-883	663	1718
3.8	16.0	3.3	22.6	50	10.6	0.0	-946	692	1753
3.9	15.0	3.8	21.8	47	9.5	0.0	-1009	719	1746
4.0	14.5	2.8	21.6	49	10.7	0.9	-1087	755	965
4.1	15.1	2.7	20.8	45	9.6	0.9	-1122	760	978
4.2	15.1	2.7	20.1	45	10.2	0.9	-1157	765	1008
4.3	15.3	2.7	19.6	43	9.7	0.0	-1194	771	981
4.4	14.9	2.5	19.2	42	10.1	0.0	-1228	775	895
4.5	14.3	3.0	18.9	41	10.0	0.0	-1259	777	790
4.6	15.8	4.0	18.1	41	9.6	0.0	-1285	776	824
4.7	15.6	4.3	17.8	41	10.1	0.0	-1318	779	875
4.8	14.8	3.8	17.5	40	10.9	0.0	-1348	780	776
4.9	16.0	5.7	16.9	39	10.5	0.0	-1374	779	783
5.0	16.2	5.1	16.4	37	9.6	0.0	-1404	780	824
5.1	15.2	3.6	16.3	37	10.5	0.0	-1433	781	780
5.2	14.4	3.6	15.6	36	10.5	0.0	-1460	780	596
5.3	15.3	4.5	15.2	35	9.8	0.0	-1476	774	538
5.4	15.0	4.3	15.0	35	9.9	0.0	-1499	771	677
5.5	14.8	5.0	15.0	34	9.3	0.0	-1525	770	864
5.6	14.7	4.5	14.4	33	10.1	0.0	-1561	774	720
5.7	14.5	5.4	14.4	33	10.0	0.0	-1577	768	455
5.8	14.5	5.3	14.0	33	10.0	0.0	-1594	763	482
5.9	14.7	5.0	14.0	32	10.5	0.0	-1550	730	772
6.0	14.7	5.8	13.8	32	9.0	0.0	-1578	731	735
6.1	14.8	6.1	13.5	31	9.5	0.0	-1603	730	634
6.2	14.4	6.3	13.2	31	9.2	0.0	-1624	728	639
6.3	14.7	6.6	13.1	31	10.6	0.0	-1649	727	736
6.4	14.5	6.4	12.8	29	9.3	0.0	-1677	728	690
6.5	14.1	6.4	12.5	29	9.9	0.0	-1699	726	615
6.6	13.7	7.0	12.2	29	10.0	0.0	-1721	724	653
6.7	14.1	8.1	12.2	29	10.8	0.0	-1746	724	738
6.8	13.4	7.9	11.9	27	9.7	0.0	-1774	725	654
6.9	12.5	9.2	11.7	27	10.6	0.0	-1793	722	405
7.0	12.9	3.5	11.5	26	10.5	0.0	-1803	716	515
7.1	13.5	3.0	11.5	27	11.6	0.0	-1830	716	719
7.2	12.8	3.1	11.2	26	10.4	0.0	-1855	716	628
7.3	11.3	3.4	11.1	25	11.0	0.0	-1875	714	439
7.4	12.1	4.4	10.9	25	10.4	0.0	-1887	708	485
7.5	12.3	4.3	10.7	25	10.2	0.0	-1910	708	698
7.6	12.4	4.1	10.7	24	10.0	0.0	-1937	708	474
7.7	11.6	4.6	10.6	24	10.8	0.0	-1944	701	374
7.8	12.3	4.5	10.6	24	11.2	0.0	-1964	699	591
7.9	13.0	3.5	10.4	23	11.3	0.0	-1987	699	698
8.0	13.5	4.9	10.3	23	10.9	0.0	-2014	699	629
8.1	12.8	5.1	10.2	23	10.1	0.0	-2032	697	524
8.2	12.8	3.2	10.1	23	10.4	0.0	-2052	695	545

Table A.9 Column $k = 4$, horizontally polarized.

f_{in}	$A_{k,max}$	$\Delta A_{k,\phi}$			SLL_θ			$\tau_{\psi,k}$	$\tau_{g,k}$
GHz	dBi	dB	$\text{HPBW}_\theta{}^\circ$	$\text{FNBW}_\theta{}^\circ$	dB	${\xi_\theta}^\circ$	${\psi_k}^\circ$	ps	ps
2.6	14.3	3.6	30.6	80	-	0.9	-59	63	2604
2.7	15.3	4.4	29.4	73	-	0.0	-153	157	2465
2.8	14.2	3.4	28.0	71	-	0.0	-237	235	2155
2.9	14.6	3.4	27.0	68	-	0.0	-308	295	1837
3.0	15.5	3.1	26.3	66	12.8	0.0	-369	342	1900
3.1	15.7	2.9	25.8	64	12.8	0.0	-445	399	2097
3.2	15.1	3.2	25.0	61	13.4	0.0	-520	451	1944
3.3	15.3	4.5	24.3	60	12.9	-1.8	-585	492	1873
3.4	15.2	3.5	23.4	59	12.0	0.9	-655	535	2010
3.5	15.7	4.5	22.4	54	12.8	0.0	-729	579	2005
3.6	15.8	5.2	21.8	55	13.3	0.0	-799	617	1846
3.7	15.5	4.1	21.4	53	12.4	0.9	-862	647	1625
3.8	16.3	4.0	20.8	51	13.0	0.0	-916	670	1688
3.9	15.6	3.5	20.3	50	13.2	0.0	-984	701	1885
4.0	15.3	3.4	20.1	49	12.4	0.0	-1057	734	980
4.1	15.4	3.5	19.7	48	12.4	0.0	-1092	740	929
4.2	15.1	3.3	19.3	45	11.8	0.0	-1124	743	916
4.3	15.2	3.4	19.0	45	11.5	0.0	-1158	748	988
4.4	15.2	3.9	18.9	43	11.4	0.0	-1195	754	910
4.5	13.8	3.7	18.1	42	9.9	0.0	-1224	755	737
4.6	15.3	4.1	18.3	42	10.6	0.0	-1248	754	780
4.7	15.6	4.3	17.6	41	11.2	0.0	-1280	756	826
4.8	15.1	3.4	17.5	41	10.8	-0.9	-1307	757	643
4.9	15.0	3.2	17.2	40	11.6	0.0	-1326	752	630
5.0	15.1	3.5	16.8	39	10.4	0.0	-1353	752	758
5.1	15.2	3.5	16.4	37	12.0	0.0	-1381	752	768
5.2	14.5	3.5	16.2	37	10.3	0.0	-1408	752	558
5.3	15.0	3.9	15.7	35	10.2	0.9	-1421	745	508
5.4	14.8	3.9	15.4	34	10.2	0.0	-1445	743	642
5.5	15.6	5.7	15.5	35	11.4	0.0	-1467	741	874
5.6	15.6	5.6	14.9	34	11.0	0.9	-1508	748	826
5.7	14.6	4.9	14.5	33	10.8	0.9	-1526	744	535
5.8	14.8	5.4	14.4	32	12.1	0.0	-1546	740	549
5.9	15.2	4.1	14.2	32	11.2	0.0	-1509	710	859
6.0	14.7	2.6	13.8	32	11.2	0.0	-1540	713	837
6.1	15.1	2.6	13.9	32	11.5	0.0	-1569	714	720
6.2	14.2	2.7	13.3	31	10.0	0.9	-1592	713	611
6.3	15.2	3.9	13.3	31	11.4	0.0	-1613	711	661
6.4	14.6	2.9	12.9	31	11.1	0.0	-1639	711	633
6.5	14.1	2.4	12.7	29	10.1	0.0	-1659	709	517
6.6	14.4	4.0	12.2	29	9.9	0.0	-1676	706	581
6.7	14.9	3.5	12.2	29	11.0	0.0	-1700	705	725
6.8	14.2	3.5	11.9	27	9.8	0.0	-1729	706	635
6.9	13.0	4.0	11.7	27	8.9	0.0	-1746	703	391
7.0	13.6	3.2	11.7	27	10.7	0.0	-1757	697	491
7.1	14.3	2.7	11.6	27	10.9	0.9	-1781	697	725
7.2	13.2	3.3	11.2	25	10.3	0.0	-1809	698	607
7.3	11.7	2.7	11.3	25	11.5	0.0	-1825	695	354
7.4	12.2	3.4	11.1	25	10.1	0.0	-1834	689	444
7.5	13.1	3.7	10.9	25	10.5	0.0	-1857	688	690
7.6	12.5	3.7	10.8	24	10.3	0.0	-1884	689	412
7.7	11.7	3.7	10.8	25	10.2	0.0	-1887	681	234
7.8	12.1	3.9	10.8	25	11.4	0.0	-1901	677	553
7.9	12.7	3.8	10.4	23	11.0	0.0	-1927	677	812
8.0	13.5	3.6	10.4	23	10.2	0.0	-1959	680	676
8.1	12.5	4.0	10.3	23	9.3	0.0	-1975	677	498
8.2	13.0	5.4	10.3	24	10.3	0.0	-1995	676	553

Table A.10 Column $k = 4$, vertically polarized.

f_{in}	$A_{k,max}$	$\Delta A_{k,\phi}$			SLL_θ			$\tau_{\psi,k}$	$\tau_{g,k}$
GHz	dBi	dB	$\text{HPBW}_\theta{}^\circ$	$\text{FNBW}_\theta{}^\circ$	dB	$\xi_\theta{}^\circ$	$\psi_k{}^\circ$	ps	ps
2.6	13.4	2.8	30.0	80	-	-1.8	-65	70	2791
2.7	14.1	3.1	28.6	83	-	0.0	-166	170	2508
2.8	13.2	2.8	28.3	74	-	0.0	-246	244	2210
2.9	12.9	2.9	27.6	68	-	0.0	-325	311	2027
3.0	14.6	2.9	28.4	66	10.2	-3.6	-392	363	2059
3.1	15.0	3.0	26.9	64	9.2	-1.8	-473	424	2052
3.2	14.5	2.6	25.8	59	11.1	-2.7	-539	468	1780
3.3	14.4	2.7	25.9	59	10.3	-2.7	-601	506	1809
3.4	14.9	3.0	24.5	55	9.5	-1.8	-670	547	1896
3.5	14.6	3.3	24.5	54	10.1	-2.7	-738	585	1841
3.6	14.9	3.8	23.7	53	9.8	-1.8	-802	619	1797
3.7	15.0	3.6	23.0	50	10.4	-0.9	-867	651	1782
3.8	15.8	3.7	22.3	49	10.5	-0.9	-930	680	1806
3.9	14.4	2.9	21.7	48	10.9	-0.9	-997	710	1849
4.0	14.5	2.8	21.2	46	10.4	-0.9	-1070	743	1107
4.1	14.9	2.5	20.8	46	11.0	0.0	-1110	752	1076
4.2	14.7	2.5	19.8	44	10.6	0.0	-1148	759	975
4.3	14.4	2.4	19.5	43	10.5	-0.9	-1180	762	911
4.4	14.7	2.4	19.4	42	10.1	-0.9	-1213	766	909
4.5	14.2	3.0	18.7	41	9.6	-0.9	-1246	769	843
4.6	15.3	3.0	18.4	41	11.1	0.0	-1274	769	789
4.7	15.0	3.2	17.8	41	11.1	-0.9	-1302	770	803
4.8	14.8	2.8	17.4	39	10.3	0.0	-1332	771	808
4.9	15.7	3.5	16.9	39	11.3	0.0	-1361	771	788
5.0	15.3	4.1	16.3	37	10.2	-0.9	-1388	771	733
5.1	14.6	3.6	16.1	38	10.9	0.0	-1413	770	710
5.2	14.1	3.6	15.9	37	10.0	0.0	-1439	769	571
5.3	15.3	4.9	15.3	35	11.5	0.0	-1454	762	525
5.4	14.7	5.2	15.0	35	11.0	0.0	-1477	760	580
5.5	15.1	6.7	15.0	35	8.2	0.0	-1496	756	781
5.6	15.4	4.9	14.7	33	10.2	0.0	-1533	761	748
5.7	14.4	5.9	14.6	34	9.7	0.0	-1550	755	496
5.8	14.8	6.0	14.0	32	10.0	0.0	-1569	752	532
5.9	15.2	5.4	14.1	32	10.1	0.0	-1531	721	833
6.0	15.0	5.7	13.7	32	8.3	0.0	-1561	723	834
6.1	14.9	6.3	13.7	32	10.3	0.0	-1591	724	700
6.2	14.4	6.1	13.4	32	9.7	0.0	-1611	722	644
6.3	15.1	6.5	12.8	30	9.6	0.0	-1637	722	762
6.4	14.7	6.9	12.9	31	10.6	0.0	-1666	723	706
6.5	13.9	8.7	12.6	30	9.1	0.0	-1688	721	566
6.6	14.1	9.5	12.2	28	9.0	0.0	-1707	718	603
6.7	14.2	3.1	12.3	30	10.5	0.0	-1731	718	705
6.8	13.5	3.2	11.8	28	9.8	0.9	-1758	718	622
6.9	12.4	4.4	11.7	28	9.2	0.0	-1776	715	498
7.0	13.3	4.3	11.8	29	10.5	0.0	-1793	712	586
7.1	13.7	3.1	11.5	27	10.1	0.0	-1818	711	678
7.2	12.9	3.2	11.0	26	9.2	0.0	-1842	711	607
7.3	12.1	3.8	11.4	26	9.9	0.0	-1862	709	375
7.4	11.6	4.4	10.8	24	9.1	0.0	-1869	702	405
7.5	12.4	3.2	10.8	24	9.8	0.0	-1891	701	646
7.6	12.4	3.1	10.8	24	9.4	0.0	-1916	700	485
7.7	11.9	5.6	10.6	24	9.5	-0.9	-1926	695	447
7.8	12.1	4.5	10.6	24	10.2	0.0	-1948	694	552
7.9	12.6	4.5	10.4	24	10.3	-0.9	-1966	691	654
8.0	13.3	5.8	10.2	23	8.7	0.0	-1995	693	683
8.1	12.4	3.4	10.2	23	9.2	0.0	-2015	691	588
8.2	12.9	3.4	10.1	23	11.0	0.0	-2037	690	618

Table A.11 Column $k = 5$, horizontally polarized.

f_{in}	$A_{k,max}$	$\Delta A_{k,\phi}$			SLL_θ			$\tau_{\psi,k}$	$\tau_{g,k}$
GHz	dBi	dB	$\text{HPBW}_\theta{}^\circ$	$\text{FNBW}_\theta{}^\circ$	dB	${\xi_\theta}^\circ$	${\psi_k}^\circ$	ps	ps
2.6	13.8	3.1	30.4	76	-	-2.7	-82	88	2502
2.7	15.1	3.6	29.9	77	-	0.9	-172	177	2424
2.8	14.1	3.4	27.6	68	-	0.0	-256	254	2165
2.9	13.5	3.1	27.0	68	-	0.0	-328	314	1863
3.0	15.3	4.2	26.2	66	13.4	-0.9	-391	362	1970
3.1	15.1	3.1	25.3	64	11.2	1.8	-470	421	2165
3.2	14.1	3.1	24.5	61	12.7	0.0	-546	474	1953
3.3	14.3	3.3	23.7	59	11.3	0.0	-610	514	1846
3.4	15.0	3.4	22.6	54	10.2	0.0	-679	555	2034
3.5	15.6	3.8	22.7	57	14.3	0.0	-757	601	2057
3.6	14.9	3.4	21.5	52	10.7	0.0	-827	638	1882
3.7	14.7	3.6	21.4	52	11.9	0.0	-892	670	1796
3.8	15.5	3.7	20.7	49	10.0	0.0	-957	699	1831
3.9	14.8	3.9	20.1	48	11.3	0.0	-1024	729	1870
4.0	14.8	3.5	20.0	47	10.5	0.0	-1095	760	837
4.1	14.5	3.7	19.6	46	10.4	0.0	-1125	762	845
4.2	15.1	3.2	19.0	44	10.7	0.0	-1155	764	909
4.3	15.2	4.0	18.2	42	9.2	0.0	-1190	769	947
4.4	14.7	3.5	18.5	42	9.8	0.0	-1224	773	845
4.5	13.8	3.4	17.7	41	9.9	0.0	-1251	772	820
4.6	15.8	3.4	17.7	41	9.6	0.0	-1283	775	892
4.7	14.7	2.8	17.2	40	10.1	0.0	-1315	777	846
4.8	14.5	2.9	17.2	40	10.8	0.0	-1344	778	687
4.9	15.1	3.0	16.7	39	11.1	0.0	-1365	774	732
5.0	14.9	3.9	16.4	37	10.4	0.0	-1396	776	845
5.1	14.5	4.4	16.2	36	9.9	0.0	-1426	776	759
5.2	13.6	4.1	15.5	34	8.5	0.0	-1451	775	619
5.3	14.4	3.6	15.8	36	11.0	0.0	-1470	771	642
5.4	13.9	4.5	15.2	33	8.3	0.0	-1497	770	650
5.5	14.5	3.3	15.2	33	9.0	-0.9	-1517	766	746
5.6	15.2	3.7	14.8	32	9.7	0.0	-1551	769	730
5.7	14.0	3.4	14.6	32	9.8	0.0	-1570	765	561
5.8	14.2	3.7	14.1	32	9.4	0.0	-1591	762	604
5.9	14.6	3.3	13.8	31	9.4	0.0	-1555	732	866
6.0	15.3	3.5	13.5	31	9.4	0.0	-1586	734	836
6.1	15.2	3.5	13.4	30	9.7	0.0	-1615	735	690
6.2	15.1	4.2	13.2	31	9.8	-0.9	-1636	733	633
6.3	15.1	4.7	13.0	30	10.4	0.0	-1660	732	724
6.4	14.9	3.7	12.5	29	9.7	0.0	-1688	732	652
6.5	14.5	3.0	12.3	28	9.0	0.0	-1707	730	506
6.6	15.0	4.1	12.3	29	9.1	-0.9	-1724	726	541
6.7	15.0	4.1	12.0	28	10.0	0.0	-1746	724	720
6.8	13.9	3.8	11.8	27	11.0	0.0	-1776	725	630
6.9	13.2	3.8	11.8	27	9.7	-0.9	-1792	721	436
7.0	13.7	5.4	11.6	27	9.7	-0.9	-1807	717	622
7.1	14.2	3.2	11.5	26	11.0	0.0	-1836	718	753
7.2	12.7	2.8	11.2	26	10.2	0.0	-1862	718	634
7.3	11.7	3.1	11.3	25	9.7	0.0	-1882	716	359
7.4	11.7	3.5	10.9	25	9.2	0.0	-1887	708	428
7.5	12.8	4.3	10.7	23	9.7	0.0	-1913	709	764
7.6	12.4	4.6	10.7	24	9.7	0.0	-1942	710	550
7.7	11.5	3.7	10.7	24	9.8	0.0	-1953	704	376
7.8	11.7	3.8	10.4	23	9.7	0.0	-1970	701	500
7.9	12.6	4.4	10.2	23	9.0	0.0	-1989	699	706
8.0	13.3	4.1	10.2	23	9.2	0.0	-2020	702	672
8.1	12.6	4.1	10.1	22	9.0	0.0	-2037	699	477
8.2	12.7	6.2	10.2	23	10.4	0.0	-2055	696	495

Table A.12 Column $k = 5$, vertically polarized.

f_{in}	$A_{k,max}$	$\Delta A_{k,\phi}$			SLL_θ			$\tau_{\psi,k}$	$\tau_{g,k}$
GHz	dBi	dB	$\text{HPBW}_\theta{}^\circ$	$\text{FNBW}_\theta{}^\circ$	dB	${\xi_\theta}^\circ$	${\psi_k}^\circ$	ps	ps
2.6	13.9	2.8	30.1	82	-	0.0	-88	94	2776
2.7	14.6	2.8	27.5	75	-	0.0	-188	193	2521
2.8	13.4	2.6	27.4	71	-	0.0	-269	267	2224
2.9	12.9	2.6	27.6	71	-	0.0	-348	333	1988
3.0	14.6	2.8	28.2	66	12.0	0.0	-412	382	2027
3.1	15.2	2.7	26.8	65	13.5	0.0	-494	442	2084
3.2	14.3	2.5	26.3	63	12.7	1.8	-562	488	1833
3.3	13.9	2.8	25.2	59	11.3	-1.8	-626	527	1790
3.4	14.1	2.5	25.0	57	12.8	0.0	-691	565	1869
3.5	14.6	2.7	24.5	55	12.6	1.8	-760	603	1898
3.6	14.4	2.9	23.9	54	12.1	-0.9	-828	639	1815
3.7	14.2	2.6	23.2	51	12.3	0.0	-891	669	1742
3.8	15.6	2.7	22.7	50	12.0	0.0	-953	697	1822
3.9	15.0	2.4	22.2	50	13.0	0.0	-1022	728	1911
4.0	14.2	2.4	21.7	49	13.1	0.0	-1100	764	940
4.1	14.6	2.5	21.1	49	12.1	0.0	-1134	768	1034
4.2	14.9	2.5	20.2	44	12.2	0.0	-1175	777	1093
4.3	15.0	2.6	19.9	45	12.8	0.0	-1213	783	1015
4.4	14.5	2.5	19.5	42	11.9	0.0	-1248	788	865
4.5	13.7	2.6	19.1	43	12.0	0.0	-1275	787	755
4.6	15.2	2.6	18.4	41	12.8	-0.9	-1302	786	810
4.7	15.1	2.7	18.0	41	12.6	0.9	-1333	788	854
4.8	14.3	2.8	17.5	41	13.0	0.0	-1364	789	684
4.9	15.1	3.5	17.0	39	12.3	0.9	-1383	784	681
5.0	15.4	4.6	16.7	40	12.4	0.0	-1413	785	830
5.1	15.2	4.8	16.3	38	12.4	0.0	-1442	786	774
5.2	14.2	5.4	15.7	37	10.9	0.0	-1469	784	603
5.3	15.0	4.9	15.7	38	12.4	0.0	-1486	779	618
5.4	14.6	4.0	15.2	36	12.5	0.0	-1513	778	767
5.5	15.7	5.2	15.0	36	9.4	0.0	-1541	778	808
5.6	15.1	4.5	14.7	34	12.3	0.0	-1571	779	655
5.7	14.5	6.1	14.6	34	11.1	0.0	-1588	774	533
5.8	14.9	5.9	14.1	33	11.9	0.0	-1610	771	594
5.9	16.7	5.0	14.0	32	11.4	0.0	-1576	742	803
6.0	16.7	4.9	13.6	32	9.5	0.0	-1605	743	802
6.1	16.4	6.1	13.5	31	10.7	0.0	-1634	744	777
6.2	16.1	7.6	13.5	31	10.8	0.0	-1661	744	699
6.3	16.4	6.9	13.2	31	10.7	0.0	-1684	743	684
6.4	15.7	6.6	12.8	30	10.2	0.0	-1711	742	668
6.5	15.3	9.1	12.5	29	10.6	0.0	-1733	740	563
6.6	15.5	3.4	12.3	29	10.8	0.0	-1751	737	541
6.7	15.8	2.9	12.1	29	10.5	0.0	-1772	734	750
6.8	14.4	3.0	11.9	28	10.4	0.0	-1805	737	664
6.9	13.5	3.3	11.8	27	11.2	0.0	-1819	732	375
7.0	14.0	3.6	11.7	27	11.3	0.0	-1832	727	561
7.1	15.0	3.1	11.8	28	11.3	0.0	-1860	728	737
7.2	13.7	3.3	11.3	27	11.4	0.0	-1885	727	551
7.3	12.6	5.7	11.2	26	11.6	0.0	-1899	723	306
7.4	13.2	5.0	11.1	26	12.0	0.0	-1907	716	505
7.5	14.0	4.1	10.9	25	10.8	0.0	-1936	717	776
7.6	13.4	4.6	10.8	25	10.2	0.0	-1963	717	522
7.7	13.1	6.5	10.7	25	11.7	0.0	-1973	712	375
7.8	13.8	6.6	10.7	25	11.6	0.0	-1990	709	628
7.9	14.2	5.4	10.4	24	11.1	0.0	-2018	710	738
8.0	14.2	3.0	10.3	23	10.7	0.0	-2043	709	609
8.1	14.4	3.5	10.1	23	10.4	0.0	-2062	707	622
8.2	14.6	3.6	10.1	23	12.7	0.0	-2088	707	710

Table A.13 Column $k = 6$, horizontally polarized.

f_{in}	$A_{k,max}$	$\Delta A_{k,\phi}$			SLL_θ			$\tau_{\psi,k}$	$\tau_{g,k}$
GHz	dBi	dB	$\text{HPBW}_\theta{}^\circ$	$\text{FNBW}_\theta{}^\circ$	dB	$\xi_\theta{}^\circ$	$\psi_k{}^\circ$	ps	ps
2.6	14.0	2.6	31.1	77	-	0.9	-82	87	2524
2.7	15.2	3.4	30.5	76	-	0.0	-172	177	2372
2.8	14.4	4.0	27.8	68	-	0.0	-252	250	2133
2.9	14.0	4.1	27.6	68	-	0.0	-326	312	2042
3.0	15.8	4.8	26.6	66	14.4	-0.9	-399	370	2151
3.1	15.0	3.3	25.7	66	11.8	2.7	-481	431	2170
3.2	14.2	2.5	24.6	61	12.8	0.9	-556	482	1905
3.3	14.6	2.9	23.9	59	12.6	0.9	-618	520	1805
3.4	15.5	3.3	23.6	59	12.5	0.9	-686	560	1978
3.5	15.7	3.2	23.1	58	13.5	0.0	-761	604	2000
3.6	15.1	3.5	22.3	54	12.5	0.0	-830	640	1892
3.7	15.3	3.9	22.1	54	13.6	0.9	-897	673	1825
3.8	16.3	4.4	21.3	51	11.2	0.0	-961	703	1858
3.9	15.4	4.2	20.5	50	12.1	0.0	-1031	734	1930
4.0	15.2	3.5	20.6	49	12.0	0.0	-1097	762	877
4.1	15.7	3.6	19.7	47	11.5	0.0	-1128	764	942
4.2	16.2	3.6	19.6	46	11.0	0.9	-1165	770	973
4.3	15.7	3.4	19.0	44	12.3	0.0	-1198	774	947
4.4	15.4	3.1	19.1	43	11.6	0.0	-1233	778	915
4.5	14.4	3.0	18.2	42	10.8	0.9	-1264	780	801
4.6	15.8	2.8	18.3	41	11.3	0.9	-1290	779	812
4.7	15.2	2.7	17.9	41	11.8	0.0	-1323	782	892
4.8	15.2	3.4	17.7	41	12.4	0.9	-1355	784	720
4.9	15.0	2.8	17.1	40	11.7	0.9	-1375	779	718
5.0	15.0	3.3	17.1	40	12.8	0.0	-1406	781	880
5.1	14.9	3.5	16.5	37	12.2	0.9	-1438	783	834
5.2	14.2	3.1	16.2	37	11.9	0.0	-1466	783	583
5.3	14.5	3.5	16.1	37	12.2	0.9	-1480	776	625
5.4	14.9	3.3	15.6	35	11.3	0.0	-1511	777	673
5.5	15.6	3.0	15.6	35	11.7	0.9	-1528	772	751
5.6	15.0	3.3	15.2	35	12.2	0.0	-1565	777	715
5.7	14.2	3.2	14.8	33	11.8	0.9	-1580	770	443
5.8	14.5	4.1	14.6	33	12.1	0.0	-1597	765	485
5.9	15.4	4.4	14.4	32	11.8	0.9	-1563	736	852
6.0	15.3	3.7	14.0	32	11.4	0.9	-1594	738	769
6.1	15.2	2.9	13.9	32	12.5	0.9	-1619	737	563
6.2	15.1	4.1	13.4	31	11.1	0.0	-1635	732	653
6.3	15.2	3.6	13.5	32	12.1	0.9	-1666	734	847
6.4	15.0	3.2	13.0	31	12.0	0.0	-1696	736	746
6.5	15.0	3.4	12.9	30	11.6	0.0	-1720	735	590
6.6	15.2	4.1	12.5	30	12.3	0.9	-1738	732	602
6.7	15.0	4.4	12.3	29	12.3	0.9	-1763	731	736
6.8	13.8	3.5	12.1	29	12.1	0.9	-1791	732	642
6.9	12.8	3.7	11.9	28	12.1	0.9	-1809	728	498
7.0	13.6	3.7	11.9	28	12.3	0.9	-1827	725	645
7.1	14.4	4.3	11.7	27	12.1	0.9	-1856	726	721
7.2	12.9	3.5	11.5	27	11.3	0.9	-1879	725	569
7.3	11.9	4.0	11.6	27	11.2	0.9	-1897	722	286
7.4	12.3	4.4	11.6	27	12.4	0.9	-1899	713	417
7.5	13.1	5.3	11.2	26	10.9	0.9	-1927	714	755
7.6	12.4	4.5	11.2	25	11.6	0.9	-1954	714	537
7.7	11.8	3.9	11.2	26	12.2	0.0	-1965	709	422
7.8	13.1	5.1	10.9	25	12.8	0.9	-1984	707	603
7.9	13.7	6.4	10.7	24	11.9	0.0	-2009	706	713
8.0	13.7	5.6	10.6	24	12.5	0.9	-2036	707	560
8.1	13.1	5.7	10.5	24	11.8	0.9	-2049	703	465
8.2	13.3	8.0	10.6	24	11.5	0.9	-2069	701	558

Table A.14 Column $k = 6$, vertically polarized.

f_{in}	$A_{k,max}$	$\Delta A_{k,\phi}$			SLL_θ			$\tau_{\psi,k}$	$\tau_{g,k}$
GHz	dBi	dB	$\text{HPBW}_\theta{}^\circ$	$\text{FNBW}_\theta{}^\circ$	dB	$\xi_\theta{}^\circ$	$\psi_k{}^\circ$	ps	ps
2.6	13.8	2.8	29.9	83	-	0.0	-78	83	2718
2.7	14.4	2.7	27.5	77	-	0.0	-176	181	2436
2.8	12.8	2.5	27.6	72	-	0.0	-253	251	2090
2.9	12.9	2.6	27.8	67	-	0.0	-326	312	1950
3.0	15.1	2.8	28.3	68	13.0	0.0	-394	364	2091
3.1	15.2	2.7	26.7	66	14.7	0.0	-477	427	2126
3.2	14.2	2.7	25.7	60	12.8	-1.8	-547	474	1855
3.3	14.0	2.6	25.7	59	11.7	-1.8	-610	514	1841
3.4	14.5	2.5	25.1	59	12.6	0.0	-679	555	1903
3.5	14.2	2.2	24.4	55	12.2	0.0	-747	593	1864
3.6	14.2	2.2	23.9	55	12.4	-1.8	-813	628	1797
3.7	14.2	2.1	23.3	51	11.9	-0.9	-877	658	1744
3.8	15.7	2.5	22.7	51	12.3	0.0	-939	686	1836
3.9	14.7	2.6	22.0	49	11.1	-0.9	-1009	719	1946
4.0	13.7	2.3	21.5	48	12.3	0.0	-1085	753	1017
4.1	14.3	2.2	21.2	48	12.4	0.0	-1121	760	1037
4.2	14.7	2.5	20.4	46	12.3	0.0	-1159	767	1080
4.3	15.0	2.7	20.0	45	12.2	0.9	-1199	775	1013
4.4	14.4	2.4	19.6	43	11.3	0.0	-1232	778	864
4.5	13.8	2.8	19.0	42	10.9	0.0	-1261	779	721
4.6	15.0	2.9	18.4	41	11.9	0.0	-1284	776	719
4.7	14.9	2.5	18.2	41	12.1	0.9	-1313	776	786
4.8	14.5	3.0	17.7	40	11.9	0.9	-1341	776	637
4.9	14.9	3.9	17.1	39	12.1	0.9	-1359	770	699
5.0	15.3	4.2	16.7	39	11.9	0.0	-1391	773	847
5.1	15.0	3.8	16.4	38	12.1	0.0	-1420	773	775
5.2	14.2	4.1	15.9	37	11.2	0.0	-1447	773	670
5.3	14.8	5.3	15.6	37	12.1	0.0	-1468	770	665
5.4	14.9	5.0	15.1	35	11.1	0.0	-1495	769	695
5.5	15.0	4.3	15.2	37	10.7	0.9	-1518	767	869
5.6	14.8	5.5	14.7	34	10.9	0.0	-1558	773	813
5.7	14.0	4.9	14.5	33	10.0	0.0	-1577	768	497
5.8	14.4	5.0	14.1	33	11.0	0.0	-1593	763	458
5.9	16.3	5.1	14.1	32	11.5	0.0	-1556	732	779
6.0	16.2	5.2	13.8	32	9.8	0.0	-1584	733	753
6.1	16.3	6.3	13.4	32	10.6	0.0	-1610	733	644
6.2	15.8	7.9	13.3	31	9.9	0.0	-1630	730	597
6.3	16.0	2.6	13.2	31	10.5	0.0	-1653	729	734
6.4	15.8	8.2	12.8	31	10.5	0.0	-1683	730	738
6.5	15.0	3.4	12.5	30	10.6	0.0	-1706	729	584
6.6	14.8	3.0	12.3	29	10.8	0.0	-1725	726	527
6.7	15.2	4.1	12.2	29	11.3	0.0	-1744	723	733
6.8	14.3	3.2	12.0	28	11.0	0.9	-1778	726	698
6.9	13.4	4.3	11.8	27	11.5	0.0	-1794	722	363
7.0	13.7	4.4	11.7	27	11.1	0.0	-1804	716	481
7.1	14.7	3.8	11.8	27	11.4	0.9	-1829	716	756
7.2	13.5	4.2	11.3	26	10.8	0.9	-1858	717	614
7.3	12.3	5.2	11.3	26	10.9	0.0	-1873	713	352
7.4	12.6	5.6	11.1	26	10.2	0.0	-1884	707	491
7.5	13.5	3.0	10.9	25	10.0	0.0	-1908	707	691
7.6	13.4	5.8	10.8	24	9.9	0.0	-1934	707	498
7.7	12.8	3.5	10.7	25	11.7	0.9	-1944	701	308
7.8	13.8	4.6	10.5	25	10.5	0.0	-1956	696	532
7.9	14.1	3.2	10.5	24	11.0	0.0	-1983	697	716
8.0	14.3	3.5	10.4	23	10.1	0.0	-2007	697	693
8.1	14.3	4.2	10.2	23	10.2	0.0	-2033	697	711
8.2	14.4	3.7	10.3	23	11.9	0.0	-2058	697	718

Table A.15 Column $k = 7$, horizontally polarized.

f_{in}	$A_{k,max}$	$\Delta A_{k,\phi}$			SLL_θ			$\tau_{\psi,k}$	$\tau_{g,k}$
GHz	dBi	dB	$\text{HPBW}_\theta{}^\circ$	$\text{FNBW}_\theta{}^\circ$	dB	${\xi_\theta}^\circ$	${\psi_k}^\circ$	ps	ps
2.6	14.1	2.9	30.9	77	-	0.9	-49	53	2653
2.7	15.4	3.4	30.4	76	-	0.0	-145	149	2422
2.8	14.4	3.6	27.9	69	-	0.0	-224	222	2168
2.9	14.6	3.9	27.5	70	-	0.0	-301	288	2100
3.0	16.3	3.8	26.7	67	14.1	1.8	-375	347	2192
3.1	15.5	3.1	25.9	66	13.0	1.8	-459	411	2188
3.2	14.8	2.2	24.9	63	12.6	0.0	-532	462	1906
3.3	15.1	2.8	24.2	61	13.0	0.0	-596	502	1779
3.4	15.8	3.7	23.5	59	12.9	0.0	-660	539	1848
3.5	15.8	3.5	23.1	57	13.6	0.0	-729	578	1855
3.6	15.9	3.5	22.2	53	12.0	0.9	-794	613	1799
3.7	15.5	4.7	22.1	54	12.3	0.9	-858	644	1751
3.8	16.5	4.3	21.3	53	11.9	0.0	-920	672	1828
3.9	15.6	3.8	20.6	50	12.4	-0.9	-990	705	1947
4.0	15.6	3.5	20.5	50	12.4	0.0	-1053	731	956
4.1	16.2	3.9	20.0	49	10.9	0.9	-1088	737	1035
4.2	16.2	3.5	19.5	46	11.8	0.9	-1128	746	1044
4.3	16.1	3.1	19.3	46	12.8	0.9	-1163	751	978
4.4	15.3	2.7	19.0	44	11.4	0.9	-1198	756	842
4.5	14.5	2.8	18.5	43	11.5	0.9	-1223	755	701
4.6	15.3	2.5	18.4	42	12.7	0.9	-1249	754	793
4.7	15.8	3.2	17.9	41	11.7	0.9	-1281	757	864
4.8	15.1	3.4	17.5	40	11.2	0.9	-1311	759	755
4.9	15.4	2.8	17.1	40	11.7	0.0	-1335	757	699
5.0	15.0	2.9	17.0	40	11.5	0.9	-1361	756	765
5.1	15.1	3.2	16.4	38	11.3	0.9	-1390	757	752
5.2	14.7	3.4	15.9	36	10.6	0.9	-1415	756	630
5.3	14.5	3.4	15.8	36	11.2	0.9	-1435	752	577
5.4	14.6	3.4	15.7	35	11.1	0.9	-1457	749	583
5.5	15.4	3.1	15.5	35	10.7	0.9	-1477	746	804
5.6	15.6	4.0	15.2	34	11.1	0.0	-1515	751	781
5.7	14.6	2.9	14.8	33	11.1	0.9	-1534	747	471
5.8	14.6	3.8	14.5	32	11.4	0.0	-1549	742	419
5.9	14.9	3.2	14.4	32	11.9	0.0	-1507	710	780
6.0	15.5	2.3	13.8	32	10.6	0.9	-1535	711	760
6.1	15.2	3.2	13.8	32	11.6	0.0	-1562	711	687
6.2	15.6	4.1	13.4	31	11.5	0.0	-1585	710	611
6.3	15.1	4.0	13.3	31	11.3	0.0	-1606	708	686
6.4	15.0	4.5	12.9	30	11.1	0.9	-1634	709	722
6.5	15.1	3.9	12.6	29	10.8	0.0	-1658	708	622
6.6	14.6	3.1	12.4	29	11.4	0.9	-1679	707	637
6.7	14.9	3.2	12.3	29	11.3	0.9	-1704	706	736
6.8	14.4	3.9	12.2	29	11.0	0.9	-1732	707	668
6.9	13.1	4.1	11.9	27	10.4	0.0	-1752	705	482
7.0	13.7	3.6	11.7	28	11.4	0.9	-1767	701	543
7.1	14.7	4.7	11.6	27	12.0	0.9	-1791	701	674
7.2	14.0	3.1	11.5	27	11.1	0.9	-1815	700	565
7.3	12.6	3.3	11.4	26	10.8	0.9	-1832	697	327
7.4	12.4	5.9	11.1	26	10.9	0.9	-1839	690	354
7.5	13.4	5.6	11.0	25	10.6	0.9	-1857	688	672
7.6	12.9	5.3	10.9	24	10.0	0.9	-1887	690	506
7.7	11.8	4.3	10.8	24	11.0	0.9	-1894	683	265
7.8	12.8	6.0	10.8	24	11.6	0.9	-1906	679	491
7.9	13.0	6.4	10.5	24	10.6	0.9	-1929	678	769
8.0	13.8	6.1	10.4	23	11.4	0.0	-1962	681	672
8.1	12.7	5.3	10.5	24	11.7	0.0	-1977	678	494
8.2	13.0	4.2	10.3	23	10.7	0.0	-1997	677	553

Table A.16 Column $k = 7$, vertically polarized.

f_{in}	$A_{k,max}$	$\Delta A_{k,\phi}$			SLL_θ			$\tau_{\psi,k}$	$\tau_{g,k}$
GHz	dBi	dB	$\text{HPBW}_\theta{}^\circ$	$\text{FNBW}_\theta{}^\circ$	dB	$\xi_\theta{}^\circ$	$\psi_k{}^\circ$	ps	ps
2.6	12.7	2.7	29.9	86	-	-0.9	-69	74	2614
2.7	13.8	2.5	27.5	75	-	0.0	-164	168	2426
2.8	12.5	2.4	27.5	74	-	0.0	-244	242	2088
2.9	10.7	2.5	25.6	60	-	0.0	-314	301	1845
3.0	14.3	2.9	28.3	66	11.1	-0.9	-377	349	2080
3.1	15.0	2.9	27.0	67	13.9	0.0	-464	415	2259
3.2	13.9	2.4	26.2	62	13.0	-0.9	-540	468	1976
3.3	13.6	2.3	24.9	57	10.2	1.8	-606	510	1868
3.4	13.8	2.4	24.9	58	12.3	-0.9	-674	551	1902
3.5	13.4	2.0	23.9	53	11.4	0.0	-743	590	1789
3.6	13.5	2.2	23.5	52	11.4	0.9	-803	620	1750
3.7	13.9	2.1	23.2	52	12.6	0.0	-869	652	1820
3.8	15.1	2.3	22.4	50	11.2	0.0	-934	683	1870
3.9	13.5	2.8	21.6	47	11.3	0.0	-1004	715	1932
4.0	13.1	2.3	21.1	47	10.0	0.0	-1072	745	991
4.1	14.3	2.5	20.6	45	12.1	0.9	-1108	751	1048
4.2	14.3	2.6	20.3	45	13.6	0.0	-1148	759	1081
4.3	13.9	2.4	19.2	42	10.2	0.9	-1186	766	977
4.4	13.7	2.2	19.4	42	11.3	0.0	-1218	769	827
4.5	13.8	2.8	19.1	42	11.8	0.0	-1245	769	788
4.6	14.3	2.9	18.0	39	10.2	0.9	-1275	770	758
4.7	13.8	2.5	17.8	40	11.6	0.0	-1300	768	673
4.8	13.5	3.0	17.4	39	11.5	0.0	-1323	766	684
4.9	15.1	3.7	16.9	39	12.9	0.0	-1349	765	861
5.0	14.5	4.2	16.7	38	10.4	0.9	-1385	769	834
5.1	13.8	3.9	16.0	37	11.0	0.0	-1409	767	649
5.2	13.4	4.4	15.6	36	10.9	0.0	-1432	765	621
5.3	14.7	5.8	15.2	35	10.5	0.0	-1454	762	717
5.4	14.4	5.4	15.1	35	10.3	0.0	-1483	763	684
5.5	14.1	4.4	15.0	35	9.7	0.0	-1503	759	777
5.6	14.5	5.2	14.3	33	10.7	-0.9	-1539	764	817
5.7	13.5	4.8	14.1	32	10.5	-0.9	-1562	761	503
5.8	13.8	5.2	13.7	32	10.2	0.0	-1576	755	384
5.9	15.7	5.4	13.8	32	10.2	0.0	-1539	724	763
6.0	15.8	6.7	13.4	31	11.0	0.0	-1566	725	717
6.1	15.9	7.4	13.2	31	10.8	0.0	-1590	724	607
6.2	15.2	3.2	12.9	30	9.8	0.0	-1610	721	631
6.3	15.1	2.5	12.8	30	10.5	0.0	-1636	721	770
6.4	14.8	3.4	12.4	29	10.5	0.0	-1665	723	706
6.5	14.7	4.6	12.2	28	9.9	0.0	-1687	721	570
6.6	14.4	3.9	12.2	29	10.3	0.0	-1706	718	593
6.7	14.7	2.9	12.1	28	9.9	0.0	-1729	717	718
6.8	13.9	2.6	11.9	27	11.2	0.0	-1758	718	666
6.9	13.1	4.4	11.8	27	11.0	0.0	-1777	716	478
7.0	13.5	4.4	11.4	26	10.4	0.0	-1793	711	549
7.1	14.4	3.9	11.6	27	10.2	0.0	-1817	711	663
7.2	13.1	3.7	11.1	25	10.2	0.0	-1840	710	566
7.3	12.6	6.0	11.1	26	11.0	0.0	-1858	707	330
7.4	12.3	5.0	10.8	25	10.7	0.0	-1864	700	437
7.5	13.3	3.5	10.6	24	10.6	0.0	-1889	700	633
7.6	12.7	3.2	10.6	24	10.3	0.0	-1910	698	551
7.7	12.9	4.1	10.6	25	11.3	0.0	-1929	696	459
7.8	12.9	4.1	10.4	24	10.4	0.0	-1943	692	581
7.9	13.5	2.9	10.2	23	10.9	0.0	-1971	693	638
8.0	13.4	3.6	10.0	23	10.6	0.0	-1989	690	573
8.1	13.6	5.3	10.1	23	10.2	-0.9	-2012	690	663
8.2	13.6	3.8	10.0	23	10.8	0.0	-2036	690	678

Table A.17 Column $k = 8$, horizontally polarized.

f_{in}	$A_{k,max}$	$\Delta A_{k,\phi}$			SLL_θ			$\tau_{\psi,k}$	$\tau_{g,k}$
GHz	dBi	dB	$\text{HPBW}_\theta{}^\circ$	$\text{FNBW}_\theta{}^\circ$	dB	${\xi_\theta}^\circ$	${\psi_k}^\circ$	ps	ps
2.6	14.3	3.5	30.9	77	-	0.0	-46	49	2706
2.7	15.6	3.4	30.1	76	-	0.0	-143	148	2444
2.8	14.2	3.4	27.9	69	-	0.0	-222	220	2215
2.9	14.6	3.7	27.0	71	-	-1.8	-303	290	2156
3.0	16.4	3.3	26.4	67	15.1	0.9	-377	349	2254
3.1	15.7	2.7	26.2	67	13.9	1.8	-465	417	2228
3.2	14.7	2.4	25.2	65	13.2	0.9	-538	467	1931
3.3	15.1	3.3	24.4	60	13.4	0.0	-604	509	1815
3.4	15.9	3.2	23.3	59	12.9	0.9	-668	546	1792
3.5	15.7	3.5	23.2	57	13.6	0.9	-733	582	1714
3.6	15.7	4.0	22.1	54	12.9	0.0	-792	611	1694
3.7	15.8	4.9	22.0	54	13.3	0.0	-855	642	1707
3.8	15.9	3.2	21.6	54	13.9	0.9	-915	669	1783
3.9	15.2	2.7	20.7	49	12.5	0.0	-984	701	1916
4.0	15.2	2.8	20.3	49	13.0	0.9	-1047	727	1082
4.1	15.8	3.9	20.1	48	12.8	0.9	-1086	736	1107
4.2	15.6	3.4	19.7	47	11.6	0.9	-1127	745	1090
4.3	15.8	3.1	19.0	45	12.1	0.9	-1165	752	1044
4.4	14.9	2.7	19.0	44	11.7	0.0	-1202	759	909
4.5	13.6	2.7	18.2	41	11.3	0.0	-1230	759	664
4.6	15.2	2.1	18.1	41	10.7	0.0	-1250	755	703
4.7	15.3	2.5	17.6	41	12.8	0.9	-1281	757	789
4.8	14.9	2.5	17.4	41	11.4	0.9	-1307	756	656
4.9	15.5	2.9	17.0	40	11.3	0.9	-1328	753	737
5.0	15.6	3.6	16.7	39	11.6	0.0	-1360	756	831
5.1	15.2	3.4	16.5	37	11.5	0.0	-1388	756	684
5.2	14.5	3.1	16.0	36	10.4	0.9	-1409	753	501
5.3	14.9	3.6	15.7	35	10.8	0.9	-1424	746	550
5.4	14.5	2.5	15.5	34	10.3	0.9	-1449	745	679
5.5	15.6	2.8	15.3	34	11.4	0.0	-1473	744	850
5.6	15.9	3.3	15.1	34	11.2	0.0	-1510	749	822
5.7	14.9	2.9	14.7	33	11.5	0.9	-1532	747	572
5.8	14.8	4.2	14.4	32	11.5	0.0	-1551	743	530
5.9	16.3	3.6	14.2	32	11.1	0.0	-1512	712	918
6.0	16.8	3.5	13.7	32	10.9	0.0	-1545	715	849
6.1	16.6	3.1	13.7	32	11.8	0.0	-1573	716	685
6.2	16.1	3.0	13.3	31	11.0	0.0	-1594	714	599
6.3	16.2	3.7	13.2	31	11.4	0.0	-1616	712	679
6.4	16.0	3.6	12.8	30	11.8	0.0	-1643	713	595
6.5	15.6	2.9	12.6	29	11.4	0.0	-1659	709	481
6.6	15.9	3.8	12.3	29	11.1	0.0	-1678	706	584
6.7	16.1	4.1	12.2	29	11.2	0.9	-1701	705	748
6.8	15.2	4.0	12.1	28	10.6	0.9	-1731	707	636
6.9	14.1	4.4	11.8	27	10.5	0.0	-1746	703	373
7.0	14.9	4.1	11.7	27	12.1	0.0	-1758	698	499
7.1	15.6	4.7	11.6	26	12.2	0.0	-1782	697	715
7.2	14.8	4.0	11.4	26	11.5	0.0	-1810	698	639
7.3	14.1	4.0	11.4	26	12.6	0.0	-1828	696	403
7.4	13.9	4.8	11.1	25	11.1	0.0	-1839	690	480
7.5	15.3	6.2	10.9	24	10.6	0.0	-1863	690	717
7.6	14.3	6.1	10.9	24	10.7	0.0	-1890	691	565
7.7	13.5	5.1	10.8	25	11.5	0.0	-1904	687	281
7.8	13.6	5.9	10.7	24	11.8	0.0	-1910	680	501
7.9	14.8	8.4	10.4	23	11.0	0.0	-1940	682	756
8.0	15.0	6.3	10.4	23	11.6	0.0	-1965	682	663
8.1	14.2	7.0	10.3	23	12.1	0.0	-1987	682	593
8.2	14.5	3.8	10.4	23	11.8	0.0	-2008	680	561

Table A.18 Column $k = 8$, vertically polarized.

f_{in}	$A_{k,max}$	$\Delta A_{k,\phi}$			SLL_θ			$\tau_{\psi,k}$	$\tau_{g,k}$
GHz	dBi	dB	$\text{HPBW}_\theta{}^\circ$	$\text{FNBW}_\theta{}^\circ$	dB	$\xi_\theta{}^\circ$	$\psi_k{}^\circ$	ps	ps
2.6	13.1	2.7	30.4	80	-	-0.9	-71	76	2480
2.7	14.0	2.5	28.1	78	-	-0.9	-160	165	2365
2.8	12.8	2.2	27.8	73	-	0.0	-241	239	2115
2.9	12.4	2.1	27.8	69	-	0.0	-313	299	1909
3.0	14.3	2.5	28.6	68	14.2	0.0	-379	351	2088
3.1	14.9	2.3	26.6	66	14.0	-1.8	-463	415	2229
3.2	14.3	2.5	26.4	64	13.4	-0.9	-539	468	1990
3.3	14.3	2.4	25.7	60	13.0	-0.9	-606	510	1910
3.4	14.8	2.4	24.8	57	12.6	-1.8	-677	553	1990
3.5	14.5	2.2	24.7	57	12.1	-0.9	-749	595	1839
3.6	14.0	2.2	24.0	55	11.6	-3.6	-809	624	1731
3.7	14.3	2.3	23.0	51	11.9	-1.8	-874	656	1778
3.8	15.4	2.5	22.8	51	12.5	-0.9	-937	685	1798
3.9	14.5	2.8	21.9	48	11.2	-1.8	-1003	715	1841
4.0	14.2	2.5	21.7	48	11.5	-1.8	-1073	745	978
4.1	14.8	2.4	21.3	48	12.6	0.0	-1108	751	1002
4.2	14.3	2.3	20.4	44	12.6	0.0	-1145	757	982
4.3	14.5	2.3	20.1	45	11.9	-0.9	-1179	761	975
4.4	14.8	2.2	19.7	42	12.3	-0.9	-1215	767	955
4.5	14.1	2.9	19.0	41	10.6	-1.8	-1247	770	806
4.6	15.0	3.4	18.8	41	12.0	-0.9	-1273	769	752
4.7	15.5	3.0	18.3	41	11.8	-0.9	-1301	769	816
4.8	14.9	2.8	17.8	40	12.6	0.0	-1332	771	799
4.9	15.0	3.3	17.2	40	13.5	-0.9	-1359	770	769
5.0	15.0	4.6	16.8	38	11.1	-0.9	-1387	771	804
5.1	14.9	4.0	16.5	38	12.3	-1.8	-1417	772	779
5.2	14.4	4.4	15.9	37	11.0	-0.9	-1443	771	568
5.3	14.8	4.5	15.7	37	11.3	-0.9	-1458	764	514
5.4	14.6	4.2	15.2	35	10.9	-0.9	-1480	761	657
5.5	15.3	4.5	15.1	34	10.9	0.0	-1505	760	779
5.6	15.2	5.0	15.0	35	12.6	-0.9	-1536	762	709
5.7	14.3	6.5	14.5	33	10.9	-0.9	-1556	758	554
5.8	14.5	6.2	14.0	33	10.8	-0.9	-1576	755	559
5.9	15.9	5.1	14.2	33	11.4	-0.9	-1540	725	749
6.0	16.0	5.7	13.8	32	10.0	-0.9	-1567	725	802
6.1	16.3	3.0	13.6	32	10.8	-0.9	-1597	727	769
6.2	16.0	3.7	13.4	31	11.6	-0.9	-1622	727	647
6.3	15.8	2.7	13.0	31	10.5	-0.9	-1644	725	669
6.4	15.5	3.1	13.0	31	10.7	-0.9	-1670	725	671
6.5	15.0	2.9	12.9	30	11.1	-0.9	-1692	723	581
6.6	15.2	4.3	12.3	28	10.7	-0.9	-1712	721	530
6.7	15.3	3.8	12.4	30	11.1	-0.9	-1730	717	671
6.8	14.8	4.0	12.2	28	10.6	-0.9	-1760	719	683
6.9	13.6	4.7	11.9	27	10.2	-0.9	-1780	716	425
7.0	14.1	5.4	11.8	28	10.6	-1.8	-1791	711	484
7.1	14.7	4.4	11.7	27	12.2	-0.9	-1814	710	681
7.2	14.2	4.5	11.4	27	10.3	-1.8	-1840	710	612
7.3	13.8	3.4	11.2	27	12.2	-0.9	-1858	707	434
7.4	13.3	3.9	10.9	25	9.5	-1.8	-1871	702	473
7.5	14.1	3.8	10.8	25	10.1	-0.9	-1893	701	670
7.6	14.0	4.4	10.9	25	10.0	-0.9	-1919	701	572
7.7	13.6	5.1	10.6	25	11.4	-0.9	-1934	698	389
7.8	13.6	4.7	10.5	24	9.8	-0.9	-1947	693	516
7.9	14.2	4.0	10.4	24	10.7	-0.9	-1971	693	676
8.0	14.7	4.7	10.3	24	10.2	-0.9	-1996	693	662
8.1	14.5	3.6	10.2	23	9.6	-1.8	-2019	692	679
8.2	14.1	3.0	10.1	23	12.5	-0.9	-2045	693	732

Table A.19 Column $k = 9$, horizontally polarized.

f_{in}	$A_{k,max}$	$\Delta A_{k,\phi}$			SLL_θ			$\tau_{\psi,k}$	$\tau_{g,k}$
GHz	dBi	dB	$\text{HPBW}_\theta{}^\circ$	$\text{FNBW}_\theta{}^\circ$	dB	$\xi_\theta{}^\circ$	$\psi_k{}^\circ$	ps	ps
2.6	14.2	3.6	30.8	83	-	0.0	-67	71	2633
2.7	14.9	2.9	31.2	80	-	-0.9	-162	166	2446
2.8	14.0	3.4	28.4	72	-	0.0	-243	241	2232
2.9	13.3	3.2	27.8	71	-	-1.8	-322	309	2086
3.0	15.2	3.2	26.9	69	15.9	-1.8	-393	364	2142
3.1	15.2	2.6	26.3	68	13.7	-2.7	-477	427	2224
3.2	14.9	2.6	25.8	65	15.1	0.0	-553	480	2036
3.3	14.6	2.5	25.2	64	15.3	0.0	-623	525	1873
3.4	15.3	2.8	23.8	60	12.9	-0.9	-688	562	1819
3.5	15.6	3.1	23.7	59	14.4	0.0	-754	598	1720
3.6	15.0	3.9	23.1	59	15.1	0.0	-812	626	1620
3.7	15.5	4.2	22.7	58	14.5	-0.9	-871	654	1650
3.8	16.1	2.7	22.0	56	14.1	-0.9	-931	680	1843
3.9	15.5	2.6	21.0	50	13.9	-0.9	-1003	715	2019
4.0	14.5	2.6	21.0	52	14.4	0.0	-1069	743	1044
4.1	15.7	4.0	20.9	50	13.9	0.0	-1107	750	1115
4.2	16.0	3.4	20.4	49	13.4	0.0	-1150	760	1146
4.3	15.6	2.8	19.4	46	12.3	0.9	-1189	768	1058
4.4	14.8	3.0	19.1	45	11.9	0.0	-1226	774	901
4.5	13.6	2.2	18.4	43	11.9	0.0	-1254	774	729
4.6	15.0	2.1	18.8	44	12.9	0.0	-1278	772	730
4.7	15.2	2.5	17.7	41	11.9	0.0	-1307	772	762
4.8	15.0	2.7	17.7	41	12.0	0.0	-1333	772	699
4.9	15.4	3.2	17.4	41	12.4	0.0	-1357	769	742
5.0	15.1	3.7	16.9	40	12.0	0.0	-1387	770	757
5.1	15.0	3.3	16.8	39	12.1	0.0	-1412	769	719
5.2	14.8	4.4	16.4	38	12.0	0.0	-1438	768	535
5.3	14.5	4.0	15.8	36	11.5	0.0	-1450	760	553
5.4	14.2	2.8	15.8	36	12.0	0.9	-1478	760	649
5.5	15.3	2.6	15.6	35	10.9	0.0	-1497	756	815
5.6	15.5	3.1	15.3	35	12.1	0.0	-1537	762	871
5.7	14.7	3.3	14.9	34	11.7	0.0	-1560	760	591
5.8	14.6	3.9	14.7	33	12.3	0.0	-1579	756	542
5.9	14.7	3.4	14.7	33	12.3	0.0	-1543	727	766
6.0	14.7	3.0	14.2	32	12.1	0.0	-1571	727	821
6.1	14.7	2.6	14.1	32	11.2	0.0	-1602	730	720
6.2	14.7	3.3	13.4	30	10.3	0.0	-1623	727	626
6.3	14.8	3.8	13.5	31	12.0	-0.9	-1647	726	692
6.4	14.3	3.3	13.2	31	12.6	0.0	-1673	726	630
6.5	14.0	3.5	12.8	31	12.2	0.0	-1693	723	505
6.6	14.2	3.9	12.2	29	11.4	0.0	-1709	719	555
6.7	14.6	3.5	12.6	30	12.8	0.0	-1733	718	718
6.8	13.7	3.3	12.2	29	11.6	0.0	-1761	719	614
6.9	12.6	3.5	11.9	27	10.5	0.9	-1777	715	403
7.0	13.2	3.6	11.8	28	12.9	0.0	-1790	710	583
7.1	13.9	4.1	11.7	27	12.4	0.0	-1819	712	785
7.2	13.1	4.9	11.4	26	11.0	0.0	-1846	712	640
7.3	11.9	3.9	11.5	26	12.3	-0.9	-1865	710	380
7.4	12.3	6.3	11.3	27	12.0	0.0	-1873	703	460
7.5	12.6	6.9	11.2	25	12.1	0.0	-1898	703	738
7.6	12.5	6.1	11.1	26	11.9	0.0	-1927	704	533
7.7	11.4	6.0	10.9	25	12.0	0.0	-1937	699	409
7.8	11.7	6.3	10.9	25	12.2	0.0	-1956	697	544
7.9	12.7	4.0	10.9	25	12.6	0.0	-1976	695	660
8.0	13.1	3.5	10.8	25	13.5	0.0	-2004	696	586
8.1	12.3	3.6	10.7	25	11.7	0.9	-2018	692	451
8.2	12.7	4.2	10.5	24	11.6	0.0	-2036	690	503

Table A.20 Column $k = 9$, vertically polarized.

f_{in}	$A_{k,max}$	$\Delta A_{k,\phi}$			SLL_θ			$\tau_{\psi,k}$	$\tau_{g,k}$
GHz	dBi	dB	$\text{HPBW}_\theta{}^\circ$	$\text{FNBW}_\theta{}^\circ$	dB	$\xi_\theta{}^\circ$	$\psi_k{}^\circ$	ps	ps
2.6	13.8	2.6	29.8	83	-	0.9	-76	81	2414
2.7	13.8	2.5	28.4	76	-	0.0	-163	168	2293
2.8	12.9	2.3	27.3	71	-	0.0	-241	239	2130
2.9	13.1	2.3	27.2	69	-	0.0	-316	303	2031
3.0	13.9	2.2	28.0	66	13.6	0.0	-387	359	2134
3.1	14.5	2.4	26.8	66	13.9	0.0	-470	421	2149
3.2	13.9	2.6	25.5	59	11.5	-0.9	-542	471	1933
3.3	14.0	2.3	25.3	59	12.8	0.0	-609	513	1899
3.4	14.6	2.3	24.7	57	12.9	0.0	-679	555	1961
3.5	14.6	2.3	24.1	54	11.8	0.0	-750	596	1948
3.6	13.7	1.9	23.8	54	12.8	0.9	-819	632	1801
3.7	13.9	2.1	23.3	53	13.2	0.0	-880	661	1650
3.8	15.4	2.3	22.6	50	12.3	0.9	-938	686	1758
3.9	15.4	2.7	22.4	50	13.0	0.0	-1007	717	1908
4.0	14.4	2.4	21.5	47	12.4	0.0	-1080	750	870
4.1	14.0	2.3	20.6	44	11.1	0.0	-1112	753	909
4.2	15.0	2.2	20.7	47	13.0	0.9	-1146	758	1023
4.3	15.0	2.3	19.8	44	11.5	0.9	-1185	766	1060
4.4	14.5	2.3	19.6	42	12.0	0.0	-1222	772	909
4.5	13.7	2.6	19.3	42	11.7	0.0	-1251	772	713
4.6	15.1	3.1	18.7	41	12.1	0.0	-1273	769	785
4.7	15.3	3.4	18.0	41	11.7	0.0	-1307	773	890
4.8	14.8	2.7	17.6	41	12.0	0.9	-1338	774	794
4.9	15.3	3.2	17.3	40	12.8	-0.9	-1364	773	781
5.0	15.4	4.3	16.7	37	11.0	0.0	-1394	774	805
5.1	14.9	3.7	16.4	37	11.3	0.0	-1422	775	744
5.2	14.5	4.2	16.1	37	12.0	0.0	-1447	773	557
5.3	15.4	4.6	15.3	34	10.6	-0.9	-1462	767	560
5.4	15.1	3.9	15.3	36	12.0	0.0	-1488	765	613
5.5	14.5	3.6	15.0	35	9.0	0.0	-1507	761	719
5.6	15.5	5.5	14.3	32	10.5	0.0	-1539	764	751
5.7	15.0	6.4	14.5	33	11.0	0.0	-1561	761	601
5.8	14.7	5.4	14.2	33	12.0	0.0	-1583	758	609
5.9	16.2	4.8	13.8	32	10.0	0.0	-1546	728	813
6.0	15.9	5.6	13.7	31	10.1	0.0	-1576	729	835
6.1	15.9	2.4	13.6	32	10.9	0.0	-1606	732	753
6.2	15.4	3.3	13.1	31	9.8	0.0	-1630	730	656
6.3	15.8	2.7	13.1	31	10.9	0.0	-1654	729	693
6.4	15.0	2.9	12.9	31	11.1	0.0	-1680	729	617
6.5	14.2	3.0	12.6	29	9.2	0.0	-1698	726	514
6.6	14.7	4.1	12.1	28	10.7	0.0	-1717	723	567
6.7	15.1	3.9	12.5	30	11.3	0.0	-1739	721	711
6.8	13.7	4.4	12.7	41	10.3	0.0	-1768	722	645
6.9	12.9	5.0	11.2	25	9.4	0.0	-1785	719	387
7.0	13.6	5.7	11.7	28	11.2	0.0	-1796	713	491
7.1	14.5	4.4	11.4	27	11.2	0.0	-1821	712	702
7.2	13.4	4.9	11.3	37	8.9	0.9	-1846	712	616
7.3	12.6	3.3	10.9	25	10.1	0.0	-1865	710	419
7.4	12.6	4.6	10.7	25	11.4	0.0	-1876	704	464
7.5	12.9	4.0	11.1	26	10.2	0.0	-1899	703	650
7.6	13.6	4.8	10.7	24	9.9	0.0	-1923	703	555
7.7	12.9	5.6	10.3	23	10.5	0.0	-1939	699	394
7.8	12.8	4.8	10.7	24	12.4	0.9	-1952	695	507
7.9	14.0	4.6	10.4	24	10.7	0.0	-1975	694	689
8.0	14.4	5.2	10.3	24	11.4	0.0	-2001	695	704
8.1	13.7	3.6	10.5	24	12.3	0.0	-2026	695	684
8.2	12.9	3.0	10.1	23	11.2	0.0	-2050	695	690

Table A.21 Column $k = 10$, horizontally polarized.

f_{in}	$A_{k,max}$	$\Delta A_{k,\phi}$			SLL_θ			$\tau_{\psi,k}$	$\tau_{g,k}$
GHz	dBi	dB	$\text{HPBW}_\theta{}^\circ$	$\text{FNBW}_\theta{}^\circ$	dB	$\xi_\theta{}^\circ$	$\psi_k{}^\circ$	ps	ps
2.6	14.0	3.2	31.8	77	-	0.0	-66	71	2667
2.7	15.2	3.1	31.2	77	-	0.0	-162	167	2450
2.8	14.6	3.6	27.9	68	-	-0.9	-242	241	2176
2.9	13.9	3.2	28.3	72	-	0.0	-319	305	2108
3.0	15.5	3.0	26.9	68	14.7	-0.9	-394	365	2196
3.1	15.3	3.6	26.5	67	12.0	-2.7	-477	427	2183
3.2	14.6	2.7	25.0	63	13.7	-0.9	-551	479	1958
3.3	14.4	2.7	25.0	63	13.2	-0.9	-618	520	1831
3.4	15.1	3.3	24.1	60	12.7	-0.9	-683	558	1889
3.5	15.4	3.3	24.0	59	12.8	0.0	-754	598	1787
3.6	15.3	3.7	22.5	55	12.5	-0.9	-812	626	1683
3.7	15.2	3.6	23.0	57	13.0	-0.9	-875	657	1712
3.8	16.3	4.2	21.4	51	11.9	-0.9	-935	684	1817
3.9	15.6	4.5	21.6	54	12.0	-0.9	-1006	716	1961
4.0	15.4	3.3	20.3	48	11.9	-0.9	-1073	745	1064
4.1	15.6	3.7	20.7	50	12.7	-0.9	-1112	753	1034
4.2	15.6	3.4	20.3	49	11.7	-0.9	-1148	759	1003
4.3	15.3	3.1	19.8	50	10.7	-1.8	-1184	765	1011
4.4	14.8	3.3	18.9	44	10.0	-0.9	-1220	770	896
4.5	13.5	2.9	19.3	45	10.9	-0.9	-1248	771	778
4.6	15.2	3.0	18.3	42	10.9	-1.8	-1276	771	809
4.7	14.9	3.2	18.6	46	10.7	-0.9	-1307	772	800
4.8	14.7	2.9	17.3	40	9.9	-0.9	-1334	772	700
4.9	15.2	3.0	17.4	41	10.3	-0.9	-1357	769	738
5.0	14.8	2.7	17.2	41	11.8	-0.9	-1387	771	814
5.1	14.5	2.8	16.6	52	10.0	-0.9	-1416	771	766
5.2	14.0	3.2	16.6	39	10.6	-0.9	-1442	770	649
5.3	14.2	3.5	16.1	38	11.2	-0.9	-1462	766	625
5.4	14.3	3.6	15.9	37	10.6	-0.9	-1487	765	684
5.5	14.6	2.5	15.7	37	10.5	-1.8	-1512	763	759
5.6	14.8	3.5	15.3	35	9.7	-0.9	-1542	765	631
5.7	14.3	3.2	15.2	35	10.5	-0.9	-1557	759	497
5.8	14.3	2.9	15.1	35	10.3	0.0	-1578	756	575
5.9	14.5	3.0	14.9	33	9.9	0.0	-1543	727	779
6.0	14.2	2.6	14.8	39	10.3	0.0	-1572	728	755
6.1	14.4	2.7	14.3	43	11.2	0.0	-1598	728	641
6.2	13.5	2.9	14.5	36	10.2	-0.9	-1618	725	625
6.3	13.8	3.8	14.5	38	10.5	-0.9	-1643	724	718
6.4	13.5	3.0	13.6	41	11.2	-0.9	-1669	725	689
6.5	13.1	3.1	13.6	40	11.0	-0.9	-1692	723	607
6.6	13.6	3.3	12.8	31	10.7	-0.9	-1713	721	627
6.7	14.3	4.1	13.0	38	10.5	-0.9	-1738	720	733
6.8	13.3	4.0	13.3	39	10.9	-1.8	-1766	721	626
6.9	12.1	4.3	12.2	28	10.3	-0.9	-1783	718	491
7.0	12.5	4.7	12.7	32	10.3	-0.9	-1801	715	604
7.1	13.2	4.7	12.4	37	9.1	-0.9	-1826	714	675
7.2	12.5	5.4	11.7	39	9.7	-1.8	-1850	714	625
7.3	11.4	4.2	12.0	36	9.9	-0.9	-1871	712	341
7.4	11.6	4.9	11.7	38	8.9	-1.8	-1874	704	290
7.5	12.3	6.5	11.4	27	8.3	-0.9	-1892	701	699
7.6	12.3	5.4	11.5	28	9.6	-0.9	-1925	703	555
7.7	11.3	5.3	11.3	35	9.2	-0.9	-1932	697	331
7.8	11.5	7.0	11.5	32	8.4	-1.8	-1948	694	508
7.9	12.2	3.7	11.2	33	9.2	-1.8	-1969	692	723
8.0	12.9	5.5	11.1	31	9.0	-0.9	-2000	695	650
8.1	12.3	5.4	11.0	33	9.7	-0.9	-2015	691	506
8.2	12.4	4.0	11.0	32	9.5	0.0	-2037	690	600

Table A.22 Column $k = 10$, vertically polarized.

f_{in}	$A_{k,max}$	$\Delta A_{k,\phi}$			SLL_θ			$\tau_{\psi,k}$	$\tau_{g,k}$
GHz	dBi	dB	$\text{HPBW}_\theta{}^\circ$	$\text{FNBW}_\theta{}^\circ$	dB	$\xi_\theta{}^\circ$	$\psi_k{}^\circ$	ps	ps
2.6	13.0	2.7	29.9	86	-	0.9	-78	84	2495
2.7	13.5	2.4	27.6	83	-	0.0	-168	173	2357
2.8	12.6	2.6	27.2	72	-	0.0	-248	246	2128
2.9	12.3	2.4	27.8	70	-	-0.9	-321	308	1942
3.0	13.7	2.2	27.6	69	13.2	0.0	-388	359	2074
3.1	14.6	2.6	26.3	68	12.5	-2.7	-471	422	2159
3.2	14.1	2.5	25.4	65	12.8	0.0	-543	472	1974
3.3	14.3	2.5	25.1	62	11.4	0.0	-613	516	1942
3.4	14.7	2.5	24.8	59	12.7	0.0	-683	558	1973
3.5	14.4	2.3	24.2	55	11.5	0.0	-755	599	1888
3.6	13.5	2.0	23.8	56	12.0	-1.8	-819	632	1760
3.7	14.0	2.2	23.4	53	11.6	-1.8	-882	662	1730
3.8	15.3	2.2	22.8	52	11.8	-0.9	-944	690	1849
3.9	14.6	2.7	22.4	50	10.8	-0.9	-1015	723	1973
4.0	13.7	2.5	22.0	49	12.6	-0.9	-1084	753	995
4.1	14.4	2.1	21.6	49	13.0	-0.9	-1120	759	1027
4.2	14.4	2.2	21.0	49	11.2	0.0	-1158	766	1058
4.3	14.2	2.5	20.3	46	11.0	-0.9	-1196	773	962
4.4	14.1	2.3	19.9	43	10.6	0.0	-1227	775	845
4.5	13.2	2.6	19.7	43	10.9	-0.9	-1257	776	789
4.6	14.9	3.0	19.1	43	10.5	0.0	-1284	775	824
4.7	14.3	2.7	19.0	43	10.7	0.0	-1316	778	780
4.8	13.8	2.9	17.7	40	10.1	-1.8	-1340	776	706
4.9	14.8	3.8	17.6	41	11.4	0.0	-1367	775	789
5.0	14.5	3.9	17.5	40	11.4	0.0	-1397	776	793
5.1	14.1	3.2	16.9	40	9.9	-0.9	-1424	776	695
5.2	13.8	4.1	16.4	39	10.1	0.0	-1447	773	657
5.3	14.6	4.9	16.2	38	11.0	-0.9	-1471	771	664
5.4	14.2	4.6	16.0	38	10.6	-0.9	-1495	769	728
5.5	14.8	4.5	15.5	37	11.2	-0.9	-1524	770	864
5.6	14.6	4.7	14.8	38	10.0	-0.9	-1557	772	699
5.7	13.4	4.8	15.0	35	10.7	-0.9	-1574	767	473
5.8	13.7	5.1	14.6	35	10.6	0.0	-1591	762	471
5.9	15.5	4.8	14.8	35	11.1	-0.9	-1554	732	862
6.0	15.2	6.0	14.3	34	12.0	0.0	-1585	734	775
6.1	15.2	6.3	14.0	32	11.3	0.0	-1610	733	602
6.2	14.7	3.2	14.4	34	11.4	-0.9	-1629	730	604
6.3	14.7	3.0	14.4	34	11.6	-0.9	-1653	729	761
6.4	14.3	3.5	13.7	33	11.2	-1.8	-1683	731	691
6.5	13.5	4.3	13.8	39	12.1	-0.9	-1703	728	535
6.6	13.7	3.8	12.7	30	10.8	-0.9	-1722	725	587
6.7	14.5	3.1	13.2	32	10.9	-0.9	-1745	724	795
6.8	13.5	2.9	13.0	33	11.0	-0.9	-1779	727	662
6.9	12.3	5.8	11.9	29	10.2	-0.9	-1793	722	417
7.0	12.9	4.4	12.2	30	11.5	-0.9	-1809	718	582
7.1	13.8	3.7	12.3	32	11.0	0.0	-1835	718	721
7.2	13.2	4.2	11.7	28	9.7	-0.9	-1861	718	575
7.3	11.9	6.3	11.4	27	10.1	-0.9	-1876	714	302
7.4	11.8	4.5	11.2	26	9.9	-0.9	-1883	707	372
7.5	12.7	3.1	11.4	27	9.5	-0.9	-1903	705	667
7.6	12.8	3.4	11.4	27	10.5	-0.9	-1931	706	597
7.7	12.4	6.4	11.0	26	9.3	0.0	-1946	702	452
7.8	12.4	4.6	11.1	26	9.7	0.0	-1963	699	535
7.9	13.0	3.1	11.1	27	11.4	-0.9	-1985	698	686
8.0	13.4	3.7	10.8	25	10.2	-0.9	-2013	699	672
8.1	13.6	5.3	10.6	24	9.8	-0.9	-2033	697	636
8.2	12.9	3.5	10.8	25	11.0	-0.9	-2058	697	703

Table A.23 Column $k = 11$, horizontally polarized.

f_{in}	$A_{k,max}$	$\Delta A_{k,\phi}$			SLL_θ			$\tau_{\psi,k}$	$\tau_{g,k}$
GHz	dBi	dB	$\text{HPBW}_\theta{}^\circ$	$\text{FNBW}_\theta{}^\circ$	dB	$\xi_\theta{}^\circ$	$\psi_k{}^\circ$	ps	ps
2.6	14.1	2.8	30.9	77	-	0.9	-63	68	2664
2.7	15.1	3.0	30.2	76	-	0.9	-159	164	2479
2.8	14.3	3.0	28.5	71	-	0.0	-242	240	2181
2.9	14.3	3.5	27.7	70	-	0.0	-316	303	2038
3.0	16.2	4.1	27.1	68	14.3	0.0	-389	360	2099
3.1	15.5	3.6	25.9	66	13.5	0.9	-467	419	2105
3.2	14.6	2.3	24.7	62	13.4	0.9	-540	469	1905
3.3	14.5	2.9	24.3	61	14.2	0.0	-605	509	1841
3.4	15.1	3.2	23.6	59	12.8	0.0	-673	550	1976
3.5	15.2	3.0	23.1	58	13.6	0.0	-747	593	1972
3.6	15.2	3.0	22.8	55	13.2	0.0	-815	629	1812
3.7	15.2	3.9	22.1	54	12.9	-0.9	-877	659	1742
3.8	16.1	3.9	21.6	52	12.0	0.0	-940	687	1798
3.9	15.8	5.2	20.6	50	11.4	0.0	-1007	717	1853
4.0	15.3	3.7	20.7	49	12.7	0.0	-1077	748	902
4.1	15.3	3.5	19.9	48	11.1	0.0	-1110	752	894
4.2	16.0	3.7	19.3	44	10.8	0.0	-1142	755	941
4.3	16.1	3.3	18.7	43	11.5	0.0	-1178	761	967
4.4	15.1	3.2	18.7	42	10.1	0.0	-1212	765	861
4.5	14.1	3.3	17.9	41	9.3	0.0	-1240	765	761
4.6	15.3	3.3	18.3	42	11.9	0.0	-1266	765	847
4.7	15.2	3.4	17.7	41	11.0	0.0	-1301	769	912
4.8	14.8	4.2	17.4	40	11.8	0.0	-1332	771	723
4.9	14.9	3.5	17.1	39	12.1	-0.9	-1353	767	675
5.0	14.7	3.7	16.8	38	12.7	0.0	-1381	767	821
5.1	14.8	3.7	16.4	37	11.1	0.0	-1412	769	806
5.2	13.8	3.2	15.9	36	11.0	0.0	-1439	768	661
5.3	14.2	3.2	15.8	35	10.9	0.0	-1459	765	654
5.4	13.8	2.9	15.6	35	11.2	0.0	-1486	764	650
5.5	14.5	2.6	15.4	34	10.2	-0.9	-1506	761	760
5.6	14.3	2.8	14.9	33	11.5	0.0	-1540	764	670
5.7	13.4	3.4	14.8	34	11.6	0.0	-1554	758	392
5.8	13.6	3.8	14.3	32	11.7	0.0	-1569	751	391
5.9	14.0	3.9	14.3	32	12.4	0.0	-1530	721	823
6.0	13.8	3.5	13.8	32	11.5	0.0	-1560	722	764
6.1	13.8	3.2	13.6	31	11.0	0.9	-1586	722	570
6.2	13.6	2.6	13.3	31	10.8	0.0	-1601	717	628
6.3	13.9	3.2	13.4	31	12.0	0.0	-1631	719	781
6.4	13.6	3.0	12.9	30	11.4	0.0	-1657	719	669
6.5	13.0	2.9	12.5	29	10.7	0.0	-1679	718	589
6.6	13.6	3.9	12.2	29	10.9	0.0	-1700	715	650
6.7	13.6	3.4	12.3	29	12.0	0.0	-1726	715	747
6.8	12.8	2.9	11.8	27	11.1	0.0	-1754	716	626
6.9	12.1	2.9	11.5	26	10.7	0.0	-1771	713	457
7.0	12.4	3.0	11.6	27	11.6	0.0	-1787	709	577
7.1	13.1	4.0	11.5	27	11.8	0.0	-1812	709	675
7.2	12.3	3.9	11.2	26	10.6	0.0	-1835	708	575
7.3	10.8	4.6	11.2	25	11.6	0.0	-1854	705	351
7.4	11.1	6.3	11.1	25	10.8	0.0	-1860	698	374
7.5	11.6	6.0	11.1	25	10.8	0.0	-1881	697	694
7.6	11.7	5.4	10.9	25	11.0	0.0	-1910	698	502
7.7	10.9	5.7	10.7	24	11.8	0.0	-1917	691	341
7.8	11.3	6.8	10.7	24	10.7	0.9	-1935	689	485
7.9	11.8	6.5	10.5	24	10.6	0.0	-1952	686	731
8.0	12.6	6.3	10.4	23	11.3	0.0	-1988	690	693
8.1	12.0	6.9	10.2	23	10.6	0.0	-2002	686	487
8.2	12.0	6.9	10.4	23	10.7	0.0	-2023	685	585

Table A.24 Column $k = 11$, vertically polarized.

f_{in}	$A_{k,max}$	$\Delta A_{k,\phi}$			SLL_θ			$\tau_{\psi,k}$	$\tau_{g,k}$
GHz	dBi	dB	$\text{HPBW}_\theta{}^\circ$	$\text{FNBW}_\theta{}^\circ$	dB	$\xi_\theta{}^\circ$	$\psi_k{}^\circ$	ps	ps
2.6	12.8	2.7	29.1	83	-	0.9	-76	81	2684
2.7	13.9	2.6	27.8	77	-	0.0	-172	177	2467
2.8	12.8	2.6	28.1	72	-	0.0	-253	251	2145
2.9	12.3	2.8	28.3	71	-	0.0	-327	313	1936
3.0	14.2	2.7	28.4	67	13.8	0.0	-393	363	2080
3.1	14.5	2.5	26.9	67	13.9	0.9	-476	427	2153
3.2	13.7	2.3	26.3	63	13.8	-0.9	-548	475	1879
3.3	13.8	2.3	26.0	59	13.8	0.0	-612	515	1855
3.4	14.1	2.4	25.6	59	14.3	0.9	-681	557	1934
3.5	14.1	2.3	24.6	56	12.5	0.0	-751	596	1855
3.6	13.5	2.1	23.9	54	12.7	0.0	-815	629	1783
3.7	13.8	2.1	23.6	53	13.1	0.9	-879	660	1777
3.8	15.0	2.2	22.8	50	12.4	0.0	-943	689	1793
3.9	14.3	2.8	22.0	49	11.9	0.0	-1008	718	1824
4.0	14.3	2.4	21.9	50	13.4	0.0	-1086	754	1179
4.1	15.0	2.5	21.1	47	12.2	0.9	-1129	765	1093
4.2	14.7	2.5	20.5	45	12.6	0.9	-1165	771	1014
4.3	14.9	3.2	19.9	45	12.2	0.0	-1202	776	949
4.4	14.6	2.8	19.6	42	12.1	0.0	-1233	779	851
4.5	13.8	2.9	19.0	41	12.4	0.9	-1263	780	758
4.6	15.2	3.0	18.5	41	12.1	0.0	-1288	778	750
4.7	14.7	2.5	18.1	40	11.8	0.0	-1317	778	759
4.8	14.2	3.6	17.8	40	11.8	0.0	-1343	777	649
4.9	15.2	3.9	17.2	40	12.8	0.0	-1364	773	729
5.0	15.2	3.7	16.6	38	12.0	0.0	-1395	775	830
5.1	14.9	3.8	16.5	38	12.3	0.0	-1424	775	732
5.2	14.3	3.8	15.9	36	11.6	0.9	-1448	773	694
5.3	15.2	5.3	15.6	36	12.2	0.0	-1474	772	744
5.4	14.9	4.3	15.3	36	11.7	0.9	-1501	772	741
5.5	14.9	5.1	15.0	34	11.0	0.9	-1527	771	852
5.6	14.4	5.5	14.8	34	11.2	0.0	-1563	775	764
5.7	14.1	5.9	14.5	33	10.6	0.0	-1582	771	508
5.8	14.5	6.2	14.1	33	11.6	0.0	-1599	766	482
5.9	15.8	4.9	14.0	32	11.5	0.9	-1558	734	780
6.0	15.7	5.8	13.7	32	10.3	0.0	-1586	734	746
6.1	15.5	5.9	13.4	31	11.0	0.0	-1612	734	608
6.2	15.0	7.5	13.2	31	10.8	0.0	-1630	730	584
6.3	15.5	2.8	13.0	31	10.5	0.9	-1654	729	788
6.4	15.1	3.1	12.9	30	11.5	0.0	-1687	732	769
6.5	14.3	4.2	12.4	29	10.0	0.0	-1710	731	551
6.6	14.2	5.5	12.1	29	10.5	0.0	-1727	727	547
6.7	15.0	3.2	12.2	28	10.8	0.0	-1749	725	767
6.8	13.6	3.5	11.9	27	9.7	0.0	-1782	728	641
6.9	12.7	4.0	11.7	27	10.3	0.0	-1795	723	346
7.0	13.3	4.7	11.6	27	10.3	0.0	-1807	717	574
7.1	14.2	4.1	11.6	28	10.9	0.0	-1836	718	759
7.2	12.5	3.7	11.2	25	10.3	0.0	-1861	718	535
7.3	11.6	5.3	11.2	25	10.6	0.0	-1875	713	353
7.4	12.1	5.4	11.0	26	10.3	0.0	-1887	708	563
7.5	13.3	3.2	10.7	24	9.1	0.0	-1915	709	722
7.6	11.8	5.3	10.8	24	9.5	0.0	-1939	709	404
7.7	12.0	3.6	10.8	25	13.0	0.0	-1945	701	273
7.8	12.7	3.8	10.5	24	10.1	0.0	-1959	697	560
7.9	13.2	2.8	10.3	24	9.8	0.0	-1985	698	701
8.0	13.3	3.4	10.3	24	9.8	0.0	-2009	698	678
8.1	13.7	4.4	10.0	23	9.4	0.0	-2034	697	754
8.2	13.8	4.0	10.1	23	11.3	0.0	-2063	699	823

Table A.25 Column $k = 12$, horizontally polarized.

f_{in}	$A_{k,max}$	$\Delta A_{k,\phi}$			SLL_θ			$\tau_{\psi,k}$	$\tau_{g,k}$
GHz	dBi	dB	$\text{HPBW}_\theta{}^\circ$	$\text{FNBW}_\theta{}^\circ$	dB	$\xi_\theta{}^\circ$	$\psi_k{}^\circ$	ps	ps
2.6	14.1	3.2	31.3	80	-	1.8	-72	77	2479
2.7	15.1	3.2	30.2	76	-	0.9	-161	166	2407
2.8	14.0	3.3	28.5	70	-	0.9	-245	243	2209
2.9	14.1	3.5	27.6	68	-	0.9	-320	307	1941
3.0	15.8	3.7	26.6	68	13.1	1.8	-385	357	1940
3.1	15.5	3.1	25.7	64	12.8	1.8	-460	412	2030
3.2	14.6	2.7	24.9	62	13.7	0.9	-531	461	1902
3.3	14.5	3.0	24.3	60	13.4	2.7	-597	502	1885
3.4	15.5	3.0	23.4	59	12.4	0.9	-667	545	2048
3.5	15.9	3.5	22.9	57	13.6	0.9	-744	591	2039
3.6	15.3	3.3	22.1	54	12.7	0.0	-814	628	1870
3.7	15.3	3.8	21.9	53	13.5	0.9	-879	660	1776
3.8	15.9	3.0	21.7	53	13.4	1.8	-942	688	1819
3.9	15.9	4.0	20.6	50	12.6	0.0	-1010	719	1902
4.0	15.5	3.4	20.4	50	12.6	0.9	-1083	752	813
4.1	16.3	4.1	20.5	50	13.3	1.8	-1112	754	876
4.2	15.7	3.8	19.8	47	11.6	0.9	-1146	758	907
4.3	16.1	3.3	19.2	46	12.7	0.9	-1178	761	892
4.4	16.0	4.1	19.0	44	11.3	0.9	-1211	764	873
4.5	15.1	3.5	18.4	43	11.3	1.8	-1241	766	805
4.6	16.2	3.1	18.1	41	11.5	0.9	-1268	766	831
4.7	15.5	2.6	17.8	41	12.3	1.8	-1300	769	862
4.8	15.3	3.3	17.5	40	11.7	0.9	-1331	770	726
4.9	15.7	3.5	17.0	39	12.4	0.9	-1353	767	715
5.0	15.3	3.5	16.7	38	11.9	0.9	-1382	768	812
5.1	15.5	4.2	16.4	37	11.2	0.9	-1411	769	780
5.2	14.6	5.5	16.1	37	11.0	0.9	-1438	768	613
5.3	14.7	4.9	15.7	35	11.2	1.8	-1455	763	575
5.4	15.0	3.4	15.4	34	10.8	0.9	-1480	761	662
5.5	15.5	3.7	15.3	34	11.3	0.9	-1503	759	845
5.6	16.1	3.6	15.0	34	11.8	0.9	-1540	764	767
5.7	14.6	2.4	14.8	33	12.4	1.8	-1558	759	513
5.8	14.7	2.9	14.4	32	11.2	0.9	-1577	755	533
5.9	14.7	2.9	14.2	32	11.4	0.9	-1537	723	891
6.0	14.8	2.7	13.9	32	11.3	0.9	-1569	726	836
6.1	14.9	3.0	13.6	31	10.8	0.9	-1597	727	679
6.2	14.5	3.8	13.2	31	10.6	0.0	-1618	725	621
6.3	14.7	3.8	13.2	30	11.1	0.9	-1642	724	678
6.4	14.7	3.2	12.7	29	11.2	0.0	-1666	723	592
6.5	14.1	2.9	12.5	29	11.5	0.9	-1684	720	515
6.6	14.2	3.6	12.5	29	11.9	0.9	-1704	717	612
6.7	14.8	3.8	12.2	28	10.8	0.9	-1728	716	778
6.8	13.8	4.1	12.0	28	11.5	0.9	-1760	719	648
6.9	12.6	3.3	11.8	27	11.3	0.9	-1775	715	394
7.0	12.9	3.9	11.7	27	11.9	0.9	-1788	709	535
7.1	13.7	4.3	11.6	27	11.8	0.9	-1813	709	737
7.2	13.0	4.2	11.3	26	11.2	0.9	-1841	710	646
7.3	11.4	4.2	11.4	25	11.1	1.8	-1860	708	390
7.4	12.0	5.8	11.2	25	11.2	0.0	-1869	702	466
7.5	12.1	5.2	11.0	25	10.6	0.9	-1893	701	740
7.6	12.4	6.0	10.8	24	10.7	0.0	-1922	703	508
7.7	11.0	5.7	10.7	24	10.7	0.0	-1930	696	386
7.8	11.7	5.3	10.6	24	10.6	0.9	-1950	694	547
7.9	12.3	5.5	10.4	23	10.1	0.9	-1969	692	701
8.0	13.2	5.5	10.3	23	10.7	0.9	-2001	695	632
8.1	12.2	4.9	10.3	23	11.4	0.0	-2015	691	433
8.2	12.1	6.0	10.2	23	10.7	0.0	-2032	688	472

Table A.26 Column $k = 12$, vertically polarized.

f_{in}	$A_{k,max}$	$\Delta A_{k,\phi}$			SLL_θ			$\tau_{\psi,k}$	$\tau_{g,k}$
GHz	dBi	dB	$\text{HPBW}_\theta{}^\circ$	$\text{FNBW}_\theta{}^\circ$	dB	$\xi_\theta{}^\circ$	$\psi_k{}^\circ$	ps	ps
2.6	13.1	2.6	29.9	84	-	0.0	-80	85	2766
2.7	13.7	2.6	27.9	75	-	0.0	-179	184	2520
2.8	12.4	2.2	27.9	72	-	0.0	-261	259	2168
2.9	12.6	2.6	27.2	68	-	0.9	-335	321	1950
3.0	14.2	2.7	28.2	66	12.7	0.0	-402	372	2060
3.1	14.9	2.6	26.5	65	13.4	0.9	-484	434	2082
3.2	13.8	2.2	26.3	60	12.1	1.8	-551	479	1820
3.3	13.8	2.7	25.5	59	12.6	0.0	-615	518	1819
3.4	14.4	2.7	25.1	58	13.2	0.0	-682	558	1925
3.5	14.6	2.6	24.3	53	11.2	0.0	-753	598	1892
3.6	13.9	2.4	23.7	53	12.0	-0.9	-819	632	1754
3.7	13.9	2.3	23.1	52	11.8	-0.9	-880	660	1743
3.8	15.6	2.6	22.7	50	12.6	0.9	-944	690	1828
3.9	14.5	2.0	22.0	48	13.0	0.0	-1011	720	1867
4.0	14.3	2.4	21.4	48	12.2	0.9	-1092	758	955
4.1	14.8	2.6	21.1	48	12.9	0.9	-1127	763	1045
4.2	15.4	2.6	20.4	45	12.5	0.0	-1167	772	1093
4.3	15.3	3.3	19.8	44	12.9	0.9	-1205	779	982
4.4	14.8	2.8	19.5	42	12.3	0.0	-1238	782	843
4.5	13.9	2.5	18.9	41	12.3	0.0	-1266	782	770
4.6	15.4	2.9	18.3	41	12.3	0.0	-1294	781	760
4.7	15.1	2.6	17.9	40	12.2	0.0	-1321	781	755
4.8	14.7	2.6	17.5	40	11.6	0.0	-1348	780	695
4.9	15.3	3.3	17.0	39	12.8	0.0	-1371	777	724
5.0	15.5	5.2	16.6	38	12.1	0.0	-1400	778	798
5.1	15.2	5.2	16.2	38	11.5	0.0	-1428	778	782
5.2	14.3	4.4	15.8	37	11.5	0.0	-1456	778	668
5.3	15.0	4.8	15.5	36	12.0	0.0	-1476	774	638
5.4	14.8	4.1	14.9	34	11.4	0.0	-1502	773	672
5.5	15.4	4.1	14.9	34	9.9	0.0	-1525	770	835
5.6	15.2	4.4	14.5	34	11.2	0.0	-1562	775	769
5.7	14.1	5.6	14.4	32	10.4	0.9	-1580	770	533
5.8	14.5	5.5	14.1	33	11.0	0.0	-1601	767	577
5.9	16.2	4.6	14.1	32	11.6	0.0	-1567	738	877
6.0	15.3	4.8	13.7	32	10.2	0.0	-1598	740	828
6.1	15.6	6.1	13.6	31	11.0	-0.9	-1626	741	707
6.2	15.3	7.6	13.1	31	9.9	0.0	-1649	739	661
6.3	15.7	6.7	13.1	31	11.4	0.0	-1674	738	685
6.4	14.8	6.6	12.7	30	11.1	0.0	-1699	737	623
6.5	14.1	3.8	12.3	29	9.1	0.0	-1719	735	574
6.6	14.1	3.4	12.2	29	11.1	0.0	-1740	732	537
6.7	14.1	2.5	12.2	29	11.2	0.0	-1758	729	685
6.8	13.2	3.5	11.9	28	11.1	0.9	-1789	731	693
6.9	12.6	3.2	11.6	27	11.3	0.0	-1807	728	382
7.0	12.6	4.0	11.6	27	11.4	0.0	-1817	721	414
7.1	13.5	3.2	11.6	27	11.3	0.0	-1837	719	688
7.2	13.0	4.1	11.1	26	11.0	0.9	-1866	720	644
7.3	11.1	4.6	11.1	25	10.6	0.0	-1884	717	325
7.4	11.9	5.4	11.0	25	11.5	0.0	-1890	709	403
7.5	12.8	4.5	10.9	25	10.9	0.0	-1913	708	768
7.6	12.7	4.3	10.7	24	10.3	0.0	-1945	711	590
7.7	12.0	6.4	10.6	25	11.3	0.0	-1955	705	360
7.8	12.7	4.0	10.5	24	11.1	0.0	-1971	702	571
7.9	13.1	2.9	10.3	24	11.6	0.0	-1996	702	676
8.0	13.0	3.6	10.3	23	10.2	0.0	-2020	701	634
8.1	13.6	3.7	10.0	23	10.6	0.0	-2042	700	639
8.2	13.2	3.3	10.1	23	12.9	0.0	-2066	700	658

Table A.27 Column $k = 13$, horizontally polarized.

f_{in}	$A_{k,max}$	$\Delta A_{k,\phi}$			SLL_θ			$\tau_{\psi,k}$	$\tau_{g,k}$
GHz	dBi	dB	$\text{HPBW}_\theta{}^\circ$	$\text{FNBW}_\theta{}^\circ$	dB	$\xi_\theta{}^\circ$	$\psi_k{}^\circ$	ps	ps
2.6	14.3	3.5	31.9	93	-	0.9	-91	98	2546
2.7	14.1	3.6	31.0	82	-	0.0	-183	188	2448
2.8	13.3	3.5	29.0	74	-	0.0	-268	265	2253
2.9	13.4	3.6	28.1	70	-	0.0	-345	331	1933
3.0	15.1	3.8	27.1	68	15.8	0.9	-407	377	1877
3.1	15.0	2.9	26.5	68	13.1	0.9	-480	430	2011
3.2	13.9	2.5	25.9	65	14.2	0.9	-551	479	1940
3.3	14.1	3.8	24.6	62	12.9	2.7	-620	522	1915
3.4	14.3	3.7	24.6	65	14.8	0.0	-689	563	2015
3.5	14.6	3.6	23.7	59	13.9	0.0	-765	607	2054
3.6	14.7	3.8	22.4	56	13.9	0.0	-837	646	1892
3.7	14.8	3.9	22.3	56	13.8	0.9	-901	677	1724
3.8	15.4	4.1	21.5	54	13.4	0.0	-961	703	1783
3.9	14.5	4.1	20.9	52	13.4	0.0	-1030	733	1896
4.0	14.9	3.9	21.1	53	15.1	0.0	-1104	767	1005
4.1	15.0	4.1	20.6	50	13.5	0.9	-1140	772	1003
4.2	14.9	3.4	20.2	50	13.8	0.9	-1176	778	997
4.3	14.8	3.0	19.2	46	12.4	0.9	-1212	783	951
4.4	14.4	3.9	19.4	46	11.2	0.9	-1245	786	815
4.5	14.0	4.4	18.7	45	11.8	1.8	-1271	784	776
4.6	15.7	4.4	18.3	42	12.4	0.9	-1301	785	896
4.7	14.8	3.5	17.9	43	13.3	1.8	-1335	789	785
4.8	14.8	3.0	17.7	41	12.1	1.8	-1357	785	640
4.9	14.9	2.7	17.5	41	12.8	0.9	-1381	783	800
5.0	14.8	3.2	17.0	41	13.3	0.9	-1415	786	830
5.1	14.4	3.4	16.3	38	11.8	0.9	-1441	785	712
5.2	13.9	4.0	16.1	37	11.8	0.9	-1466	783	562
5.3	14.8	3.1	16.1	38	12.4	0.9	-1481	776	612
5.4	14.1	4.8	15.8	37	12.1	0.0	-1510	777	590
5.5	14.7	3.4	15.7	39	12.5	0.9	-1524	770	815
5.6	15.0	4.5	15.3	35	11.8	0.9	-1569	778	933
5.7	14.1	4.4	15.1	34	12.4	1.8	-1591	775	580
5.8	14.3	4.2	14.7	34	11.9	0.9	-1611	771	540
5.9	14.1	3.9	14.7	34	12.6	0.9	-1569	739	929
6.0	14.5	3.6	14.3	32	11.4	0.9	-1602	742	900
6.1	14.3	2.6	14.1	32	12.7	0.9	-1634	744	715
6.2	13.7	2.3	13.7	32	11.8	0.9	-1654	741	623
6.3	14.5	3.3	13.8	32	13.8	0.9	-1679	740	711
6.4	13.9	3.1	13.4	31	13.1	1.8	-1705	740	654
6.5	13.6	3.1	13.0	31	13.1	0.9	-1726	737	531
6.6	13.8	3.4	12.7	30	11.7	1.8	-1743	734	548
6.7	14.3	3.5	12.4	29	11.5	1.8	-1765	732	730
6.8	14.0	3.5	12.4	29	11.9	0.9	-1796	734	684
6.9	12.5	3.5	11.9	28	12.5	0.9	-1814	730	451
7.0	13.1	4.1	11.8	29	13.4	0.9	-1828	725	618
7.1	13.9	3.7	11.7	28	12.6	0.9	-1859	727	812
7.2	12.4	3.8	11.6	28	11.9	0.9	-1887	728	705
7.3	10.9	4.5	11.6	28	13.3	0.9	-1910	727	322
7.4	11.2	4.6	11.4	27	12.6	0.9	-1910	717	362
7.5	12.5	5.4	11.2	26	11.4	0.9	-1936	717	780
7.6	11.3	4.3	11.2	27	12.7	0.0	-1966	719	541
7.7	10.5	4.5	11.4	28	13.1	0.9	-1975	712	321
7.8	11.2	4.7	11.2	27	12.8	0.9	-1989	708	517
7.9	11.7	4.5	11.0	25	11.3	0.9	-2012	707	695
8.0	11.9	4.4	10.9	26	12.7	0.9	-2039	708	567
8.1	11.3	5.1	11.0	34	13.0	0.9	-2053	704	474
8.2	11.5	5.2	10.7	26	11.9	0.9	-2073	702	577

Table A.28 Column $k = 13$, vertically polarized.

f_{in}	$A_{k,max}$	$\Delta A_{k,\phi}$			SLL_θ			$\tau_{\psi,k}$	$\tau_{g,k}$
GHz	dBi	dB	$\text{HPBW}_\theta{}^\circ$	$\text{FNBW}_\theta{}^\circ$	dB	$\xi_\theta{}^\circ$	$\psi_k{}^\circ$	ps	ps
2.6	12.2	2.8	29.6	82	-	0.0	-65	69	2769
2.7	13.3	2.8	27.3	79	-	0.9	-165	169	2550
2.8	11.9	2.3	28.0	75	-	0.9	-248	246	2205
2.9	11.2	2.3	27.4	69	-	0.0	-323	310	1930
3.0	13.0	2.9	27.6	67	13.1	2.7	-387	359	2042
3.1	14.1	2.8	26.4	68	13.8	2.7	-470	421	2064
3.2	13.3	2.3	25.6	62	12.6	1.8	-536	465	1765
3.3	12.9	2.3	25.2	59	12.4	2.7	-597	503	1786
3.4	13.6	2.4	24.7	59	12.6	0.0	-665	543	1934
3.5	13.8	2.7	24.2	55	11.1	2.7	-737	585	1866
3.6	13.2	2.9	23.9	56	10.9	0.0	-799	616	1734
3.7	13.3	2.1	23.0	51	11.3	0.9	-862	647	1731
3.8	14.6	2.8	22.5	50	11.8	0.9	-924	675	1795
3.9	13.8	2.5	21.9	49	11.6	1.8	-991	706	1867
4.0	14.0	2.5	21.7	49	11.8	0.9	-1070	743	1087
4.1	14.8	2.5	21.1	47	11.9	0.9	-1109	751	1053
4.2	15.0	2.7	20.5	46	12.0	0.9	-1145	758	1016
4.3	15.0	2.6	19.9	44	11.6	0.9	-1182	763	1012
4.4	14.6	2.6	19.7	42	11.5	0.9	-1218	769	882
4.5	13.6	2.5	19.3	42	11.6	1.8	-1245	769	694
4.6	15.4	3.5	18.8	41	11.9	0.9	-1268	766	790
4.7	15.2	2.8	18.6	41	11.7	1.8	-1302	770	883
4.8	14.5	3.2	17.9	40	11.6	1.8	-1332	771	734
4.9	15.2	3.1	17.4	40	12.3	1.8	-1355	768	715
5.0	14.8	3.7	16.8	39	11.1	1.8	-1383	768	815
5.1	14.7	3.8	16.5	38	11.4	1.8	-1414	770	795
5.2	13.6	4.7	16.1	37	11.0	0.9	-1440	769	552
5.3	14.8	5.4	15.8	37	12.1	1.8	-1454	762	422
5.4	14.5	5.2	15.4	36	11.6	0.9	-1471	757	571
5.5	15.3	5.1	15.2	37	9.0	1.8	-1495	755	841
5.6	14.7	4.5	14.9	35	10.5	1.8	-1531	760	730
5.7	14.0	5.1	14.7	34	10.9	0.9	-1547	754	488
5.8	14.5	5.5	14.3	34	11.3	0.9	-1567	750	537
5.9	14.7	4.7	14.3	33	10.0	1.8	-1527	719	765
6.0	15.1	5.0	13.7	32	9.9	0.9	-1555	720	806
6.1	14.8	5.2	13.8	32	10.7	1.8	-1585	722	762
6.2	14.3	5.8	13.4	32	9.3	0.9	-1610	721	672
6.3	14.8	6.2	13.4	32	9.8	1.8	-1634	720	663
6.4	14.4	6.6	12.9	30	9.7	1.8	-1657	719	644
6.5	13.9	7.8	12.8	30	8.9	0.9	-1680	718	605
6.6	13.9	3.4	12.4	30	10.1	0.9	-1701	716	610
6.7	14.1	3.4	12.6	30	10.3	0.9	-1724	715	703
6.8	13.6	2.8	12.2	29	10.1	1.8	-1752	715	667
6.9	12.5	4.6	11.9	28	9.2	0.9	-1772	713	550
7.0	12.8	4.3	12.0	28	10.7	0.0	-1791	711	606
7.1	13.0	2.6	12.0	28	10.6	0.9	-1816	710	653
7.2	12.4	2.9	11.6	28	10.3	0.9	-1838	709	544
7.3	11.1	3.9	11.5	27	10.0	0.9	-1855	706	330
7.4	11.2	4.9	11.1	26	9.7	0.9	-1862	699	390
7.5	11.6	2.8	11.2	26	10.3	0.9	-1883	697	620
7.6	11.7	3.1	11.1	26	11.1	0.9	-1907	697	472
7.7	11.0	6.0	10.9	26	11.0	0.9	-1917	692	395
7.8	11.0	5.7	10.8	25	10.4	0.9	-1935	689	507
7.9	11.9	4.3	10.7	26	11.9	0.9	-1953	687	688
8.0	12.5	5.7	10.6	25	9.3	0.9	-1984	689	662
8.1	11.6	3.6	10.3	25	9.8	0.9	-2001	686	516
8.2	12.1	3.5	10.3	25	12.6	0.9	-2022	685	573

Table A.29 Column $k = 14$, horizontally polarized.

f_{in}	$A_{k,max}$	$\Delta A_{k,\phi}$			SLL_θ			$\tau_{\psi,k}$	$\tau_{g,k}$
GHz	dBi	dB	$\text{HPBW}_\theta{}^\circ$	$\text{FNBW}_\theta{}^\circ$	dB	$\xi_\theta{}^\circ$	$\psi_k{}^\circ$	ps	ps
2.6	13.8	4.0	30.4	77	-	1.8	-65	69	2645
2.7	13.7	4.4	30.0	77	-	0.9	-160	165	2511
2.8	13.3	3.2	28.4	73	-	0.0	-246	244	2180
2.9	12.6	3.0	27.1	68	-	0.0	-317	304	1831
3.0	14.7	3.5	26.6	67	13.9	0.9	-378	350	1838
3.1	14.5	2.5	25.7	64	12.7	0.0	-449	403	2023
3.2	14.8	3.2	25.2	63	13.3	0.9	-523	454	1954
3.3	15.0	4.0	24.3	61	12.6	0.9	-590	497	1926
3.4	15.5	3.3	23.4	59	12.3	-0.9	-662	541	2037
3.5	15.5	3.3	23.0	56	13.5	0.0	-737	585	1975
3.6	14.6	4.7	22.2	53	12.3	0.0	-804	620	1704
3.7	15.1	5.5	21.7	53	12.5	0.9	-860	645	1531
3.8	16.8	5.0	21.3	52	12.4	0.0	-914	668	1780
3.9	16.1	4.8	20.3	49	11.6	0.9	-988	703	2039
4.0	15.2	3.6	20.0	48	11.0	0.9	-1064	739	971
4.1	16.4	3.8	19.9	49	12.3	0.9	-1099	745	1049
4.2	16.5	3.4	19.3	46	11.1	0.0	-1140	754	1085
4.3	16.3	3.0	18.7	44	10.1	0.0	-1177	761	1100
4.4	15.8	3.8	18.7	43	10.3	0.9	-1219	770	856
4.5	15.4	4.1	17.9	41	9.5	0.0	-1239	765	665
4.6	15.7	3.4	18.3	43	11.7	0.0	-1267	765	788
4.7	16.4	4.4	17.7	41	11.8	0.9	-1296	766	774
4.8	14.2	4.6	17.2	39	9.5	0.0	-1323	765	720
4.9	15.8	4.3	16.9	38	10.5	0.0	-1348	764	752
5.0	15.4	4.2	17.0	39	11.8	0.0	-1377	765	785
5.1	15.5	5.0	16.5	37	10.4	0.0	-1404	765	590
5.2	14.4	4.1	16.0	37	10.8	0.0	-1419	758	532
5.3	15.1	4.6	15.6	35	9.9	0.0	-1442	756	517
5.4	14.2	3.8	15.7	36	10.2	0.9	-1456	749	653
5.5	15.9	3.4	15.4	35	11.5	0.9	-1489	752	887
5.6	15.7	4.0	15.3	35	10.9	0.0	-1520	754	720
5.7	15.3	3.5	14.6	33	10.1	0.0	-1541	751	538
5.8	15.2	3.1	14.3	32	10.3	0.0	-1559	747	495
5.9	15.3	3.9	14.5	32	12.2	0.0	-1518	715	758
6.0	15.5	3.9	14.0	32	11.3	0.0	-1545	715	735
6.1	15.0	3.9	13.7	31	10.6	0.0	-1571	715	712
6.2	15.5	4.0	13.6	32	11.7	-0.9	-1596	715	693
6.3	15.1	3.5	13.2	31	12.4	0.0	-1621	715	706
6.4	14.7	2.9	12.8	30	11.4	0.0	-1647	715	709
6.5	14.6	3.4	12.7	30	11.0	0.0	-1672	714	621
6.6	14.8	3.4	12.3	29	10.5	-0.9	-1692	712	643
6.7	15.1	3.7	12.3	29	11.8	0.0	-1718	712	733
6.8	14.5	3.5	12.2	29	10.7	0.0	-1745	713	664
6.9	13.1	3.5	12.1	28	11.0	0.0	-1766	711	535
7.0	13.5	3.9	12.0	28	11.7	0.0	-1783	708	583
7.1	14.1	4.1	11.7	27	11.1	0.0	-1808	707	633
7.2	13.4	3.9	11.4	26	10.9	0.0	-1829	706	567
7.3	11.9	4.5	11.7	27	11.2	0.0	-1848	703	371
7.4	11.4	4.6	11.4	25	11.2	0.0	-1855	696	327
7.5	12.0	3.8	11.3	26	11.4	0.9	-1872	693	610
7.6	12.4	3.7	11.0	25	11.1	0.0	-1899	694	512
7.7	11.2	4.2	10.9	25	10.5	0.0	-1909	689	316
7.8	11.8	4.2	10.8	25	11.5	0.0	-1922	684	450
7.9	12.1	4.0	10.6	24	11.1	0.0	-1941	683	733
8.0	12.9	2.9	10.5	23	11.8	0.0	-1975	686	679
8.1	11.8	3.4	10.5	23	11.5	-0.9	-1990	682	459
8.2	11.7	5.2	10.4	23	11.5	0.0	-2008	680	494

Table A.30 Column $k = 14$, vertically polarized.

f_{in}	$A_{k,max}$	$\Delta A_{k,\phi}$			SLL_θ			$\tau_{\psi,k}$	$\tau_{g,k}$
GHz	dBi	dB	$\text{HPBW}_\theta{}^\circ$	$\text{FNBW}_\theta{}^\circ$	dB	$\xi_\theta{}^\circ$	$\psi_k{}^\circ$	ps	ps
2.6	13.1	3.1	29.9	82	-	0.0	-79	84	2722
2.7	13.9	3.3	29.4	77	-	0.0	-177	182	2536
2.8	12.9	2.9	27.7	76	-	0.0	-261	259	2266
2.9	12.4	2.8	27.8	72	-	0.9	-340	325	2061
3.0	13.9	3.4	28.6	68	12.6	-2.7	-410	379	2045
3.1	14.5	2.8	26.7	64	12.9	1.8	-487	436	2056
3.2	13.9	2.6	26.4	61	11.9	-1.8	-558	484	1833
3.3	13.3	2.4	25.8	60	12.5	-0.9	-619	521	1758
3.4	14.0	2.4	24.9	58	12.5	-0.9	-684	559	1922
3.5	14.7	2.7	24.6	56	12.6	0.0	-757	601	1973
3.6	14.6	2.5	23.8	54	12.1	-0.9	-826	638	1843
3.7	13.8	3.2	23.4	53	11.7	0.0	-890	668	1634
3.8	15.3	3.2	22.8	50	12.4	-0.9	-944	690	1689
3.9	14.8	2.7	22.1	49	12.6	-0.9	-1012	721	1882
4.0	15.2	2.8	21.7	48	12.6	0.0	-1094	760	979
4.1	14.3	2.5	20.8	47	11.7	-0.9	-1130	765	959
4.2	14.7	2.6	20.6	46	12.5	0.0	-1163	769	960
4.3	15.3	2.5	19.6	44	13.0	-0.9	-1199	774	1030
4.4	15.5	2.8	19.5	42	11.8	0.0	-1238	781	880
4.5	14.9	2.7	18.9	42	12.2	-0.9	-1262	779	799
4.6	15.9	3.9	18.4	41	12.0	-0.9	-1295	782	861
4.7	15.4	3.9	17.9	41	11.9	0.0	-1324	783	784
4.8	14.8	3.6	17.4	40	11.8	0.9	-1352	782	835
4.9	16.3	4.7	17.0	40	12.4	0.0	-1384	785	885
5.0	16.0	3.7	16.5	38	12.1	0.0	-1415	786	807
5.1	15.4	3.2	16.2	37	12.3	0.0	-1442	786	672
5.2	15.1	3.2	15.5	36	11.5	0.0	-1464	782	680
5.3	15.6	3.9	15.5	37	11.9	0.0	-1491	782	625
5.4	14.4	4.5	15.1	36	11.3	0.0	-1509	776	589
5.5	15.9	4.0	15.2	35	11.5	0.0	-1534	775	773
5.6	15.8	4.0	14.5	34	11.6	0.0	-1564	776	721
5.7	15.2	4.4	14.4	33	11.5	-0.9	-1586	773	542
5.8	15.4	5.2	14.1	33	11.8	-0.9	-1603	768	495
5.9	15.5	4.8	14.0	32	11.2	0.0	-1564	736	868
6.0	15.4	5.1	13.7	32	11.0	0.0	-1595	738	747
6.1	15.2	5.2	13.5	32	10.7	0.0	-1617	736	616
6.2	15.3	5.0	13.4	32	10.5	0.0	-1639	734	655
6.3	15.1	5.6	13.1	31	11.6	0.0	-1665	734	785
6.4	15.1	5.5	12.7	30	11.3	0.0	-1696	736	782
6.5	14.4	5.6	12.6	30	10.9	0.0	-1721	735	610
6.6	13.7	7.2	12.3	29	11.2	0.0	-1740	732	536
6.7	14.4	8.1	12.4	29	11.6	0.0	-1759	729	729
6.8	14.0	8.0	12.1	29	11.2	0.0	-1792	732	709
6.9	12.7	3.5	11.9	28	11.6	0.0	-1810	729	408
7.0	12.5	3.4	11.8	27	11.1	0.0	-1821	723	458
7.1	13.6	3.0	11.7	27	12.5	0.0	-1843	721	721
7.2	13.0	2.8	11.4	27	11.1	0.0	-1873	723	709
7.3	11.4	3.5	11.4	27	11.3	0.0	-1895	721	397
7.4	11.3	4.9	11.2	26	11.4	0.0	-1902	714	371
7.5	12.3	4.7	10.9	25	10.7	0.0	-1921	712	746
7.6	12.6	4.2	11.0	26	11.0	0.0	-1956	715	591
7.7	11.3	4.4	10.8	25	12.2	0.0	-1964	708	362
7.8	11.7	4.5	10.7	24	11.7	-0.9	-1982	706	479
7.9	12.4	3.9	10.6	24	11.1	0.0	-1998	703	636
8.0	13.3	4.2	10.4	23	10.9	0.0	-2027	704	671
8.1	12.9	4.7	10.2	23	11.0	0.0	-2047	702	533
8.2	13.0	5.7	10.3	23	11.7	0.0	-2066	700	533

Table A.31 Column $k = 15$, horizontally polarized.

f_{in}	$A_{k,max}$	$\Delta A_{k,\phi}$			SLL_θ			$\tau_{\psi,k}$	$\tau_{g,k}$
GHz	dBi	dB	$\text{HPBW}_\theta{}^\circ$	$\text{FNBW}_\theta{}^\circ$	dB	$\xi_\theta{}^\circ$	$\psi_k{}^\circ$	ps	ps
2.6	13.5	3.7	32.7	93	-	-1.8	-58	62	2940
2.7	14.9	4.0	30.8	79	-	-0.9	-164	169	2643
2.8	13.4	3.3	28.8	93	-	-1.8	-249	247	2167
2.9	13.9	3.2	28.1	73	-	-0.9	-320	307	1968
3.0	15.9	4.3	27.4	72	13.8	-3.6	-390	361	2091
3.1	14.2	3.4	27.2	68	11.1	-2.7	-471	422	2137
3.2	14.3	4.6	25.7	87	12.8	-4.5	-544	472	1962
3.3	13.9	4.3	25.4	64	11.9	-1.8	-612	515	1836
3.4	14.4	3.0	24.4	80	10.3	-2.7	-676	553	1917
3.5	14.4	2.7	24.6	60	12.2	-0.9	-750	595	1805
3.6	14.2	3.3	22.7	74	10.2	-3.6	-806	622	1674
3.7	14.6	4.7	24.2	62	12.1	-0.9	-870	653	1641
3.8	15.4	4.5	22.1	68	9.9	-2.7	-924	676	1757
3.9	15.0	5.0	23.0	56	11.3	-2.7	-997	710	2015
4.0	14.9	4.2	20.8	70	8.5	-2.7	-1063	738	1277
4.1	15.6	4.6	21.9	57	10.0	-1.8	-1109	752	1162
4.2	15.5	4.3	20.5	51	10.0	-1.8	-1147	759	1124
4.3	15.1	4.7	21.5	51	10.4	-1.8	-1190	769	1043
4.4	14.6	4.6	20.5	57	8.4	-3.6	-1222	772	870
4.5	14.2	4.7	19.7	47	9.0	-2.7	-1253	773	726
4.6	15.5	4.5	18.8	54	9.6	-3.6	-1274	770	767
4.7	14.9	3.1	20.5	50	10.4	-0.9	-1308	773	824
4.8	14.6	3.5	17.6	52	8.2	-2.7	-1334	772	720
4.9	14.9	3.4	18.4	48	9.0	-2.7	-1360	771	790
5.0	14.7	3.7	18.0	47	10.5	-1.8	-1391	773	845
5.1	14.3	3.2	18.6	46	6.8	-1.8	-1421	774	846
5.2	13.9	3.0	17.8	46	9.9	-1.8	-1452	775	649
5.3	14.7	3.4	17.0	44	8.5	-1.8	-1468	769	586
5.4	14.1	5.3	16.9	44	9.0	-1.8	-1494	768	676
5.5	14.1	3.9	17.2	41	7.4	-2.7	-1516	766	833
5.6	14.5	4.3	16.6	43	8.0	-2.7	-1554	771	740
5.7	13.7	4.5	17.5	41	8.1	-2.7	-1570	765	377
5.8	13.6	3.5	15.9	40	8.3	-1.8	-1581	757	314
5.9	13.8	3.6	16.7	40	7.1	-1.8	-1542	726	662
6.0	13.9	3.8	16.3	40	8.5	-1.8	-1566	725	689
6.1	13.1	3.0	16.8	38	7.8	-0.9	-1592	725	542
6.2	12.9	3.5	15.2	38	8.0	-2.7	-1605	719	626
6.3	13.6	3.7	16.3	36	9.5	-1.8	-1637	722	843
6.4	12.8	2.9	15.4	35	8.2	-1.8	-1666	723	690
6.5	11.7	2.7	16.7	36	8.4	-1.8	-1687	721	528
6.6	12.5	2.9	14.3	35	8.0	-1.8	-1704	717	612
6.7	13.5	3.6	14.5	34	8.6	-1.8	-1731	718	862
6.8	12.5	3.2	15.4	34	9.8	-0.9	-1766	721	724
6.9	10.3	3.3	16.4	33	7.4	-1.8	-1783	718	386
7.0	11.8	4.0	13.6	33	8.5	-2.7	-1794	712	543
7.1	13.1	3.1	13.9	32	8.7	-1.8	-1822	713	849
7.2	11.5	4.7	15.2	32	8.6	-0.9	-1855	716	597
7.3	9.9	4.5	14.8	32	7.2	-1.8	-1865	710	248
7.4	10.7	5.2	13.2	32	8.5	-1.8	-1873	703	478
7.5	11.4	4.4	13.8	31	8.0	-0.9	-1899	703	849
7.6	11.0	4.1	14.3	30	8.2	-1.8	-1934	707	584
7.7	9.7	4.9	13.5	31	7.9	-1.8	-1941	700	375
7.8	10.5	5.1	13.6	30	8.6	-1.8	-1961	698	550
7.9	11.0	4.6	13.3	29	8.0	0.0	-1981	697	750
8.0	11.2	4.0	13.6	28	7.5	0.9	-2015	700	730
8.1	10.3	4.1	13.8	27	7.8	0.0	-2034	697	463
8.2	10.2	5.3	13.8	27	6.9	0.0	-2048	694	410

Table A.32 Column $k = 15$, vertically polarized.

f_{in}	$A_{k,max}$	$\Delta A_{k,\phi}$			SLL_θ			$\tau_{\psi,k}$	$\tau_{g,k}$
GHz	dBi	dB	$\text{HPBW}_\theta{}^\circ$	$\text{FNBW}_\theta{}^\circ$	dB	$\xi_\theta{}^\circ$	$\psi_k{}^\circ$	ps	ps
2.6	11.6	3.5	30.2	90	-	0.0	-63	67	2674
2.7	13.1	3.9	27.9	83	-	0.0	-159	164	2548
2.8	12.1	3.9	25.5	78	-	0.0	-247	245	2273
2.9	10.9	3.4	28.8	77	-	-0.9	-323	309	1976
3.0	13.0	3.8	29.0	71	9.9	-1.8	-389	360	2051
3.1	13.3	3.3	26.4	67	8.2	-2.7	-471	422	2104
3.2	13.1	3.1	26.3	68	11.1	-1.8	-540	469	1884
3.3	12.9	2.9	24.9	65	8.0	0.0	-606	510	1887
3.4	13.2	2.8	25.8	64	10.5	0.0	-676	552	2020
3.5	13.3	3.0	24.9	59	8.9	0.0	-752	597	1937
3.6	11.8	2.7	24.8	62	8.8	0.0	-816	629	1651
3.7	13.1	2.8	23.4	63	9.3	-1.8	-871	654	1682
3.8	14.2	2.6	23.3	57	9.2	-0.9	-937	685	1864
3.9	13.2	2.7	22.5	52	9.0	-1.8	-1005	716	1895
4.0	13.1	2.8	23.2	55	10.4	0.0	-1076	747	872
4.1	14.2	2.8	22.5	56	9.8	-0.9	-1108	750	974
4.2	14.0	2.9	21.6	54	8.7	-1.8	-1146	758	1055
4.3	14.4	2.8	20.9	49	9.1	-0.9	-1184	765	983
4.4	13.9	2.5	20.9	54	8.9	-0.9	-1217	768	850
4.5	13.2	2.5	20.5	47	8.7	0.0	-1245	768	769
4.6	14.7	3.3	20.4	50	9.1	-1.8	-1273	768	854
4.7	14.6	3.2	19.3	47	9.3	-0.9	-1306	772	847
4.8	13.4	3.3	19.2	48	8.1	-2.7	-1333	772	728
4.9	14.8	4.9	18.2	43	8.3	-0.9	-1359	770	814
5.0	14.7	3.4	18.5	43	9.6	-0.9	-1392	773	868
5.1	13.8	5.1	18.4	42	7.8	-0.9	-1421	774	768
5.2	13.2	6.0	18.1	41	7.7	0.0	-1447	773	610
5.3	14.4	5.3	17.0	41	7.8	-1.8	-1465	768	598
5.4	14.0	4.9	16.6	40	7.2	-0.9	-1490	767	673
5.5	12.4	5.4	16.6	38	7.7	-0.9	-1513	764	874
5.6	13.0	4.1	16.4	40	7.7	-1.8	-1553	771	805
5.7	12.9	4.4	16.3	38	7.1	-1.8	-1571	766	447
5.8	13.0	4.3	15.6	39	7.7	-0.9	-1586	759	394
5.9	13.4	4.3	15.8	37	8.4	-0.9	-1549	729	760
6.0	12.7	4.8	15.4	36	7.4	-0.9	-1576	730	737
6.1	12.5	4.3	15.8	36	7.9	-1.8	-1602	729	571
6.2	12.6	5.3	15.2	36	8.5	-1.8	-1617	724	596
6.3	13.1	5.8	15.1	35	8.7	-0.9	-1644	725	738
6.4	13.1	6.0	14.2	35	7.8	-1.8	-1670	725	681
6.5	12.0	5.6	15.0	34	9.0	-0.9	-1693	724	552
6.6	12.0	6.2	13.7	32	7.7	-1.8	-1710	720	608
6.7	12.8	6.5	14.1	32	9.3	-0.9	-1737	720	769
6.8	11.9	6.2	14.0	32	9.5	-0.9	-1765	721	592
6.9	10.7	7.1	13.4	32	8.0	-1.8	-1780	717	388
7.0	11.3	8.8	13.0	32	10.1	-0.9	-1793	712	569
7.1	12.3	9.0	13.3	32	10.2	-0.9	-1821	712	704
7.2	11.2	3.3	13.0	31	8.5	-0.9	-1844	711	565
7.3	9.7	3.4	12.8	30	8.9	-0.9	-1862	708	337
7.4	10.6	3.6	12.3	29	9.7	-0.9	-1868	701	451
7.5	11.5	3.6	12.5	29	10.2	0.0	-1894	702	729
7.6	10.8	3.0	12.5	29	10.3	0.0	-1921	702	547
7.7	10.1	3.4	12.7	29	8.8	0.0	-1933	697	438
7.8	10.4	3.7	12.7	28	9.2	0.0	-1952	695	556
7.9	11.7	3.5	12.5	28	10.5	-0.9	-1973	694	737
8.0	12.2	4.1	11.9	27	9.1	0.0	-2005	696	730
8.1	11.1	5.0	12.1	27	8.5	-0.9	-2026	695	530
8.2	11.7	4.6	12.1	27	8.1	-0.9	-2043	692	482

Table A.33 Column $k = 16$, horizontally polarized.

f_{in}	$A_{k,max}$	$\Delta A_{k,\phi}$			SLL_θ			$\tau_{\psi,k}$	$\tau_{g,k}$
GHz	dBi	dB	$\text{HPBW}_\theta{}^\circ$	$\text{FNBW}_\theta{}^\circ$	dB	${\xi_\theta}^\circ$	${\psi_k}^\circ$	ps	ps
2.6	17.0	8.4	31.1	79	-	-1.8	-90	96	2743
2.7	16.3	7.4	31.1	88	-	-1.8	-189	194	2407
2.8	15.1	8.1	28.1	73	-	-0.9	-263	261	2064
2.9	15.6	7.0	28.0	71	-	-2.7	-337	323	2046
3.0	15.4	5.4	27.7	71	15.3	-1.8	-411	380	2162
3.1	16.5	7.0	25.7	63	12.2	-1.8	-493	442	2182
3.2	16.3	7.4	25.5	64	13.6	-0.9	-568	493	1840
3.3	15.9	8.5	25.0	60	11.9	-1.8	-625	526	1555
3.4	16.4	8.3	23.0	54	10.1	-0.9	-680	555	1504
3.5	16.3	7.7	24.4	59	13.3	-1.8	-734	582	1672
3.6	15.5	7.7	23.0	56	11.3	-0.9	-800	617	1766
3.7	15.7	7.3	22.0	52	11.1	-0.9	-861	646	1792
3.8	18.3	8.7	23.0	56	13.3	-0.9	-929	679	1978
3.9	16.8	7.8	21.1	50	10.5	-2.7	-1003	715	2062
4.0	15.9	6.2	21.5	50	11.2	-0.9	-1075	747	982
4.1	15.9	5.2	21.7	53	12.3	0.0	-1110	752	1042
4.2	16.9	6.8	20.7	49	10.9	-0.9	-1150	761	1127
4.3	16.6	7.1	19.8	47	11.4	-0.9	-1192	770	1050
4.4	16.3	6.5	20.0	47	11.5	-0.9	-1226	774	807
4.5	16.2	6.4	19.1	44	9.6	-0.9	-1250	771	875
4.6	17.0	5.6	19.0	44	10.7	-0.9	-1289	778	970
4.7	16.2	6.3	18.3	43	10.7	0.0	-1319	780	837
4.8	15.6	5.9	18.1	42	10.4	0.0	-1349	781	749
4.9	17.3	6.4	17.5	41	10.2	-0.9	-1373	779	808
5.0	16.6	6.9	17.7	41	10.3	-0.9	-1407	782	871
5.1	15.9	5.6	17.0	40	10.0	-0.9	-1436	782	696
5.2	14.2	6.3	16.4	38	8.9	-0.9	-1457	778	713
5.3	16.1	6.5	16.6	39	10.5	-0.9	-1487	780	796
5.4	15.4	5.6	16.6	39	8.8	-0.9	-1515	779	753
5.5	16.0	5.4	15.9	36	9.9	-0.9	-1542	779	716
5.6	15.4	4.4	16.1	38	10.8	-0.9	-1566	777	605
5.7	15.6	4.9	15.3	35	9.5	-0.9	-1585	772	556
5.8	15.3	5.5	15.1	34	9.3	-0.9	-1606	769	585
5.9	15.0	4.7	15.0	35	9.8	-0.9	-1563	736	802
6.0	15.0	4.5	14.6	33	9.5	-0.9	-1592	737	773
6.1	15.3	4.7	14.4	33	10.5	-0.9	-1618	737	716
6.2	15.5	4.7	14.1	32	9.0	-0.9	-1643	736	683
6.3	14.8	4.7	13.9	32	9.7	-0.9	-1668	735	638
6.4	14.7	4.8	13.7	33	10.3	-0.9	-1689	733	577
6.5	14.4	4.7	13.3	32	10.5	-0.9	-1709	730	531
6.6	14.6	4.6	12.9	31	9.9	-0.9	-1727	727	579
6.7	14.3	4.2	12.8	30	9.4	-0.9	-1751	726	714
6.8	13.4	5.0	12.7	31	9.7	-0.9	-1779	727	658
6.9	12.6	4.8	12.3	30	9.8	-0.9	-1798	724	433
7.0	12.6	6.0	12.1	29	10.2	0.0	-1810	718	571
7.1	13.2	5.1	12.3	31	9.9	0.0	-1839	720	679
7.2	12.2	4.7	11.7	28	8.2	-1.8	-1859	717	649
7.3	10.5	4.3	11.7	27	9.9	-0.9	-1886	718	454
7.4	10.1	4.1	11.5	26	10.3	-0.9	-1892	710	405
7.5	10.2	4.2	11.5	26	9.8	-0.9	-1915	709	660
7.6	11.4	4.3	11.5	27	9.8	-1.8	-1939	709	518
7.7	9.9	4.6	11.3	36	8.4	-1.8	-1952	704	506
7.8	9.8	3.8	11.0	26	10.2	-1.8	-1976	704	424
7.9	10.1	4.4	11.2	26	9.7	-0.9	-1983	697	604
8.0	11.6	4.3	10.8	25	8.5	0.0	-2019	701	710
8.1	10.8	3.8	10.7	25	8.9	-0.9	-2034	698	538
8.2	10.5	4.7	10.6	24	8.4	-1.8	-2058	697	657

Table A.34 Column $k = 16$, vertically polarized.

f_{in}	$A_{k,max}$	$\Delta A_{k,\phi}$			SLL_θ			$\tau_{\psi,k}$	$\tau_{g,k}$
GHz	dBi	dB	$\text{HPBW}_\theta{}^\circ$	$\text{FNBW}_\theta{}^\circ$	dB	$\xi_\theta{}^\circ$	$\psi_k{}^\circ$	ps	ps
2.6	11.3	3.7	29.8	79	-	-0.9	-67	72	2646
2.7	12.7	4.7	28.9	76	-	0.0	-162	167	2506
2.8	12.0	4.7	29.0	77	-	-0.9	-247	245	2217
2.9	11.3	4.2	27.2	63	-	-0.9	-322	308	2029
3.0	12.9	4.1	28.0	61	8.8	-2.7	-393	364	2080
3.1	13.6	4.2	27.0	62	10.2	-2.7	-472	423	2143
3.2	13.0	3.1	25.5	57	9.1	-2.7	-548	475	2006
3.3	12.4	3.3	25.8	57	10.4	0.9	-616	518	1876
3.4	12.4	3.9	23.7	51	8.7	-2.7	-683	558	1878
3.5	12.6	3.8	24.4	53	9.3	-1.8	-751	596	1866
3.6	13.6	3.3	23.2	50	9.3	-0.9	-817	630	1838
3.7	12.8	3.3	22.6	50	9.3	-1.8	-883	663	1715
3.8	13.7	3.3	22.8	50	11.9	-1.8	-941	688	1818
3.9	12.7	3.1	22.2	48	9.9	-0.9	-1014	722	2050
4.0	13.8	3.1	20.7	45	9.5	-2.7	-1079	749	981
4.1	13.5	3.0	21.3	49	11.7	-0.9	-1115	755	941
4.2	13.8	2.7	20.7	46	11.4	-0.9	-1147	759	981
4.3	14.5	2.8	19.9	44	9.7	-0.9	-1185	766	996
4.4	14.3	3.2	19.5	42	10.0	-0.9	-1219	769	781
4.5	13.2	2.7	18.8	41	9.2	-0.9	-1241	766	762
4.6	15.2	2.7	18.5	41	10.9	-0.9	-1273	769	857
4.7	14.8	3.0	18.7	44	10.5	-0.9	-1303	770	765
4.8	14.4	3.0	17.2	39	9.7	0.0	-1329	769	685
4.9	14.8	3.0	17.2	41	10.4	0.0	-1352	767	697
5.0	15.0	3.2	17.2	40	10.6	-0.9	-1379	766	763
5.1	14.9	4.0	16.4	38	9.0	-0.9	-1407	767	733
5.2	14.1	3.0	15.8	36	10.5	-0.9	-1432	765	720
5.3	15.1	3.5	15.9	38	9.9	-0.9	-1459	765	712
5.4	14.8	3.8	15.5	37	9.5	0.0	-1483	763	736
5.5	16.6	4.3	15.4	37	9.5	-0.9	-1512	764	857
5.6	14.7	5.2	14.8	34	9.3	-0.9	-1545	766	675
5.7	14.3	5.1	14.8	35	8.4	0.0	-1561	761	523
5.8	14.5	4.7	14.5	33	9.1	0.0	-1582	758	594
5.9	14.4	4.3	14.4	34	9.0	-0.9	-1549	729	858
6.0	14.3	4.2	14.1	33	9.6	0.0	-1580	731	793
6.1	14.2	4.7	13.5	32	8.6	0.0	-1606	731	726
6.2	14.2	4.6	13.7	32	9.3	0.0	-1632	731	664
6.3	14.5	5.0	13.5	32	8.2	-0.9	-1654	729	697
6.4	14.3	5.1	12.9	30	8.5	-0.9	-1682	730	676
6.5	13.0	5.2	12.8	30	9.4	0.0	-1703	728	515
6.6	12.7	5.7	12.7	30	9.4	0.0	-1720	724	533
6.7	13.5	6.3	12.7	31	8.2	-0.9	-1741	722	770
6.8	12.5	6.4	12.6	41	9.2	-0.9	-1775	725	695
6.9	11.4	6.8	11.8	27	8.2	0.0	-1791	721	414
7.0	11.1	7.6	12.0	28	10.4	0.0	-1805	716	534
7.1	12.3	6.5	12.1	39	9.8	-0.9	-1830	716	733
7.2	11.7	7.8	11.4	27	7.8	-0.9	-1858	717	609
7.3	10.0	8.2	11.1	26	9.3	-0.9	-1873	713	279
7.4	9.8	5.0	11.2	27	9.3	0.0	-1878	705	373
7.5	11.4	4.7	11.4	38	8.9	-0.9	-1900	704	659
7.6	11.6	4.0	10.9	36	8.6	-0.9	-1925	704	444
7.7	11.0	5.4	10.3	24	8.5	-0.9	-1932	697	354
7.8	11.2	4.2	10.7	34	9.4	-0.9	-1951	695	488
7.9	12.1	3.7	10.6	34	9.6	-0.9	-1967	692	687
8.0	12.8	3.7	10.4	33	8.2	-0.9	-2000	694	737
8.1	12.4	3.9	10.3	23	9.9	-0.9	-2020	693	573
8.2	12.4	3.6	10.2	32	8.8	0.0	-2041	692	584

Appendix B. Command-Line Interface for Mid-Atlantic Tuners: Source Code

The following program is a command-line front-end to control Mid-Atlantic's LCR series tuners. Without a front-end, Mid-Atlantic's GUI alone can not interface with Matlab or any other application. This front-end program accepts a numeric argument from 0.500 to 18.000, and then passes the argument into the GUI which drives the tuners. This application was developed in C using Microsoft Visual Studio and Microsoft Platform Software Development Kit (SDK), and compiles into an executable called LCR100CL.exe. The Mid-Atlantic GUI, shown in Fig. 3.4, must be running before LCR100CL.exe is called. From the command line, for example, the user could enter

```
LCR100 6.123
```

which would set the tuners on 6.123 GHz. Equivalently, from Matlab, the command

```
dos('LCR100 6.123')
```

would accomplish the same thing. LCR100CL.exe functions as follows. First, it searches the operating system for the window with the title "LCR100 Tuner - Mid-Atlantic RF Systems", i.e. the GUI. It then emulates the mouse and keyboard to set the GUI on the desired frequency; this in turn sets the tuners on the desired frequency. The source code is contained in LCR100CL.c; the supporting files STDAFX.c and STDAFX.h are also used with Visual Studio. This code, including the executable product, are available in electronic form upon request from [12].

Listing B.1 STDAFX.h

```
1  // stdafx.h : include file for standard system include files,
2  // or project specific include files that are used frequently,
3  // but are changed infrequently
4
5  #pragma once
6
7  #define WIN32_LEAN_AND_MEAN
8      // Exclude rarely-used stuff from Windows headers
9  #include <stdio.h>
10 #include <tchar.h>
```

```
11 #include <windows.h>
12 #pragma comment(lib, "user32.lib")
13
14 // TODO: reference additional headers your program requires
      here
```

Listing B.2 STDAFX.c

```
1 // stdafx.c : source file that includes just the standard
      includes
2 // LCR100CL.pch will be the pre-compiled header
3 // stdafx.obj will contain the pre-compiled type information
4
5 #include "stdafx.h"
6
7 // TODO: reference any additional headers you need in STDAFX.H
8 // and not in this file
```

Listing B.3 LCR100CL.c

```
1 /*************************************************************
2 *
3 * LCR100CL.c
4 *
5 * by Capt Christopher Allen
6 * Air Force Institute of Technology
7 * September 2009
8 *
9 *************************************************************
10 *
11 * This program is a command-line front-end for Mid-Atlantic's
12 * LCR100 tuner software (LCR100 V2_5.exe).  This program makes
13 * it possible to tune the LCR100 via the command line.  It
14 * works by emulating mouse clicks and keystrokes in
15 * Mid-Atlantic's Graphical User Interface (GUI) window.
16 *
17 * Command-line usage:
18 *
19 * LCR100CL xxxxxx
20 * where each x is a numeral from 0 to 9, or a decimal point.
21 *
22 *************************************************************/
23 //#define _UNICODE
```

```
24 #include "stdafx.h"
25
26 void errormessage();
27
28 int _tmain(int argc, _TCHAR* argv[])
29 {
30     HWND hWnd;          // window handle
31     RECT lpRect;
32         // coordinates of the LCR100 GUI window (in pixels)
33     long ScreenWidth, ScreenHeight;
34         // width and height of the desktop (in pixels)
35     DWORD dx, dy;
36         // coordinates of the "Frequency" box (in mickeys)
37     BYTE bScan[6];
38         // hardware scan codes used by keybd_event
39     unsigned int i;    // index counter
40     char point = 0;    // used for error checking; makes sure
          you only use one decimal point
41     char leadingone = 0;
42         // determines if the first digit is a 1
43     char channelselect = 0;
44         // determines if we're using Channel Select A or B
45
46     // Make sure the user passed the parameter via the command
47     // line, and it was formatted correctly. If not, then quit
48     if (argc < 2) {
49         errormessage();
50         return 1; }
51     for (i = 0; i < wcslen(argv[1]); i++) {
52         if ((i > 5) || (((*(argv[1]+i) < '0') || (*(argv[1]+i)
              > '9')) && (*(argv[1]+i) != '.'))) {
53             errormessage();
54             return 1; }
55         if (*(argv[1]+i) == '.') {
56             // if argv[1]+i is a decimal point
57             // make sure there's only one decimal point
58             if (point > 0) {
59                 errormessage();
60                 return 1; }
61             point++;
62             // prepare for keybd_event
63             *(argv[1]+i) = VK_DECIMAL;
64             bScan[i] = 0x34; }
```

```
65          else {
66              // if argv[1]+i is not a decimal point
67              // prepare for keybd_event
68              bScan[i] = *(argv[1]+i) - 0x2F;
69              if (point == 0) {
70                  if ((leadingone>0) || (*(argv[1]+i) > '5')) {
71                      // if 6 GHz or greater, use Channel B
72                      channelselect++;   }
73                  else if (*(argv[1]+i) > '0') {
74                      // make note if the first digit is > 0
75                      leadingone++;   } } }
76      }
77
78      // Find the window for the LCR100 GUI.
79      hWnd = FindWindow(NULL, L"LCR100␣Tuner␣␣-␣␣Mid-Atlantic␣RF
           ␣Systems");
80      if (!hWnd) {
81          errormessage();
82          return 2;   }
83
84      // Make sure the GUI is displayed on top.
85      ShowWindow(hWnd, SW_SHOWNORMAL);
86      SetWindowPos(hWnd, HWND_TOPMOST, 0, 0, 0, 0, SWP_NOMOVE |
           SWP_NOSIZE | SWP_SHOWWINDOW);
87      SetWindowPos(hWnd, HWND_NOTOPMOST, 0, 0, 0, 0, SWP_NOMOVE
           | SWP_NOSIZE | SWP_SHOWWINDOW);
88
89      // Get the screen coordinates of the GUI window.
90      GetWindowRect(hWnd, &lpRect);
91
92      // mouse_event does not use the same coordinate system as
93      // GetWindowRect.  Convert from pixels to mickeys.
94      ScreenWidth = GetSystemMetrics(SM_CXSCREEN);
95          // width of the desktop in pixels
96      ScreenHeight = GetSystemMetrics(SM_CYSCREEN);
97          // height of the desktop in pixels
98      dx = 0xFFFF * (lpRect.left+39) / ScreenWidth;
99          // channel A or B select button location, X
100     if (channelselect == 0) {
101         // channel A select button location, Y
102         dy = 0xFFFF * (lpRect.top+162) / ScreenHeight;   }
103     else {
104         // channel B select button location, Y
```

```
105          dy = 0xFFFF * (lpRect.top+204) / ScreenHeight;   }
106
107      // Move the cursor to the frequency box, and simulate a
             mouse click.
108      mouse_event(MOUSEEVENTF_MOVE | MOUSEEVENTF_ABSOLUTE, dx,
             dy, 0, 0);
109      mouse_event(MOUSEEVENTF_LEFTDOWN, 0, 0, 0, 0);
110      mouse_event(MOUSEEVENTF_LEFTUP, 0, 0, 0, 0);
111
112      // Move the cursor to the frequency box, and simulate a
             mouse click.
113      dx = 0xFFFF * (lpRect.left+150) / ScreenWidth;
114          // frequency box location, X
115      dy = 0xFFFF * (lpRect.top+80) / ScreenHeight;
116          // frequency box location, Y
117      mouse_event(MOUSEEVENTF_MOVE | MOUSEEVENTF_ABSOLUTE, dx,
             dy, 0, 0);
118      mouse_event(MOUSEEVENTF_LEFTDOWN, 0, 0, 0, 0);
119      mouse_event(MOUSEEVENTF_LEFTUP, 0, 0, 0, 0);
120
121      // Simulate keystrokes in the frequency box.
122      for (i = 0; i < wcslen(argv[1]); i++) {
123          keybd_event((BYTE) *(argv[1]+i), bScan[i], 0, 0);
124          keybd_event((BYTE) *(argv[1]+i), bScan[i],
                 KEYEVENTF_KEYUP, 0);
125      }
126
127      // Tab over to the "Tune" button, and press enter.
128      keybd_event(VK_TAB, 0x0F, 0, 0);
129      keybd_event(VK_TAB, 0x0F, KEYEVENTF_KEYUP, 0);
130      keybd_event(VK_RETURN, 0x1C, 0, 0);
131      keybd_event(VK_RETURN, 0x1C, KEYEVENTF_KEYUP, 0);
132      return 0;
133  }
134
135  void errormessage()
136  {
137      printf("Usage:␣␣LCR100CL␣xxxxxx\n");
138      printf("␣␣␣␣␣␣␣␣where␣each␣x␣is␣a␣numeral␣from␣0␣to␣9,␣or␣
             a␣decimal␣point.\n");
139      printf("The␣Mid-Atlantic␣GUI␣must␣be␣running␣before␣you␣
             call␣LCR100CL.\n");
140  }
```

Bibliography

1. Evans, Merran, Nicholas Hastings, and Brian Peacock. *Statistical Distributions* (Third Edition). Hoboken, NJ: Wiley-Interscience, 2000.

2. Hollander, Myles and Douglas A. Wolfe. *Nonparametric Statistical Methods* (Second Edition). New York, NY: John Wiley & Sons, Inc., 1999.

3. Kutner, Michael H., Christopher J. Nachtsheim, John Neter, and William Li. *Applied Linear Statistical Models* (Fifth Edition). Boston, MA: McGraw-Hill Irwin, 2005.

4. Near Field Systems, Inc. *NSI2000 Operating Manual (Near-Field Edition), Version 4*. Torrance, CA, May 2005.

5. Saville, Michael A., Kenneth Monroe, Christopher Allen, and Rick Martin. "Processing-based Tuner Gain Correction in a Wideband Multi-channel Receiver." *Proceedings of the IEEE International Radar Conference*. May 2010.

6. Tseng, Ching-Yih and Lloyd J. Griffiths. "A Unified Approach to the Design of Linear Constraints in Minimum Variance Adaptive Beamformers," *IEEE Transactions on Antennas and Propagation*, *40*(12):1533–1542 (December 1992).

7. Tsui, James B. *Microwave Receivers with Electronic Warfare Applications* (Second Edition). Raleigh, NC: SciTech Publishing, Inc., 2005.

8. VanTrees, Harry L. *Detection, Estimation, and Modulation Theory, Part 1*. New York, NY: John Wiley and Sons, Inc., 2001.

9. Vincent, F. and O. Besson. "Steering Vector Errors and Diagonal Loading," *IEE Proceedings - Radar, Sonar, and Navigation*, *151*(6):337–343 (December 2004).

10. Wax, Mati and Yosef Anu. "Performance Analysis of the Minimum Variance Beamformer in the Presence of Steering Vector Errors," *IEEE Transactions on Signal Processing*, *44*(4):938–947 (April 1996).

11. Yu, Zhu Liang, Qiyue Zou, and Meng Hwa Er. "A New Approach to Robust Beamforming Against Generalized Phase Errors." *IEEE 6th CAS Symposium on Emerging Technologies: Mobile and Wireless Communications*. 775–778. May-June 2004.

12. Air Force Research Laboratory, Sensors Directorate, RF/EO Subsystems Branch. http://www.wpafb.af.mil/afrl/ry.

REPORT DOCUMENTATION PAGE

Form Approved
OMB No. 074-0188

1. REPORT DATE *(DD-MM-YYYY)*	**2. REPORT TYPE**	**3. DATES COVERED** *(From – To)*
12-03-2010	Thesis	Sep 2008 – Mar 2010

4. TITLE AND SUBTITLE

Effects of Channel Mismatches on Beamforming and Signal Detection

5a. CONTRACT NUMBER
N/A

5b. GRANT NUMBER
N/A

5c. PROGRAM ELEMENT NUMBER
N/A

6. AUTHOR(S)

Christopher I. Allen

5d. PROJECT NUMBER
N/A

5e. TASK NUMBER
N/A

5f. WORK UNIT NUMBER
N/A

7. PERFORMING ORGANIZATION NAMES(S) AND ADDRESS(S)

Capt Christopher Allen
AFIT/ENG
2950 Hobson Way
Wright-Patterson AFB, OH 45433-7765

8. PERFORMING ORGANIZATION REPORT NUMBER
N/A

9. SPONSORING/MONITORING AGENCY NAME(S) AND ADDRESS(ES)

Seng M. Hong, PhD
Air Force Research Lab
2241 Avionics Circle, Bldg 620
Wright-Patterson AFB, OH 45433-7765
(937) 904-9098
Seng.Hong@wpafb.af.mil

10. SPONSOR/MONITOR'S ACRONYM(S)
AFRL/RYDR

11. SPONSOR/MONITOR'S REPORT NUMBER(S)

12. DISTRIBUTION/AVAILABILITY STATEMENT
Approved for public release; distribution unlimited.

13. SUPPLEMENTARY NOTES
N/A

14. ABSTRACT

Tuner gain measurements of a multichannel receiver are reported. A linear regression model is used to characterize the gain, as a function of channel number, tuner set-on frequency, and intermediate frequency. Residual errors of this model are characterized by a *t* distribution. Very strong autocorrelation of tuner gain at various frequencies is noted. Tuner performance from one channel to the next is diverse; several defects at specific frequencies are noted. The Wilcoxon signed rank test is used to test normality of tuner gain among devices; normality is rejected.

Antenna directivity and phase pattern measurements are also reported. An antenna element pattern is presented, along with residual errors. An array pattern model is constructed using steering vectors. Simulated gain and phase mismatches are used to predict their effects on antenna beamforming and signal detection.

15. SUBJECT TERMS
Wideband receiver; radar; ELINT; mixer performance; mixer modeling; regression modeling; antenna pattern; antenna modeling; signal detection; beamforming.

16. SECURITY CLASSIFICATION OF:			**17. LIMITATION OF ABSTRACT**	**18. NUMBER OF PAGES**	**19a. NAME OF RESPONSIBLE PERSON**
REPORT	**ABSTRACT**	**c. THIS PAGE**			Richard K. Martin
U	**U**	**U**	**U U**	211	**19b. TELEPHONE NUMBER** *(Include area code)* (937) 255-3636 x4625 Richard.Martin@afit.edu